2012

Numerical Evaluation Of Different Retrofitting Techniques Of New Orleans Floodwalls And Implementation Of Advanced Constitutive Model In Flac3D

Sudarshan Adhikari
University of Mississippi

NUMERICAL EVALUATION OF DIFFERENT RETROFITTING TECHNIQUES OF NEW ORLEANS FLOODWALLS AND IMPLEMENTATION OF ADVANCED CONSTITUTIVE MODEL IN FLAC^{3D}

A Dissertation

Presented for the

Doctor of Philosophy

Degree

The University of Mississippi

Adhikari, Sudarshan

November, 2012

ABSTRACT

The objective of this study was to re-examine some but the crucial established failure mechanism, and also to establish other failure mechanisms of the floodwalls due to hurricanes in New Orleans so that the necessary retrofitting techniques could be sought out. Depending on the failure mechanisms, two of the proposed retrofitting techniques such as "structural cap" to maintain integrity by tying adjacent panels of I-type floodwalls, and "bentonite apron" to self seal gaps that occur between the floodwall and foundation soil were chosen, for which their performances had to be evaluated. This dissertation documents all the numerical analysis conducted to address those tasks.

At first, this study utilized the field monitoring results from a full scale loading test in London Ave. Canal in New Orleans, LA to calibrate/back-calculate soil moduli. From this study, it turned out that the moduli of the field soils are mostly higher (1 to 12 times) than predicted magnitudes from laboratory tests or empirical relations, and quantitatively confirmed that the gap formation and strength reduction in the water glazed marsh layer greatly decreased the stability of floodwall. Using the calibrated parameters and the failure mechanism established, effectiveness of the structural cap was evaluated and it was found that the structural cap is effective in restricting the relative displacement of the adjacent panels maintaining integrity.

In order to justify the application of retrofitting techniques design to seal these gaps (Bentonite Apron), this study conducted numerical and analytical evaluations to investigate the in-depth mechanism of gap formation using an effective stress approach. It was found that

question of whether gap is the cause or the result of failure depends on soil properties and site conditions. But improving the existing foundation soil for the case where gap is the result of failure tends to cause the formation of gap which necessitates the implementation of gap sealing mechanism in any circumstances. The study also showed that swelling potential of the Bentonite Apron was such that it can seal the gap effectively, and at the same time it is not that large to cause the excessive displacement of the wall and the peripheral soil.

Incorporation of anisotropy in numerical analysis is very important since most of the soils are anisotropic in nature. So far, none of the researchers of New Orleans flood protection system have incorporated this behavior in their numerical analysis as they are not readily available in commercial codes .So, to fill this gap, as a second objective, this study implemented the new user defined constitutive model (**A**nisotropic **M**odified **C**am **C**lay **M**odel) in FLAC^{3D}, by taking the advantage of user defined model capability. The implemented Model was well verified and validated with the mathematical model and the experimental results respectively. When applied to the New Orleans floodwall sections, the results showed that isotropic Mohr Coulomb might be good for evaluating overall behavior in moderate deformation problems, while Anisotropic Modified Cam Clay Model was good even for large strain problems where more accurate evaluation of yielding is needed.

.

Dedication

This work is dedicated to my late father and family

LIST OF SYMBOLS

Following is the lists of the symbols which are not described in the text. The symbols described in the text are not listed here.

$\mathbf{I_{uncr}}$	=	moment of Inertia for the uncracked RCC section
b	=	width of the section
D	=	Overall depth of the I-wall section
n	=	modular ratio
$\mathbf{A_s}$	=	area of steel in tension zone
$\mathbf{A'_s}$	=	area of steel in compression zone
$\mathbf{h_s}$	=	distance of the centroidal axis of the tension steel bar to the centroidal axis of the section
$\mathbf{h'_s}$	=	distance of the centroidal axis of the compression steel bar to the centroidal axis of the section
$\mathbf{I_{cr}}$	=	moment of Inertia for the cracked RCC section
d	=	effective depth of the section
d'	=	cover at the compression zone
ρ	=	ratio of the area of steel in tension zone to the effective area of the section
ρ'	=	ratio of the area of steel in compression zone to the effective area of the section

$\mathbf{E_c}$ = concrete elastic modulus

$\mathbf{I_c}$ = moment of inertia of the concrete section

$\mathbf{E_e}$ = equivalent modulus of elasticity corresponding to cracked or uncracked RCC section

$\mathbf{t_e}$ = equivalent thickness of the section corresponding to cracked or uncracked section

$\mathbf{f_{ct}}$ = tensile strength of concrete

$\mathbf{f'_c}$ = compressive strength of the concrete

$\mathbf{M_{cr}}$ = cracking moment

$\mathbf{I_e}$ = effective moment of inertia for the cracking section

$\mathbf{M_a}$ = maximum moment in the member at the loading stage

$\mathbf{M}$ = bending moment at any element of the structural element

$\boldsymbol{\phi}$ = factor for resistance

$\boldsymbol{\phi M_n}$ = factored resisting moment

$\mathbf{M_n}$ = resisting moment

$\boldsymbol{\nu}$ = Poisson's ratio

$\mathbf{c_{11}, c_{22}}$ = Stiffness in the global system

$\mathbf{c_{12}, c_{33}}$ = Stiffness in the global system

$\mathbf{c'_{11}, c'_{22}}$ = Stiffness in the local system

$\mathbf{c'_{12}, 'c_{33}}$ = Stiffness in the local system

c'^{b}_{11}, c'^{b}_{22} = bending Stiffness in the local system

c'^{b}_{12}, c'^{b}_{33} = bending Stiffness in the local system

c'^{m}_{11}, c'^{m}_{22} = membrane Stiffness in the local system

c'^{m}_{12}, c'^{m}_{33} = membrane Stiffness in the local system

M_x = Bending moment about the vertical axis of the wall

M_y = Bending moment about the lateral axis of the wall

f_y = yield strength of steel

C_s = Compressive force in steel

C_c = compressive force in concrete

a = depth of the compression stress block

ε'_s = strain at the compression steel

ACKNOWLEDGEMENTS

I wish to express my heartfelt gratitude to Dr. Chung R. Song for his keen interest and guidance to supervise this important study work as a part of the Ph. D. Degree. His co-operative nature has always been an impetus not only to complete the present study but also to carry out research in future. I am equally grateful to other members of my dissertation committee, Drs. Alexander H.-D. Cheng, Ahmed Al-Ostaz, and P. Raju Mantena for their comments and suggestions.

A sacred tribute of eternal dedication and devotion goes to my late father whose blessings are always with me. My love and respect goes to my mother who has always taught me to lead a disciplined life and her sharing in all my difficulties and has always bolstered my self confidence.

Thanks are also extended to all my relatives and friends in Nepal and abroad for their moral support dedicating wishes, for all my endeavours.

I am very grateful for the Department of Homeland Security, SERRI Project, Department of Civil Engineering, and Graduate School for sponsoring and supporting my study.

I especially like to express my gratitude to my wife Dipti Adhikari for her support to make this study success. Only through her endless support and love during the difficult time have this work been successful.

Last but not least, I would like to express my heartfelt thanks to one and all that is one way or the other, directly or indirectly, supported me for achieving this work.

TABLE OF CONTENT

LIST OF TABLES

LIST OF FIGURES

1. INTRODUCTION

1.1 MOTIVATION OF THE RESEARCH

New Orleans Flood protection system is one of the storm damage reduction infrastructures that alone comprise 350 miles of levee and floodwall. Most of the floodwall is of I-wall type which propels about 6 to 10 feet (old design) above the earthen levees and is 1 foot wide at the top and 2 feet wide at the bottom supported by the sheet pile underneath. The project which was initially designed in 1960s but reanalyzed during 1980s was constructed piecewise rather than one unit having many transitions in regards of height, shape, size and the quality of the structures. In additions to these transitions, factors such as coastal land loss and settlement; over population and increased man made infrastructures; and the climate change induced increased storm surge are the other challenges of the New Orleans hurricane protection system. These challenges have resulted in the need to improve the existing flood protection system.

The improvement of these structures might be done either by complete replacement program or by retrofitting the existing ones. While replacement program can be of huge economical burden, retrofitting technique may be viable. The retrofitting programs for the next hurricane season can be designed considering the lessons learned from hurricane Katrina 2005 which caused lots of human and economical loss. The causes of the failure of the New Orleans floodwall system are clearly documented in IPET (Interagency Performance and Evaluation Taskforce) and ILIT (Independent levee Investigation Team) reports. Both these reports, with

some exceptions, stood on the common ground to point out two categories of the failure mechanism in which the first is related to the erosion and the other to the stability.

With reference to the IPET and ILIT reports, stability related failures were primarily due but not limited to the gap formation on the backside of wall, the higher uplifting seepage pressure on the levee toe (promoting heaving) and the shearing of the weak soil. Most of those failures were the localized failure (maximum 600 feet in length) since the floodwall didn't behave as one integral unit. This integrity was compromised in the original design to avoid the crack formation due to the shrinkage and expansion of concrete capping by constructing floodwall as a combination of different panels with gaps in between.

While the erosion related failure mechanism has been already studied and the retrofitting techniques been addressed as a Ph.D. dissertation (Jang 2010), this study is focused on the stability related failure mechanism and the retrofitting techniques related to it. Currently, the retrofitting techniques that are in common practices in New Orleans are relief well installation (relief seepage pressure), construction of seepage berms, and deep soil mixing. But due to the high cost and a demand of wide right of way for their implementation, new, innovative, effective and economical techniques have been sought out. The new techniques that have been looked upon in this study is the structural cap to tie the different panels to maintain system integrity; and the use of the bentonite apron to self seal the gap between the soil and the wall due to rise in water level. To justify that these mechanism are effective, it is utmost necessary to evaluate their performance. Numerical analysis is one of the reliable measures to evaluate the effectiveness of these proposed techniques. So, this study is motivated to evaluate the performance of these techniques using FLAC^{3D}. If the retrofitting techniques perform well, then these techniques that are economical to implement can be used by the practitioners.

Incorporation of anisotropy in numerical analysis is very important because most of the soils are undergone K_0 consolidation during the successive deposition and at the same time the construction of the levee on top of them causes the rotation of the principal stresses. The recent experimental results have also shown that the soil behavior deviate pronouncedly from the fundamental area of classical soil plasticity.

In reference to the New Orleans levees and floodwalls, so far, numerical analysis as reported in IPET and ILIT reports were primarily done using three constitutive models either in PLAXIS or FLAC. In these reports, it is seen that the analysis were primarily done using Mohr Coulomb Model. Apart from that, analysis was also done using the Bounding surface hypoplastic model for sand (Wang et al. 1990) to represent the behavior of sand. ILIT team had incorporated the critical state soil mechanics in their analysis and used Modified Cam Clay Model (Roscoe and Burland 1968) to simulate the behavior of soft soils (ILIT 2006). But, none of the researches of New Orleans flood protection system have incorporated anisotropic behavior of soils in their numerical analysis as they are not readily available in commercial codes. So this study is motivated to incorporate the anisotropy in soft soil.

1.2 AIMS AND OBJECTIVES

Though the IPET report (IPET 2007) pointed out that that there were four failure mechanism that led to the failure of the New Orleans Levee and floodwall system, they can be primarily divided into two modes such as the one due to the erosion on the backside of the levee and the other related to the stability. The gap formation, seepage induced failure and the shearing of the weak layer all comes into the second category. The failure related to the erosion and its retrofitting technique has already been studied as the Ph.D. dissertation by Jang (2010). So, in this study, only failures related to stability and retrofitting techniques against it was dealt.

The objectives of this study are given as follows.

General objectives

1. To re-examine the established failure mechanisms, and to establish new failure mechanism of the floodwalls especially I-walls due to hurricanes to devise proper retrofitting technique
2. To evaluate effectiveness of chosen retrofitting techniques using numerical simulation
3. To develop, implement and apply the advanced constitutive soil model

Specific objectives

1. To calibrate with some degree of accuracy the soil stiffness to be used in the numerical analysis while evaluating the retrofitting techniques.
2. To reconfirm the effect of gap on the overall performance of the floodwall as stated in the IPET report (IPET 2007) and purpose an appropriate method of modeling the occurrence gap in numerical simulation. This means the study determines whether the gap caused the failure or is the result of the failure.
3. To predict the other failure mechanism of the floodwall in New Orleans
4. To evaluate numerically the proposed retrofitting techniques such as the bentonite apron and the structural cap for the integrated and resilient floodwall.
5. To implement the new soil constitutive model (Anisotropic Modified Cam Clay Model) in FLAC^{3D} for soft clay (lacustrine clay) and apply it in the numerical simulation of New Orleans levee/ floodwall section.
6. To establish the approach in developing the deflection based failure criterion that aid in developing the effective tool in monitoring the performance of floodwalls.

1.3 SCIENTIFIC SIGNIFICANCE

The main significant contribution of this research is to highlight the major component of the new and innovative retrofitting techniques to improve the performance of the floodwalls and levees that can be used in the common practice. It also contributes in developing the levee failure monitoring tool using the deflection base failure criterion. This monitoring tool can be utilized in evacuation program and emergency levee repairing scheme during the hurricanes. Secondly, this research also aims to add one new user defined constitutive model in FLAC^{3D} which could obviously be used not only in analyzing New Orleans floodwall sections but also for any other research or practice which involves soft soil exhibiting anisotropy.

1.4 WORK SCOPE

This study is composed of seven chapters

Chapter 1 presents the introduction, the objectives of the study, the significance of the study and the work scope.

Chapter 2 presents the literature review where the major failure mechanism of the floodwalls and levees are addressed. In addition to that, the current retrofitting techniques for levees that are in practice are also addressed. And later some constitutive soil models which are used in the numerical analysis of New Orleans levees and floodwall sections are also presented.

Chapter 3 presents the calibration of the soil parameters and analysis of I-wall using the calibrated parameters. In this chapter, apart from calibrating the parameters using the field load test data, the failure mechanism of the floodwall was identified which has been overshadowed in the IPET and ILIT report. This study was conducted so that the reliable result will be obtained from the further numerical Analysis.

In Chapter 4 using the calibrated parameters in Chapter 3, the performance of the structural cap is evaluated. The cap has been proposed to be used as one of the retrofitting technique in New Orleans levees and floodwall system.

In chapter 5, effective stress based analysis is done to re-evaluate gap on the performance of the floodwall and to see if the gap is the cause or the consequence of the failure of floodwalls. Ultimately, for the case where gap is the cause of the failure of wall, then the performance of the Bentonite Apron is evaluated to check if the Bentonite Apron does not apply excessive pressure to the floodwall.

In Chapter 6, implementation of an Advanced Constitutive model in FLAC^{3D} is presented. At the same time, the model is verified with the analytical solution and also validated with the experimental results. Ultimately, the model is applied in the numerical simulation of the Floodwall section in New Orleans.

In chapter 7, an initial effort to develop and apply deflection based criterion with the example case is demonstrated.

In Chapter 8, the summary and conclusions from this study are presented and some recommendations for the future study are demonstrated.

2. LITERATURE REVIEW

2.1 NEW ORLEANS FLOODWALL SYSTEM AND GEOLOGICAL SET UP

The geological set up is the key component to determine the engineering property of the soils and thus to evaluate the performance of the floodwalls. Dunbar and Britsch (2008) did an extensive study to find out the geomorphologic set up of New Orleans. According to them, the geology consists of the Pleistocene surface at the bottommost layer. Overlying this surface is the Estuarine (Bay sound) clay which is the fine grained shallow water sediments. Above this layer is the Beach sand above which lays the Soft clay known as the lacustrine clay and Plaudal (marsh) deposits depending upon the locations.

According to Kolb and Van Lopic (1958) via Rogers et al.(2008), the New Orleans canals constructed between 1833 and 1878 are primarily seated on the interdistributary bayments which are underlain basically by fat clays such as of marsh and Lacustrine type.

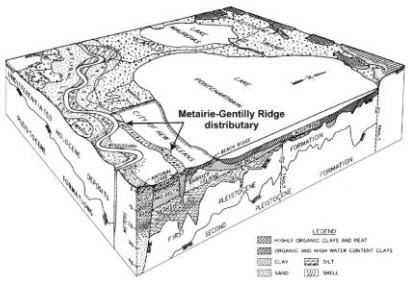

Figure 2.1. Block diagram of geology underlying New Orleans (adapted from Kolb and Saucier, 1981)

About 90 percent of New Orleans excluding filled areas is covered by swamps and Marsh (Rogers et al, 2008). These are the most weak soil deposits which are to be looked upon carefully when designing any kind of protection system in New Orleans. Apart from marsh layers, the area also consists of lacustrine clay which is fat clays with organic mix and is very weak in shear strength.

2.2 KATRINA AND MAJOR FAILURE MECHANISMS OF THE FLOODWALL

Lesson learned from Hurricane Katrina is the main basis on which the principles for design of the floodwall for the next hurricane season are formulated. Hurricane Katrina occurred in August 29, 2005 and was the costliest natural disaster and one of the five deadliest hurricanes in the history of United States which took 1836 lives with a total property damage of $81 billion (Knabb et al 2006.). Due to the Hurricane 53 levee and floodwall breaches in New Orleans and St Bernard Parish areas. Due to these breaches about 80 % of the city of New Orleans and 100% of St. Bernard parish flooded.

After Hurricane Katrina, many studies were conducted to find the failure mechanisms that led the catastrophic failure of the floodwalls in New Orleans. Though there are minor controversies between the two major studies conducted by IPET team (IPET 2007) and ILIT team (ILIT 2006), they stood on the common ground to point out that there were four major failure mechanisms that led the catastrophic event such as gap formation on the canal side; overtopping of the floodwall; shear failure of the weak soil layer; and the under seepage induced failure. Each of these failure mechanisms are discussed as follows:

2.2.1 Gap Formation

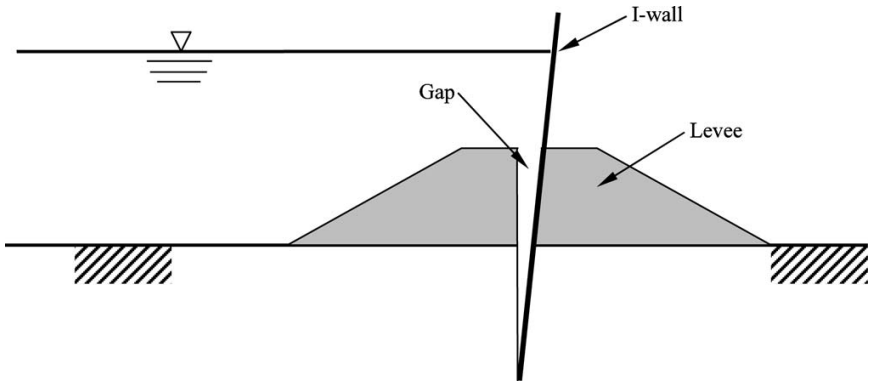

Figure 2.2. Example of I-wall gap (adapted from Brandon et al. 2008)

Gap formation was not included in the initial design of the floodwall. This phenomenon turned out to be a very important issue after the Hurricane Katrina and was considered to be the one of the most important candidate that led to the failure of floodwall, mostly I type during Hurricane Katrina. Both IPET report (IPET 2007) and ILIT report (ILIT 2006) highlighted the importance of its inclusion in the design guidelines. There are others papers which were published after these reports such as Sills et al. (2008) which highlighted the effects of gap on the stability of I-walls in New Orleans.

Brandon et al. (2008) has studied the effect of gap on the stability of I-wall and has formulated some closed form equations to calculate the depth of gap for homogenous and layered soil. According to them the depth of the gap is equal to the depth where the active horizontal pressure and the water pressure are equal. In other words, the depth is equal to the one upto which the positive effective stress exists. For cohesive soil where the angle of internal friction angle is zero,

$$\sigma_{ha} = \gamma_w(z_w - z) + \gamma z - 2c \qquad (2.1)$$

$$\sigma_w = \gamma_w z_w \tag{2.2}$$

If z_0 is the depth where the horizontal active earth pressure and the water pressure is zero, then the depth of gap for this can be given as:

$$z_0 = \frac{2c}{\gamma - \gamma_w} = \frac{2c}{\gamma'} \tag{2.3}$$

In above equations, σ_{ha} is the horizontal active earth pressure; γ is the saturated unit weight of the soil, γ_w is the unit weight of the soil; γ' is the effective unit weight of the soil; z is the depth below the ground surface; z_w is the depth below the water surface and c is the cohesion of the soil. Since the internal friction angle of the soil is zero, then the coefficient of active earth pressure for that case is 1.

If in case the soil is not uniform but composed of different soil layers with varying unit weight then the active horizontal pressure has been proposed as following:

$$\sigma_{ha} = \gamma_w h_w + \sum(\gamma_i h_i) - 2c_i \tag{2.4}$$

Where h_i is the height of the i^{th} individual soil layer above the depth of interest; h_w is the height of the water above the ground surface; and c_i is the cohesion of the soil layer at the depth of interest.

The above equations are valid for the total stress analysis and when the soil layers are cohesive in nature. But the author has not proposed the equations for the case of effective stress analysis where the coefficient of active horizontal stress are not equal to one and the soil effective pressure and the water pressure are treated separately. But even this is only viable for the limiting case when the enough deformation has been developed to build the active condition.

Otherwise for the effective stress analysis where the internal frictional angle is taken into account, the coefficient of lateral earth pressure varies between at rest condition to the active condition.

Brandon et al (2008) have also proposed a methodology in modeling the gap formation in their paper. After the analytic calculation of the depth of gap, they proposed to remove the soil on the active side from their model and apply a water pressure instead .This has been illustrated in the figure below.

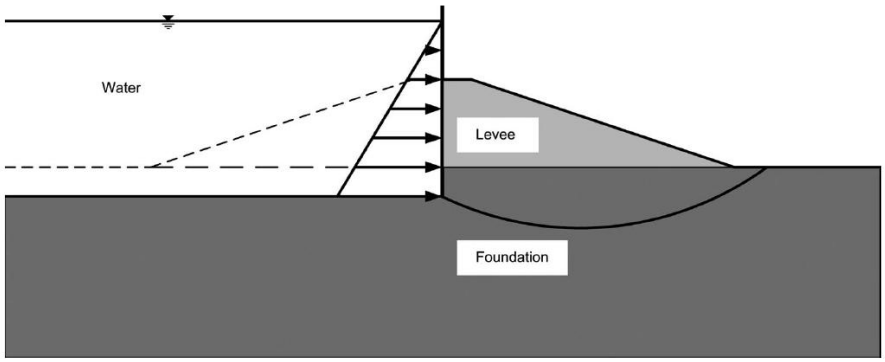

Figure 2.3. Modeling gap formation (adapted from Brandon et al. 2008)

The above proposal may be good for the case when the sheet pile is rigid and rotates about its tip. But this may not be true when the sheet pile is flexible and the centre of rotation is not at the tip of the pile but at some point above the tip. Since the water level is not constant and calculating the rotation center analytically is very tiresome, the stress and strain analysis has to be done and monitor the stress at the interface of the soil and wall. The tensile stress on the interface of the soil and wall confirms the development of the gap. The method proposed by Brandon et al. (2008) is applicable for the limit equilibrium analysis and for the cohesive soil since the coefficient of lateral earth pressure is always one no matters how much the displacement of the wall is.

2.2.2 Shear Failure of the Weak Layer

This is the other type of failure mechanism that led to the failure of the floodwalls in New Orleans. Both the IPET report (IPET 2007) and ILIT report (ILIT 2006) and other journal papers (almost all) has also categorized this failure mechanism to be the important one for the floodwall breach at North breach of the IHNC east bank and the breach of the 17th street canal by Katrina. The main cause for this type of failure mechanism is due to the soft gray clay layer which lies below the embankment fill. This soft clay layer whose strength depends upon the overburden pressure has a strength profile of $s_u / \sigma_v^{'}$ of 0.24 as suggested by the IPET report (IPET 2007) where the strength varies from 200 psf at the shallow depth to 400 psf for the larger depth. The illustration of this type of failure mechanism is shown in the Figure 2.4.

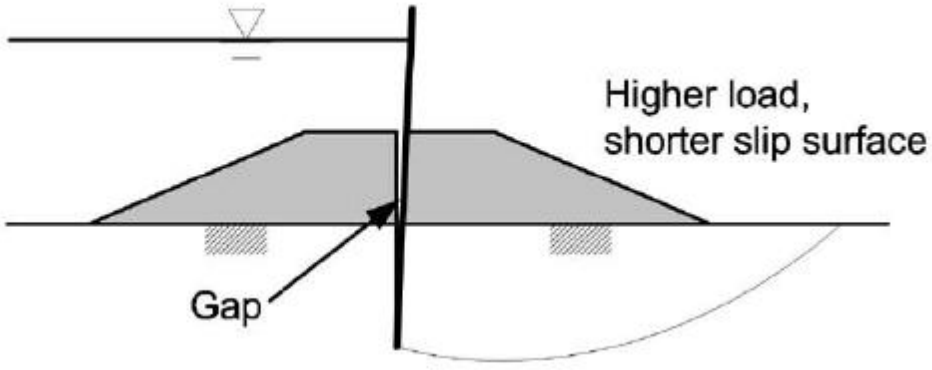

Figure 2.4. Foundation instability through clay (adapted from Duncan et al. (2008))

2.2.3 Under seepage Removal of Foundation Sand

According to IPET report and other journal papers like Duncan et al. (2008) accepted that this is best candidate for the failure of the London Avenue south during Katrina 2005.

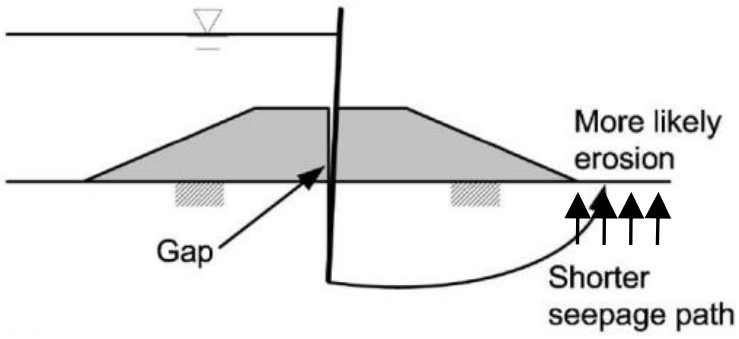

Figure 2.5. Underseepage and erosion through sand (adapted from Duncan et al. 2008)

This phenomenon of failure of foundation soil is also known as the piping or internal erosion. This phenomenon may be defined as the internal erosion caused by the groundwater flow that removes the fine grained deposits which starts from the toe of the structure progressing backwards making a tubular hollows (Haggerty 1991) or low strength layers (Rossa et. al. 2003).There has been a extensive works done regarding the piping phenomenon such as fromVon Ritchhofen, (1886);Col. Clibborn, (1895); Forchmeir, (1900); Bligh (1910); Lane, (1934); Terzaghi, (1922,1939,1943,1948); Casagrande, (1937); Betram, (1939) etc. These studies proposed the different method of evaluating the piping phenomenon specific to the geotechnical structure.

The most popular and used equation to evaluate the piping by heaving is the one proposed by Terzaghi (1943). He proposed the following equation.

$$F_s = \frac{W'}{U_e} \tag{2.5}$$

Where W' is the effective weight of the most critical soil prism Fs is the factor of safety against piping by heave and U_e is the uplift pressure at the base of the soil prism. So at the critical

condition when F_s is 1, then he defines the hydraulic gradient as the critical hydraulic gradient which is given by the following relation.

$$i_c = \frac{\gamma'}{\gamma_w} = \frac{G_s - 1}{1 + e} \tag{2.6}$$

Where i_c is the critical hydraulic gradient, G_s is the specific weight of the soil grain and e is the void ratio of the soil at the point of interest.

The IPET Report (IPET 2007) and ILIT report (ILIT 2006) both reported that the exit hydraulic gradient at the toe of the levee of London Avenue south was much higher than the critical hydraulic gradient. This is mainly because the soil profile of this section is composed of beach sand which has a high coefficient of permeability. Even the forensic investigation showed that there were sand boils on this section which confirms the failure mechanism at this section.

2.2.4 Overtopping Erosion of the Levee

The IPET report (IPET 2007) and the ILIT report (ILIT 2006) including Duncan et al. (2008) confirmed that this was the another failure mechanism of the catastrophic event during Katrina 2005 and this phenomenon occurred mainly in IHNC west bank north breach and IHNC east bank south breach (Duncan et al. 2008).

The main consequence of this phenomenon is that the resistance on the passive side of the wall is reduced due to scoring which contributes to the instability of the wall. There has been a numerous studies taken place for the erosion effect due to plunging water and is a complete study which is beyond the scope of this study and is regarded not relevant to include in this study

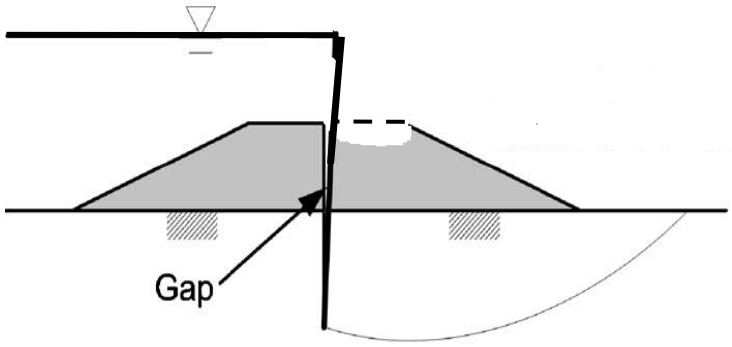

Figure 2.6. Failure due to the overtopping Erosion

2.3 CURRENT RETROFITTING TECHNIQUES

One of the main objectives of the project is to propose the retrofitting technique. There are many retrofitting techniques that are in practice for the levees and dams. Out of these, the practice that are currently in use in New Orleans are like Installation of relief wells to reduce seepage risk; installation of seepage berms; impermeable canal bed blanket, cutoffs; drainage blankets or trenches; raising the floodwall heights; and grouting (deep soil mixing). Out of these, the most applicable techniques are discussed one by one below.

2.3.1 Relief Wells

Relief wells are normally installed on the land side toe of the levees to discharge the seep water in a controlled manner so that the seepage stress under the levee is relieved so that the heaving of the soil is controlled. The schematic sketch of the relief well is shown in figure below.WES (1956); and Mansur and Kaufman (1957) have given the account for the detailed design of the relief wells and its construction procedures in Mississippi river levees. Likewise Middlebrookes and Jevris (1947); Turnbull et al. (1949): Turnbull and Mansur (1954) gave the

comprehensive description of the studies undertaken for controlling seepage and sand boils using the relief well along the lower Mississippi River levees. Mansur et al (2000) has in addition given the outline on the monitoring and the routine maintenance of the relief wells to achieve the best performance of the levees.

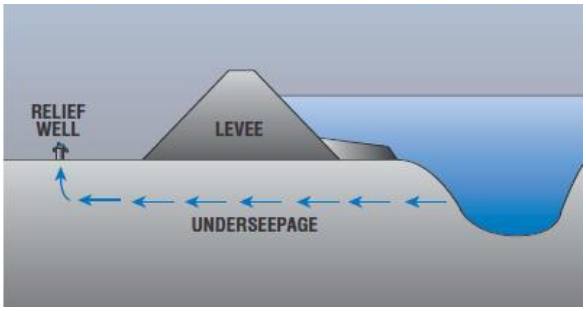

Figure 2.7. Relief wells control underseepage (Mississippi Levee Board)

2.3.2 Seepage Berms

Thick blanket of the soil can be placed on the adjacent to the landside slope of the levee to increase the weight of the soil and to increase the flow length of the water to decrease the exit gradient and at the same time to increase the weight of the soil so that the heaving and rupturing of the soil on this side can be minimized. One of the main disadvantages of this type of method is that they are very wide requiring large right of way and a tremendous amount of borrow material.

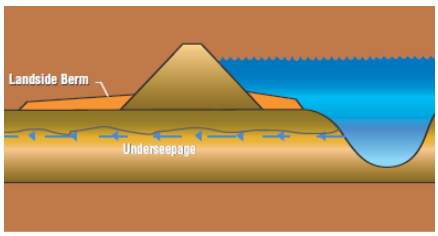

Figure 2.8. Landside berms controlling underseepage (Mississippi Levee Board)

Sometimes in scarcity of the borrowed materials, the canal bed itself can be dredged to make the Seepage berms. This type of berm is known as the dredged berms. The detailed design of the berms can be found in U. S. Army Engineer Waterways Experiment Station EM 1110-2-1913(2000) which is the revised form of TM 3-424 (Hess and Sills 2004)

2.3.3 Deep Soil Mixing

Grouting or Deep soil mixing is highly effective ground treatment system used to improve the load performance (such as reducing foundation settlements, increasing shear strength to improve the slope stability, and prevent soil liquefaction) of the weak soils like peat, soft clays etc

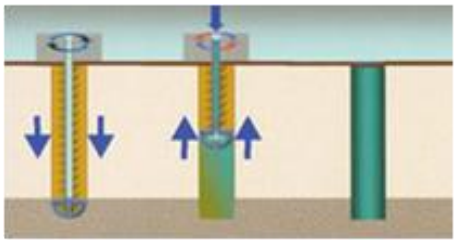

Figure 2.9. Schematic of Deep Soil Mixing

A wide range of strength can be achieved by varying the proportion of lime, cement or other admixtures. The deep soil mixing consists of mixing the soil with the admixtures in the form of coloums. The designing creterion depends on the failure mode which may be the failure of the coloumn or the soil.

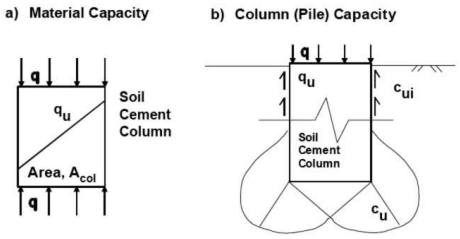

Figure 2.10. Failure mode of the pillar and the underneath soil (adapted from Terashi 2009)

Since New Orleans soil profile consists of the layers of weak soils, after Katrina, the retrofitting plans includes the deep soil mixing program as well. This method will be typically used in the IHNC at ninth ward point. This method will improve the performance of the I-wall sections in those areas

2.3.4 Using Erosion resisting Materials

One of the major failure mechanisms of the New Orleans levees during Katrina was the erosion of the levee crest on the land side due to the plunging water. Jang (2010) conducted an extensive research regarding erosion resisting materials and come to the conclusion that the dispersive soil having high degree of compaction and non dispersive soil having both high degree of compaction and low permeability can be a good resisting material. Similarly, certain admixtures like cement, poss and using the vetiver plants have a higher resistance to the erosion.

2.4 SOIL CONSTITUTIVE MODELS

2.4.1 Background

There are many soil constitutive models to model the stress deformation relationship of the soil. Out of these models, we are considering three models such as Mohr Coulomb Model,

Modified Cam Clay Model and Bounding Surface Hypoplasic model since these models have been used in the numerical analysis of the floodwall and levee sections in New Orleans.

2.4.2 Mohr Coulomb Model

Mohr coulomb is the simplest model which represents the first-order approximation of the soil or rock behavior**.** This is the linear elastic perfectly plastic model which is obtained from combining the Mohr's circle of stress with Coulomb's Friction law.

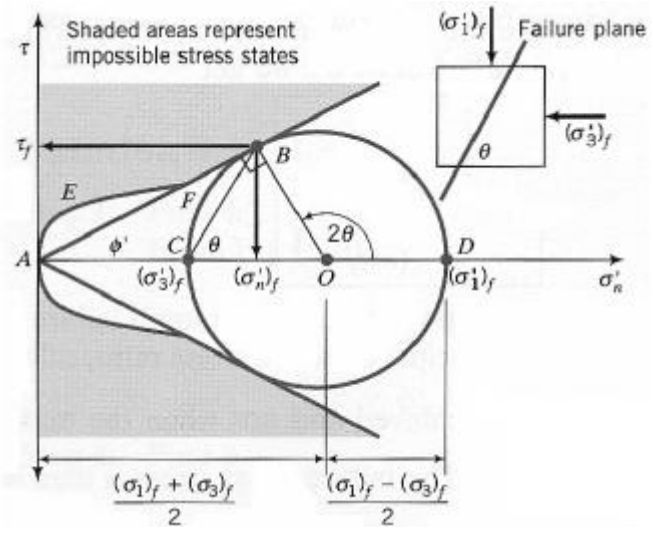

Figure 2.11. Mohr Coulomb Model (Budhu 2000)

The figure above illustrates the Mohr-Coulomb Model. The state of the soil is elastic within the conical conical area enclosed by the Coulomb's failure line and the Curve AEF representing the peak stresses. At the same time the state soil is at yielding on the Coulomb failure line. It should also be remembered that the soil cannot have the stress state that lies in the shaded area outside the Coulomb's failure line and the curve AEF of peak stresses.

Actually due to the simplicity of this model, it is recommended to use this model for a first analysis of the problem. Since for each soil layers a average stiffness is estimated, due to which computations are really fast and one can obtain the first estimate of the deformations only. The failure mechanism for the Mohr Coulomb model can be given by:

$$\sigma_{1f} - \sigma_{3f} = \frac{2c\cos\phi + 2\sigma_{3f}\sin\phi}{1-\sin\phi} \qquad (2.7)$$

Where *c* is the cohesion, ϕ is the internal angle of friction,σ_{1f} and σ_{2f} are the principal stresses

2.4.3 Modified Cam Clay Model

Early constitutive soil (elastic and elastic-perfectively) model over- idealized the soil behavior and was basically based upon the theories related to solid mechanics. These constitutive models do not take into account the volumetric changes that occur in the soil during shearing which is actually the most important and fundamental characteristics of the soil. Therefore these models though have been used widely in the practical field are inappropriate to represent the actual behavior of the soil. It was first time in 1958 that Roscoe, Schofield and Wroth (1958) incorporated the volumetric changes in the soil through which the critical state soil mechanics evolved.

The first constitutive model based on the critical state soil mechanics that incorporates the volumetric strain during shearing and also the hardening rule was Cam clay model (Roscoe and Schofield 1963). The formulation of this model is based on the assumption of simple work hardening rule proposed by Drucker et al. (1957). In this model, the state variables are described in the *q* (shear), *p* (mean effective pressure) and *e* (void ratio) space. At the critical state, change

in these state variables is zero (e.g. *dp = dq = dv = 0*) with the continuous increase in the shear strain.

Later the main problem of Cam Clay Model was realized. The main problem associated with the cam clay model was that there is a unrealistic estimation of the strain at lower stress ratio. To overcome this problem, the model was further modified by Burland (1965) and Roscoe and Burland (1968) by introducing the new formulation of work dissipation.

$$pd\varepsilon_v^p + qd\varepsilon_q^p = p\left\{(d\varepsilon_v^p)^2 + M^2(d\varepsilon_q^p)^2\right\}^{1/2} \tag{2.8}$$

The yield envelop for the Modified Cam Clay model is shown in the figure below.

The yield function for Modified Cam Clay model can be given in the equation below:

$$f = q^2 + M^2 p(p - p_o) = 0 \tag{2.9}$$

And the flow rule is given by the following equation

$$dp_o = \frac{vp_o\, d\varepsilon_v^p}{\lambda - \kappa} \tag{2.10}$$

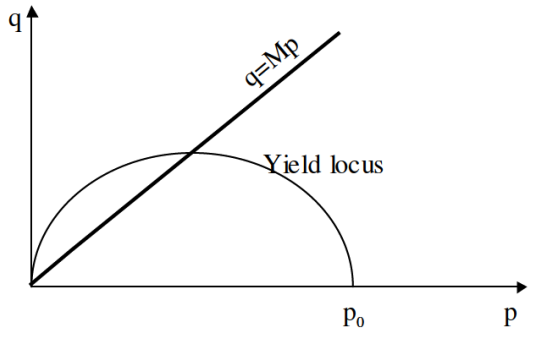

Figure 2.12. Modified Cam Clay yield criterion (Roscoe and Burland, 1968)

Where M is the slope of critical line p_o is the preconsolidation pressure (which determines the size of the yield locus) dp_o is the change in the preconsolidation pressure de_v^p is the change in the plastic volumetric strain, v is the specific volume, λ and κ are the slope of the virgin compression line and the swelling line in the v vs. $ln(p)$ plane which is shown in Figure 2.13.

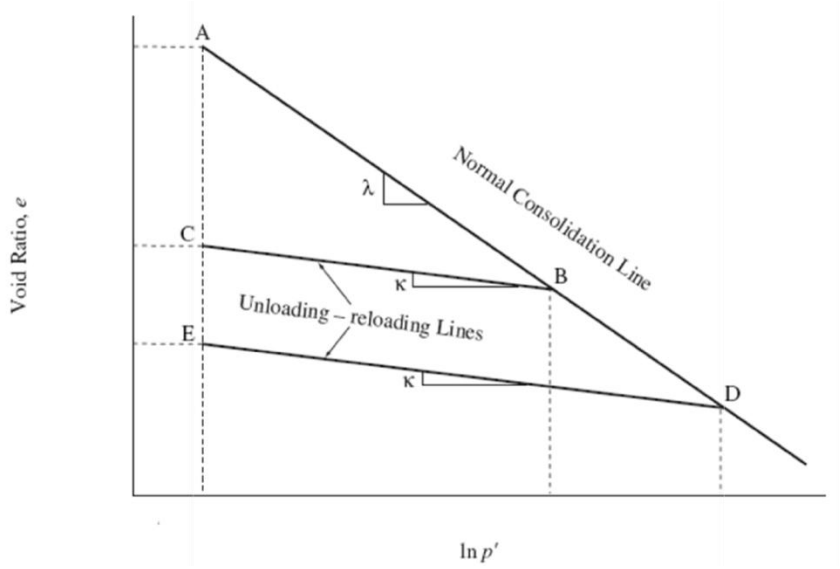

Figure 2.13. Loading and unloading Parameters

During shearing there is a change in volume associates a change in the Bulk Modulus and is given by:

$$K = \frac{vp}{\kappa} \tag{2.11}$$

And using the flow rule, the incremental form of the deviator and volumetric strains can be given by:

$$\begin{bmatrix} d\varepsilon_v^p \\ d\varepsilon_q^p \end{bmatrix} = \frac{1}{H}\begin{bmatrix} (M^2-\eta^2)p^2 & 2\eta(M^2-\eta^2)q^2 \\ 2\eta(M^2-\eta^2)p^2 & 4q^2 \end{bmatrix}\begin{bmatrix} dp \\ dq \end{bmatrix} \tag{2.12}$$

Where

$$\eta = \frac{q}{p} \tag{2.13}$$

And H is the Plastic Modulus which is given by the following relation

$$H = \frac{(1+e)p^3(M^4 - \eta^4)}{\lambda - \kappa} \tag{2.14}$$

ILIT (ILIT 2006) has used this model (soft soil model) in Plaxis to simulate the behavior of lacustrine clay and marsh in New Orleans floodwall sections.

2.4.4 Bounding Surface Hypoplastic Model for Sand

The two dimensional version of this model has been used to analyze the floodwall and levee section in New Orleans and is clearly documented in IPET report (IPET 2007). The model was formulated by Wang et al. (1990) within the framework of bounding surface hypoplasticity in which the main feature is the dependence of the loading and plastic strain rate direction on the stress rate direction that yield an incremental non linearity of the stress strain rate relations. So this model is particularly used for the successive simulation of the rotational shear due to the hypoplastic character. Specifically, the model was formulated by combining the bounding surface and hypoplasticity (e.g. Dafalias, 1986); and the creation of new loading surfaces upon reverse loading (Mroz and Zienkiewicz, 1984).

Since the original model which was written in general stress and strain tensors was not used in the numerical simulation of New Orleans levee section , the original model is not

described in detail this study (for details see Wang et. al. 1990). Only the formulations that confirm the plane strain conditions (Wang and Makdisi, 1999) are briefly describe here.

The model consists of two features such as the representation of the ultimate state of sandy soils by failure surface defined by the friction angle; and the dependency of soil modulus for each stress increment with the distance from the maximum pre-stressed surface to the failure surface (or the loading-stress condition). The model is capable of simulating shear stress induced volumetric change (excess pore water pressure for the undrained test).

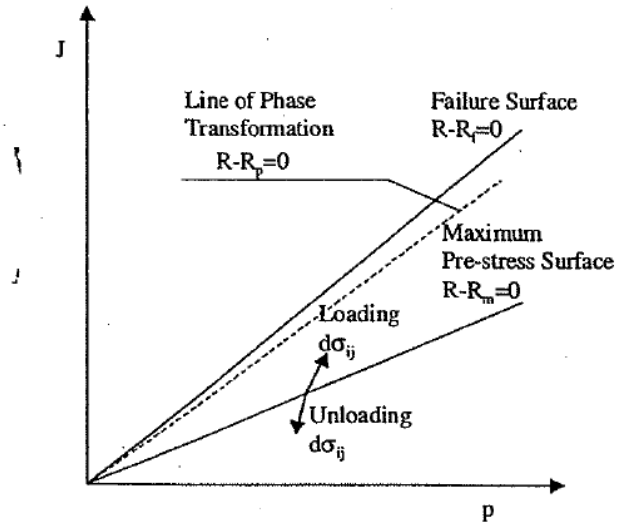

Figure 2.14. Surface and Stress variable in *p- J* plane for Bounding surface Hypoplastic Model (Wang and Makdisi, 1999)

Figure 2.14 shows the three surfaces and the stress variables in *p-J* space where *p* is the mean effective pressure and *J* is the deviator second invariant ($J = (1/2 s_{ij} s_{ij})^{1/2}$). Out of these three surfaces, two are the bounding surface and remaining one is the phase transformation surface. Phase transformation surface is the transit between the dilative and contractive behavior of soil. These surfaces can be formulated as the following equations.

Failure Surface: $R - R_f = 0$ (2.15)

Loading surface: $R - R_m = 0$ (2.16)

Phase transformation surface: $R - R_p = 0$ (2.17)

In which, $R_f = 2\sqrt{3}\sin\phi/(3-\sin\phi)$, where ϕ is the friction angle ; R_m is the variable that has the initial value that depends on the initial static stress and is automatically updated during computation; and R is the stress ratio invariant and is defined as ($R = J / p$).

The loading surface is cone in the stress space with apex at the origin. If the loading stress vector points outside the surface, the surface is expanded updating the current stress state. When the stress vector is pointing inside, then, this will be the unloading phase where the current stress conditions the projection center of the unloading phase.

The stress and strain relationship can be expressed as the increment $d\sigma_{ij}$ as the linear function of strain increment $d\varepsilon_{ij}$ as:

$$d\sigma_{ij} = \Lambda_{ijkl} d\varepsilon_{kl} = E_{ijkl} d\varepsilon_{kl} + A_{ijkl} d\varepsilon_{kl} \quad (2.18)$$

Where the first term is the elastic response and the second term is the plastic response. The details of the elastic stiffness matrix and the plastic stiffness matrix can be found in Wang and Makdisi (1999) and Wang et al. (1990) and are not described fully. All those stiffness can be defined in terms of shear and bulk moduli (both elastic and plastic) associated with the stress ratio ($r_{ij} = s_{ij} / p$) increment and mean pressure increment. This model has altogether 8 parameters.

3. PARAMETERS CALIBRATION AND SIMULATION OF I-WALL USING TOTAL STRESS ANALYSIS

3.1 BACKGROUND

The failures of I-walls during hurricane Katrina were the major causes for many breaches of the flood protection systems in New Orleans. After Katrina many research papers have been published regarding the failure mechanisms of the floodwall system such as gap formation behind the floodwalls, instability of the floodwall system due to the shearing of the weak foundation soil, the development of high uplift pressure in the sand layer, reduction of the strength of foundation soil due to the under seepage induced pore pressure, and scouring on the front side of the floodwall (IPET 2007; Seed et al. 2008; Brandon et al. 2008; Dunbar and Britsch III 2008; Duncan et al. 2008; Sills et al. 2008). To counteract those failure mechanisms and to enhance the performance of the flood protection system, some retrofitting techniques might be the improved floodwall sections to counteract the overturning; the use of expansive plugs to restrict gap formation; use of composite sheet piles to increase the stiffness; and the protection on the front side of the floodwalls against erosion. The numerical analysis is particularly important for the reliable analysis of those counter measures.

For the numerical analysis, appropriate numerical approach and accurate soil parameters are essential. So the study presented in this paper had two objectives. The first objective of the study was the development and verification of the numerical approach to capture the realistic behavior of floodwall system due to water load.

The numerical approach included the development of two dimensional geometric model of the floodwall and soil system incorporating the elasto- plastic material behavior of the soils and soil/wall interfaces. The simulation procedure was also accompanied with the algorithm to model the occurrence of gap and the prediction of its depth compatible with the deformation of the soil and wall system. At the same time the numerical procedure also included the reduction of the shear strength of the weak marsh soil susceptible to the high pore pressure during high flood level. The verification of the numerical technique was conducted by comparing its results with those of the full scale load test done in the London Avenue Canal of New Orleans.

The second objective of the study was to calibrate the soil parameters that will be used for further numerical analysis. Though there has been a wide variability of the soil strength parameters in New Orleans region, especially for marsh and the levee fill (Duncan et al. 2008), the IPET strength model which is used to provide the representative soil strength for levee and marsh of that region and which is based on the strength parameters obtained by actual shear strength test of the soil samples from the borings (this model is based on the samples from 17th Street canal) can be used for the two dimensional numerical analysis in London Avenue Canal as well . The inclusion of the variation of the soil strength in the analysis is beyond the scope of two dimensional analyses since it can only be captured by three dimensional analyses .So a major concern regarding the soil parameters in the two dimensional numerical analysis is the prediction of stiffness parameters. In most of the cases, there is a direct correlation of undrained shear strength with the stiffness of the soil. Duncan and Buchignani (1976) have proposed a relationship of these parameters with the function of over consolidation ratio and plasticity index. But it is seen that the relationship exists for a wide range .Similarly Mayne and Swanson (1981) also proposed a cam clay prediction of undrained initial tangent modulus with respect to

undrained shear strength in terms of over consolidation ratio, Cc and friction angle. With this method, the range is smaller than proposed by Duncan and Buchignani (1976) but still the relationship exists for certain range.

Specific to study site, in IPET report, V-19(IPET 2007), the stiffness of the soil was estimated by using the relation as E/S_u to be 92. Hurricane Protection Office (HPO) (2008) did the soil structural analysis for the same site in February 2007 before the full scale load test in which two analysis were conducted, one using the soil modulus obtained from tri-axial shear strength testing (TXT) and the other from in situ Pressure Meter Test (PMT) performed at the outfall canals where E/S_u for TXT was 48-68 and G/S_u for PMT was 100-220. So comparing all this approaches, it is seen that there is not a unique value of stiffness parameters and uncertainties certainly exist in estimating stiffness parameters by any kind of empirical equations. So it is necessary to treat these uncertainties by calibrating them accurately. In this study, back numerical analysis was done by using inclinometer measurement of the full scale test as the datum to calibrate the stiffness parameters of the individual soil layers. Though the complete report of parametric study has not been presented in this paper, the paper has recommended the final calibrated moduli required for the further numerical analysis.

As an outline of this paper, the brief description about the full scale test is given in the second section of this chapter. In the third section, a detailed account on the modeling has been presented. The main focus and the uniqueness of this study is the development of the algorithm for the initialization of the model which suits for the total stress analysis; proper modeling of the gap occurrence ; and the alteration of the shear strength of marsh layer for different loading condition. In the fourth section of the chapter, the results from the numerical simulations are evaluated and finally the conclusion from the study is presented in the last section.

3.2 FULL SCALE LOADING TEST

Since the data and the information from the full scale loading test were used as the datum of this study, it is relevant to discuss briefly about the full scale loading test.

3.2.1 Objectives

The full scale load test was conducted in the critical section of the I-wall in the London Avenue canal of New Orleans by US Army Corps of Engineer (USACE), New Orleans District from August 17, 2007 to August 31, 2007 with the main objective to find out whether the safe water elevation (SWE) can be increased within the city's outfall canals during the closure of the temporary gated structure during the hurricane season or not. The closure of the temporary gated structure is needed to prevent the storm surge to enter the outfall canals from Lake Pontchartrain. Since the pumping capacity of the gate is not equal to city's inland drainage system, it is necessary to increase the safe water elevation to reduce the interior flooding during the closure of the gate. Increasing the safe water elevation would allow the city to pump the water into the canal at higher rate which reduces the risk of flooding inland and at the same time it would also allow the flood gates to remain open for the longer time.

The other objective of the test was to calibrate the models in order to study the behavior of the floodwalls.

3.2.2 Test procedure and the measurements

A cofferdam was built along 150 feet of the critical section of I-wall on the east side of the London Avenue canal to isolate the I-wall section from the rest of the water in the canal and to aid the slow, incremental and controlled raising of water level against the wall. Then the

sophisticated instruments were installed to monitor the response of the wall and the foundation soil underneath due to the impact of different water level. The Instruments that were used during the test were the inclinometers to measure the horizontal soil deformation; tilt meters to record the rotation of the monolithic base; piezometers to measure the pore pressure; and the distance measuring device to measure the deflection of wall. Once the site set up was ready, the water was raised in controlled incremental manner and the response of the wall and the foundation was monitored by scientists and engineers. The data like the load deflection curve and the inclinometer readings presented in the documents (HPO 2008; Conroy and Berry 2008) was used for this study. Figure 3.1 shows the fluctuation of water level and the deflection of the monolithic base for different water level (HPO 2008; Conroy and Berry 2008).In Figure 3.1, it can be seen that the loading of the wall was done in two phases.

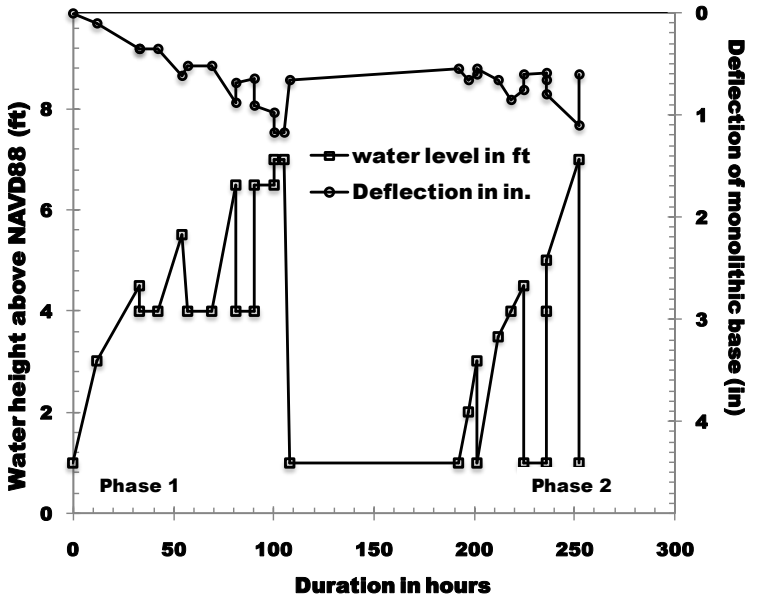

Figure 3.1. Loading sequence and deflection pattern during the full scale load test (Source: Conroy et al, 2008)

3.3 NUMERICAL MODEL

3.3.1 Modeling Tool and Condition

Fast Lagrangian Analysis of Continua ($FLAC^{3D}$) developed by ITASCA was used for the numerical analysis of the floodwall. It is a finite difference code which uses the mix discretization technique and explicit dynamic solution scheme (Hart and Detournay 2005) to solve quasi- static problem. To model the static response of a system, damping is used to absorb kinetic energy. It has the capability of large strain calculation mode. The main advantage of this scheme is that it can handle any complex problems which are physically instable (collapse problems), path dependent and non linear of stress-strain without concerning the numerical stability issue. Here the full dynamic equation of motion are included in the formulation where the static state of the system is reached when the kinetic energy are absorbed by the inertial terms absorbed in the formulation. Specifically, the grids are represented by the combination of the grid points where the mass are concentrated and are connected by the springs.

Apart from having its own built in constitutive models, $FLAC^{3D}$ also provides the user interface so that the new constitutive model can be implemented. This versatility of the software is the main reason for its use in this study.

To reflect the short period of loading condition and the undrained behavior of the embankment and the foundation soil (marsh stratum) total stress analysis was conducted. The other reason of selecting the total stress analysis is that the total stress strength parameters are readily available in the literature (IPET 2007) whereas effective stress strength parameters are not and estimation of effective stress parameters using empirical relations may add uncertainty in the simulation.

3.3.2 Model Geometry

Since I-wall is a long system with the homogenous property, the system can be analyzed using the plane strain model. To mimic the plane strain behavior using FLAC^{3D} ,only one zone was constructed along the out of plane direction and the velocity of the grid points lying on the front and the back plane along this direction was constrained to zero.

Dunbar and Britsch III 2008 and Rogers et al. 2008 have given the detail outline of the geologic set up of the New Orleans area and the history of its formation. The load test site consists of four layers of foundation soil and the embankment backfill soil layer. The FLAC^{3D} is constructed to represent those layers with sheet pile and the concrete capping. The lower most soil layer is the stiff clay known as Bay sound clay. This layer extends below -44.4 ft measured in NAVD88 scale. The stiff clay is overlain by beach sand that extends from -44.4 ft to -21.4 ft. Above beach sand layer, up to -11.4 ft, is the silty-sand layer which is overlain by the marsh layer. The marsh layer is divided in to two parts namely Marsh-crest and the Marsh-toe as they exhibits different shear strength. The embankment with backfill material extends up to 2.2 ft above the marsh layer. The sheet pile is embedded inside the reinforced concrete for 2.75 ft from the base of I-wall. The reinforced concrete capping extends from 0.2 ft up to 13.2 ft and the tip of the sheet pile is at -21.4 ft.

The main characteristics of the FLAC^{3D} numerical model were that soil was represented by the brick type zones each having eight grid points possessing elasto- plastic behavior. Similarly, sheet pile was represented by linearly elastic two dimensional shell type finite elements known as the ‘embedded liner’ slaved with an interface. The reinforced concrete I-wall was represented by the brick type zones having eight grid points possessing isotropic linearly elastic behavior and the soil/wall interface was represented by three nodes triangular elements.

The typical I-wall section is shown in Figure 3.2 which has the base of 1.75 feet and tapered to 1 foot above.

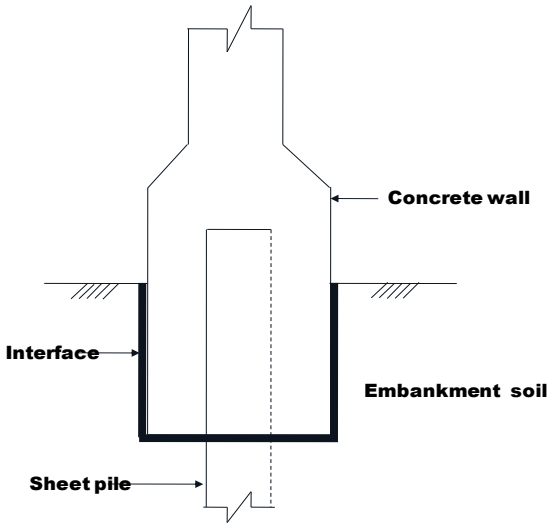

Figure 3.2. Typical I -wall section

The model geometry is illustrated in Figure 3.3

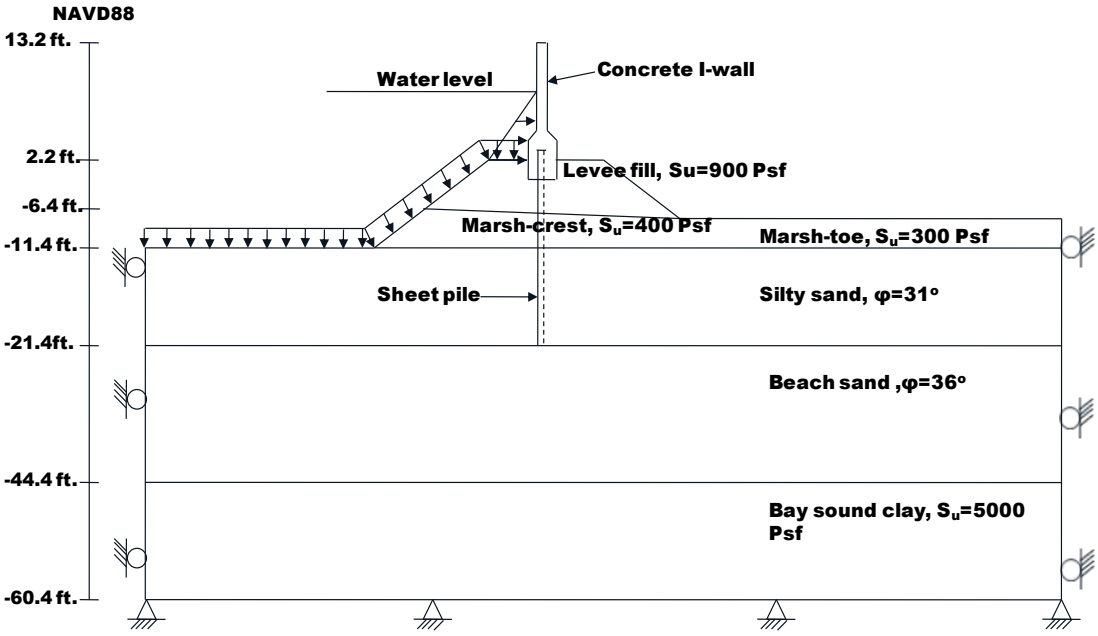

Figure 3.3. Model geometry with soil profile

3.3.3 Initial Soil Model Parameters

The Mohr Coulomb constitutive model was used to represent the stress strain behavior of the soil**.** This model was used since it is simple and has less parameter than other advanced constitutive model so that it has the lower degree of uncertainty. This model requires basically five parameters: cohesion, *c*; internal friction angle, ϕ; mass density ,ρ; shear modulus, *G*; and bulk modulus, *K***.** For the numerical analysis, the strength parameters and the young's modulus of soil in IPET report, Volume V, Appendix 19, (IPET 2007) were taken as the starting parameters. The Poisson's ratio was taken as 0.48 to account the undrained behavior of the soil for the cohesive soil and for silty sand and beach sand; poison's ratio was estimated using the relation derived from the theory of elasticity (e.g. Terzaghi 1943):

$$\upsilon = \frac{K_0^t}{1 + K_0^t} \tag{3.1}$$

Where, *v* is the Poisson's ratio and K_0^t is the equivalent coefficient of lateral earth pressure at rest condition for total stress analysis. K_0^t is estimated using Eq. (3.12)

Once the undrained elastic young's modulus and the Poisson's ratio were known, the bulk modulus and the shear modulus were calculated using the following relations:

$$G = \frac{E}{2(1+\nu)} \tag{3.2}$$

$$K = \frac{E}{3(1-2\nu)} \tag{3.3}$$

where *G* and *K* denote the shear modulus and bulk modulus respectively and *E* denotes the elastic young modulus of the soil. The elastic modulus in IPET report was estimated to be 92 times the undrained strength. The elastic moduli of sand and silty sand layers were calculated with the same relation for cohesive soil assuming the undrained strength of sand to be 1500 (this value was used to calculate the young's modulus only).The starting model parameters for the soil are given in Table 3.1:

Table 3.1. Initial soil model parameters

Soil layer	**Shear Strength**	**Saturated density (Slug/ft^3)**	**Elastic modulus (psf)**	**Poisson's ratio**
Levee-fill	s_u=900 psf,ϕ_u=0°	3.39	8.28e4	0.48
Marsh(Toe)	s_u=300 psf,ϕ_u=0°	2.49	2.76e4	0.48
Marsh(Center)	s_u=400 psf, ϕ_u=0°	2.49	3.68e4	0.48
Silty Sand	c'=0 ,ϕ'=31°	3.66	1.38e5	0.43
Relic Beach Sand	c'=0 ,ϕ'=36°	3.79	1.38e5	0.41
Bay sound Clay	s_u=5000 psf,ϕ_u=0°	3.89	4.60e5	0.48

The parameters of silty sand were assumed to be the one for the topmost sand layer of London Avenue Canal which is given in IPET report, Volume V- Appendix 19, (IPET 2007).

3.3.4 Model parameters for the I-wall and sheet pile

To model the sheet pile, structural element of the FLAC^{3D}, known as "embedded liner" was used. The structural element is basically the shell element having resistance to both

membrane loading and the bending loading. The shell element in FLAC^{3D} can possess either of the isotropic, orthotropic or anisotropic properties. In this analysis, the sheet pile was assumed to possess an isotropic elastic property. It requires three parameters to define the mechanical properties of these elements: density, ρ; elastic modulus, E; Poisson's ratio, υ; and the thickness, t. Elastic modulus, density and the poisons ratio can be found in any steel tables. The sheet pile used in London Avenue canal is CZ-101(HPO 2008). The geometrical parameters of this type of sheet pile are found in the manufacturer table (sheetpile.net). To account the simple geometry of the shell element used in the simulation against the complex one of the real Z-type sheet pile, equivalent thickness of the shell element was estimated using the relation:

$$t_{eq} = \sqrt[3]{I} \tag{3.4}$$

Where, t_{eq} denotes the equivalent thickness of the embedded liner element in *in* used in the simulation and I denotes moment of inertia in in^4 per unit foot width of the sheet pile

To model the concrete I-wall section, FLAC^{3D} zones were used. Elastic model was used to model the stress strain behavior of the concrete. The main parameters required for this model are: the density, ρ; bulk modulus, K and shear modulus, G. The density of the concrete is readily available in any literature. Bulk and shear modulus are calculated using the Eq. (3.2) and Eq. (3.3) where E is young's modulus of concrete estimated from Eq. (3.5). The Poisson's ratio of concrete can vary from 0.15 to 0.2 (Bowles, 1982). In this simulation the Poisson's ratio was assumed to be 0.2. The young's modulus of normal weight concrete was estimated using the relation (Wang and Salmon1998):

$$E_c = 57{,}000.\sqrt{f_c^{'}} \tag{3.5}$$

Where, E_c is the elastic modulus of concrete in psi and $f_c^{'}$ is the compressive strength of the concrete that varies from 3500 to 5000 psi for usual non pre-stressed reinforced concrete (Wang and Salmon 1998). In this numerical simulation, it was taken to be 3925 psi. This value is the average value of the compressive strength measured by taking samples from the existing I-wall. The details can be found in Appendix 15, Volume V of IPET report (IPET 2007). For plane strain condition, the elastic modulus estimated using the Eq. (3.5) was modified using the relation given in FLAC structural elements manual (Itasca 2006):

$$E_{c,plane\text{-}strain} = \frac{E_c}{(1-\nu^2)} \tag{3.6}$$

Where, ν denotes the poison's ratio.

Actually, the reinforcement was disregarded while calculating the elastic modulus, because the moment of inertia for the transformed reinforced cement concrete section is only 5% and 7% more than that of the plain cement for the upper portion and the lower portion of the existing I-wall. And as far as the cracking is concerned, the tensile stress developed in the concrete for maximum 7 feet of loading condition is below the tensile strength of the concrete given by the equation (4-7) (ACI 318-05, 2005)

$$f_{ct} = 7.5\sqrt{f_c^{'}} \tag{3.7}$$

So the cracking was not considered in the numerical analysis.

3.3.5 Model parameters for the soil–wall interface

As described in the previous section, structural element of the FLAC^{3D}, known as "embedded liner" was used to model the sheet pile. Apart from having structural behavior of the

shell type element, the embedded liner has also the tangential and normal interaction between it and the FLAC^{3D} grid. This tangential and the normal behavior is controlled by the "embedded liner" interfacial properties. This means that the embedded liner has the interface slaved with it so that building of separate interface is not necessary.

The normal behavior of the soil- sheet pile interface is governed by the normal coupling springs properties like the stiffness per unit area, K_n and the tensile strength f_t. The tangential or the shear behavior of the soil sheet pile interface is governed by the shear coupling springs properties like stiffness per unit area, K_s; cohesive strength c; residual cohesive strength c_r ; the friction angle ϕ and the interface normal stress σ_n. The tangential behavior of the interface is so modeled that if the interface fails in tension, then the effective cohesion drops from c to residual cohesion c_r and the tensile strength is reduced to zero. But if the relative displacement is such that there is no more separation between the soil and the sheet pile, then the normal stress will again develop. This behavior of the liner interface in FLAC^{3D} provides the possibility of modeling gap occurrence and closing of it very accurately. Figure 3.4 and Figure 3.5 show the normal and shear directional behavior of the interface.

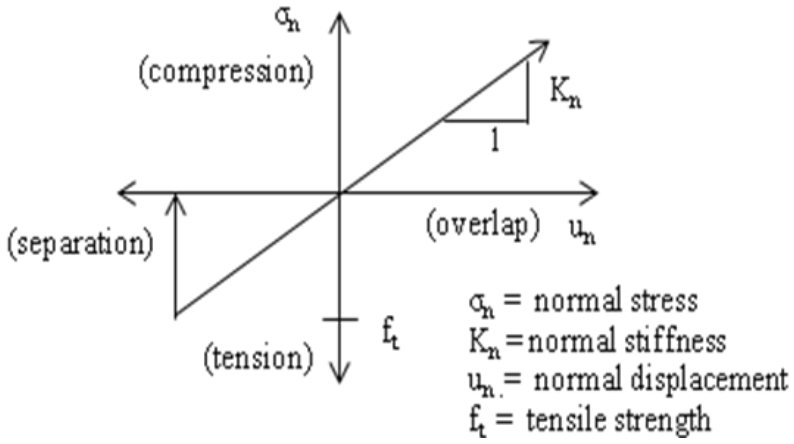

Figure 3.4. Normal directional interface behavior for sheet pile (Replotted from Itasca, 2006)

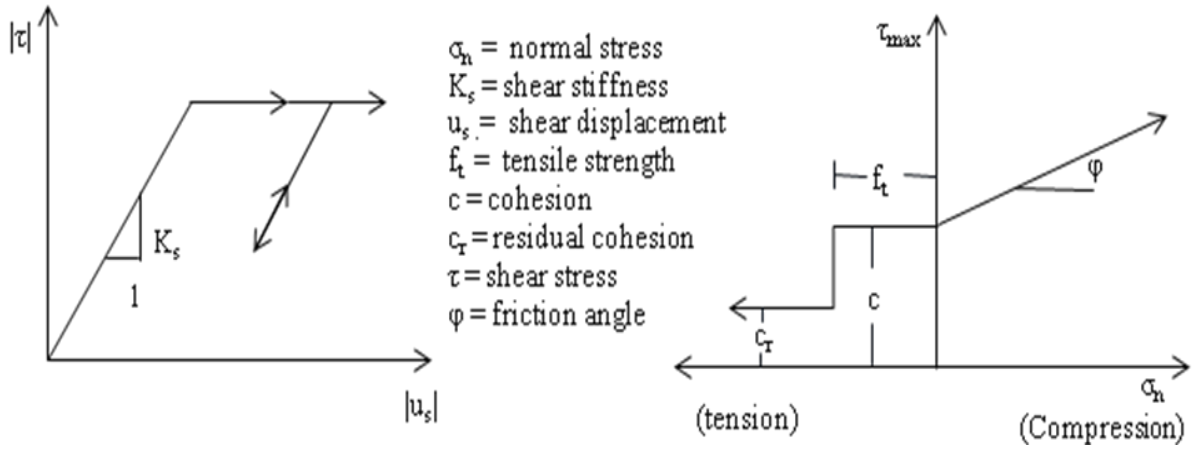

(a) Shear stress versus total relative displacement (b) shear-strength criterion

Figure 3.5. Shear-directional interface behavior for sheet pile (Replotted from Itasca, 2006)

In the case of interface between the reinforced concrete capping and the soil, a separate interface represented by triangular elements with 3 nodes was built up. These elements are characterized by the normal and shear stiffness with sliding properties. The constitutive model of these interfaces is defined by linear Coulomb shear strength model which limits the shear force acting in the interfacial node.

For both cases of sheet pile-soil interface and reinforced concrete wall-soil interface, a schematic of the FLAC^{3D} interface elements showing constitutive behavior are shown in Figure 3.6.

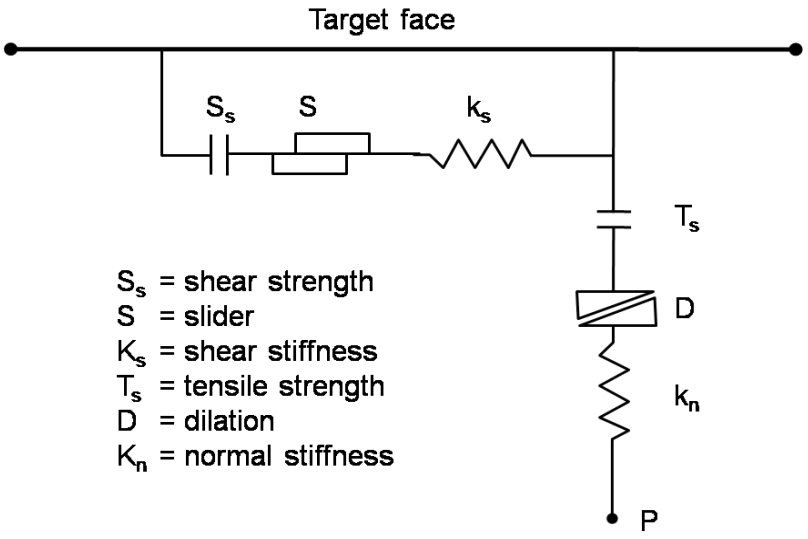

Figure 3.6. Components of soil/wall interface constitutive model (Replotted from Itasca, 2006)

As mentioned earlier, the main interfacial properties required for the simulation are the stiffness and the strength parameters. The FLAC^{3D} manual (Itasca 2006) points out that the strength properties of the interface are important, but the stiffness properties are not. But if there is a large contrast of the stiffness in the system, it takes a lot of time for numerical simulation to converge. So to economize the simulations, the FLAC^{3D} Theory and Background Manual (Itasca 2006) recommend that the K_n and K_s can be estimated by thumb of rule which is to be 10 times the stiffest neighboring zone.

$$K_n \approx K_s \approx 10.\max\left[\frac{K+\frac{4}{3}G}{\Delta z_{\min}}\right] \tag{3.8}$$

Where K & G are the bulk and shear moduli respectively and Δz_{min} is the smallest width of an adjoining zone in the normal direction. The max [ ] notation indicates the maximum value over all the zones adjacent to the interface to be used.

As far as the strength parameters of the interface are concerned, for cohesive soil, they are given in terms of adhesion which is equal to 0.5 to 0.7 times the undrained strength of the adjacent soil (Bowles 1996). In this Simulation, the cohesion was estimated using the relation:

$$c \approx 0.67.s_u \qquad (3.9)$$

Where, s_u denotes the undrained shear strength of the adjacent soil and c is the cohesion of interface.

For the case of cohesion less soil, the strength parameters are given in terms of angle of friction. For steel pile embedded in silty sand (dirty sand), the interface angle of friction, δ was taken to be 14^o (Bowles 1996; USACE 1994).

3.3.6 Modeling Hypothesis

As discussed earlier, the main objective of this study was to develop proper analytical procedures that reflect the realistic behavior of the floodwall system. What happens in the system is not always tangible. So it was necessary to develop some hypothetical tool which had to be verified using numerical experiment. Two major hypotheses were made to study the behavior of the I-wall due to water load. The validity of these hypotheses was tested by comparing the results from numerical analysis with the measurements from the full scale load test.

3.3.6.1 Hypothesis 1: formation of gap

The gap formation was not considered in the previous design of floodwalls system in New Orleans. Most of the design guidelines then published by USACE considered the formation of tension cracks to some depth formed due to the cohesion of the soil but didn't take into account the formation of gap due the relative deformation of the soil/wall system. After Katrina,

investigations made by IPET (IPET 2007) showed that the major aspect relating to the performance of floodwall system is related to the formation of gaps between I-wall and the levee embankment soil or foundation soil. After this, many papers have been published pointing out the significant effect of the gap formation on the overall stability of the floodwall system. The observations made during the field visits after the Hurricane Katrina showed that gap occurred at several places due to canal water loads. But at the same time, during the field visits, occurrence of gap was not observed at all places. To elaborate more, even for the two sections adjacent to each other having the seemingly identical soil conditions and the same loading conditions is liable to gap occurrence for one section and not liable to gap occurrence for the other one. So, the factors governing the gap occurrence in the floodwall system might not be only very few. Therefore it is not always possible to predict whether the gap will occur or not. So incorporation of the gap formation can only be regarded as the hypothesis which has to be tested using the numerical experiments. In this study, the numerical simulation results have been compared for the system when gap occurs and when it doesn't with the measured one. In the case when gap formation was considered, it was assumed that the formation of the gap allows water to penetrate through it and exert a direct hydrostatic force on the exposed sheet pile and the soil adjacent to it.

However, unlike in numerical analysis, in the case of design of floodwalls, as the hydrostatic force acting on the exposed sheet pile is more than the active earth pressure that the wall would experienced if there were no gap, gap formation is taken to be more critical and recommended to be incorporated for the safe and conservative design, no matter whether gap occurs or not.

3.3.6.2 Hypothesis2: under seepage induced strength reduction of marsh layer

The investigation performed by IPET has pointed out that the subsurface erosion/piping is the main cause of the failure of I-walls in London Avenue Canal. Most of the papers published aftermath of Katrina has also indicated the same thing. Some paper (e.g. IPET 2007) indicated the evidences of sink holes and sand boils at the crest and toe of the levees in London Avenue Canal after Katrina .Though the full scale load test was taken on London Avenue canal (the section near to the one where piping and subsoil erosion was reported to be more prevalent during Katrina), it might be misleading to adopt that piping occurred during the load test, since there were no evidence reported during the load test regarding piping/erosion. It is obvious that the piping will occur for the sand layer. But the subsurface setup of the full scale test location shows that the sand layer is overlain by the marsh stratum which is fairly impermeable than the sand layer. So the occurrence of piping failure for such geological setup cannot be justified since piping is the process of removing soil from the exit point advancing up gradient. Piping might occur in the case where there are discontinuities in the marsh stratum exposing the sand layer to the ground surface or due to the development of the tensile stresses in the marsh layer promoting the propensity of vertical piping in this layer. And since piping is a progressive event, the duration of the full scale test was not long enough to lead such event.

From the above discussion, I (author) am not trying to advocate that the load test section will not suffer from the piping failure at all. The section is liable to piping problem for the large and sustained loading condition. This is because the sustained and large hydraulic loads generate higher seepage force which might be potential enough to rupture the marsh layer and break it throughout its depth that promote vertical piping through this layer. But before this action could take place, the marsh layer on the land side might face some strength reduction which is justified

by the explanation in the following paragraph. In other words, the strength reduction of the marsh might be the case which when exacerbated by the high seepage force on the sand layer underneath causes it to rupture making vertical path to promote piping.

So in this study, another aspect for impending failure is considered. Formation of gap causes the shortening of the water path to weak marsh layer which causes an under seepage induced strength reduction of the layer. Since the strength of the marsh is dependent on the effective stress, the seepage force in the marsh would decrease the effective stress thus decreasing the strength. This aspect has also been discussed by Seed et al. (2008) and Ubilla et al. (2008). IPET 2007 on page V-42 has also given the similar explanation regarding the reduced shear strength for the London Avenue North breach near the load test site. The strength is however recovered when the water level drops increasing the effective stress in the marsh.

Most of the literature indicates that there is a correlation between the shear strength of the marsh and the effective vertical stress but have not proposed the unique correlation factor. So the quantitative reduction of the of shear strength using any theoretical expression is not possible. So in this study the reduction of the strength was taken to be only hypothetical which had to be tested and calibrated using the numerical experiment. Reduction of shear strength can only be realized when there is a gap and since the marsh is about 100 times impermeable than the levee fill material (IPET 2007), the reduction of strength in the levee fill material would not be that dominant as compared to the marsh layer. So reduction of strength was considered only in the marsh layer.

The motivation toward the reduction of the strength during the high flood level was evolved by observing the load deflection curve of the full scale load test. From the measured load deflection curve (Figure 3.1), it is seen that some portion of the deformation was not

recovered during the unloading indicating the yielding of some soil portion. The curve also indicates that some soil already started yielding when the water level reached 5.5 feet. And since for the initial original soil strength, the system behaves elastically, the load deflection curve indicates implicitly that there might be a reduction of the strength of certain soil layer during the high flood level which leads to the unrecoverable deformation. Some might argue of using the low shear strength starting from the low water level, but experience showed that this would affect in increasing the deflection at lower water level as well which contradicts the measured load deflection curve.

3.3.7 Simulating Procedure

In this section, the detailed numerical procedure has been discussed. First, the general procedure which is common to any type of geotechnical numerical analysis is discussed. Apart from these general procedures, the special and unique numerical approaches that have been formulated and implemented in this study such as the initialization procedures, the gap formation, and the strength reduction are discussed separately.

3.3.7.1 General procedure

The natural soil layer up to marsh layer was built up and run for the initial state. For this, gravity was turned on gradually in an incremental manner to reduce the dynamic impact. Alternately, the initialization of the existing natural soil layer could also have been done layer by layer of small thickness.

Then the embankment of backfilled material was built on above the natural soil layer. The sheet pile was erected and reinforced cement concrete capping was constructed with suitable interface between the reinforced cement concrete and the embankment soil. Again the model was

run for the elastic equilibrium. Elastic equilibrium was chosen so that the plastic flow would not occur during the initial equilibrium state.

The suitable sub routine was used to initialize the accurate horizontal stress. For this, the equivalent coefficient of lateral earth pressure at rest (K_0) for total stress analysis was calculated using the K_0 values of the corresponding soils at effective stress condition.

The water was then added up to Mean Water Level (MWL) and run for elastic equilibrium. The water was added in an incremental manner to avoid dynamic effect. Then the soil was changed to Mohr Coulomb elastic perfectively plastic model and again run for the equilibrium. After the equilibrium was reached, the displacement and the velocity of the whole system were initialized to zero.

The water level in the canal was raised according to the loading sequence in the full scale load test. To reduce the dynamic impact, water level was raised in an incremental manner. The response of the system was observed for each water level.

The above procedure was repeated for each modified set of parameters.

3.3.7.2 Initialization

The initial stress condition in the system is very important in the numerical simulation of many geotechnical problems since the stress strain behavior of the soil depends on the stress level. It is difficult to achieve the initial stress in numerical simulation when there are discontinuities in the geometry since plastic flow occurs at these points (Itasca 2006). To avoid this problem, the initialization was done in two steps, as discussed earlier, initially by bringing the model into elastic equilibrium to inhibit the yielding of soil before assigning the elasto-plastic properties of the soil.

During the initialization process, FLAC^{3D} calculates the vertical stress accurately but the calculation of the horizontal stress might not be the one as per the appropriate value coefficient of lateral earth pressure at rest (K_0). So an algorithm was devised to assign the appropriate value of K_0 for different soil layers.

Actually, evaluation of the K_0 is very difficult since it depends on the geological and the stress history of the soil layers. There are many theoretical and empirical correlations to estimate this value for normally consolidated soils and over consolidated soils. But these correlation are valid for over consolidated soil only if the over consolidation is due to simple unloading (Lancellota 1995). The over consolidation due to the other effects like desiccation cannot be addressed with those formula. For the study site, luckily the soil deposits are from normally consolidated state to only slightly over-consolidated state (IPET 2007). So, the existing theoretical and empirical correlations can be applicable to evaluate K_0 with confidence.

In the literatures, K_0 values are referred for the effective stress case. Since the numerical simulation was done for the total stress case using the saturated unit weight, equation (4-9) was developed to calculate the "equivalent K_0" for the total stress analysis. The "equivalent K_0" incorporates the effect of horizontal pressure due to water as well. The relation was derived assuming that the total horizontal stress developed for the effective stress case and the total stress case will be the same.

$$K_{0,i}^{t} = \frac{K_{0,i}\Sigma\sigma_{vi}^{'} + \sigma_w}{\Sigma\sigma_{vi}} \tag{3.10}$$

Evaluating the stress term in Eq.(3.10),

$$K_{0,i}^{t} = \frac{K_{0,i}\Sigma\gamma_i^{'}h_i + \gamma_w\Sigma h_i}{\Sigma\gamma_{sati}h_i} \tag{3.11}$$

Simplifying,

$$K_{0,i}^{t} = \frac{K_{0,i}\gamma_i^{'} + \gamma_w}{\gamma_{sat}} \tag{3.12}$$

Where, $K_{0,i}^{t}$ denotes "equivalent coefficient of lateral earth pressure at rest condition for total stress analysis for the ith layer", $K_{o,i}$ is the coefficient of lateral earth pressure at rest condition for effective stress condition for the ith soil layer, $\sigma_{vi}^{'}$ is the effective overburden pressure for the ith layer, σ_{vi} is the total overburden pressure for the ith layer, σ_w is the water pressure, h_i of depth of ith layer, $\gamma_i^{'}$ is the effective unit weight of soil of ith layer and $\gamma_{sat\,i}$ is the saturated unit weight of soil of ith layer

With Eq. (3.11), the equivalent coefficient of lateral earth pressure for total stress analysis can be used for the FLAC^{3D} simulation. The Eq. (3.11) is simplified to Eq. (3.12) to ease its use in devising a subroutine in the simulation and the K_0^t calculated using Eq. (3.12) gives an average error of only 2.5 % when compared to that using Eq. (3.11).

To use Eq. (3.12), K_0 value for the case of effective stress is needed for different soil layers. Since embankment clay, marsh and the stiff clay are from normally consolidated to slightly consolidated soils (IPET 2007), K_0 are within the range between 0.60 and 0.63 (Seed et al 2008).The value of 0.6 was chosen in this study.

Similarly, for beach sand and silty-sand, which are also normally consolidated, K_0 was estimated using the relation (Jaky, 1944):

$$K_0 = 1 - \sin(\phi') \tag{3.13}$$

3.3.7.3 Gap formation

Different papers have devised different logics regarding the likelihood of formation of gaps and their depths. In the IPET report (IPET 2007), the depth of the gap is estimated numerically by checking the effective stress of the soil in the neighborhood of the sheet pile and has assumed that the gap occurs if the soil undergoes the tensile stress.

The same principle is echoed in the paper by Brandon et al. (2008), in which the depth of gap has been calculated analytically by comparing the total lateral earth pressure and the water pressure for different depths. In their paper it has been concluded that the depth of the gap solely depends upon the cohesion and the submerged unit weight of the soil independent of the load condition.

In the above discussions, the theory behind the calculation of the depth of the gap assumes that the sheet pile is rigid which rotates about its tip developing active earth pressure on the flood side and the passive earth pressure on the protected side. The method proposed by Brandon et al. (2008) can be an effective way for the calculation of an approximate depth for the hand calculation. But this might not be the case if the sheet pile is flexible. So the logics in predicting the depth of gap should be compatible with respect to the soil/ structure deformation and is only possible through numerical simulation.

In this study, the relative displacement between the sheet pile and the soil adjacent to it was monitored. If the relative displacement was such that the soil/wall interface was in tension, the soil pile interface was removed and the water load was applied to the sheet pile and the soil adjacent to it. This was achieved by deleting the link element that connects the soil zones with the structural nodes. The link in FLAC^{3D} is actually a special element which provides the means by which the structural element (sheet pile) interacts with the grid (soil). The removal of the link

allows the structure and the soil adjacent to behave independently. The sub routine was so developed that the link was reinstalled when the soil/wall interface undergoes compression. This reflects the case when the wall is unloaded.

3.3.7.4 Strength reduction

As the gap forms reducing the seepage path to marsh layer, the strength of the marsh layer was reduced when the water level was high and was resumed to the original strength when the water level dropped to the MWL.

As discussed earlier, the correlation factor recommended by different papers that correlates the shear strength of the marsh to the effective stress is not unique .So trial values of the reduced strength were used for the marsh beneath the crest (since the under seepage is dominant at this section) when the water level reached 5.5 feet, 6.5 feet and 7 feet and the response of the floodwall system is observed. As the shear strength of the marsh soil of similar site at 17th Street canal near to the load test site varies from 50 to 920 psf (Sasankul et al 2008) the trial values that have been used were within this range.

Since the stiffness and the undrained shear strength of the soils have a direct correlation, the reduction of the shear strength should induce a decrease in the stiffness of the marsh soil. This will also influence the stiffness and strength of soil/wall interface as well. But incorporation of all these effects cannot be handled manually in the numerical simulation as they add complexity. This study has only been limited to the fact that the influence of gap will reduce the seepage path of the water increasing the pore pressure in the marsh layer thus decreasing the effective stress resulting in reduction of the strength for the high flood level and vice versa. This is not that implausible. But at the same time, this concept has opened the door for further study to

introduce new constitutive model for the marsh layer and the soil/ wall interface which can handle all those effects.

3.4 COMPARISON OF MODEL PREDICTIONS AND TEST DATA

3.4.1 Summary of Comparison

One purpose of this study is to calibrate the soil parameters which are required for the evaluation of retrofitting techniques. Full scale load test (London Avenue Canal) data are available for the calibration of soil parameters. Since the stiffness parameters are important than the strength parameters, the calibration is basically focused on the stiffness parameters rather than the strength parameters.

If larger number of the parameters is to be calibrated to match the many data sets, then it can be facilitated by the optimization technique (Yang and Elgama, 2003). There are many optimization schemes such as analytical, semi-analytical and numerical optimization techniques which can be applied for the judicious calibration of the model parameters. Many authors such as Anandrajah and Agrawal (1991); and Mattsson et al. (2000) have studied regarding the optimization while doing the systematic and convenient calibration.

According to Yang and Elagama (2003), optimization procedure look for the set of parameters systematically that can simultaneously minimize the large number of experimental data to the corresponding numerical results. Whereas in the complex modeling, the numerical optimization algorithms (e.g.Rosenbrock,1960; Powell,1964; Gill,1981;Dennish and Schanbel,1983) are used for the optimization techniques, in the case of more simpler case the closed form analytical equations may be sufficient.

To build the analytical method for optimization, Rosenbrock (1960) and Fletcher (1980) proposed an equation which is based on the least square method that minimizes the sum of the squares of the difference between the numerical predictions and the experimental observations and is given by:

$$F(x) = \sum_{i=1}^{n} w_i [\, f\ (x, t_i) - y(t_i)]^2 \tag{3.14}$$

Where x is the set of the parameters, $F(x)$ is the scalar function; $f(x,t_i)$ is the model (numerical) prediction at a certain time, loading condition or location; $y(t_i)$ is the corresponding observation in the field; and t_i is the attribute of the experiment, and w_i are the weighting factors associated with the experiment point i. By minimizing the function $F(x)$ one can find the best set of model parameters x^* to match the available data.

In the case of the unconstrained optimization where, the bound of the parameters are not important, then one may find the gradient and the Hessian of the function $F(x)$ by:

$$g(x) = \frac{\partial F}{\partial x} \tag{3.15}$$

And

$$H(x) = \frac{\partial^2 F}{\partial x^2} \tag{3.16}$$

So that for the optimum parameters, the sufficient conditions are that the gradient of the function with best set of parameters should be zero and the Hessian of the same function should be positive definite (Rosenbrock, 960 and Fletcher, 1980)

According to Abifadel (1998), there are three approaches where one can do the optimization

1. Zero -order optimization where on the evaluation of *F(x)* is required. (Mattsson ,2001 via Yang and Elgamal, 2003)
2. First- order optimization where the evaluation of the Function *F(x*) and the gradient, *g(x)* are required (Gill et al., 1981 via Yang and Elgamal, 2003)
3. Second- order optimization where both gradient, *g(x)* and the Hessian, *H(x)* are to be evaluated

Within the scope of this study, the zero order optimization schemes was adopted where Eq. (3-1) was modified to calculate the Root Mean Square (RMS) value by

$$F(x) = \sqrt{\sum_{i=1}^{n} [\frac{f(t_i) - y(t_i)}{y(t_i)}]^2} \qquad (3.17)$$

In Eq. (3.17), instead of taking weighting factor for each data points, the discrepancy is normalized with the measured data to account that weighting factor for smaller measured value is more than that for the larger measured value.

Three cases each of which with considering the gap formation and without gap formation were compared. The result from each of these cases were compared with the deflection curve of the monolithic base measured during the full scale load test and the Root Mean Square (RMS) of the discrepancy using Eq.(3.17) between the measured and computed deflection at different WL were compared for each case. This is illustrated in Table 3. 2.

Table 3.2. RMS values for the different cases

Case	With Gap	Without gap
1. IPET elastic modulus	0.37	0.35
2. Adjusted elastic modulus without strength reduction	0.38	0.46
3. Adjusted elastic modulus with strength reduction	0.15	0.23

3.4.2 Load Deflection Curves

The load deflection curves in terms of water level versus deflection of the wall at monolithic base was plotted and compared with the measured load deflection curve for the different cases discussed in 3.1.

When comparing the load deflection curves for different cases, it is seen that the IPET Elastic modulus is highly underestimated (Figure 3.7). It can be seen that though the underestimation is not that significant for the higher water level, it is much significant for the low water level.

When the elastic modulus is adjusted to match the inclinometer results (discussed in next section), the load deflection curve is somewhat different (Figure 3.8). The adjustment has not made that much improvement in predicting the behavior. In this case, it is seen that the deflection from the simulation for the low water level is in close agreement with that of the measured one but it fails to predict the behavior for higher water level.

When the elastic modulus of the soil layer is adjusted and the strength of the marsh layer beneath the crest is reduced during the high water level, there has been a significant

improvement in the approximation of the behavior of the system as reflected by load deflection curves for the numerical simulation and measured one (Figure 3.9). Due to the reduction of the strength, part of the deformation of the system has not been recovered. On top of that, when comparing the load deflection curves for this case, the approximation is again improved when the gap formation is incorporated than when it is not. So this implies that the hypothesis regarding the gap occurrence and strength reduction best represent the phenomena occurring in the floodwall system during the load test as reflected through the load deflection curve. Though the phenomenon of the strength alteration of the marsh layer at higher water level cannot be observed visually, there were some evidences that proved the occurrence of the gap during the load test.

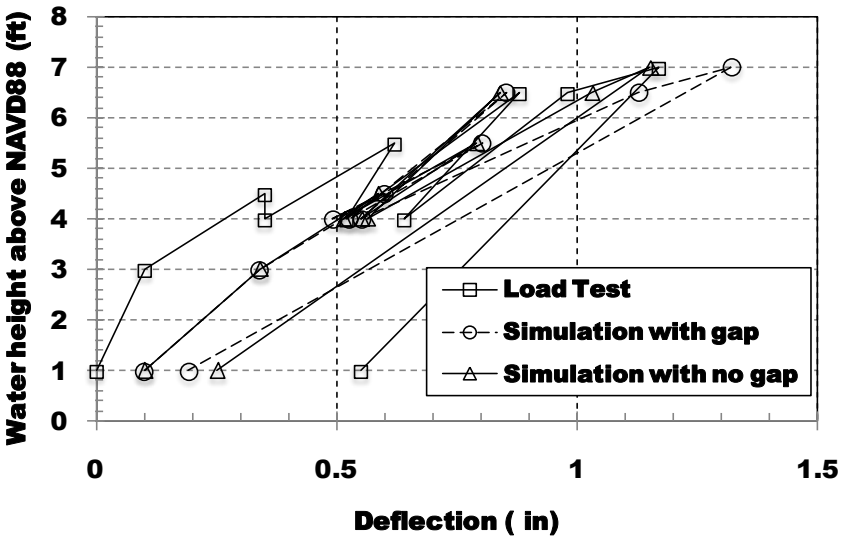

Figure 3.7. Load deflection curve for the numerical simulation with IPET elastic modulus

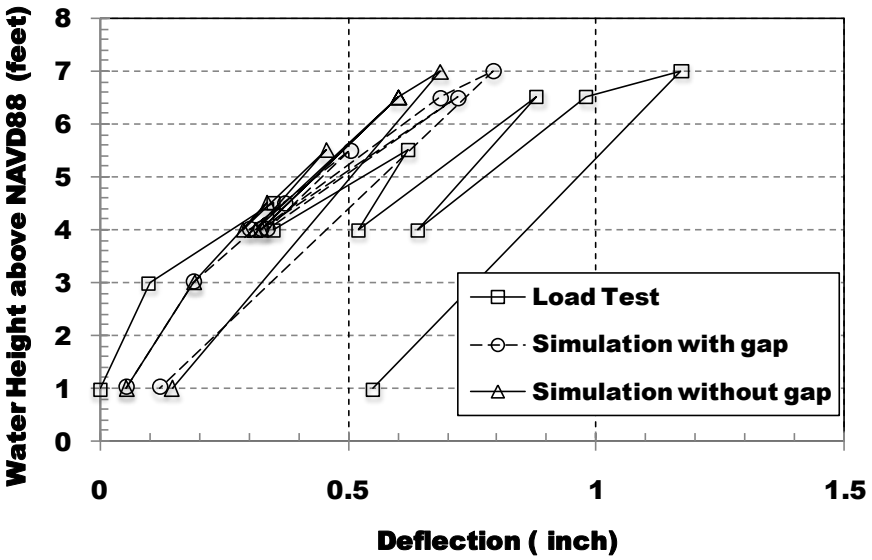

Figure 3.8. Load deflection curve of the numerical simulation with adjusted elastic modulus

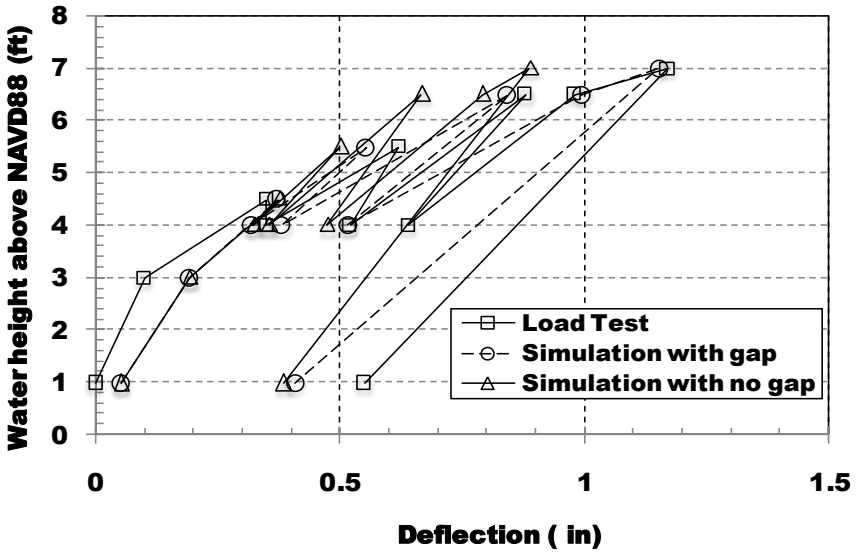

Figure 3.9. Load deflection curve of the numerical simulation with adjusted elastic modulus and strength reduction

3.4.3 Soil Deformation along the Depth

The verification of the calibrated soil stiffness parameters can only be justified by comparing the soil deformation along the depth. During the full scale load test, the differential inclinometer was used in measuring the soil deformation (HPO 2008). The inclinometer measurement was done below the crest and the toe represented by IP-2 andIP-3 respectively. Since the measurement were done for all the water heights of the full scale load test and it was not convenient to include all the measurements, the measurements corresponding to typical loading conditions were taken into consideration for the comparison with the simulated results.

Figure 3.10 shows the measured deformation of the soil along the depth for the hydraulic pressure corresponding to 6.0 ft. height of water during the first phase test and 7.0 ft. height of water during the second phase and the simulated results corresponding to the same loading conditions for the calibrated parameters. Though there are some discrepancies between the measured deformations with that from the simulation, the calibration of the parameters has given a close approximation of the behavior of the system.

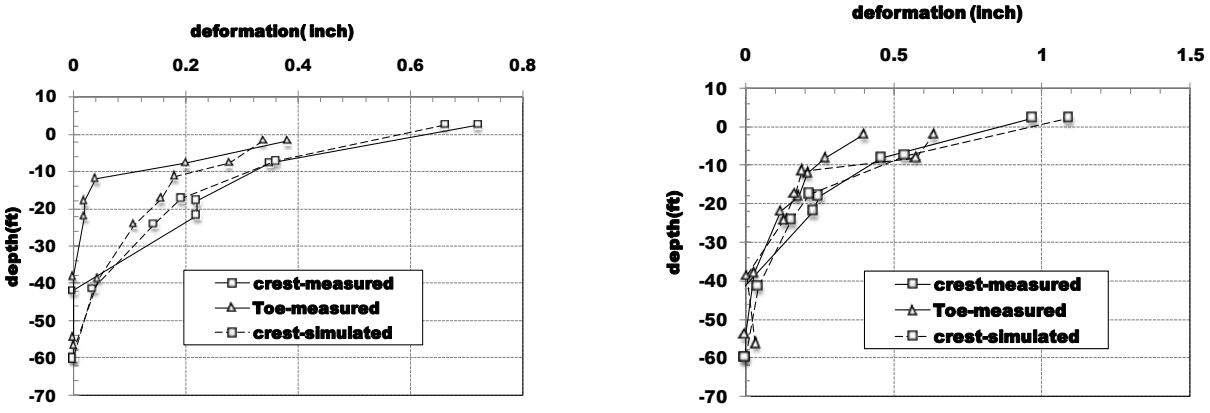

(a) First phase at 6 ft. WL (b) Second phase at 7 ft. WL

Figure 3.10. Deformation of soil at different depths

To verify the possibility of this significant strength reduction in the marsh layer, field vane tests were conducted in this study. As shown in Table 3.3, the intact shear strength was in 1879 – 3842 psf range, and disturbed strength was in 1670-4009 psf range during the dry season.

Table 3.3. Shear Vane results

Date	Depth (ft)	Undisturbed Strength (psf)	Remolded Strength (psf)	S_t	Remarks
Apr 15, 2011	1.67	3006.7	919.48	3.27	Dry Surface
	1.67	3841.92	4008.96	1.00	
	3.34	1879.20	1670.40	1.13	
	5.01	3257.28	2380.32	1.37	
	8.35	2714.40	2171.52	1.25	
Dec 15, 2011	1.67	960.48	292.32	3.29	Wet Surface
	3.34	375.84	167.04	2.25	
	5.01	417.6	167.04	2.5	
Dec 26, 2011	1.67	626.4	167.04	3.75	Wet Surface
	1.67	208.8	0	∞	Water Added
	1.67	668.16	250.56	2.67	Wet Surface
	1.67	417.6	0	∞	Water Added
	2.51	626.4	41.76	15	Wet Surface
	3.34	83.52	0	∞	Water Added
	3.34	584.64	125.28	4.67	Wet Surface
	3.34	83.52	0	∞	Water Added
	5.00	208.8	0	∞	
	3.34	1336.32	501.12	2.67	Wet Surface
	3.34	83.52	0	∞	Water Added
	5.00	83.52	0	∞	

However, one hole showed much lower disturbed strength (up to 920 psf or St=3.27). For this hole, the retrieved field vane blade and rod showed the water-glazed surface indicating that a small amount of water can further decrease the strength of the marsh layer significantly.

The glazed surface felt like a well lubricated surface with grease. To see the effect of water on the vane shear strength, a second set of field vane shear tests were conducted during the wet season. Tests performed Dec. 15, 2011 showed much lower strength but higher sensitivity in overall indicating the strength characteristic of these soils may be affected by water. To further explore the effect of the water content, a third set of field vane shear tests were conducted by manually introducing water for measuring the remolded strength into the holes after measuring the undisturbed strength. In these cases, the introduction of water significantly reduced the strength well down to 0 psf and failed instantaneously in the remolded state.

Therefore, the adjustment of the strength of marsh layer at higher water level is understandable which is due to the infiltration of water into the marsh layer through the gap and the disturbances caused by higher stress.

3.4.4 Horizontal Deformation of Embankment

The verification of the calibrated parameters was also done for the soil and wall deformation at different points of the levee and floodwalls. The points that were chosen were the top of the wall, the bottom of the wall and the edge of the crest. The load deformation curves were measured for hydraulic pressures corresponding to different water level during the first and second phase of the full scale load test. Comparing the results from the numerical analysis with the measured one, it shows that the calibration of the parameters is in close approximation of the behavior of the system. This is shown in Figure 3.11.

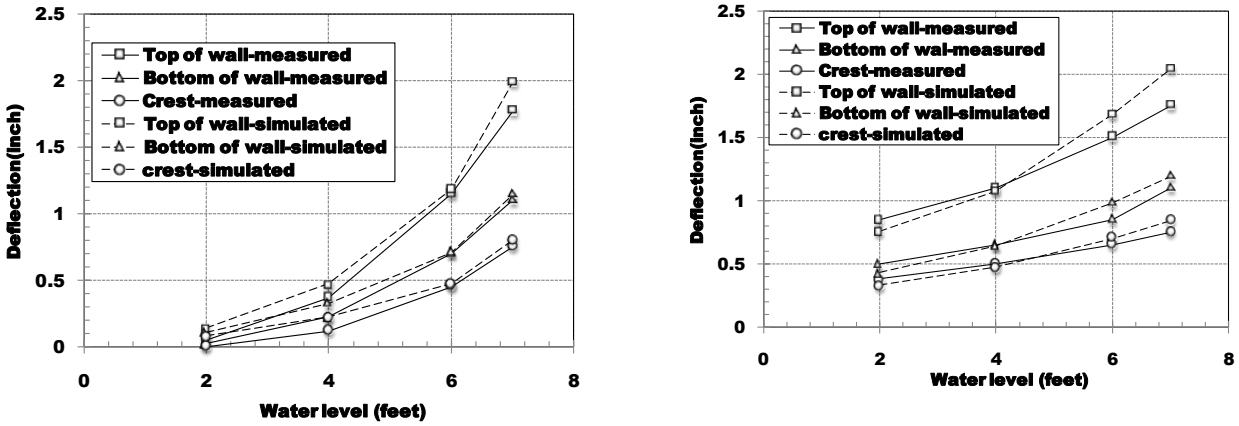

(a) First Phase

(b) Second Phase

Figure 3.11. Deformation of soil and wall at different points

3.4.5 Bending Moments, Wall Configuration and the State of Soil

Though report on the bending moments, soil/wall configuration and the state of the soil has not been provided in the documents presented by HPO (2008) or Conroy and Berry (2008) so that the comparison can be made, author of this paper noticed that it is necessary to present them to give an insight of the behavior of the floodwall system so that it can pave a path for the improved design procedure. Fig. 4.12 shows the comparison of the bending moments for the hydraulic pressure corresponding to 7 feet of water level for the system with calibrated stiffness and reduced strength of the marsh for the case with - and without gap. It is seen that the bending moment corresponding to gap formation is more critical than that without gap formation. Fig. 4.13 shows the exaggerated view of soil and wall configuration for the same loading condition. From this figure, it is seen that the gap was only partially developed for the water load corresponding to 7 feet height. This result contradicts with other literatures in which they point out that the gap normally occurs up to silty sand layer. These literatures assume that the sheet pile is a rigid structure but from Figure 3.12, it can be seen that the sheet pile in this study

behaved as if it a flexible structure. Figure 3.14a shows that the marsh layer lying between the toe of the levee and the center of the levee has been yielded. This is reflected in the load deflection curve and the history of the deflection of the monolithic base which is given in Figure 3.14b. Unfortunately, we don't have any evidences supporting the yielding of the marsh layer in the full scale load test.

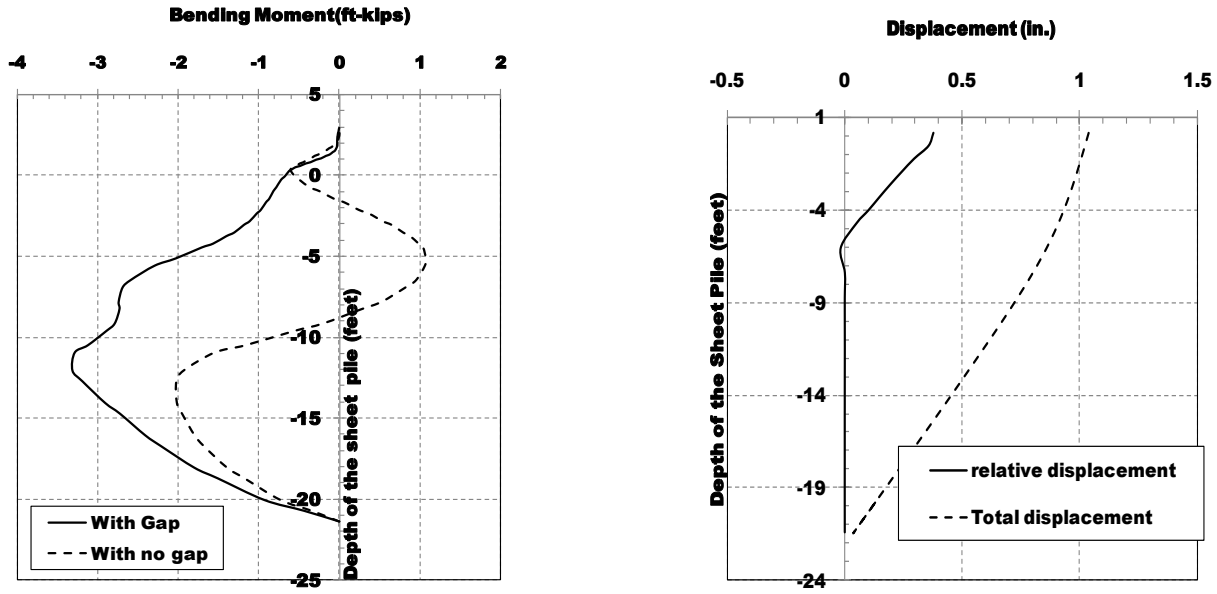

Figure 3.12. Bending Moment distribution and displacement along the sheet pile

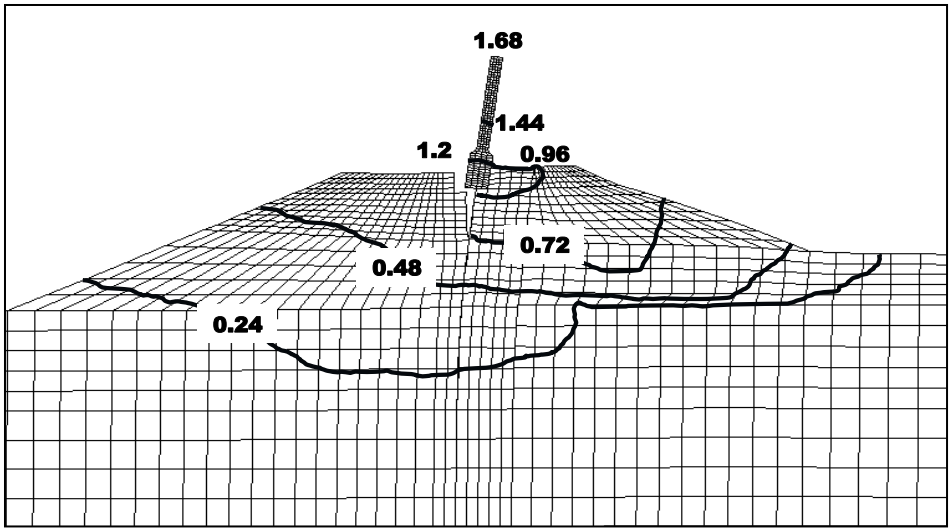

Figure 3.13. Configuration of wall at 7 ft. water level showing the contours of horizontal displacement (in.)

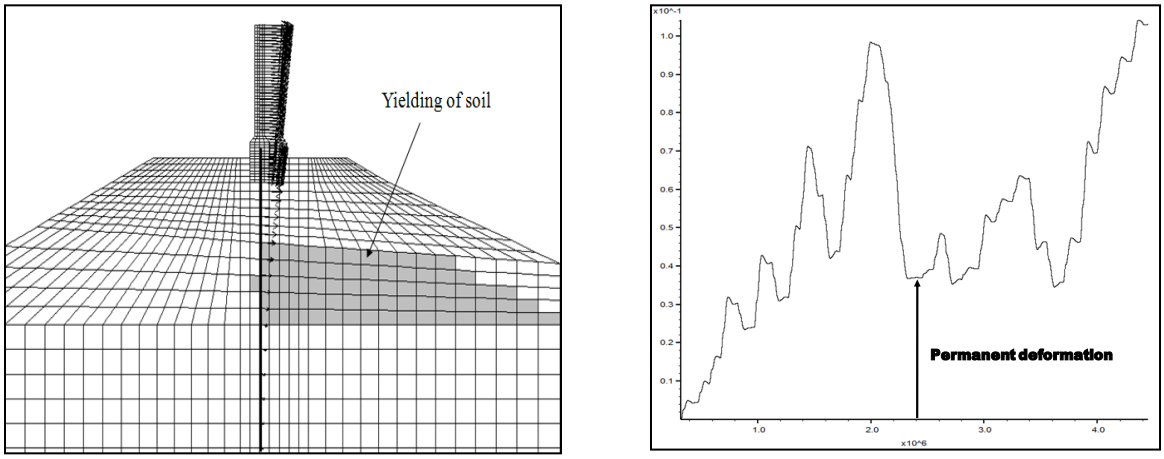

(a) State of soil (b) History of base deflection

Figure 3.14. State of the soil at 7 feet loading and horizontal displacement history

3.5 SUMMARY

The objective of this study was to develop a proper numerical procedure to study the behavior of the floodwall system and to calibrate the soil parameters that can best represent the

site characterization by comparing the model predictions with the full-scale test program. From the study it can be concluded that the adjustment of the modulus of the soil in IPET report and the reduction of the strength in the marsh layer during high flood with incorporation of gap gives the better result which matches closely with that of the field data. This implies that the numerical procedures adopted in this study and the calibrated modulus (1 to 12 times the IPET modulus) gives a better approximation of the behavior of the floodwall system.

From the study, it was also found out that the marsh layer is the most susceptible layer to yielding and this yielding was primarily due to the strength reduction of the marsh layer (upto 70 psf from the 400 psf) induced by increase in moisture content and the high underwater seepage during larger load promoted by the opening of the gap reducing the seepage path. Though the seepage analysis was not conducted in this study, many papers (e.g., IPET 2007) have already proved that the opening of gap induces the high pore pressure on the land side of floodwall system. So, we recommend that this situation should also be incorporated while analyzing and designing the I-wall in New Orleans area because, apart from the high uplift pressure above the sandy layer, the strength reduction of the marsh layer might contribute significantly for the instability of the I-wall.

During the full scale loading test, the levee experienced early stage of yielding. However, the proper management of field instrumentation system and proper field action prevented the failure.

Because the gap development was the main triggering mechanism of the failure of I-wall in London Ave. Canal area, a technique that may prevent the gap development could be an effective technique to countermeasure the failure of I-walls in this area.

Using the numerical technique that has been adopted in this study and the calibrated stiffness parameter, the further analysis of the floodwall system to evaluate the proposed

retrofitting techniques will be significantly more reliable. The final calibrated parameters is shown in Table 3.4

Table 3.4. Adjusted stiffness parameters for the soil

Soil layer	**Adjustment in elastic modulus**
Levee-fill	1 times the IPET elastic Modulus
Marsh	3 times the IPET elastic Modulus
Silty Sand	2 times the IPET elastic Modulus
Relic Beach Sand	3.5 times the IPET elastic Modulus
Bay-sound Clay	12 times the IPET elastic Modulus

Note: The IPET elastic modulus corresponds to modulus in Table 3.1.

4. NUMERICAL PRE-EVALUATION OF STRUCTURAL CAP

4.1 BACKGROUND

During the Hurricane Katrina, the major causes of the breaches were due to the instability of I-wall sections. There are many reasons that led to the failure of I-walls. One of those reasons that led to the failure of this type of floodwall is that the floodwall didn't behave as if it is one integral system. This non integrity of the system might arise from the improper or weak bondage between the concrete capping and the sheet pile depth wise or the composition of I-wall as different panels of varying length (USACE 2001) length wise acting individually without behaving in mutually supportive manner so that the intolerable stresses developed in one of the individual panel has to be bear individually without getting any chance of sharing them with the adjacent section leading to the localized failure.

Three cases which cause the localized failure of I-wall in New Orleans were dealt in this study. The spatial variation of the soil strength in the New Orleans region having weak spots is one of the main causes for the local levee breaches in that region. For example in 17th street Canal, according to USACE (2006), the measured shear strength of levee fill material varies widely from 120 psf to 5000 psf. Similar is the case for peat where the measured shear strengths vary from about 50 to 920 psf. So the strength parameters used in the design may not represent fully the actual strength of the soil of that region. This can be understood by illustration in Fig. 5.1.

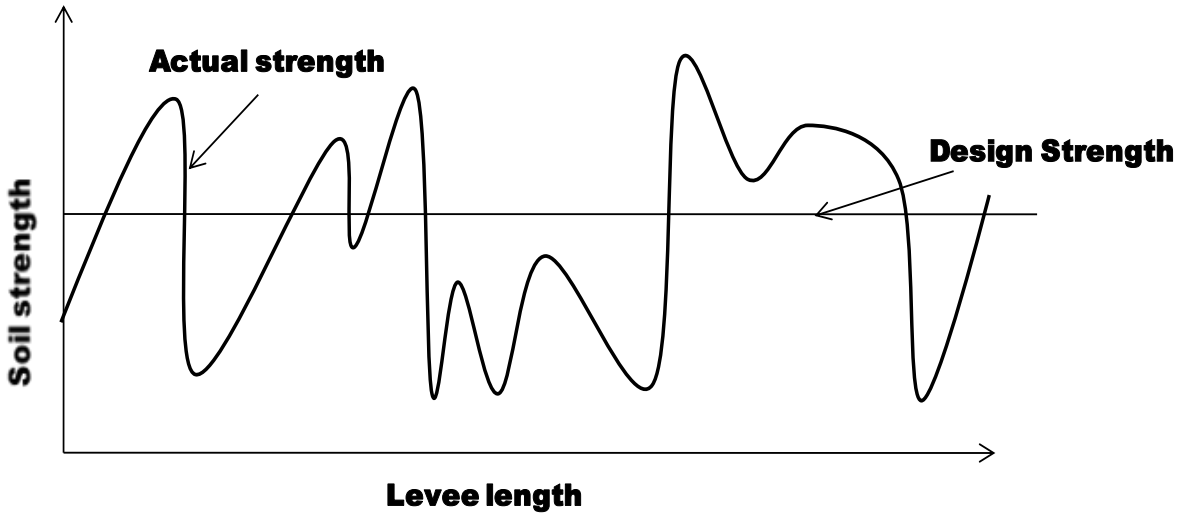

Figure 4.1. Conceptual graph showing the difference of actual and design strength

From Figure 4.1, it can be inferred that the I-wall sections having actual strength above the design strength will have the factor of safety more than what is required in the design guidelines but the sections where the strength falls below the design strength will have the factor of safety lower than the required one. So from the figure, it can be concluded that the region where the actual strength falls below the design strength will have higher probability of failure as compared to the regions where the actual strength is above the design strength. This indicates that only some sections of I-walls are vulnerable to instability. But in terms of the catastrophe induced by this local failure, no matter how small it is, it is not insignificant. And at the same time reducing the design strength to the lower bound of the actual strength distribution or improving the soil to bring up the actual strength up to design strength may be too uneconomic. So it is necessary to find an alternative mechanism which is economic and at the same time effective to get rid of this problem.

Figure 4.2. Local Failure of one panel (IPET V-14-64)

The other cause of the local failure is related to the erosion of some weak erodible soil portion of I-wall section. During hurricane Katrina, it was observed that some parts of I-wall section were suffered from erosion. This caused two adjacent concrete panels to separate resulting uncontrolled erosion induced by entrance of the flood water through the gap of separation promoting the expansion of the scour leading catastrophe.

Last but not least, the local failure of the I-wall might be caused by the local structural failure of the individual panel due to the weak bondage between the sheet pile and the concrete capping. Though there was no evidence of such failure during hurricane Katrina, this case was felt to be investigated since it has the potential to occur in future as the I-wall system in New Orleans is very old that the interface between the concrete capping and the sheet pile is so weak promoting the propensity of developing plastic hinge at the junction between the two.

The main objective of this study is to find the mechanism to integrate the isolated panel into one system so that the whole I-wall will act as if it is one unit. This integral unit will take the advantage of the stress redistribution in the unit so that the weak section enjoys the sharing of the stresses with the strong section relieving the overstressed zone and thus preventing it from the progression of failure.

One of the mechanisms of integrating the floodwall system that the project has proposed is the use of the structural cap. The structural cap is simply a structural element combining two adjacent panels at the top of the wall devised to restrict the relative displacement between them and aid in distributing the stresses from the overstressed panel to the under-stressed panel. The schematic of the location of the cap and the individual panel is shown in Figure 4.3.

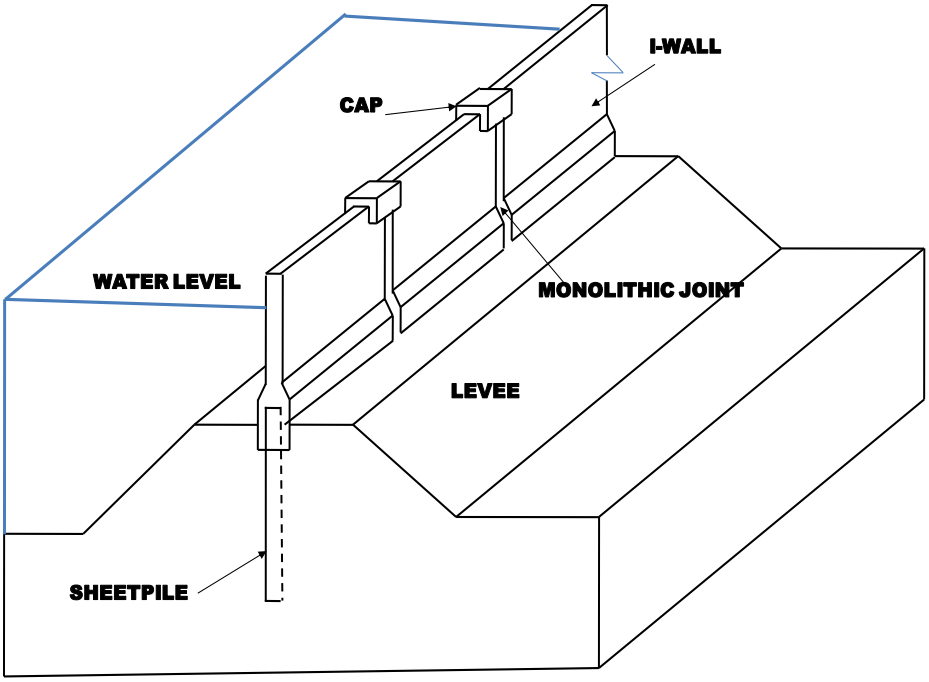

Figure 4.3. Schematic of I-wall showing individual panels with structural cap

4.2 NUMERICAL SIMULATION

4.2.1 FLAC^{3D} Geometric Model

For numerical modeling, one of the critical sections of London Avenue Canal was taken. The geological set up of the site consists of four natural soil layers such as bay sound clay, beach sand, silty sand and the marsh. The embankment of lean or fat clay overlay the marsh layer up to 2.2 feet in NAVD88 Scale. Above the embankment is the I-wall which propels up to 13.2 feet.

Sheet pile is embedded in to the soil up to -21.4 feet. The depth of each of these layers represented in NAVD88 scale is shown in Figure 4.4.

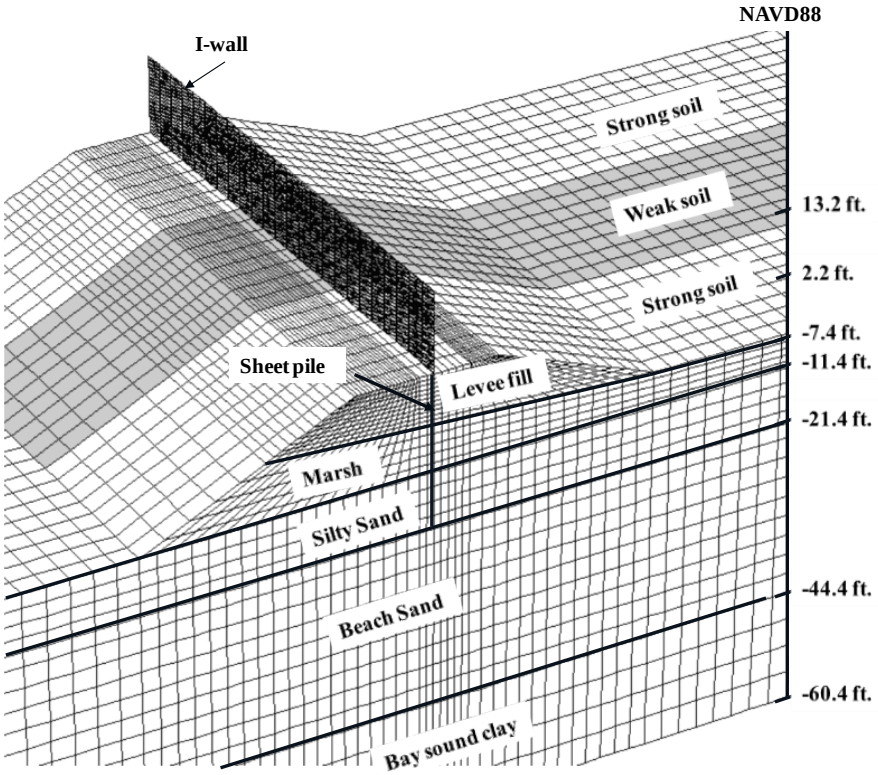

Figure 4.4. FLAC^{3D} Geometric Model

The characteristics of the FLAC^{3D} numerical model are that the Soil was represented by the brick type zones each having eight grid points possessing elastic perfectly plastic behavior. Sheet pile and the concrete capping were represented by linearly elastic two dimensional shell type finite elements known as the 'embedded liner' slaved with an interface. As the boundary condition, all the movement at the bottom level of the computational domain was restricted whereas, at the lateral exterior sides, the lateral movement was restricted. To simplify the building up of FLAC^{3D} model, sheet pile was assumed to be installed up to crest level which was joined to the concrete capping above it. The use of shell element for the concrete capping against

solid zones was to capture the bending effects accurately and to reduce the computational time. The sheet pile is created to be one unit but as far as the concrete capping was considered, it was separated into three separate units which idealized three different panels of realistic I-wall. The geometrical simplification used in the modeling is shown in Figure 4.5.

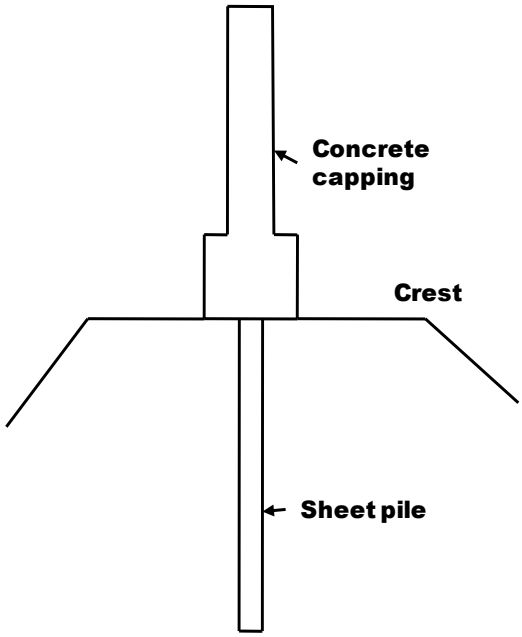

Figure 4.5. Model simplification at the sheet pile and the concrete capping joints

To model cap, the ideal case was adopted in which the top 2 feet of the adjacent panels were rigidly connected which was possible by using the link elements of FLAC^{3D} possessing rigid degree of freedoms in all directions. In this study, we only tried to investigate the performance of cap in ideal case, the details of the cap structure and its interaction with the concrete panel was beyond the scope of this study and should be investigated separately.

To account the soil strength variation of first case of this study, the model was idealized to be divided in to three sections in out of plane direction of equal lengths (the length of the panel of I-wall, in this study: 24 feet) in which the section with weak soil was sand-witched

between the sections with strong soil as shown in Figure 4.4. But in other two cases, the soil in longitudinal direction was taken to be homogenous of intermediate strength.

4.2.2 Soil Parameters and Soil Constitutive Model

The soil parameters derived in chapter four was used for the second and third cases. For the first case**,** main concern of the study was the effect of the soil strength variation in the longitudinal direction to the overall behavior of the floodwall system and the remedy action required to reduce the problem created by this situation. It can be seen that in one of the region (17th Street Canal) near the study site, there is a wide variability of the shear strength of the soil for marsh and levee fill materials whereas the variation is not of much significance for the sand layer and stiff clay underneath (IPET 2007). So in the 3D numerical analysis, the variation of the soil strength was related to the embankment soil and the marsh soil only. Two extreme strengths were taken where the lower bound of the strength represents the strength for weak soil and the upper bound represents the strength for the strong soil. In Figure 4.6, two extreme bounds of soil strengths are categorized as weak and strong soil strength.

Stiffness parameters were calculated using the undrained elastic modulus using some calibrated factors from our previous study. As far as the poisons ratio was considered, it was assumed to be 0.48 for the cohesive soil; 0.41 for beach sand and 0.43 for silty sand respectively. The details of soil strength parameters are discussed in our previous paper. The soil parameters are shown in the Table 4.1.

As far as the constitutive model is considered, elastic perfectly plastic Tresca constitutive model was used to simulate the behavior cohesive soil layers and Mohr Coulomb constitutive model was used to simulate the behavior of cohesion less soil layers.

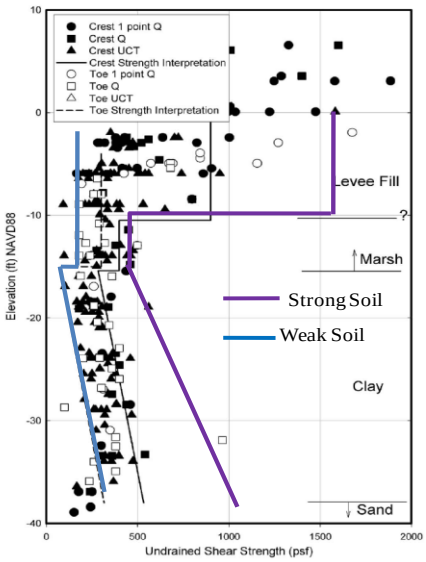

Figure 4.6. Scattered undrained shear strength for cohesive soil in 17th Street Canal (IPET, 2007) with upper and lower bound strengths

Table 4.1. Soil parameters

Soil layer	**Shear Strength**			**Saturated density (Slug/ft^3)**	**Elastic modulus (psf)**			**Poisson's ratio**
	weak	**medium**	**strong**		**weak**	**medium**	**strong**	
Levee-fill	s_u=200 psf, ϕ_u=0°	s_u=900 psf,ϕ_u=0°	s_u=1600 psf, ϕ_u=0°	3.39	1.84e4	8.28e4	1.47e5	0.48
Marsh(Toe)	s_u=200 psf, ϕ_u=0°	s_u=300 psf,ϕ_u=0°	s_u=450 psf, ϕ_u=0°	2.49	5.52e4	8.28e4	1.24e5	0.48
Marsh(Center)	s_u=200 psf, ϕ_u=0°	s_u=400 psf, ϕ_u=0°	s_u=450 psf, ϕ_u=0°	2.49	5.52e4	1.10e5	1.24e5	0.48
Bay sound Clay		s_u=5000 psf,ϕ_u=0°		3.89		5.52e6		0.48
Relic Beach Sand		c'=0, ϕ'=36°		3.79		4.83e5		0.41
Silty Sand		c'=0, ϕ'=31°		3.66		2.76e5		0.43

The soil –interface parameters were calculated in accordance to the method described in the chapter 3.

4.2.3 Model Parameters for I-wall

4.2.3.1 Capping

To model concrete capping and sheet pile, structural element of the FLAC^{3D}, known as "embedded liner" was used. The structural element is basically the shell element having resistance to both membrane loading and the bending loading. The shell element in FLAC^{3D} can possess either of the isotropic, orthotropic or anisotropic properties. In this simulation, initially, I-wall was assumed to possess an isotropic elastic property (if the moment is beyond the limiting tensile strength, then the cracking was considered resulting anisotropic property). It requires three parameters to define the mechanical properties of these elements: density, ρ; elastic modulus, E; Poisson's ratio, υ; and the thickness, t. Density of concrete are readily available in any literature. The Poisson's ratio of concrete v can vary from 0.15 to 0.2 . In this simulation the Poisson's ratio was assumed to be 0.2. The young's modulus of normal weight concrete was estimated using the relation (Wang et al. 1998):

$$E_c = 57{,}000.\sqrt{f_c^{'}} \qquad (4.1)$$

Where, E_c is the elastic modulus of Concrete in psi and $f_c^{'}$ is the compressive strength of the concrete that varies from 3500 to 5000 psi for usual non pre-stressed reinforced concrete (Wang et al. 1998). In this numerical simulation it was taken to be 3925 psi. This value is an average value of the compressive strength measured by taking samples from the existing I-wall. The details can be found in Appendix 15, Volume V of IPET report (IPET 2007)

For the reinforced concrete structures, the moment of inertia for uncracked section can be estimated using Eq. (4.2):

$$I_{uncr} = \frac{1}{12} bD^3 + (n-1)A_s h_s^2 + (2n-1)A_s' h_s'^2 \tag{4.2}$$

In the analysis, the flexural stiffness corresponding to the moment of inertia calculated by Eq. (4.2) could be used provided that the bending moment induced by the analysis was less than the cracking moment $M_{cr.}$ If the bending moment was more than the cracking moment, then the flexural stiffness corresponding to moment of inertia for the partially or fully cracked section should be used.

The moment of inertia for cracked section can be estimated using Eq. (4.3) (Everad 1993):

$$I_{cr} = \frac{b(kd)^3}{3} + (2n-1)A_s'(kd-d')^2 + nA_s(d-kd)^2 \tag{4.3}$$

Where n is the modular ratio given by the relation:

$$n = \frac{E_s}{E_c} \tag{4.4}$$

Taking E_s to be 29,000,000 psi and E_c to be 3,571,040 psi, n turns out to be 8.12 and

$$k = \sqrt{\left[n\rho + (2n-1)\rho'\right]^2 + 2\left[n\rho + (2n-1)\rho' d'/d\right]} - \left[n\rho + (2n-1)\rho'\right] \tag{4.5}$$

$$\rho = \frac{A_s}{bd} \tag{4.6a}$$

$$\rho' = \frac{A_s'}{bd} \tag{4.6b}$$

In modeling, to account the composition of reinforcement in the section, we can either use the actual thickness of the wall section with equivalent modulus with moment of inertia corresponding to cracked or uncracked section; or the modulus of concrete with equivalent thickness interpreted from the moment of inertia for the cracked or uncracked section.

The equivalent modulus of elasticity can be calculated adopting that the rigidity for two aforementioned conditions are same i.e.

$$I_{uncr(cr)}E_c = I_c E_e \tag{4.7}$$

Evaluating,

$$E_e = \frac{I_{uncr(cr)}E_c}{I_c} \tag{4.8}$$

Where I_c corresponds to the real section of the wall.

And the equivalent thickness of the shell element can be estimated using Eq. (5-9)

$$t_e = \sqrt[3]{\frac{12 * I_{uncr(cr)}}{b}} \tag{4.9}$$

To see the effect of crack and the reinforcement on the deflection and the bending stress development in I-wall, sensitivity analysis was conducted for stiffness corresponding to plain concrete section, uncracked reinforced concrete section and the cracked reinforced concrete section .The result is shown and discussed as below:

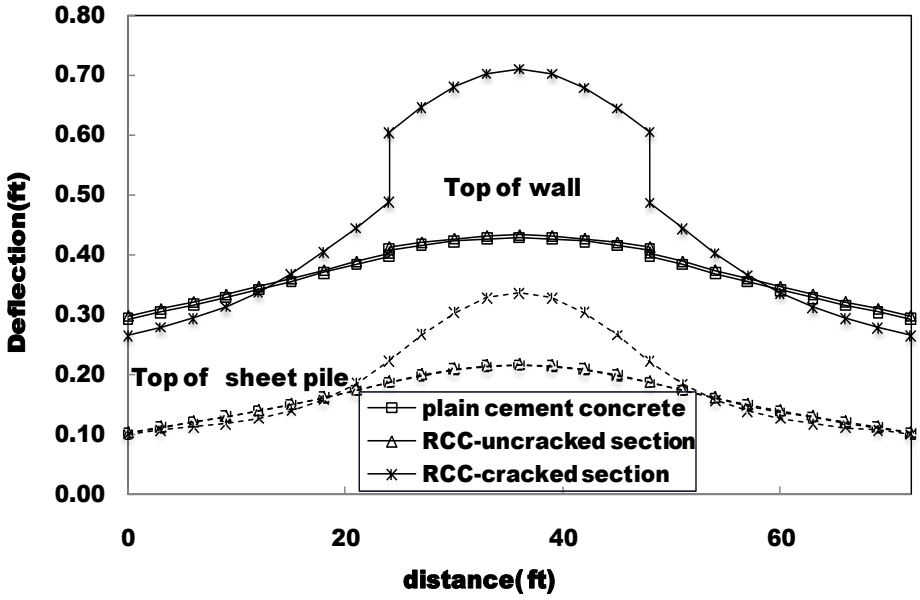

Figure 4.7. Deflection of the wall and the sheet pile

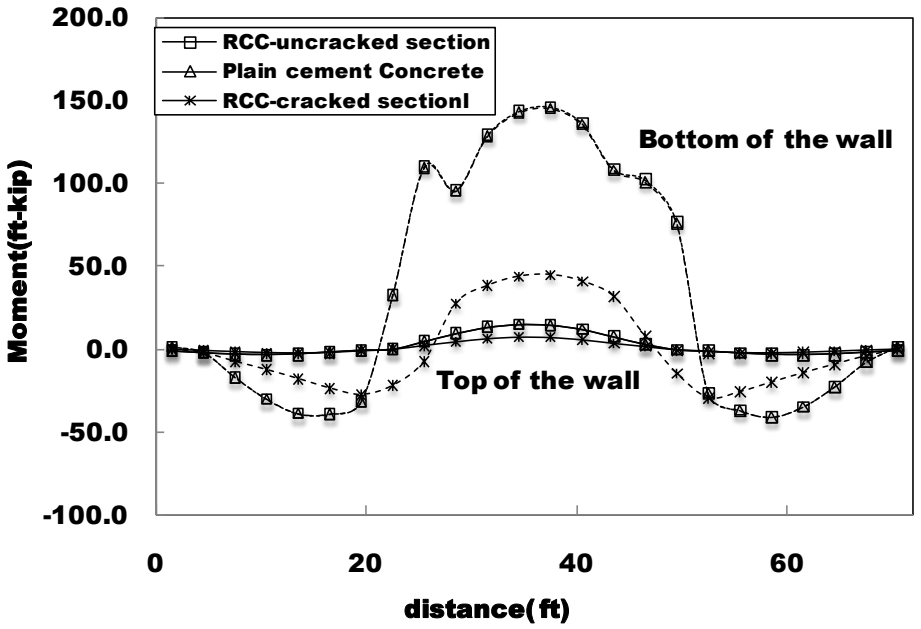

Figure 4.8. Moment about the vertical axis of the wall

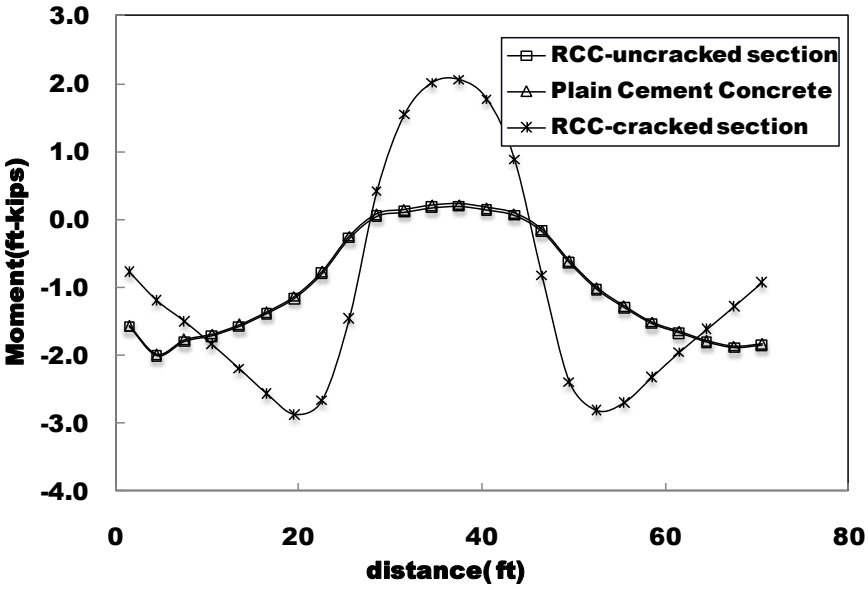

Figure 4.9. Moment at the sheet pile about the vertical axis of the wall

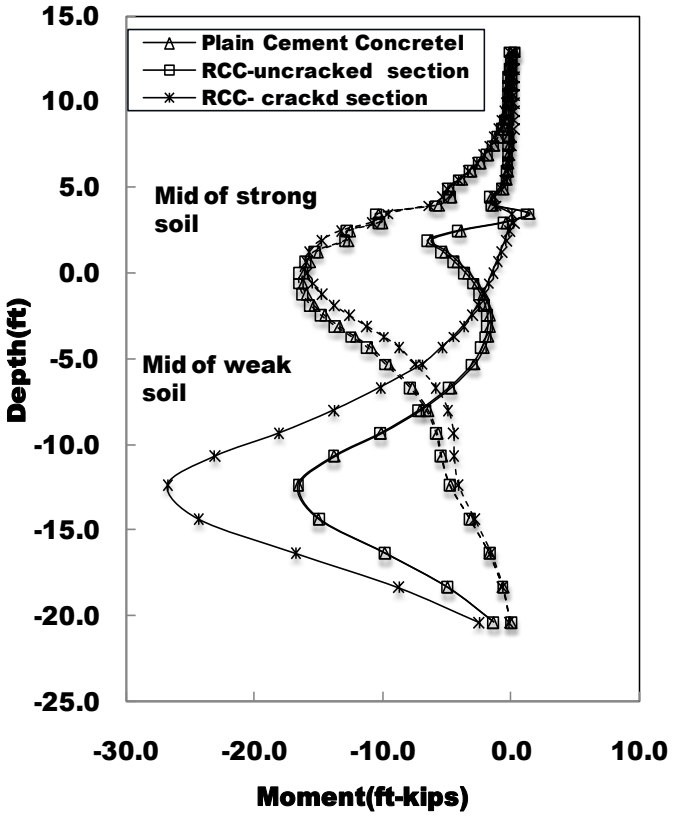

Figure 4.10. Moment about horizontal axis of the wall

From the result it can be seen that as far as the crack is not considered in the concrete section, the deflection and the moment distribution is not different for the composite reinforced cement concrete and the plain cement concrete sections. But if the cracked section is used to calculate the stiffness of I-wall section, then the difference is very large. From this result, it might be wrong to disregard the cracking of the concrete in the analysis which otherwise will result in overestimation of the bending moment developed.

The main concern in this study was that which modulus should be taken during the numerical analysis. Normally when the deflection (serviceability) is the main concern, the cracked moment of inertia should be taken into account (Everad 1993). But still it is customary to use uncracked section and see if the concrete on the tensile side is within the tensile strength given by the Eq. (4.10a) (ACI 318-05, 2005) or not

$$f_{ct} = 7.5\sqrt{f_c'} \qquad (4.10a)$$

or,

$$M_{cr} = \frac{2.f_{ct}I_{uncr}}{D} \qquad (4.10b)$$

Only in case when the tensile stress is beyond that given in Eq. (4.10), the reduced stiffness may be used.

Actually, for reinforced concrete, however, three different flexural stiffness values can be considered: the uncracked stiffness; transition from uncracked to cracked stiffness; and the cracked stiffness. This can be illustrated using a moment curvature diagram for a length of beam shown in the Figure 5.14 shows the distribution of *EI* along the beam where the stiffness varies from the uncracked value at points where the moment is less than the cracking moment to a

partially cracked value at points of higher moment. Therefore in the transition from the uncracked condition to the fully cracked condition, the reinforced concrete section may have the different flexural stiffness depending upon the curvature or the moment induced in the structure.

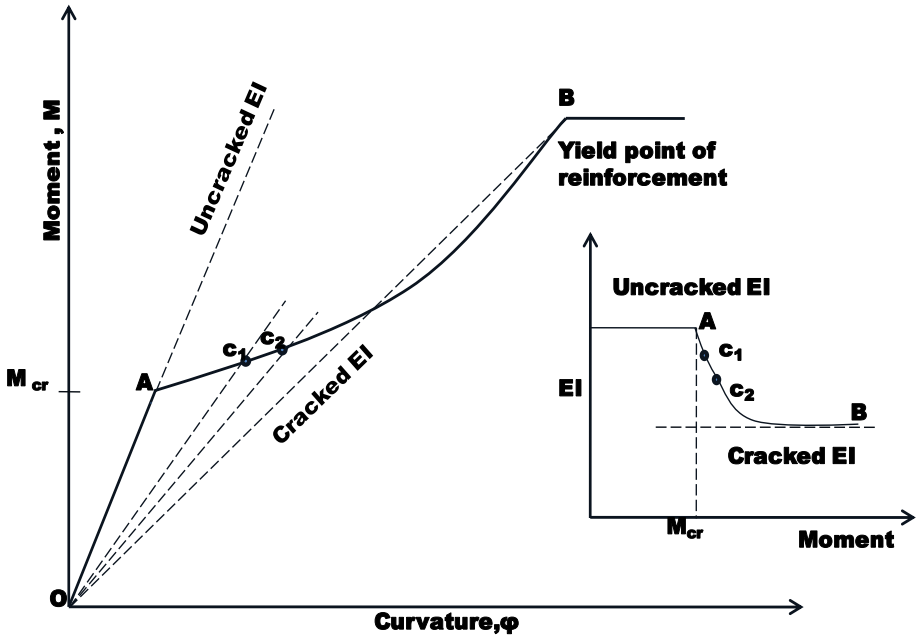

Figure 4.11. Moment–curvature curve for the reinforced cement concrete section (Replotted from MacGregor 1992)

Actually, modeling the crack propagation was beyond the scope of this study and not incorporated in this study. But still it was possible to incorporate the variation of the flexural stiffness due to the variation of the curvature or moment induced in the system. Though the yielding of the reinforced cement concrete cannot be modeled for the FLAC structural element (linear elastic model), but using this procedure, it was still possible to judge accurately whether the loading condition had already reached the moment capacity or not.

The other method to capture the cracking of the RCC section is to calculate the effective moment of inertia which can be calculated Eq. (4.11) (Branson 1971). This method is more

appropriate in hand calculation since the distribution of the *EI* is very hard to be incorporated in such case.

$$I_e = \left(\frac{M_{cr}}{M_a}\right)^a I_{uncr} + \left[1 - \left(\frac{M_{cr}}{M_a}\right)^a I_{cr}\right] \tag{4.11}$$

Where, M_a is the maximum moment in the member at the loading stage for which the moment of inertia is being computed or any previous loading stage.

But as long as we are using numerical simulation, it is more appropriate to use the stiffness calculated using the first criterion discussed above. So in this study, we conducted the analysis using the uncracked section and checked whether the tensile and the compressive strength were within the compressive and the tensile strength of the concrete or not. If tensile stress crossed the limiting stress provided in Eq. (5-10a), we repeated the analysis using the cracked moment of inertia. The following relationships were derived for different conditions:

$$EI = (EI)_{uncracked} \qquad \text{if} \quad M < M_{cr} \tag{4.12}$$

$$EI = \frac{M}{M_{cr}/(EI)_{uncracked} + \dfrac{(M - M_{cr}) * (\phi M_n/(EI)_{cracked} - M_{cr}/(EI)_{uncracked})}{(\phi M_n - M_{cr})}} \qquad \text{if } M > M_{cr} \tag{4.13}$$

$$EI = (EI)_{cracked} \qquad \text{if} \quad M > \phi M_n \tag{4.14}$$

Using the equations above, the variation for the stiffnesses for the real I-wall sections (New Design Guidelines) were calculated and the variations are shown in Figure 4.12.

From Figure 4.12 it is seen that the I-wall section recommended in the new design guidelines is seen to be quite brittle. Since the ductility is provided mostly by the steel

reinforcement, it can be inferred that the I-wall sections are provided with very less reinforcement which exhibits brittleness.

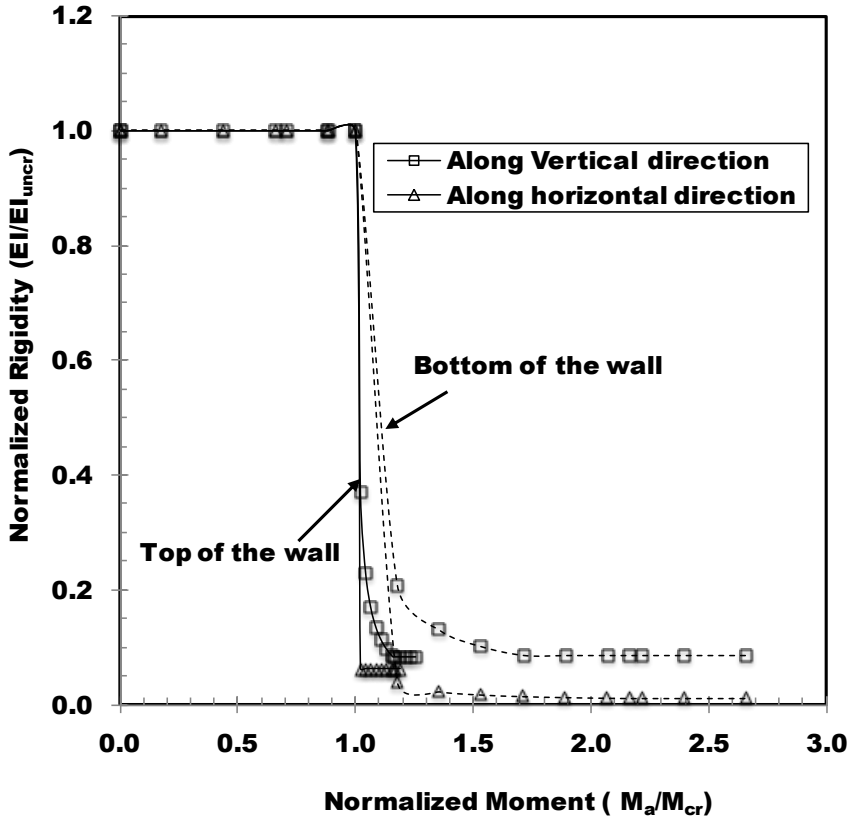

Figure 4.12. Variation of the stiffness of the reinforced cement concrete with moment for I-wall section of New Orleans

4.2.3.2 Sheet pile

The sheet pile used in London Avenue canal is CZ-101(USACE 2008). The geometrical parameters of this type of sheet pile are found in the manufacturer table (sheetpile.net). To account the simple geometry of the shell element used in the simulation against the complex one of the real Z-type sheet pile, equivalent thickness of the shell element was estimated using the relation:

$$t_{eq} = \sqrt[3]{I} \tag{4.16}$$

Where, t_{eq} denotes the equivalent thickness in in. of the embedded liner element used in the simulation and I denotes moment of inertia in in^4 per unit foot width of the sheet pile

A variation of soil strength along the longitudinal direction in a three dimensional analysis has a prominent effect of anisotropy of bending stiffness on the bending moment and the deflection of wall. Since the degree of anisotropy is an uncertain parameter and to see to what extent of anisotropy has its significant effect on the bending and deflection of I-wall, sensitivity analysis was conducted. The results were compared for five cases: the isotropic case; and the orthotropic case with 10, 100, 1000 and 1000 times reduced rigidity in horizontal direction.

The stiffness matrix for the isotropic plate can be estimated by Eq. (5-17) (FLAC^{3D} 2006):

$$\begin{aligned} c_{11} &= c_{22} = \frac{E}{1-\upsilon^2} \\ c_{33} &= \frac{E}{2(1+\upsilon)} \\ c_{12} &= \upsilon\left(\frac{E}{1-\upsilon^2}\right) \\ c_{13} &= c_{23} = 0 \end{aligned} \tag{4.17}$$

For the orthotropic material, the constitutive equation can be represented as Eq. (4.18)

$$\{\sigma'\} = \begin{Bmatrix} \sigma_{x'} \\ \sigma_{y'} \\ \sigma_{z'} \end{Bmatrix} = [E']\{\varepsilon'\} = \begin{bmatrix} c'_{11} & c'_{12} & 0 \\ & c'_{22} & 0 \\ sym. & & c'_{33} \end{bmatrix} \begin{Bmatrix} \varepsilon_{x'} \\ \varepsilon_{y'} \\ \gamma_{x'y'} \end{Bmatrix} (orthotropic shell) \tag{4.18}$$

The stiffness matrix for orthotropic material can be divided into membrane stiffness and the bending stiffness, which can be estimated using Eq. (4.19) (Ugural 1981):

$$c_{11}^{'} = \frac{E_{x'}^{'}}{1-\upsilon_{x'}\upsilon_{y'}}$$

$$c_{22}^{'} = \frac{E_{y'}^{'}}{1-\upsilon_{x'}\upsilon_{y'}} \qquad (4.19)$$

$$c_{33}^{'} = G$$

$$c_{12}^{'} = \frac{E_{x}^{'}\upsilon_{y'}}{1-\upsilon_{x}^{'}\upsilon_{y}^{'}} = \frac{E_{y}^{'}\upsilon_{x'}}{1-\upsilon_{x}^{'}\upsilon_{y}^{'}}$$

Where $E'_{x'}, E'_{y'}, \nu_{x'}, \nu_{y'}$ are the modulus and poisons ratio along the local axes x' and y' respectively.

$$c_{11}^{b'} = \frac{12}{t^3} D_{x'}$$

$$c_{22}^{b'} = \frac{12}{t^3} D_{y'} \qquad (4.20)$$

$$c_{33}^{b'} = \frac{12}{t^3} G_{x'y'}$$

$$c_{12}^{b'} = \frac{12}{t^3} D_{x'y'}$$

Where $D_{x'}, D_{y'}, D_{x'y'}$ and $G_{x'y'}$ represent the flexural rigidities and the tortional rigidities respectively. If $D_{x'}$ and $D_{y'}$ are known then $D_{x'y'}$ and $G_{x'y'}$ can be calculated using Eq. (4.21). (Ugural 1981)

$$G_{x'y'} = \frac{1-\upsilon}{2}\sqrt{D_{x'}D_{y'}} \qquad (4.21)$$
$$D_{x'y'} = \upsilon\sqrt{D_{x'}D_{y'}}$$

To see the effect of anisotropy, deflection at top and the center of the wall; deflection at the bottom and the center of the wall; moment M_x at top and bottom of the wall; moment at the top of the sheet pile; and moment M_y at center of the sheet pile were compared. The results are shown in Figure 4.13 and Figure 4.14.

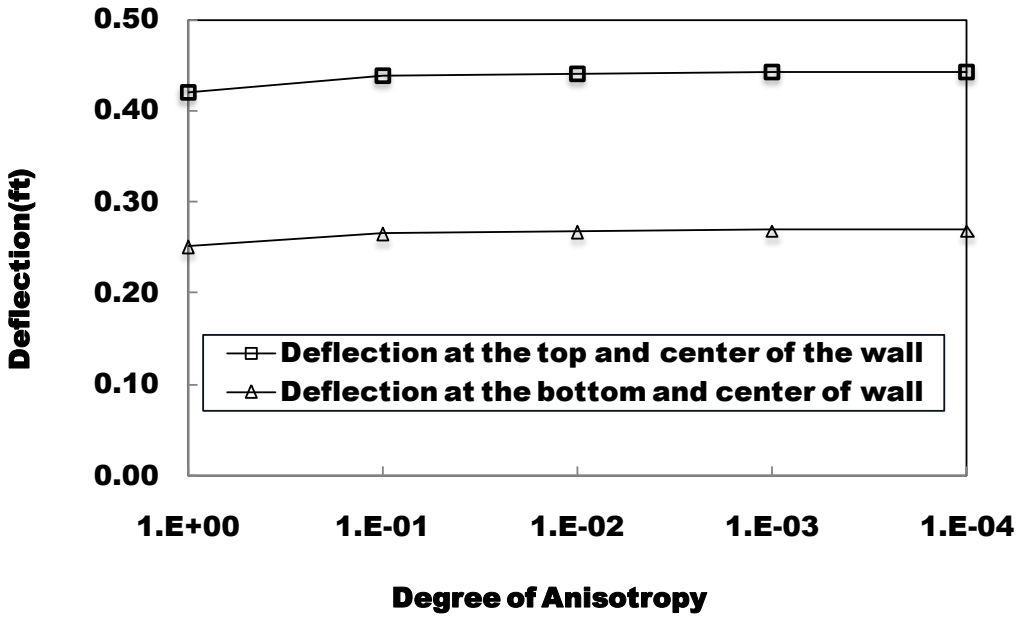

(a)

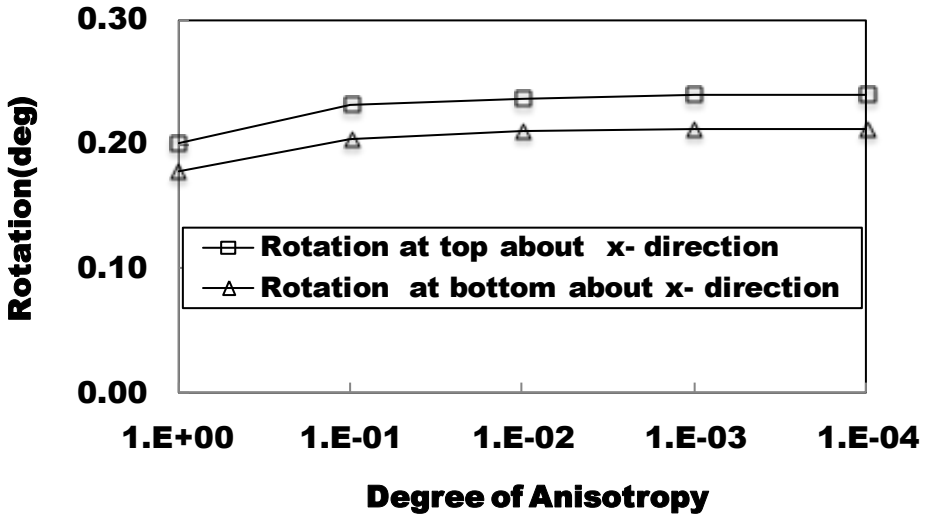

(b)

Figure 4.13. Deflection (a) and rotation (b) of the wall for different degree of anisotropy

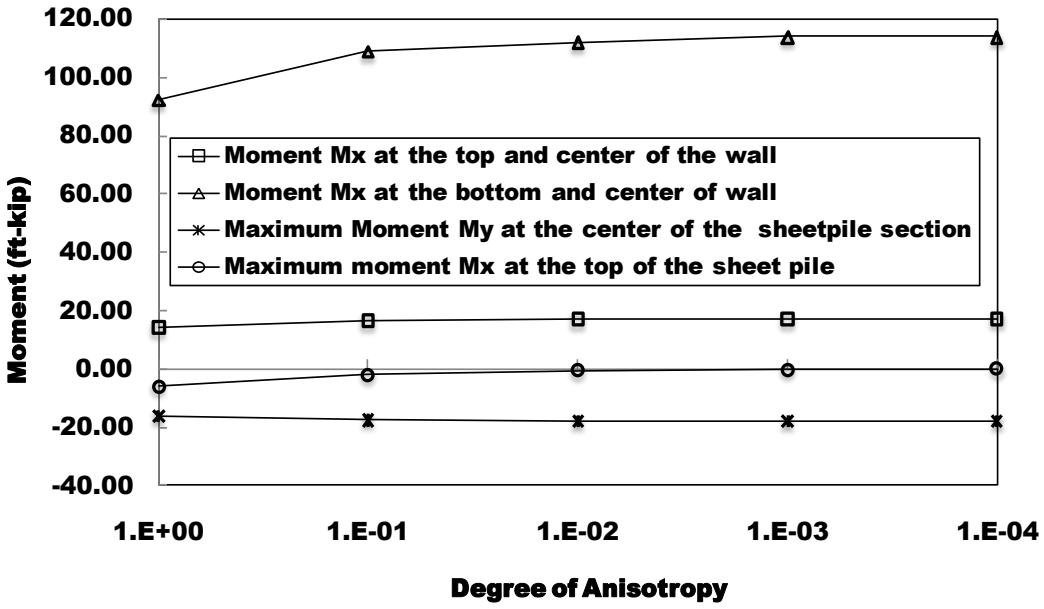

Figure 4.14. Moment at the wall and Sheet pile for different degree of anisotropy

In Figures 4.13 and 4.14, the degree of anisotropy indicates the ratio of the horizontal stiffness to the vertical stiffness. From Figures 4.13 and 5.14, it can be seen that as the anisotropy increases, the deflection and the moment about vertical axis of the wall increases but the moment on sheet pile section decreases. From the figures, it can also be seen that the anisotropy is much influential when the degree of anisotropy is 0.1. The increase in anisotropy beyond this magnitude is seen to be not that influential, so that the degree of anisotropy of any magnitude beyond 0.1 can be used without significantly altering the result.. In this study, the degree of anisotropy was assumed to be 0.1.

4.3 CASES OF STUDY

There are many potential causes for the localized failure of I-wall. Out of those potential failure modes, three cases were investigated in this study: variation of soil strength along I-wall section; localized erosion of certain part of the soil section along the I-wall; weak bondage

between the sheet pile and the concrete capping due to the result of the rusting of the sheet piles or due to the poor workmanship during the casting of the sheet pile rendering the concrete capping and the sheet pile to act as the separate entities at certain location of the I-wall section. Each of these cases was investigated to find out for which case the cap would be more effective.

4.3.1 Case 1: Variation of Soil Strength

One of the failure mechanisms of the failure of I-wall in New Orleans during Katrina was due to soil instability at weak soil spots. During hurricane Katrina, instead of the collapse of the whole system, only some portions were breached. The example of such breach was that of the 17^{th} Street Canal breach which was of the length 450 feet (Duncan 2008). This wide breach was not developed abruptly but was developed by the sequence of inception and progression of the local and small scale breaches which occurred due to the localized weaker zones. So if only the onset of these small scale breaches is inhibited by some mechanism, the development of the larger breaches might be controlled. So effectiveness of the cap as the mechanism to restrict the onset of this localized failure was investigated in this study.

In the analysis, to model the extreme case, the development of the gap up to sand layer and the reduction of strength of the marsh stratum at higher water level were incorporated in the soil section having weak strength.

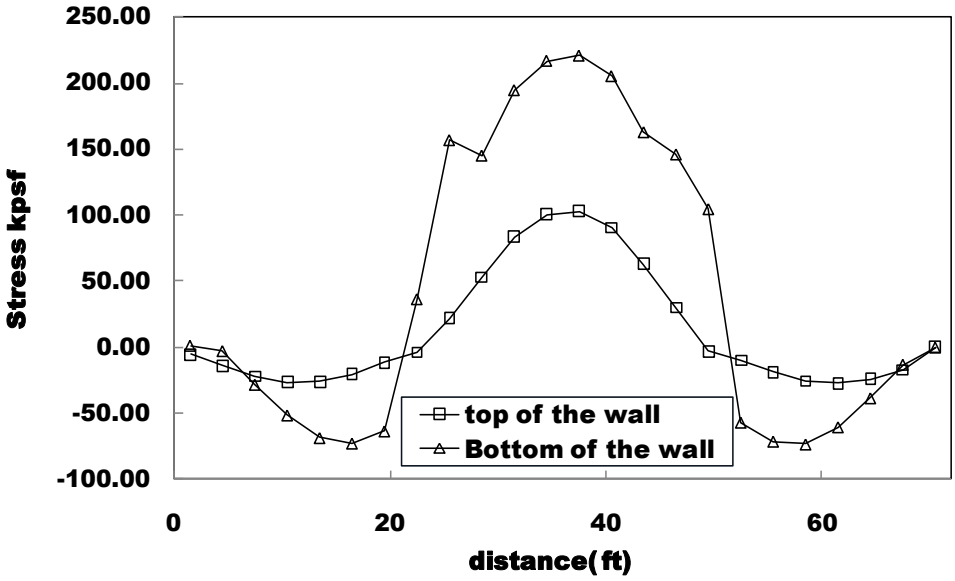

Figure 4.15. Lateral stress on the wall surface

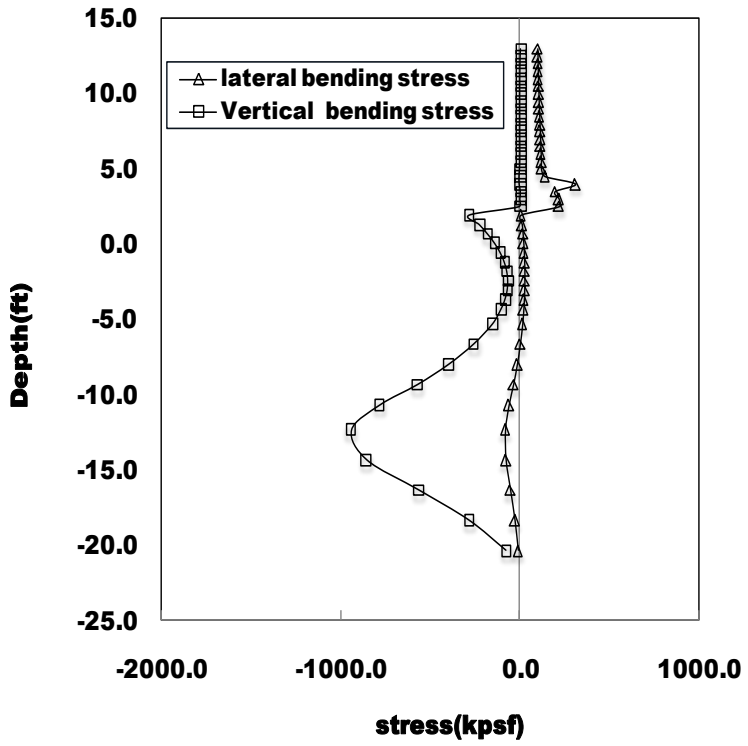

Figure 4.16. Stress distribution along the depth at surface at mid section

Two steps were conducted during the analysis as mentioned earlier. In the first step the cracking was not included in the analysis and it was checked if the stresses were within the tensile strength of the concrete or not. Then if the stresses crossed the limit, then the cracking was incorporated using the relation given by the Eq. (4.12) to Eq. (4.14). The stiffness was assigned differently for longitudinal and horizontal direction using the orthotropic material properties of FLAC$^{3D.}$ This is because the reinforcement distribution in vertical and longitudinal direction is different.

From Figure 4.15, it is seen that the bending stress has already reached the tensile strength of the concrete given by Eq. (4.10a) which is 67.7 ksf. So it was necessary to use the stiffness of the concrete derived by incorporating cracking.

To see the effect of cap, deflection at top of the wall; deflection at the bottom of the wall; deflection along the center of the wall; moment at the top of the wall; moment at the bottom of the wall; and moment at the center of the wall were compared for the I-wall with and without cap. These are illustrated in the figures below.

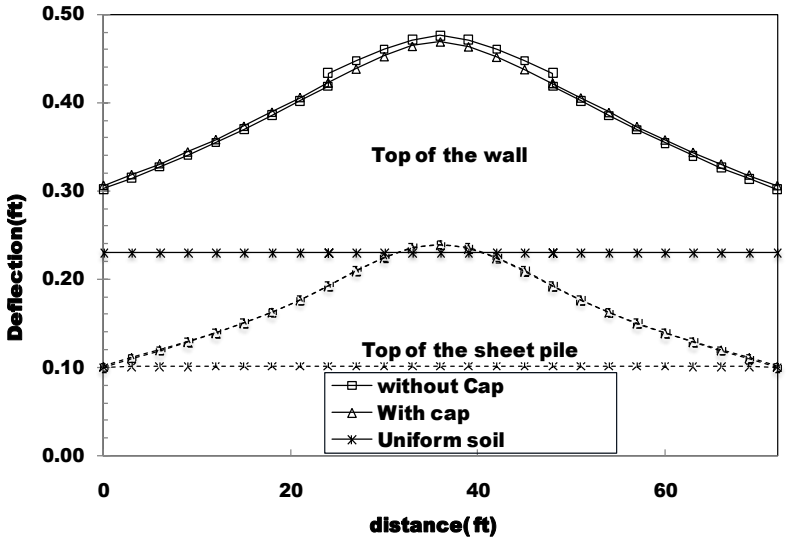

Figure 4.17. Deflection of the wall and the sheet pile

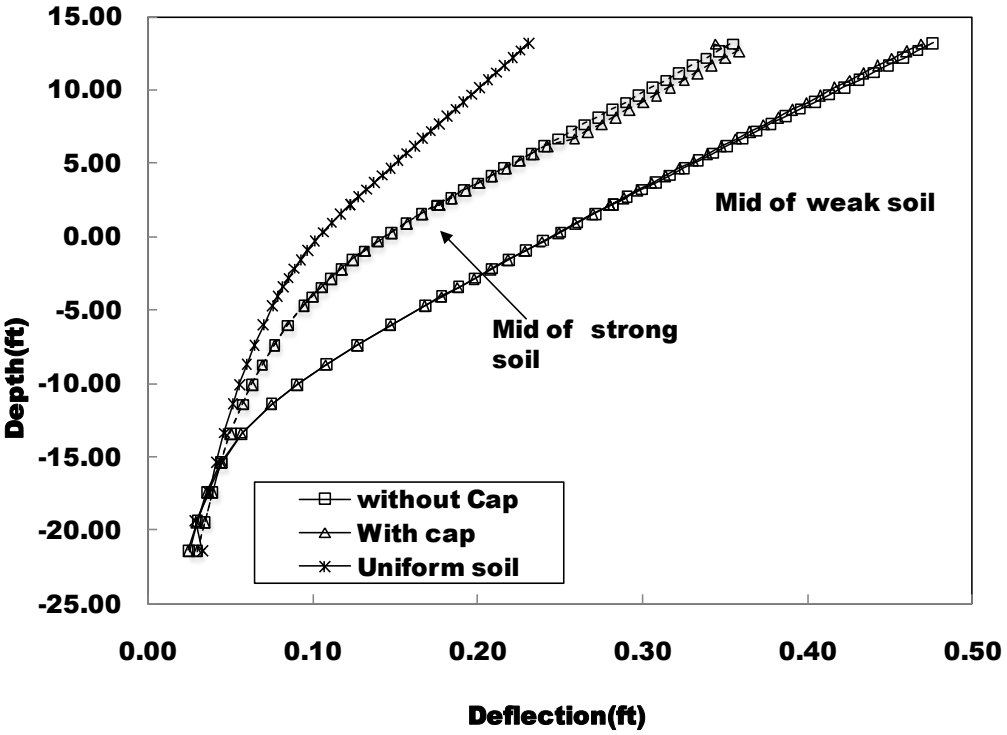

Figure 4.18. Deflection of the wall and the sheet pile along depth

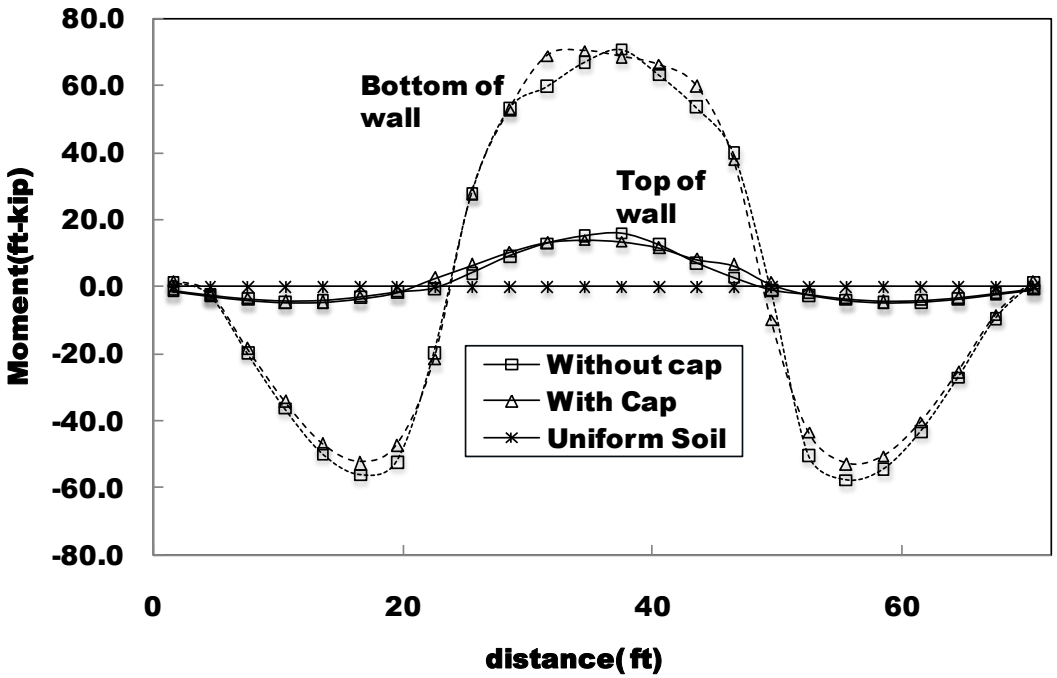

Figure 4.19. Moment about the vertical axis of the wall

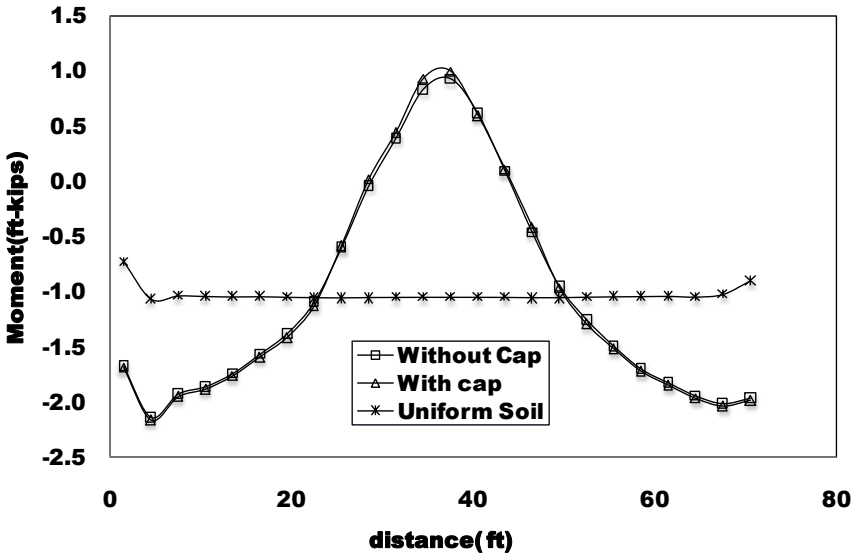

Figure 4.20. Moment at the sheet pile about the vertical axis of the wall

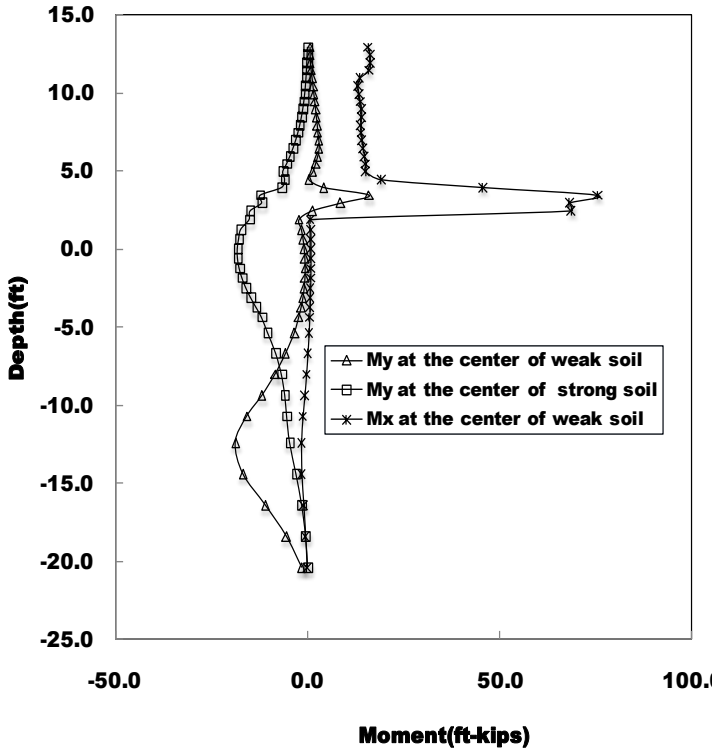

Figure 4.21. Moment about vertical axis of the wall (Mx) and about horizontal axis of the wall (My)

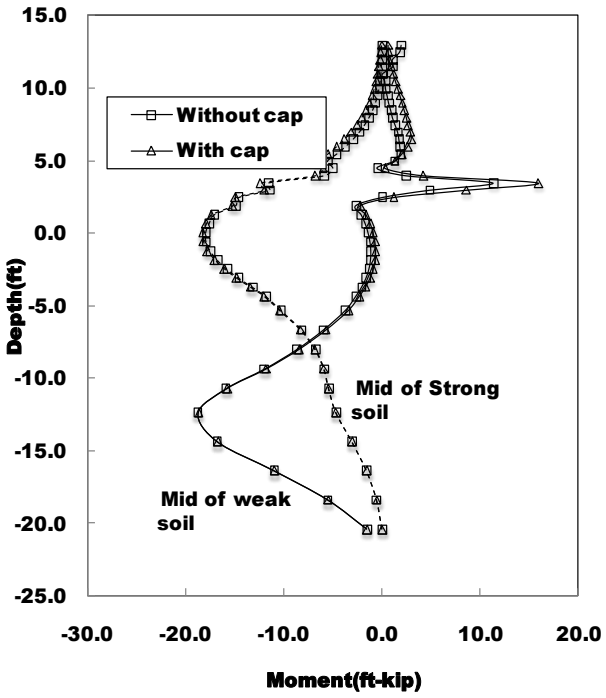

Figure 4.22. Moment about horizontal axis of the wall

4.3.1.1 Discussion of the result

From Figure 4.17, it can be seen that the relative displacement for two adjacent panels at the top of the wall is reduced when the cap is used. But at the same time the incorporation of the cap is not that effective in reducing the overall displacement of I-wall. There is also not much significant improvement of the moment distribution in the wall when the cap is used. With this result, we can still stick to the point that since the relative displacement of two adjacent panels is not allowed; the impending failure of the weak panel is resisted to some extend by the strong panel inhibiting the local failure of the weaker panel.

From the result, it can also be seen that the moment induced by the variation of the soil strength about the vertical direction is much greater than the moment about the lateral direction due to the hydrostatic loading. This provokes us to think whether the I-wall section related to

the current design guidelines is strong enough to resist the moment attributed to the spatial variation of the soil strength or not. To investigate this, we compare the moment of resistance of the available section of the typical I-wall of New Orleans with the computed bending moment. Figure .4.23 shows the typical cross section of I-wall used for the analysis.

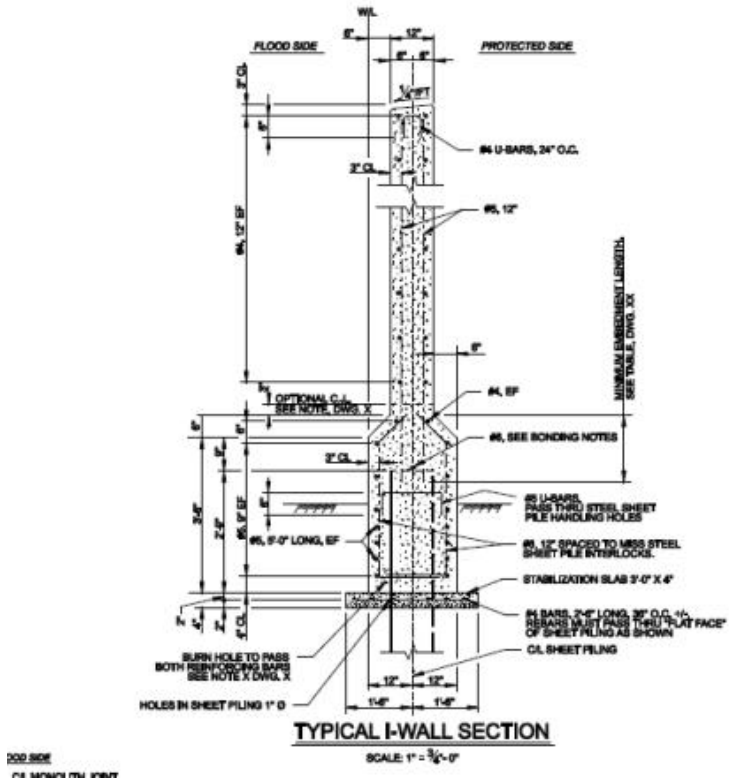

Figure 4.23. Typical cross section of I-wall (USACE, 2008)

The cross sections at the top of the wall and the bottom of the wall above the ground level are shown in Figure 4.24.

The design check was done for the true strength available from the testing of samples collected and design strength recommended in ASTM code.

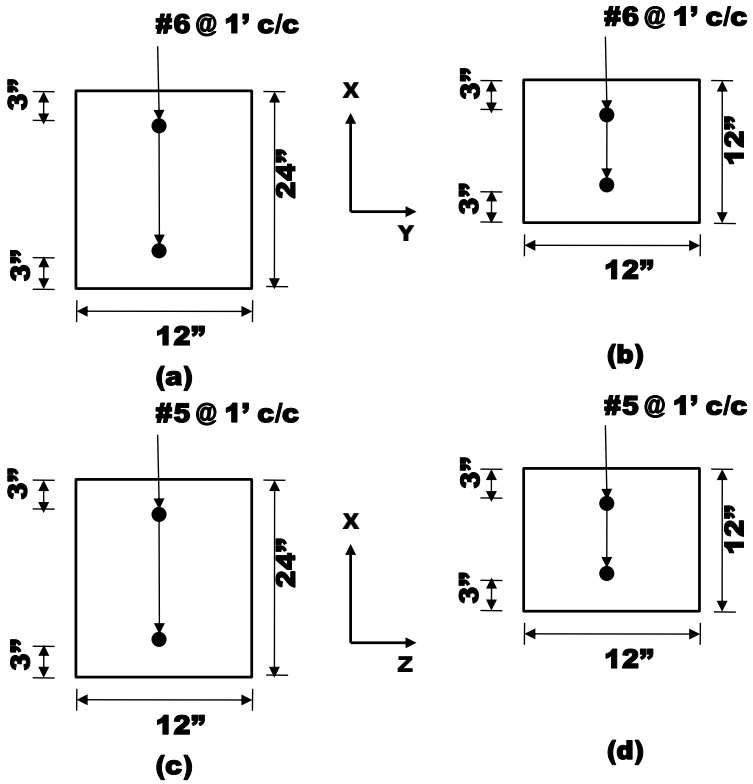

Figure 4.24. Typical cross section of the wall

(a): Lengthwise per unit foot at the bottom of the wall

(b): Lengthwise per unit foot at the top of the wall

(c): Depth wise per unit foot at the bottom of the wall

(d): Depth wise per unit foot at the top of the wall

From the IPET report, Volume 5, Appendix 15 (real value from the sampling), the compressive strength of the concrete, f'_c is 3925 psi and yield strength of the steel bar, *fy* is 71 ksi. And for the design value recommended by ASTM A 615, *f'c* is 3 ksi and fy is 60 ksi

Two assumptions were adopted to calculate the moment of the resistance of the wall and were compared with the bending moment computed from FLAC^{3D}. But since the compression steel and the tension steel are of equal in area for the typical section, assumption 2 was to be taken for the comparison, since the compressive reinforcement would not subjected to the yield

stress. The Moment of resistance were calculated using the following equations (MacGregor 1992)

Assumption 1: Compressive reinforcement subjected to yield stress

$$M_n = \phi\left[(A_s - A_s^{'}) f_y (d - a/2) + A_s^{'} f_y (d - d^{'})\right] \tag{4.22}$$

Assumption 2: Compressive reinforcement not subjected to yield stress

$$M_n = \phi\left[C_c\left(d - \frac{a}{2}\right) + C_s\left(d - d^{'}\right)\right] \tag{4.23}$$

where,

$$C_c = 0.85 f_c^{'} ba \tag{4.24}$$

and

$$C_s = \left(E_s \varepsilon_s^{'}\right) A_s^{'} = E_s A_s^{'}\left(1 - \frac{\beta_1 d^{'}}{a}\right) 0.003 \tag{4.25}$$

Where a is given by the relation,

$$(0.85 f_c^{'} b)a^2 + (0.003 E_s A_s^{'} - A_s f_y)a - 0.003 E_s A_s^{'} \beta_1 d^{'} = 0 \tag{4.26}$$

In the above equations, β_1 was taken to be 0.85

Using above relations, the moment of resistance for the four sections listed above were calculated and compared with the computed bending moment. The comparison is shown in the Table 4.2.

From Table 4.2, it can be seen that the sections a and b are in the precracking stage since the computed moment is less than the cracking moment. Section d on the other hand is in the postcracking service load stage, since the computed moment is in between the cracking moment and the moment capacity. Section c was already in the post serviceability cracking stage as seen

from Table 4.2 because the moment has already crossed the moment capacity of the beam. From practical point of view, the moment above moment capacity is not allowed to develop, but it can be inferred that this section experienced a pronounced increase in the deformation and the section can be considered to be structurally failed by initial yielding of tension steel. This may lead to the development of compression failure leading to the total crushing of concrete followed by the rupture.

Table 4.2. Comparison of bending moment with the moment of resistance

S/N	**Section**	**Moment of resistance (ft-lb)**				**Computed moment (ft-lb)**
		Real strength		ASTM design strength		
		Assumpt.1	*Assumpt.2*	*Assumpt.1*	*Assumpt.2*	
1	a	40,416.75	**52,629.62**	34,155.00	**44,045.38**	**18200**
2	b	12,593.63	**24,430.92**	10,642.50	**20,222.76**	**5990**
3	c	28,681.78	**39,175.00**	24,238.13	**32,825.03**	**70500**
4	d	8,872.78	**19,366.00**	7,498.13	**16,085.03**	**13390**

Similarly we also investigated if the sheet pile is yielded or not. As far as the moment in the sheet pile is considered, the tensile stress in the sheet pile can be calculated as:

$$\sigma_t = M / z \tag{4.27}$$

where z is the section modulus and is given by:

$$z = \frac{bt^2}{6} \tag{4.28}$$

Where t is the thickness of the sheet pile .The section modulus per unit foot of the sheet pile of this study was 0.2178 ft^3

In this case, maximum moment in the sheet pile computed by FLAC^{3D} was 18800 lb-ft (M_y) and 2140 lb-ft (M_x). For these moments, the stresses developed in the sheet pile using Equation (5-27) due to M_y is 0.60 ksi and due to M_x is 0.068 ksi which are far below the yield strength of the sheet pile. The yield strength of the sheet pile measured by getting the sample was 56.6 ksi whereas the value recommended using the ASTM A 328 is 39 ksi. From this comparison, it is seen that the sheet pile will still be safe on account of soil strength variation.

4.3.2 Case 2: Erosion

In this case, erosion was so idealized that it was considered to be taken place on the soil section corresponding to central panel whereas the other parts were not affected by the erosion. During hurricane Katrina, the largest depth of the scour was found to be 6.5 feet (Seed et al. 2008) and the longest breach that took place during Katrina due to overtopping was of 920 feet (Seed et al. 2008). Seed et al. (2008) points out that this length of breach probably occurred in a progressive manner incepting from the small scale scouring. This small scale scouring might have brought the non uniform deflection of the I-wall resulting in a misalignment of floodwall system. This misalignment might have resulted a gap formation between the individual panels making a way for the water to flow through it and leading to uncontrolled erosion. The uncontrolled erosion would result in the expansion of the scouring along the length making a wider breach. So the main point is if some mechanism is there to restrict the misalignment of the I-wall section due to the small scale scouring, then this might restrict the uncontrolled erosion which ultimately reduces the width of the scouring and thus preventing it from having a wider breach. This scenario was investigated in this study and we had the following results.

In this case also, two steps of analysis were conducted as mentioned earlier. In the first step, the cracking was not included in the analysis and the stresses were checked if they were

within the tensile strength of the concrete or not. Then if the stresses crossed the limit then the cracking was incorporated using the relation given in Eqns. (4.12 to 4.14).

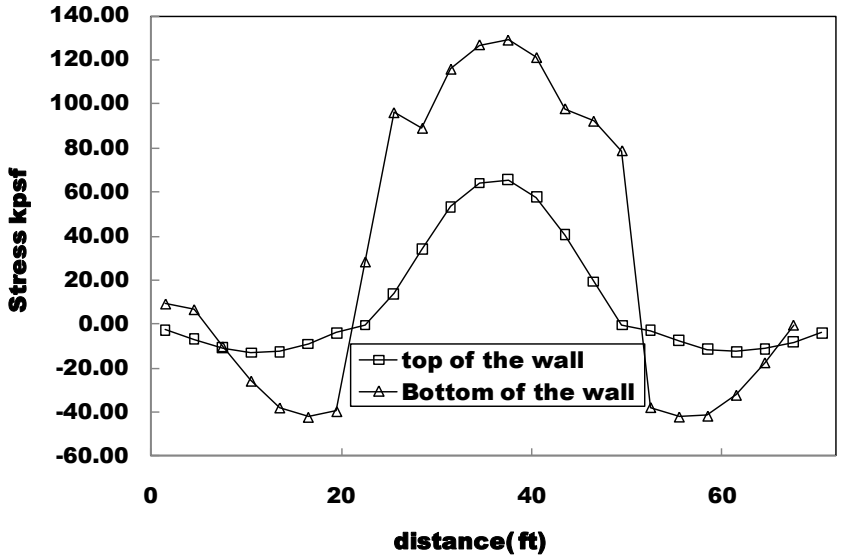

Figure 4.25. Lateral stress on the wall surface

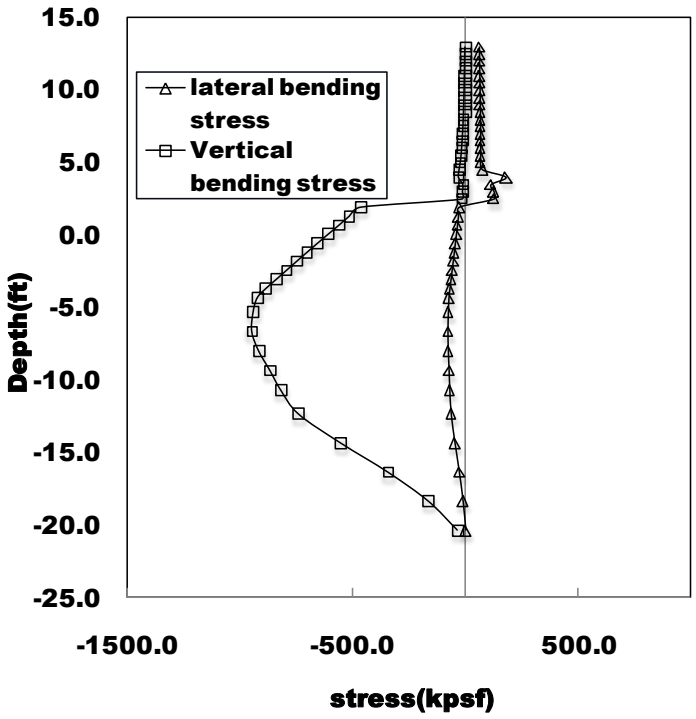

Figure 4.26. Stress distribution along the depth at surface at mid section

From Figure. 4.25, it is seen that the bending stress exceeded the tensile strength of the concrete given in Eq. (4.10a) which is 67.7 ksf. So it was necessary to use the stiffness derived from the relationships that incorporate cracking. So the second step of the analysis was conducted.

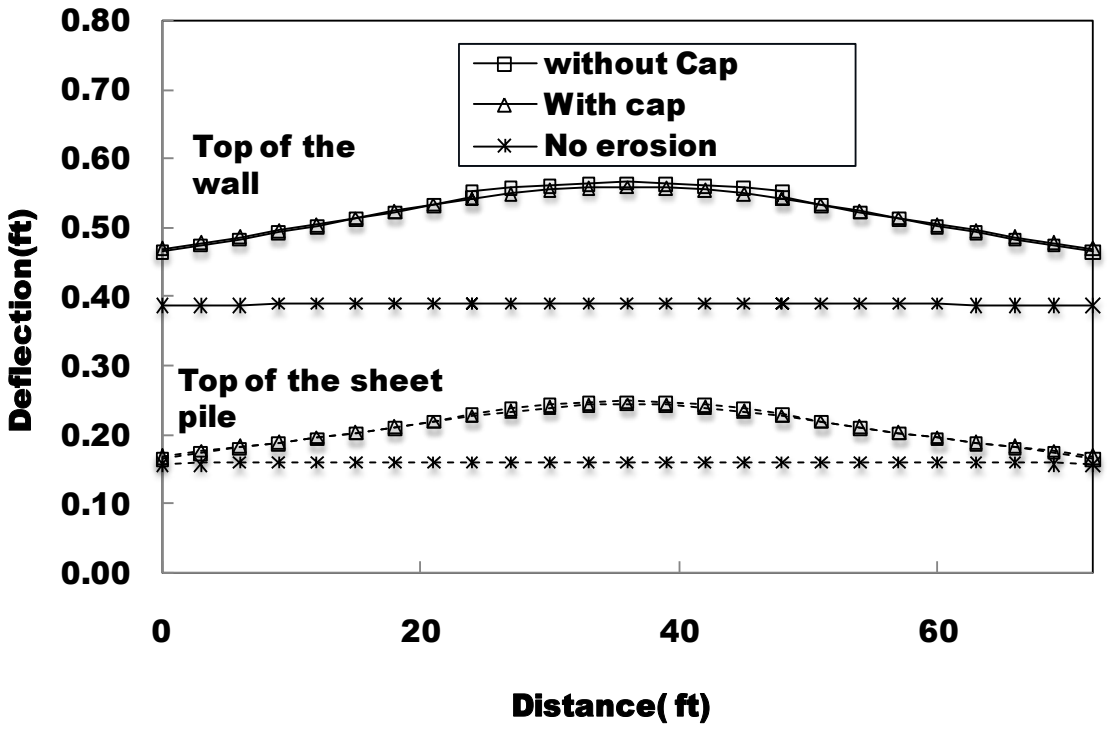

Figure 4.27. Deflection of the wall and the sheet pile

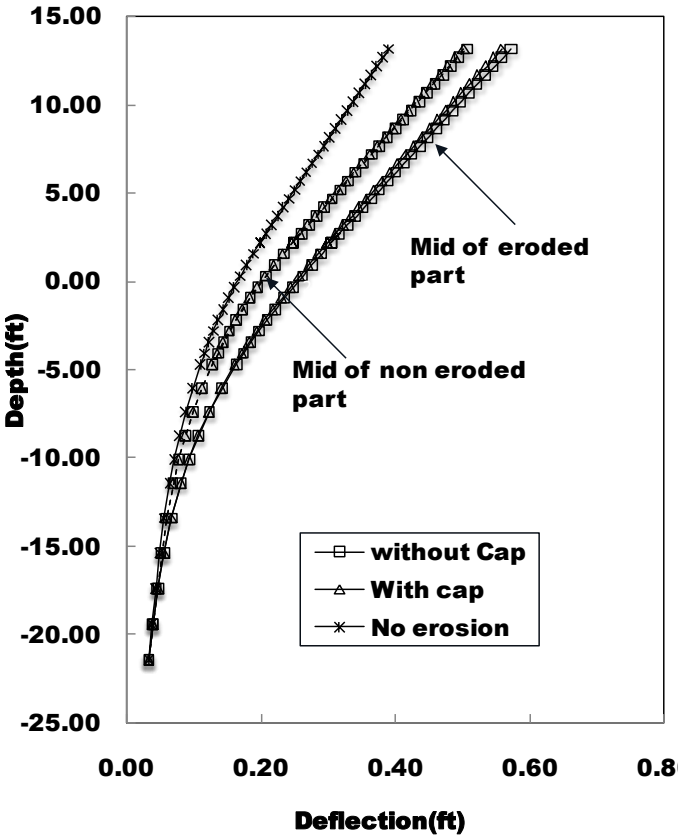

Figure 4.28. Deflection of the wall and the sheet pile along depth

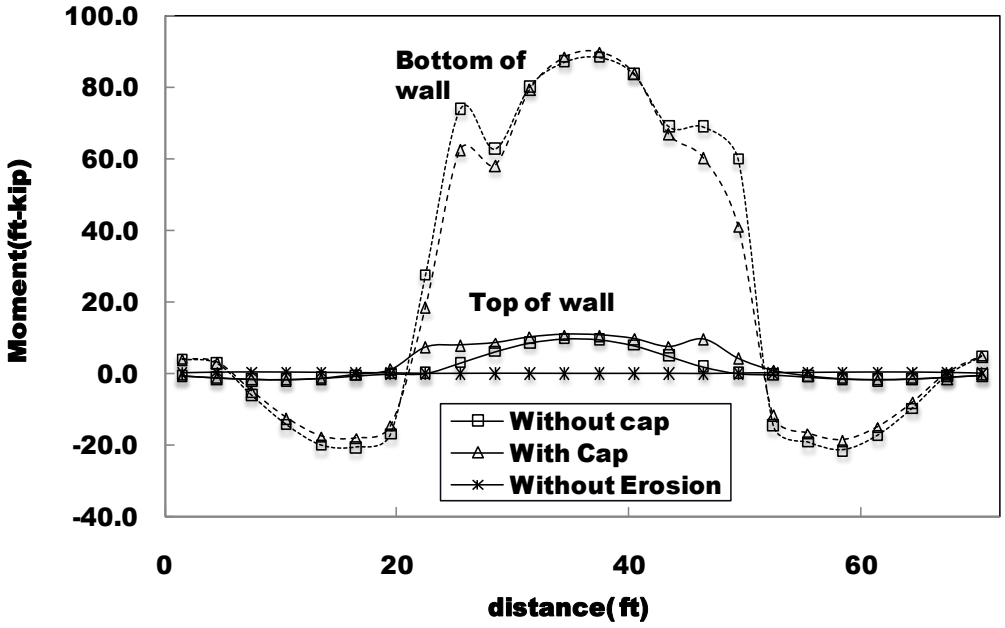

Figure 4.29. Moment about the vertical axis of the wall

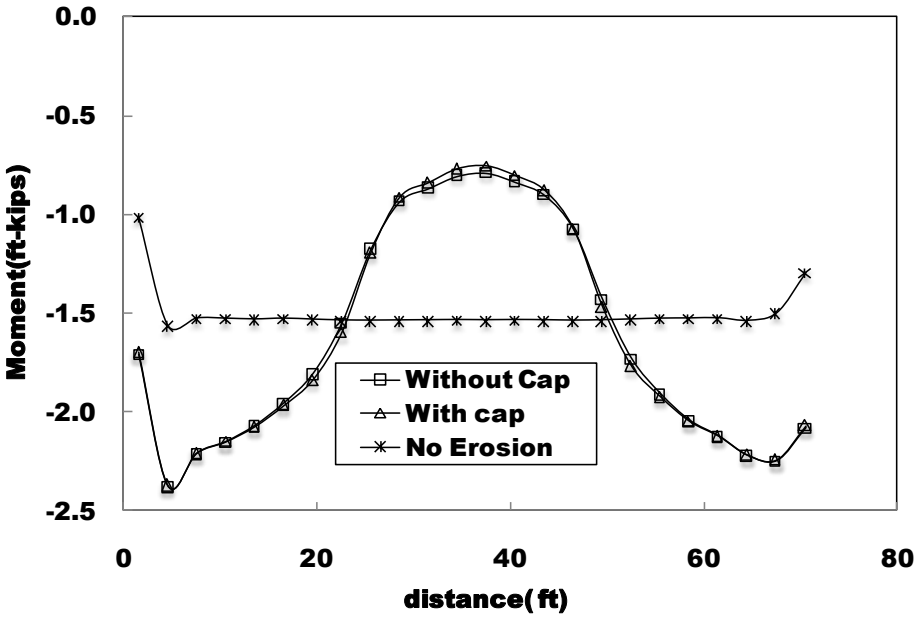

Figure 4.30. Moment at the sheet pile about the vertical axis of the wall

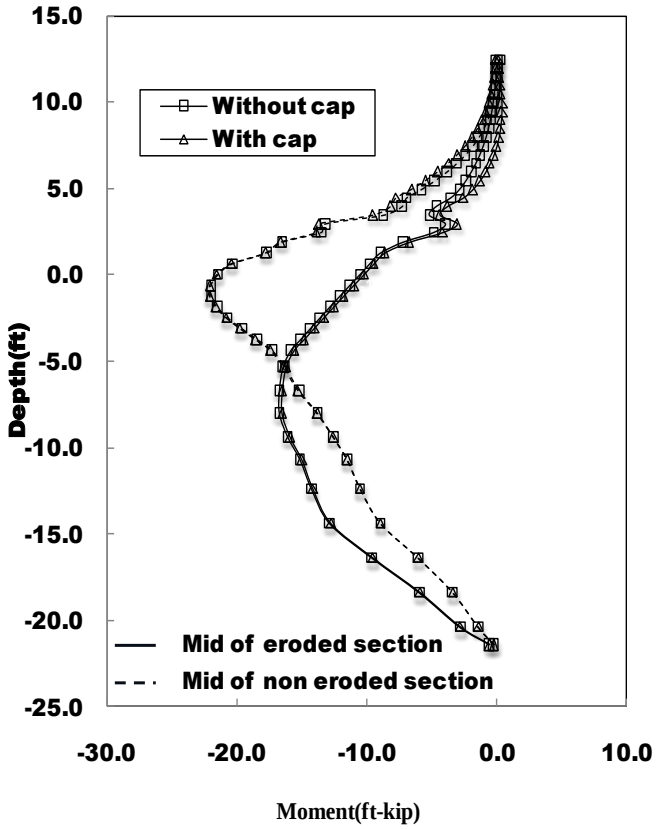

Figure 4.31. Moment about horizontal axis of the wall

As in the first case, there was a reduction of the relative displacement on the two adjacent panels when cap was installed but the overall deflection and the distribution of the moment was not improved. As in the first case, the computed moment and the moment of the resistance of the typical I-wall was compared and is shown in the Table 4.3. This gives the similar result as discussed in the previous section where section c could experience a severe crushing whereas the other three sections are still in the precracking stage.

Table 4.3. Comparison between the computed bending moment and the moment of resistance

S/N	**Section**	**Moment of resistance (ft-lb)**				**Computed moment (ft-lb)**
		Real strength		ASTM Design Strength		
		Assumpt.1	*Assumpt.2*	*Assumpt.1*	*Assumpt.2*	
1	a	40,416.75	**52,629.62**	34,155.00	**44,045.38**	**16500**
2	b	12,593.63	**24,430.92**	10,642.50	**20,222.76**	**8150**
3	c	28,681.78	**39,175.00**	24,238.13	**32,825.03**	**90200**
4	d	8,872.78	**19,366.00**	7,498.13	**16,085.03**	**11000**

To see if the sheet pile was yielded or not, we compared the stresses developed in the sheet pile with its yield strength. In this case also, maximum moment in the sheet pile computed by FLAC^{3D} was 16700 ft-lb (M_y) and 2380 lb-ft (M_x). For these moments, the stresses developed in the sheet pile due to M_y was 0.53 ksi and due to M_x was 0.074 ksi which are far below the yield strength of the sheet pile. So the sheet pile was not yielded for this case as well.

4.3.3 Case 3: Plastic Hinge

In this case, the weak bondage between the sheet pile and the concrete capping was considered. Here, the weak bondage was simulated using the plastic hinge at the joint between

the sheet pile and the concrete capping. This type of failure mechanism was not observed during Katrina but it was felt to be important since this might be the potential failure for the old levee system like New Orleans which is attributed to the deterioration of the material through the rusting. The results are shown in the figures below.

In this case also, two steps of analysis were conducted as mentioned earlier. In the first step, the cracking was not included in the analysis and the stresses were checked if they were within the tensile strength of the concrete or not. Then if the stresses crossed the limit then the cracking was incorporated using the relation given in Eqns. (4.12 to 4.14).

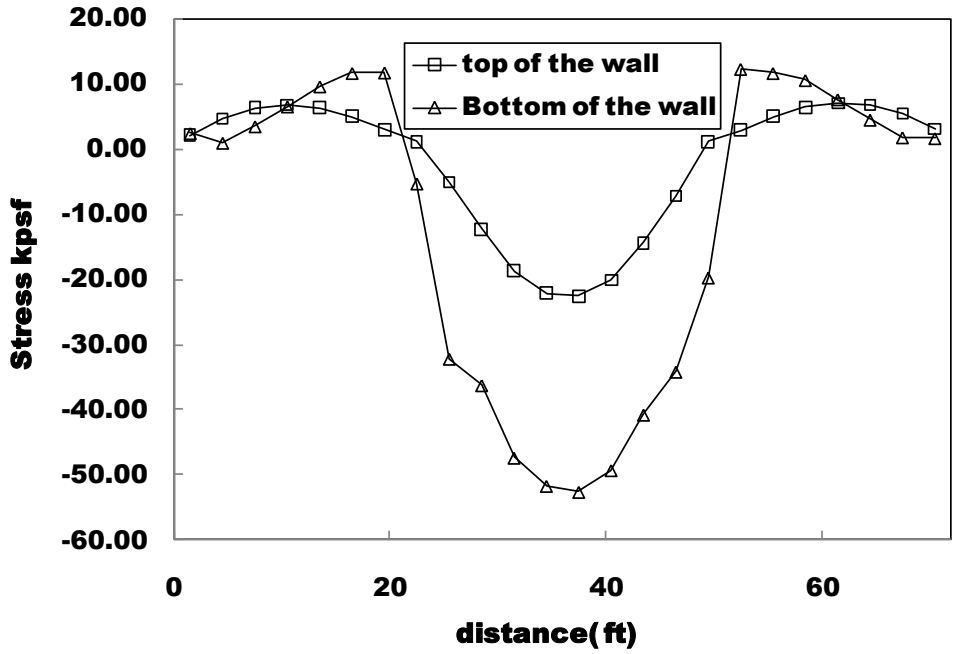

Figure 4.32. Lateral stress on the wall surface

From Figures 4.32 and 4.33, it is seen that the bending stress is below the tensile strength of the concrete given by Eq. (4.10a) which is 67.7 ksf. So it was not necessary to use the stiffness derived from the relationships that incorporate cracking. The stiffness of the uncracked section could be used for the analysis in this case.

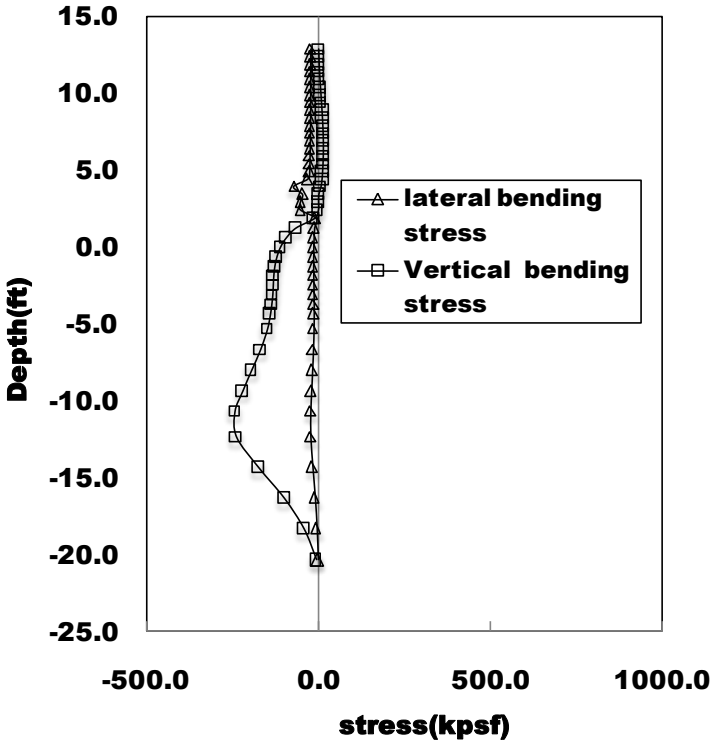

Figure 4.33. Stress distribution along the depth at surface at mid section

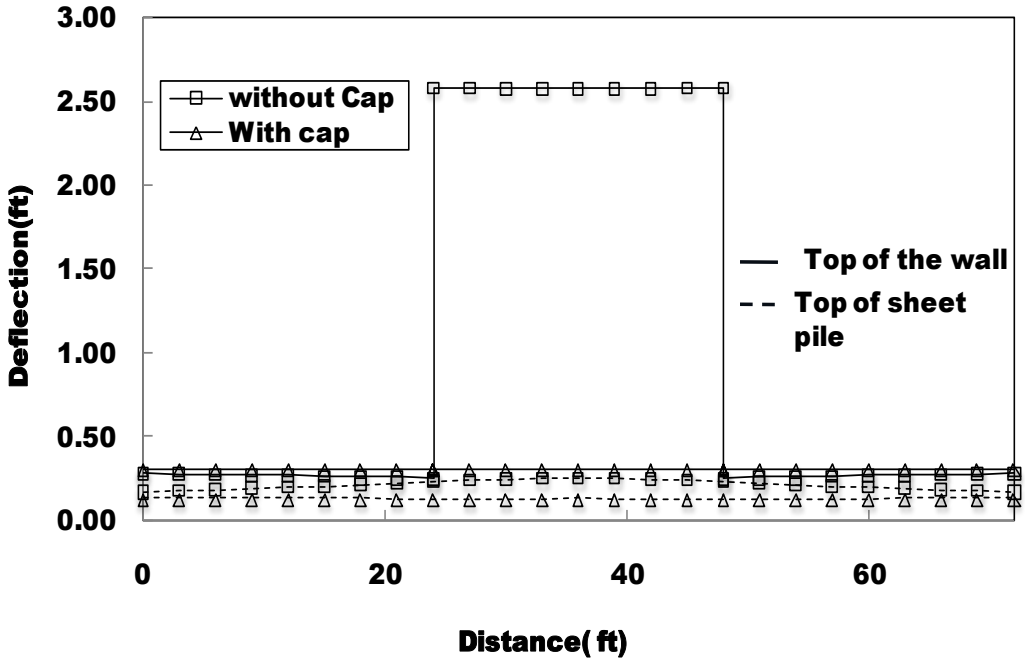

Figure 4.34. Deflection of the wall and the sheet pile

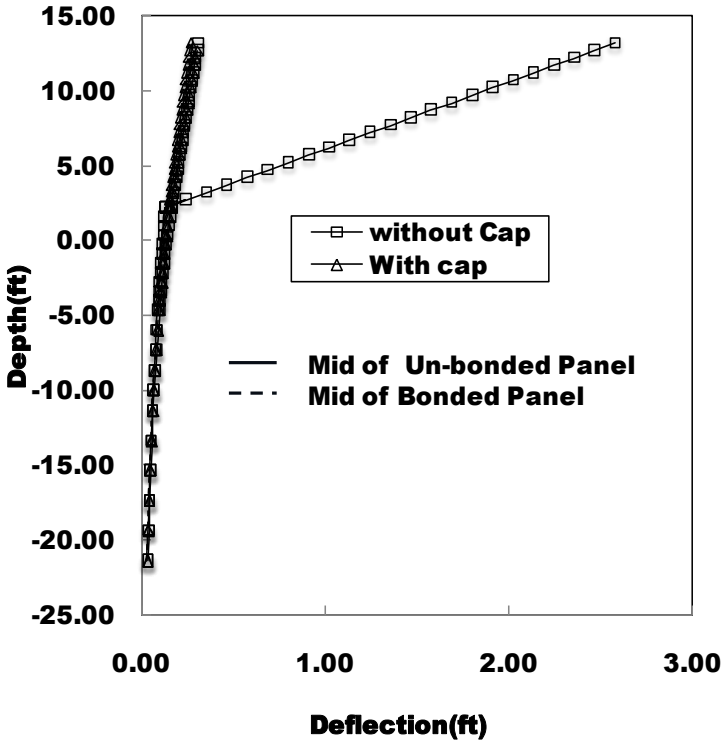

Figure 4.35. Deflection of the wall and the sheet pile along the depth

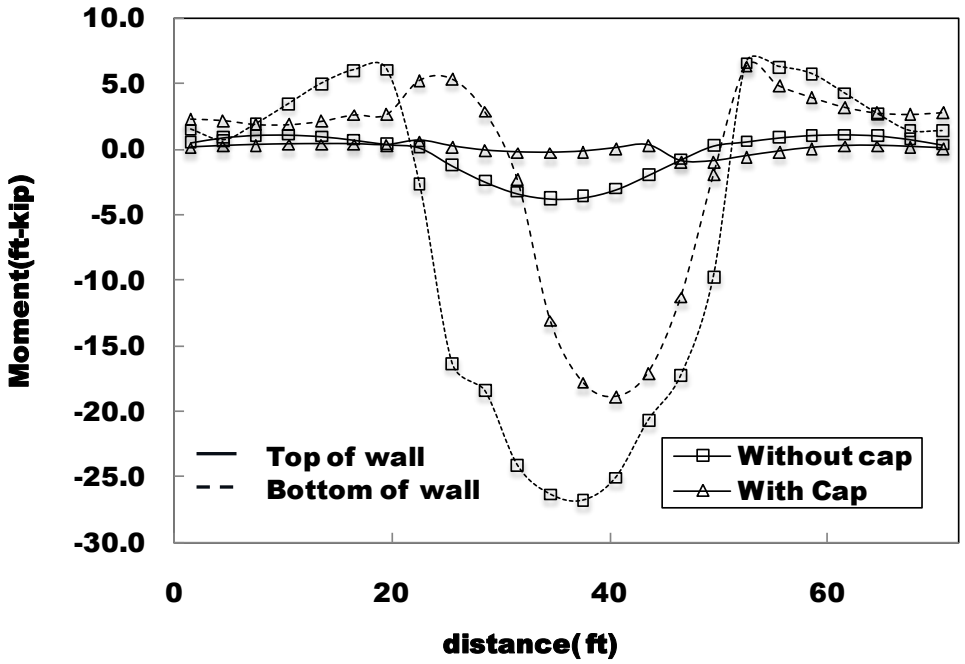

Figure 4.36. Moment about the vertical axis of the wall

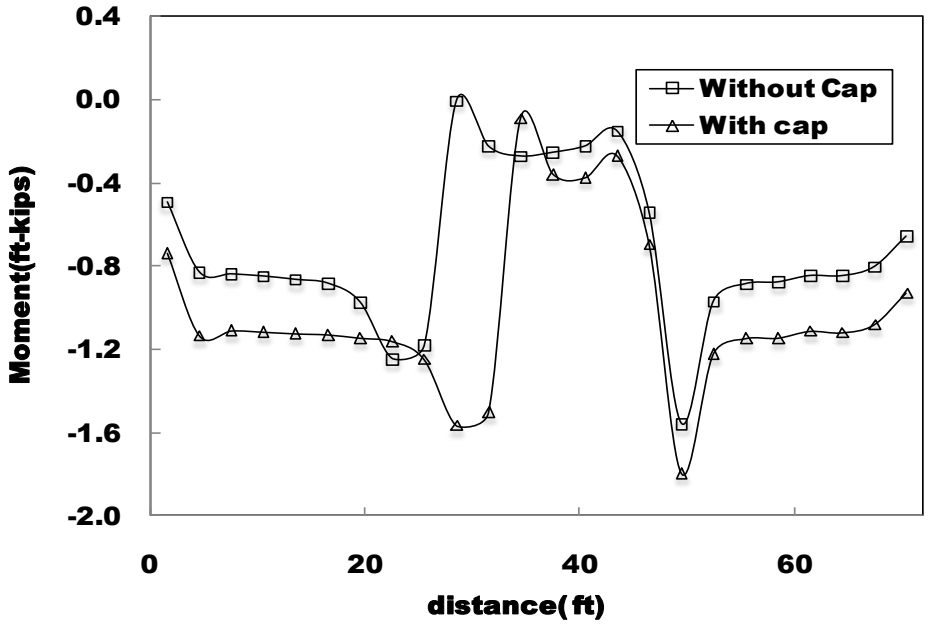

Figure 4.37. Moment at the sheet pile about the vertical axis of the wall

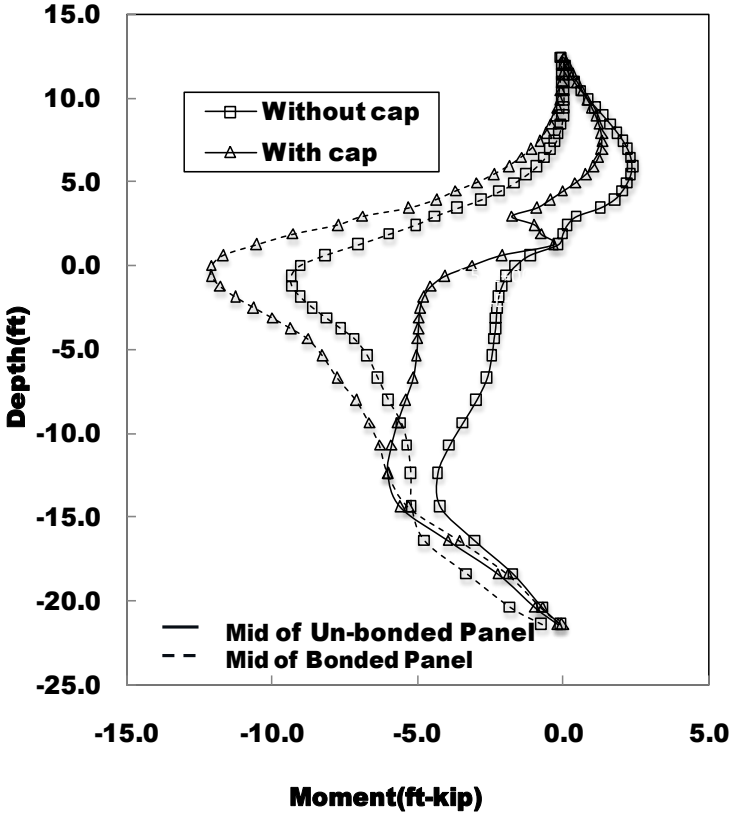

Figure 4.38. Moment about horizontal axis of the wall

In this case, from the above figures, it is seen that there was a significant reduction of both the relative displacement and the overall displacement on the two adjacent panels when cap was installed. Also the moment distribution was significantly changed due to the installment of the cap. As in the previous cases, the computed moment and the moment of the resistance of the typical I-wall were compared and are shown in the Table 4.4. From the table it can be seen that for the whole section of the wall, the developed moment is below cracking moment, which means the loads associated with this case are still in the pre cracking stage.

Table 4.4 Comparison between the computed bending moment and the moment of resistance

S/N	**Section**	**Moment of resistance (ft-lb)**				**Computed moment (ft-lb)**
		Real strength		ASTM Design Strength		
		Assumpt.1	*Assumpt.2*	*Assumpt.1*	*Assumpt.2*	
1	a	40,416.75	**52,629.62**	34,155.00	**44,045.38**	**12100**
2	b	12,593.63	**24,430.92**	10,642.50	**20,222.76**	**4380**
3	c	28,681.78	**39,175.00**	24,238.13	**32,825.03**	**26800**
4	d	8,872.78	**19,366.00**	7,498.13	**16,085.03**	**3770**

To see if the sheet pile was yielded or not, we compared the stresses developed in the sheet pile with its yield strength. In this case, maximum moment in the sheet pile computed by FLAC^{3D} was 12100 lb-ft (M_y) and 1570 lb-ft (M_x). For these moments, the stresses developed in the sheet pile due to M_y was 0.39ksi and due to M_x is 0.05 ksi which are far below the yield strength of the sheet pile.

4.4 SUMMARY

The main objective of this study was to evaluate the performance of the structural cap. After the comprehensive analysis, the results were apparently not that persuasive to confirm the effectiveness of the cap in reducing the overall displacement of the system. From the study, it was found that the structural cap is very effective in the third case to reduce the relative displacement of the adjacent panels as well as the overall displacement of the floodwalls. In the first two cases, though it was not that effective in reducing the overall displacement of the system significantly, it was effective in restricting the relative displacement of the adjacent panels. The moment distribution was also not improved by the incorporation of the cap in the first two cases. Though the result was not that persuasive apparently, we can still convince our self to one point that since the relative displacement was totally restricted; the cap helps to integrate the panels in one system. This would eventually prohibit the localized weak panel to fall individually.

The other outcome of this analysis was that the variation of the soil strength and non uniform erosion along the I-wall results the higher bending moment about the vertical axis (lateral bending stress) which is not addressed in the current design guidelines of New Orleans floodwalls. This can be seen by comparing the moment of resistance of the typical cross section with the computed bending moment. The typical section of the I-wall fails to satisfy the minimum reinforcement requirement which is given in Eq. (4.29) (ACI 1984):

$$\rho_{\min} = \frac{200}{f_y} \tag{4.29}$$

For f_y = 60 ksi, ρ_{min} is 0.0033, but for the typical section, calculated ρ was only 0.0029 for the section at top of the wall and 0.0012 for the section at the bottom of wall.

As an evidence to support the limitations in design guidelines, Seed et al. (2008) pointed out that most of the concrete capping of the South breach of IHNC was spalled since the concrete couldn't withstand the tensile stress caused by the excessive bending of the I-wall due to erosion. As already discussed, the final breach scenario that was observed during Katrina was only possible due to the progression of the local breaches. The initiation of the breach might have started by the localized spall of the concrete panel due to high bending stress. This spall of the concrete capping would result in the uncontrolled erosion and thus expanding the breach wider and wider in an exponential manner. So if only the initiation of the breach can be restricted, the large global breach would eventually not occur.

Modeling the full phase breach is not possible numerically. From the numerical simulation we can only observe the onset of the breach and the factors that led to such failures. But it can still be explained that the full breaching of I-wall during hurricane Katrina must be a result of the propagation of the small scale localized failure and this propagation rate must be higher and higher as time elapses within the time span between the onset of the localized breach and the final global breach.

From the above discussion, it is relevant to point out that the lateral bending stresses developed due to the local breaches and the erosion should be looked upon seriously and should be incorporated in the design guidelines. Some may argue that the bending stresses developed due to this condition are manifold high that construction of such structure will be very uneconomical. But the main point is that the bending stress developed for the final breach may be high but it is not that high during the onset of the failure (stresses found from this study). And

if we can design the section to withstand the onset of the localized structural failure, we may eventually prevent the large breaching.

So from this study, it may be logical to conclude that though we have to include cap for the integrity of the I-wall system, the moment induced by the variation of the shear strength and non uniform erosion along the I-wall section should be in the forefront of the factors while designing the I-wall section for the new construction. The specific conclusions from this study are summarized as followings

- The structural cap are effective in reducing the relative displacement of the adjacent panels, thus restricting the gap between them which otherwise would add further instability of the system.
- The lateral bending stress developed due to the soil strength variation and the non uniform erosion is manifold higher than the vertical bending stress developed due to the hydraulic load. So incorporation of this issue is recommended in the future design of the floodwall.
- The inclusion of cracking in the modeling has a prominent effect on the computed moment and the deflection of the wall
- The anisotropy of the sheet pile has effect upto 0.1. Anisotropy more than this magnitude does not have significant effect on the computed deflection and the rotation of the wall.
- The existing I-wall in New Orleans is brittle in nature i.e. the service load region on the moment curvature curve is very narrow.

5. ANALYTICAL AND NUMERICAL SIMULATION TO EVALUATE THE EFFECT OF GAP AND TO EVALUATE THE SELF HEALING MECHANISM OF THE BENTONITE APRON

5.1 BACKGROUND

Lessons learned from Hurricane Katrina can be the main basis on which the principles for improved design of the floodwalls for the next hurricane season can be formulated. Hurricane Katrina occurred in August 29, 2005 and was the costliest natural disaster and one of the five deadliest hurricanes in the history of United States which took 1836 lives with a total property damage of $81 billion (Knabb et al 2006). Due to Hurricane Katrina, 53 levee and floodwall sections were breached in New Orleans and St Bernard Parish areas. Due to these breaches, about 80 % of the city of New Orleans and 100% of St. Bernard parish were flooded.

After Hurricane Katrina, many studies were conducted to find the failure mechanisms that led the catastrophic failure of the floodwalls in New Orleans. Though there are minor controversies between the two major studies conducted by IPET (2007) and ILIT (2006), they stood on the common ground in pointing out that there were four major failure mechanisms such as gap formation on the canal side; overtopping of the floodwall; shear failure of the weak soil layer; and the under seepage induced failure. In this paper, the failure induced by gap formation, and the countermeasures to control its development is discussed in detail.

The effect of gap formation was not included in the initial design of the floodwall (Brandon et al. 2008). This phenomenon turned out to be an important issue after Hurricane Katrina, and many studies considered it to be one of the most important candidates that led the failure of floodwalls, especially I-walls during Hurricane Katrina. It is also worthwhile to note that both IPET (2007) and ILIT (2006) proposed an entrenched inclusion of gap formation in the improved design guidelines.

There have been a lot of researches conducted about the gap formation. Duncan et al. (2008), Brandon et al. (2008), Sills et al. (2008) IPET (2007), and ILIT (2006) have common explanations about the unfavorable conditions associated with it as shown in Fig. 1. They pointed out that the formation of the gap allows the water to penetrate through the gap exerting a direct hydrostatic pressure that is greater than the earth pressure that would act on it if there were no gap. The other implication of the gap formation is that it shortens the water path towards the sub surface soil, increasing the pore pressure in sandy soils causing an uplift pressure on the base of the layer above, and subsequently increasing the instability. The formation of the gap also reduces the shear resistance of the soil in the flood side because the failure plane does not extend beyond the base of the sheet pile reducing the weight of the soil wedge to be displaced.

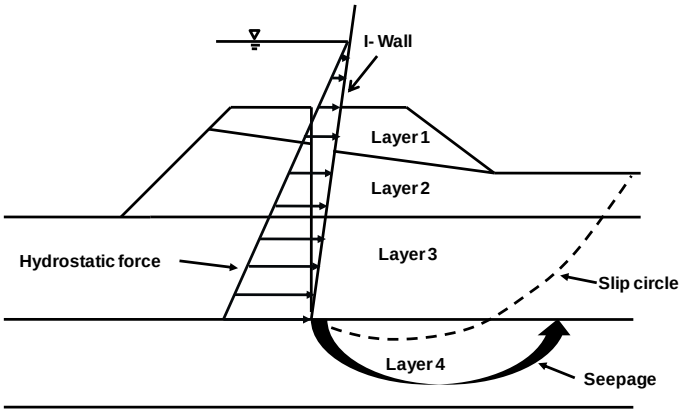

Figure.5.1. Implications of gap formation

The analytical evaluation conducted by Brandon et al (2008) showed that gap formation is the natural occurring phenomenon once the wall is loaded horizontally and was therefore regarded as the frequent cause of the failure. They studied the effect of gap on the stability of I-wall, and formulated some closed form equations to calculate the depth of gap for homogenous and layered cohesive soil using total stress approach and the limit state equilibrium principle. In an attempt to overcome the limitation of total stress approach, this study formulates the closed form equations for the effective stress approach, where the pore water pressure and the stresses due to soil are taken separately. Apart from that, this study also evaluates the effect of gap numerically using the same approach where the underground seepage is incorporated so that the coupled effect of both the shear stress and the pore pressure generation is incorporated to investigate the effect of seepage force on the stability of the levees and floodwalls.

Though formation of gap worsens the stability of the floodwall and levee section both during the pre- and post-failures, there might be controversy regarding weather those gap is the cause or the result of the failure. So in this paper, author investigates this issue for two typical floodwall sections which are different in geometry and soil conditions. The underlying hypothesis of this investigation is, whether gap is the cause or the result of failure depends upon the geometric configuration of the levee section, and the relative differences of the stiffness of the layered soil. Again, for those conditions where gap is the cause of the failure, it was again necessary to investigate whether the gap is the primary or the secondary cause of the failure so that the effective retrofitting technique can be devised. So this study also investigates this issue to distinguish the conditions where the gap is the sole or the secondary cause of the failure.

No matter whether gap is the primary, or the secondary cause of the failure, bentonite apron has been proved experimentally in the lab fabricated small scale floodwall (Kidd 2011) as

an effective mechanism for self sealing gaps. Bentonite apron is the buried layer of bentonite and sand mixture which has the potential to swell, and restrict gap development to prevent water infiltrating those gaps. However, it is still necessary to verify that the bentonite apron doesn't apply excessive pressure on the wall, and at the same time it has the potential to swell at all water levels, so that the effectiveness of self sealing mechanism can be confirmed. So in this study, the author addresses this issue by evaluating the effectiveness of the bentonite apron in real floodwalls in real loading conditions

This study is primarily divided into two sections. In the first section, an analytical evaluation is conducted to compare the total horizontal pressure acting on the wall for gap condition and no gap condition. Then the numerical evaluation is conducted where the comparison of the deflection at the top of floodwall is performed for those conditions. Subsequently, the study also investigates and identifies the situations where the gap is the cause or the result of the failure. For the situation where gap is the cause of the failure, author tries to investigate the effect of gap on the overall behavior of the real floodwall of New Orleans to justify the use of gap sealing material (bentonite apron). Ultimately, in the second section of this study, author evaluates the effectiveness of the bentonite apron for real conditions.

5.2 ANALYTICAL EVALUATION OF THE EFFECT OF GAP

The effect of gap can be evaluated analytically before the numerical analysis is conducted. Brandon et al. (2008) evaluated it for the total stress analysis. In this study, author developed an effective stress approach to quantify the effect of gap. For layered soil profile and effective stress analysis (for drained parameters), horizontal effective earth pressure may be calculated differently for steady state and transient flow conditions.

For the steady state flow condition, the total horizontal pressure acting on the wall and sheet pile at a depth z from the levee surface due to soil and water in no gap condition is approximately given by (Figure 5.2a)

$$\sigma_h = K.\sigma_v^{'} + u \tag{5.1}$$

For the layered soil, expanding Eq. (5.1), Eq. (5.2) is obtained.

$$\sigma_h = K_i.(\sum(\gamma_i{'}h_i) + iz\gamma_w) + \gamma_w(h_w + z) - iz\gamma_w \tag{5.2}$$

In above equations, K_i = coefficient of horizontal earth pressure for ith layer whose value lies between active, and at rest conditions; u = pore water pressure; h_w = height of water above the levee crest; h_i = height of the individual soil layer above the point of interest; z = depth of the point of interest below the levee crest; $\gamma_i{'}$ and γ_w = submerged unit weight of the soil and the unit weight of the water, respectively; and i = hydraulic gradient. In the above formulations, it is assumed that the hydraulic load is distributed infinitely on the levee crest neglecting it on the levee slope and the canal bed for simplicity.

The total horizontal pressure of the water exerting on the wall and sheet pile for the gap condition is given by (Figure 5.2b)

$$\sigma_{hw} = \gamma_w(h_w + z) \tag{5.3}$$

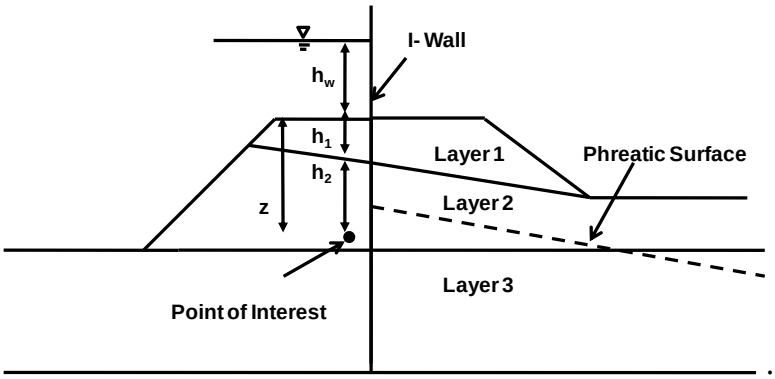

(a) No gap condition

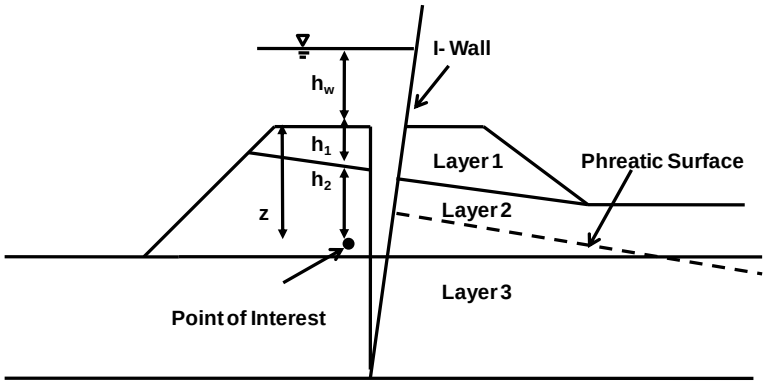

(b) Gap condition

Figure 5.2. The schematic of the geometry and location of phreatic surface for the steady state fluid flow condition

From above equations, it can be seen that the magnitude of total horizontal pressure during the steady state flow condition is governed by the hydraulic gradient. This is because the total horizontal pressure during no gap condition is decreased as the hydraulic gradient is increased as given by

$$\frac{\partial \sigma_h}{\partial i} = \gamma_w z(K_i - 1) < 0 \qquad (5.4)$$

Since, K_i is usually less than one for normally consolidated soils, $\frac{\partial \sigma_h}{\partial i}$ is always negative.

When the pressure on the wall and sheet pile in no gap condition and in gap condition is equal, hydraulic gradient may be evaluated by equilibrating Eq.(5.2) and Eq.(5.3), and Eq.(5.5) is obtained.

$$i_t = \frac{K_i}{1-K_i} \frac{\sum \gamma'_i h_i}{\gamma_w z} \tag{5.5}$$

where, i_t = threshold hydraulic gradient, above which the horizontal pressure on the wall for gap condition is higher than that for no gap condition. If in case, i is zero (steady state, no flow condition or hydrostatic condition), then obviously, the total horizontal pressure in the case for no gap condition is much higher than the water pressure for gap condition. If such condition prevails, then the system won't allow the gap to occur.

In the case of the transient flow analysis, above equations need to be modified as follows because of the unstable phreatic surface. Since the soil condition of the study site is undrained, and the loading duration of hurricane is very short, the author assumes that the phreatic surface does not change that much from the steady state Mean Water Level (MWL). Again, the total horizontal pressure acting on the wall and sheet pile at a depth z from the levee surface due to soil and water in no gap condition is approximately given by (Figure 5.3a)

$$\sigma_h = K.\sigma'_v + u \tag{5.6}$$

where,

$$\sigma'_v = \sum (\gamma_{ti} h_i + \gamma_i' h_i') \tag{5.6a}$$

and

$$u = \gamma_w z' + \gamma_w h_w \tag{5.6b}$$

In Eq. (5.6b), first term is associated with the hydrostatic condition whereas the second term is the excess pore water pressure as the soil condition is undrained. So, substituting Eq. (6a) and Eq.(6b) in Eq.(6), Eq.(7) is obtained.

$$\sigma_h = K_i \cdot \sum (\gamma_{ti} h_i + \gamma_i' h_i') + \gamma_w z' + \gamma_w h_w \tag{5.7}$$

Simplifying,

$$\sigma_h = K_i \cdot \sum (\gamma_{ti} h_i + \gamma_i' h_i') + \gamma_w (z' + h_w) \tag{5.8}$$

where, γ_{ti} = moist unit weight of the soil of ith layer; h_i = height of soil of the ith layer above the phreatic surface; and z' = depth of the point of interest below the phreatic surface. Other symbols represent the same physical quantities as described earlier. The schematic of the geometry and the location of phreatic line are shown in Figure 5.3a.

The expression for the gap condition should be the same as Eq. (5.3) and is shown in Figure 5.3b.

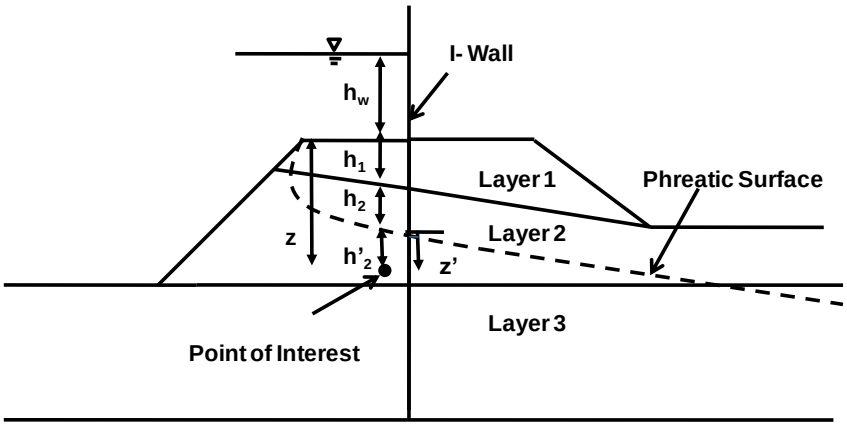

(a) No gap condition

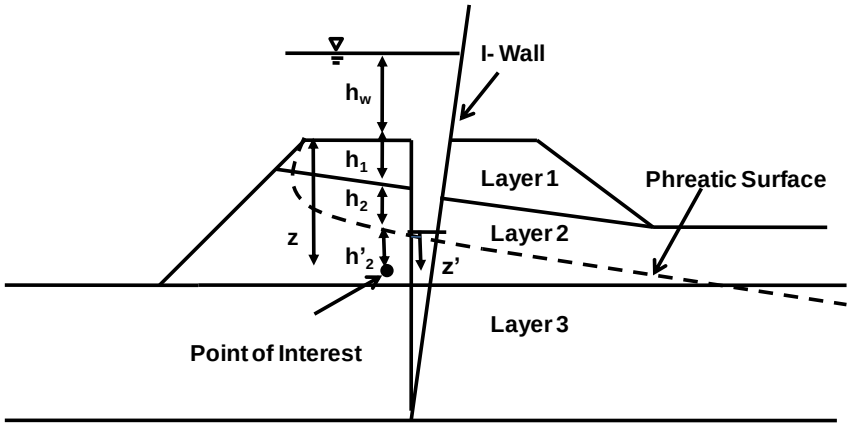

(b) Gap condition

Figure 5.3. Schematic of the geometry and phreatic surface for the transient fluid flow condition

In transient flow condition, water pressure in gap condition is always higher than the total horizontal stress due to soil and water in no gap condition. This is why for the transient flow analysis; there is always a higher chance of gap formation. To justify this, comparison of the depth wise distribution of horizontal pressure exerted on the wall and sheet pile for the gap and no gap conditions for the transient flow condition are made and are shown in Figure 5.4.

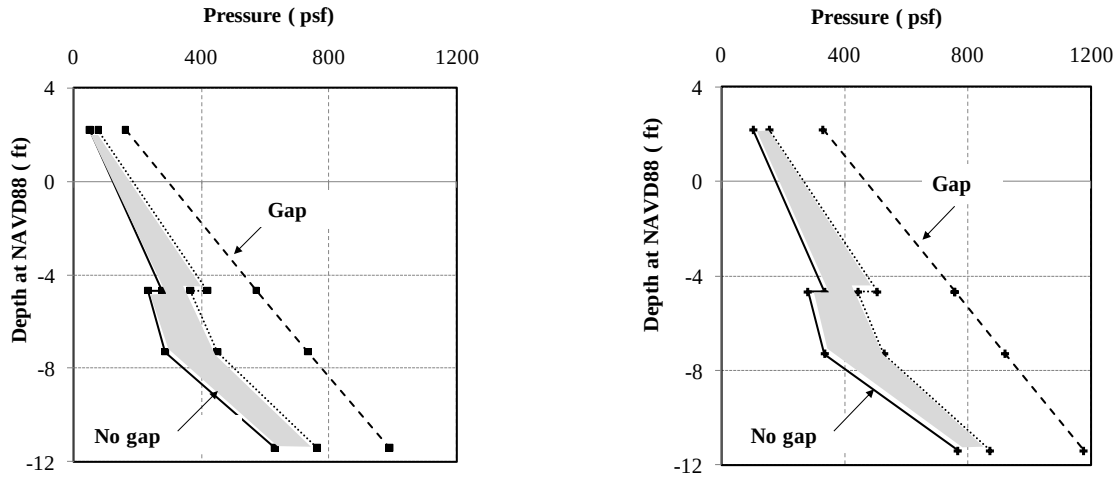

(a) At water level 4.5 ft at NAVD88 Scale (b) At water level 7.5 ft at NAVD88 Scale

Figure 5.4. Comparison of the horizontal pressure acting on the sheet pile at gap condition and no gap condition

From the figure, it can be seen that the water load for the gap condition is always greater than the total horizontal pressure for no gap condition. Therefore, it can be inferred that the gap condition is more critical than the no gap condition in transient flow condition. And this could be the reason why gaps caused the failure of levees and floodwalls in New Orleans. Therefore, from this evaluation, relevancy of any methodology to seal the gaps is fully justified.

5.3 NUMERICAL EVALUATION OF THE EFFECT OF GAP ON OVERALL PERFORMANCE OF WALL

Numerical simulation was conducted to advocate the findings from the analytical solution regarding the effect of gap on the overall performance of the floodwall. The details are described in the flowing subsections.

5.3.1 Modeling tool and Condition

Fast Lagrangian Analysis of Continua or FLAC^{3D} (Itasca consulting group 2006) was used for the numerical analysis of the floodwall. It is a finite difference code to solve quasi-static problem using dynamic approach. To model the static response of a system, damping is used to absorb all the kinetic energy. It has the capability of large strain calculation mode.

To mimic the real behavior of the floodwall, and to account the effect of the pore water distribution on the mechanical stress strain calculations, effective stress analysis was conducted. With this analysis, the effect of the hydro-mechanical behavior of the soil can be fully accounted.

5.3.2 Model site, Geometry and Soil Profile

The specific floodwall section of the London Avenue Canal of New Orleans was taken in the study. This floodwall section was not the breached one during Hurricane Katrina but was the one where the full scale load test (Hurricane Protection Office or HPO 2008) was conducted in 2007. The geometry and the soil profile of the model section are shown in Figure 5.5.

Since this study was done to find the effect of the gap on the overall performance of the wall, a fictitious cofferdam was built at the toe of the levee on the canal side so that the influence of the loading and the seepage from the base of the canal would be negligible and only the effect of gap could be studied independently.

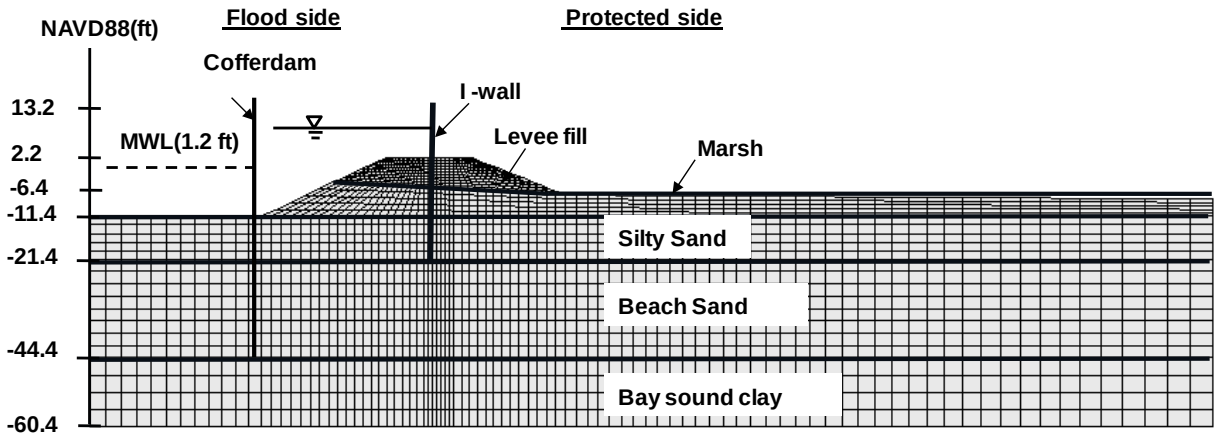

Figure 5.5. Model geometry showing soil Profile

The soil profile consists of the embankment soil with four layers of foundation soil. The embankment soil is basically the clay layer of CL/CH consistency (IPET 2007). This layer extends from Elevation (EL.) 2.2 feet to EL. -4.7 ft in North American Vertical Datum of 1988 (NAVD 88) scale at the center of the levee section. Underneath the embankment layer, there is a marsh layer which is categorized as the peat layer and extends up to EL. -11.4 feet. The peat layer is underlain by the silty sand layer extending upto EL. -21.4 feet. Underneath silty sand layer lies the sand layer categorized as the beach sand by HPO (2008) that extends up to EL. -44.4 ft. Below this layer lies the stiff clay layer which is categorized as Baysound clay.

5.3.3 Soil, Structural and Soil–Structure Interfacial Parameters

Mohr Coulomb (MC) model was used to represent the constitutive behavior of soils while elastic model was used for the concrete capping and the sheet pile. In case, if the stresses in the sheet pile and concrete capping are more than the yield strength, then the plastic model should be used. But this was not the case in this study, since the stresses in the sheet pile and concrete capping were below the yield strength.

The strength and the stiffness parameters; and the coefficient of hydraulic conductivity of each soil layer in Figure 5.4 were taken from IPET (2007) and Seed et. al. (2008[a]) and is shown in Table 5.1. Since the hydro-mechanical simulation was done, effective stress parameters were adopted for this study. As the value of shear modulus has no significant difference in the drained and the undrained conditions, same shear modulus for the undrained case in IPET (2007) was taken and the bulk modulus, K, was calculated by

$$K = \frac{2G(1+\nu)}{3(1-2\nu)} \tag{5.9}$$

where, G = shear modulus; and ν = Poisson's ratio of the soil.

Poisson's ratio may be derived from the theory of elasticity (e.g. Terzaghi, 1943) ($\nu = K_0/(1+K_0)$) for silty sand and beach sand. And since most of the soil layers in New Orleans are in normally or slightly overconsolidated state, coefficient of the lateral earth pressure may be estimated from Jaky's (1944) relation ($K_0 = 1-\sin\phi$). For cohesive soils on the other hand, which are comparatively in undrained condition, Poisson's ratio was taken to be equal to 0.35. (Seed et al. 2008[a])

The permeability of marsh layer taken from the IPET (2007) is necessarily the same one that was found during the parametric study by Seed et al. (2008[b]).For simplicity, isotropic hydraulic conductivity was used in this study.

As far as the stiffness and the permeability of silty sand are concerned, it depends upon the percentage of fine content in the sand. According to Salgado et al. (2000), the stiffness of silty sand for the same confining pressure and the void ratio (20-50 kPa effective stress and void ratio of 0.57) is: 50 to 80 MPa for clean sand; 30 to 65MPa for 5% fine content; 25 to 55 MPa

for 10 % sand and 10 to 25 MPa for 20 % fine content. From this trend of the effect of fine content on the stiffness of the silty sand, it is seen that the silt content can reduce the stiffness upto 30 % of the clean sand. Since the fine content of the silty sand for the concerned site was not known, the stiffness was assumed to be about 60 % of that of beach sand. This relation is consistent with the calibrated parameters by Adhikari et al. (2009). As long as the permeability of silty sand is concerned, Bandini and Sathiskumar (2009) confirmed the reduction of permeability by upto 200 times for the 20 percent of fine content whereas for the 10 percent of fine content, it reduces by about 25 times (6e-4 cm/s) that of clean beach sand. So in this simulation, two cases were taken where the permeability of silty sand was 25 and 250 times less than that of the beach sand. According to Terzhagi et al (1996), the permeability of sillty sand is between 1e-3 to 1e-7 cm/s which is consistent with the range used in the analysis.

Table 5.1. Soil Parameters

Soil layer	ϕ'	γ_d **(pcf)**	**G (psf)**	**v**	**n**	**k (ft/s)**
Levee-fill	32	83.96	2.81e4	0.35	0.4	3.2e-8
Marsh(Toe)	36	57.58	9.39e3	0.35	0.4	3.2e-6
Marsh(Center)	36	57.58	1.25e4	0.35	0.4	3.2e-6
Silty Sand	31	90.72	2.81e4	0.32	0.4	2e-5/ 2e-6
Relic Beach Sand	36	95	4.69e4	0.29	0.4	4.9e-4
Bay sound Clay	36	99.7	1.56e5	0.35	0.4	3.2e-8

Note: ϕ' = Internal friction angle; γ_d = dry unit weight of the soil; G = Shear Modulus of the soil; v = Poisson's ratio; n = porosity; k = hydraulic conductivity.

The sheet pile was modeled using FLAC^{3D}'s structural element called "embedded liner", which is a modified shell element enslaved with interface and has the capability of incorporating sliding and gap development between the sheet pile and soil. According to Itasca (2006), strength properties of interface are important, but stiffness properties are not. So, to reduce the

computation time for the varying stiffness of the soil layers, the maximum interface spring constants can be evaluated as Eq. (5.10) as recommended by Itasca (2006):

$$k_s \approx k_n \approx 10 \cdot \left[\frac{\left(K + 4/3G\right)}{\Delta z_{\min}} \right] \tag{5.10}$$

Where *Δzmin*= smallest width of an adjoining zone in the normal direction; and *K* and *G* = bulk modulus and shear modulus of soil, respectively.

As far as the strength parameters of the interface are concerned, for effective stress analysis, they are given in terms of the interface angle of friction, δ to be 0.67 times the friction angle of the adjacent soil (Bowles 1996). In the case of silty- sand (dirty sand), the interface angle of friction, δ was taken to be 14^o (Bowles 1996; USACE 1994).

The concrete capping of I-wall was modeled using FLAC^{3D} zones. Elastic model was used to model the stress strain behavior of the Concrete. Around the concrete block, interface elements were used to simulate the interaction between the concrete and the soil, so that the gapping and slippage were considered at the interface. The same interface springs used for sheet piles were used in this case also.

5.3.4 Loading Condition

The loading condition for the simulation was taken the same as the load time history of the navigation canals of New Orleans during Hurricane Katrina (IPET 2007) and is illustrated in Fig. 6. To investigate the effect of gap on the overall deformation of the system, only upto EL. 7.0 feet (2.1m) of water level (WL) was taken to save the computational time.

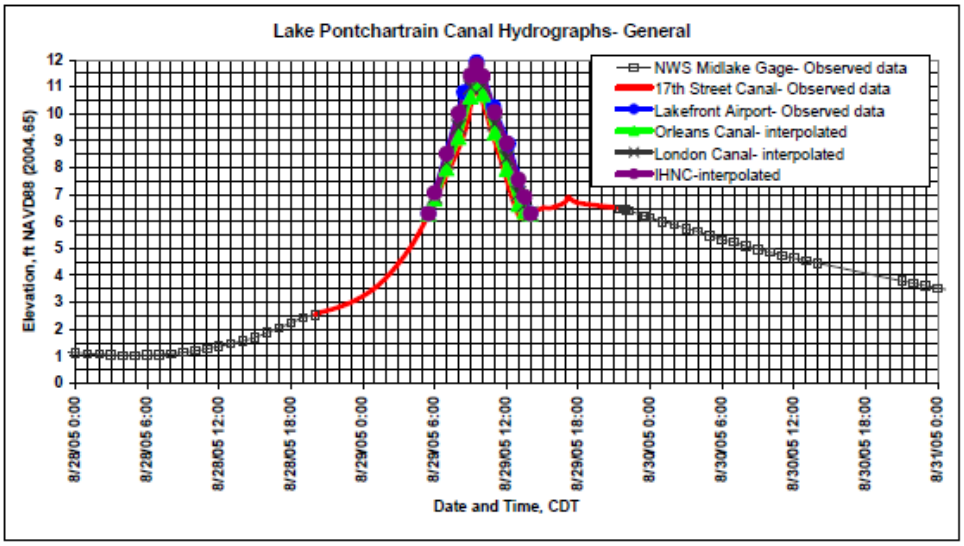

Figure 5.6. Hydrograph of lake Pontachrain canal (IPET 2007)

5.3.5 Simulation procedure

To obtain the realistic field conditions, the construction sequence of the soil, sheet pile, and the concrete capping was followed. For the numerical simulation, the initial stress condition and pore water pressure for the Mean Water Level (MWL) of 1.2 ft was established initially by bringing the system into elastic equilibrium by turning on the gravity slowly to avoid the dynamic oscillation of the system, and later by increasing the water level condition in small increments upto MWL. Initial pore water pressure condition was maintained using the measured piezometrical height as reported in HPO (2008). Then the model was re run for the MC elasto-plastic soil model. To maintain the K_0 condition of the foundation and embankment soil, "fish function' of FLAC^{3D} code was used to recalculate the initial stress condition and the deformation was initialized to zero.

Then the hydraulic pressure and the pore water pressure were applied on the levee surface and the floodwall with an increment of 1 ft to avoid dynamic oscillations of the system. Since the

fully coupled analysis could take a longer time, the uncoupled hydro-mechanical analysis was conducted. For the fluid flow analysis, transient analysis was conducted for which the fluid flow time for each load increment was taken from hydrograph shown in Figure 5.6.

One of the main problems when conducting a transient flow analysis is it takes a longer computational time especially when there is a vast contrast of hydraulic conductivities for different soil layers. This is specifically obvious when there is a presence of sand layer (high conductivity) since the time step taken for computation for sand layer is very small, and this time step is the governing time step for the whole grid .To overcome this problem, two step fluid flow analysis was conducted for each water level increment.

In the first step, the conductivity of the sand layer was decreased by two orders maintaining the actual conductivity of other soil layers. This would increase the time step and hence the computational speed by two orders. Then in the next step, the conductivity of the sand layer was maintained the actual value. But this time, the transient flow analysis was not run for the actual time but reduced to the time known as the 'characteristic time' that would allow the steady state flow condition in the sand layer. This characteristic time for the diffusion process was calculated using (Itasca 2006)

$$t_c^f = \frac{L_c^2}{c} \tag{5.11}$$

where, L_c = characteristic length (i.e. the average length of the flow path through the medium); c = diffusivity defined by (Itasca 2006)

$$c = \frac{k.K_f}{n} \tag{5.12}$$

where, k =mobility coefficient; K_f = bulk modulus of the fluid; and n = porosity of the soil layer.

Since t_c^f is much smaller than the actual fluid flow time in the field, this would not affect the diffusion process in other layers maintaining the accuracy of the solution.

It should also be noted that the effective stress parameters for the cohesive soils are the equivalent parameters to produce the undrained strength. So undrained effective stress analysis was conducted for the cohesive soils.

5.3.6 Result and discussion

Since the main objective of this study was to evaluate the mechanism that seals the gap opening during the loading condition so that the undesirable effect of gap could be minimized, the performance of the floodwall in gap and no gap conditions was compared in the numerical simulation. In this case, two other conditions were also included to see the effect of the mechanical load and the seepage force separately. In the first case, only the mechanical force was applied without applying pore pressure on the gap; and in the other case, the sheet pile was considered to be permeable that mimics the loosened interlock of cold rolled sheet piles while driving in dense sand (Sills et al. 2008). Different physical quantities like load deflection response; the shear strain distribution; and the effective vertical stress were evaluated for those conditions.

To see if gap is not always the cause, but sometimes the consequence of failure, the author also compared the performance of current floodwall section with the 17th street canal section. Subsequently, since silty sand has the wide range of permeability (depends on the fine content) the author also compared the simulations considering those variations to identify the conditions (permeability) in which the gap formation is not the primary, but the secondary cause of the failure.

5.3.6.1 Load displacement curve

The load vs. displacement at the top of the wall was drawn to compare the four conditions such as 1) no gap condition; 2) gap with water pressure but no pore pressure acting on the soil adjacent to the sheet pile; 3) gap with pore pressure acting on the soil adjacent to the sheet pile; and 4) the gap condition for the permeable sheet pile. The load vs. displacement curve for these four cases is sown in Figure 5.7.

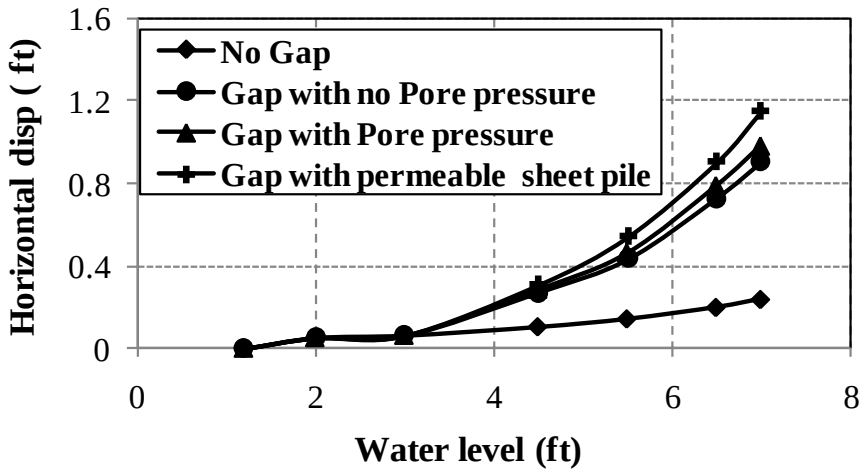

Figure 5.7. Load deflection curve

From the figure, it is clear that the gap condition is more critical than the no gap condition when considering the deflection pattern of the floodwall. From the figure, it can also be inferred that the severity of the gap condition evolves not only through the higher pressure acting on the wall and sheet piles, but also through the higher pore pressure caused by the gap opening as depicted through the difference in deflections for the second and third cases. On top of that, if the sheet piles are permeable, then the gap condition is even more critical.

5.3.6.2 Shear strain with deformed shape

To justify the unfavorable effect associated with gap opening, the author also looked upon the shear strain in soil elements on the protected side of the levee. The shear strain for the four cases is shown in Figure 5. 8.

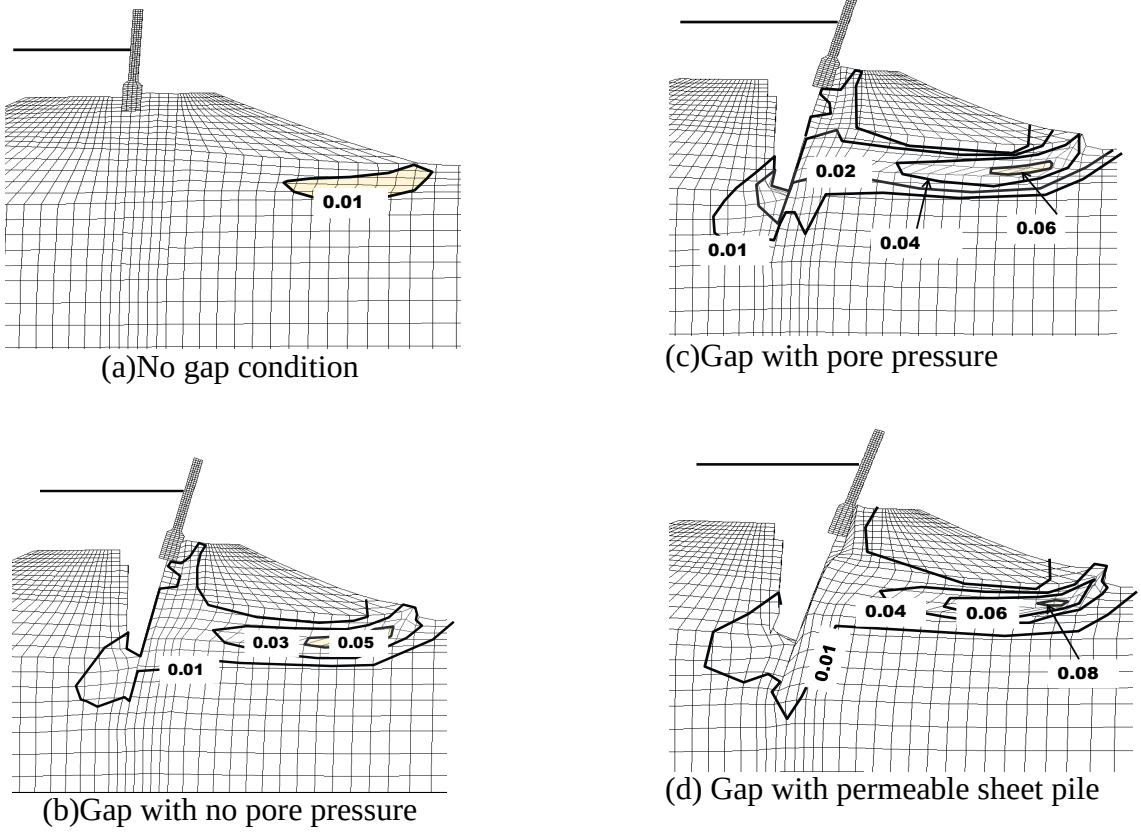

(a)No gap condition

(c)Gap with pore pressure

(b)Gap with no pore pressure

(d) Gap with permeable sheet pile

Figure 5.8. Shear strain at 7 ft loading condition (ten times exaggerated)

From the figure, it is seen that, in comparison to no gap condition, there has been a significant increase in the value of shear strain in the soil for gap condition with no pore pressure acting on the soil adjacent to the sheet pile. If the pore pressure was allowed to act on the soil adjacent to the sheet pile during the gap formation, then the shear strain increased even more. This is due to the increase in the pore pressure in the soil causing a decrease in the effective

stress as other conditions are the same. In the case where the sheet pile was assumed to be a permeable one, the shear strain was increased even substantially. The increase in the shear strain was because there was a direct contact of marsh layer with water increasing the pore pressure dramatically, and thus decreasing the effective vertical stress. With this, there was shear yield of the soil at the marsh and silty sand interface causing the sliding of the of soil block along the yielded elements. Evaluating these scenarios, it can be concluded that there is a negative impact of the gap formation on the overall performance of the floodwalls.

5.3.6.3 Effect of gap on horizontal stress and effective vertical stress

To investigate the causes of an increase in deflection and shear strain increment due to the gap condition, the effect of gap on the total horizontal stress and effective vertical stress of soil was also evaluated. Since horizontal stress is the major principal stress in the protected side of the floodwall, it has a greater impact on the instability of the floodwall. To see the effect of gap on the horizontal stress, no gap condition and gap condition without the distribution of the pore pressure on the adjacent soil of the gap was compared and is shown in Figure 5.9. Pore pressure distribution (seepage from gap) was not incorporated as the boundary condition on the soil elements adjacent to the gap to investigate the effect of gap formation on the development of mechanical stress only.

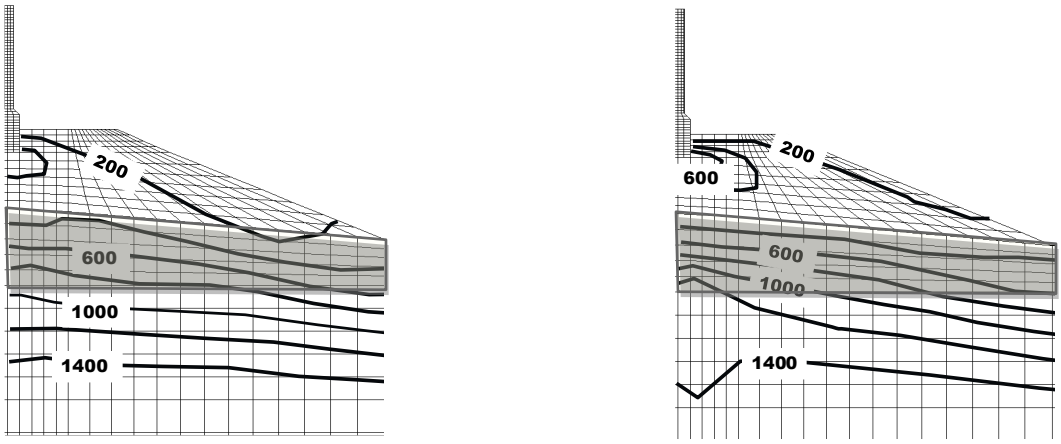

(a) No gap (a) Gap with no pore pressure

Figure 5.9. Total horizontal stress (psf) on the soil at 7 ft (2.1m) Water Level (WL)

From the figure, it is seen that in the gap condition, the soil on the land side is horizontally stressed more than that during no gap condition.

Apart from increasing the stress on the soil, there was also the reduction in the shear strength of the soil on the passive side due to the opening of the gap. This reduction in the shear strength was primarily due to the decrease in effective vertical stress during the gap condition. This is evident from the comparison of the vertical effective stress on the landside of the floodwall for four different cases and is shown in the Figure 5.10.

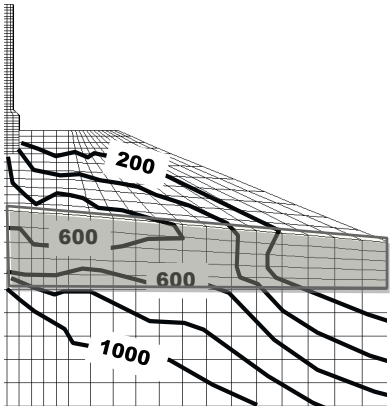

(a) No gap

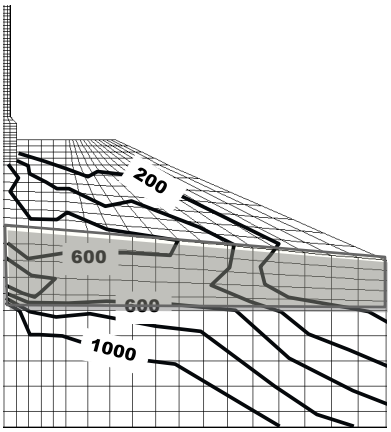

(c) Gap with pore pressure distribution

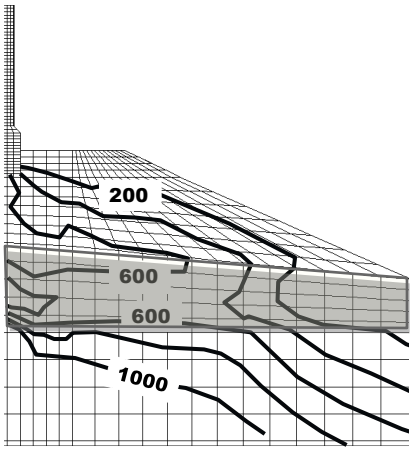

(b) Gap with no pore pressure distribution

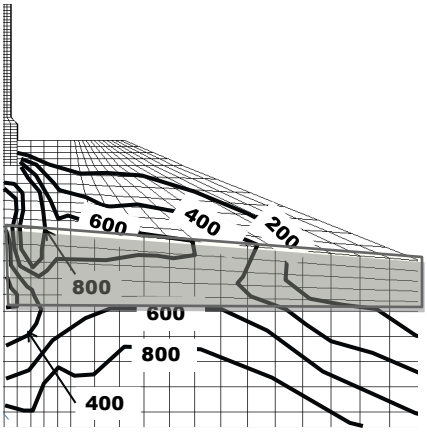

(d) Gap with permeable sheet pile

Figure 5.10. Distribution of effective vertical stress (psf) on the soil at 7 ft

From the figure, it is seen that for the gap condition, even when there is no pore pressure distribution in the adjacent soil (case b), there is a reduction in the effective vertical stress because of the development of transient pore pressure due to the undrained characteristics of the marsh layer which is in direct contact with the hydraulic load due to gap opening. To advocate that that transient pore water pressure is more severe, the drained and undrained analyses were performed for case (b) and are shown in Figure 5.11.

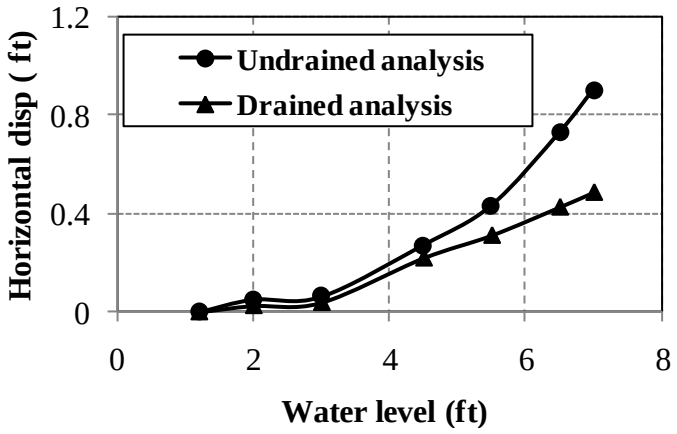

Figure 5.11. Load deflection curve for case (b) using drained and undrained analysis

From the figure, it is seen that the undrained condition of the soil induces a higher pore pressure which result in the decrease of the effective vertical stress of the soil as reflected by the larger deflection of the wall top in Figure 5.7.

Again, from Figure 5.10, if case (b) and (c) are compared; there is not much difference in the effective vertical stress. But if the sheet pile is permeable (e. g. case d), there is a significant reduction of the effective stress in the marsh and silty- sand zone due to high seepage pore pressure. From this result, it is seen that there is a reduction of the shear strength of marsh layer due to the gap opening.

5.3.6.4 Effect of permeability of silty sand

In the previous section, the author mentioned that depending on the fine content, there is a wide range of permeability of silty sand. The model site is located on the London Avenue Canal where two major breaches occurred during Hurricane Katrina induced primarily due to under seepage, which depends basically on the permeability of the silty sand layer. So, it is

relevant to study the effect of permeability of silty sand on the overall performance of the floodwall.

From the previous result, it was seen that the gap opening always exacerbates the stability condition of the floodwall. But at the same time, it should also be noted that there might be other factors that play together with the gap opening so that other countermeasures should be implemented in conjunction with controlling gap formation. Therefore, author investigated this issue by choosing no gap condition in the analysis to see if other failure candidate exists or not depending on the permeability of the silty sand layer.

In the previous analysis, the cofferdam was built on the flood side to see the effect of the gap solely without incorporating seepage from the base of the canal. In this section, the cofferdam was removed to see the effect of the seepage from the base of the canal for the case of two extreme values of permeability of silty sand, and the result is shown in Figure 5.12. From the result, it is seen that for the higher water level, even no gap condition for the higher permeability of silty sand is critical, whereas that for the lower permeability, it is not that critical. Even more, in the case of higher permeability, due to the higher seepage pressure, there was a heave at the toe of the levee on the protected side. But in the case of lower permeability, there was no heave observed at that place. So from this result, it may be concluded that though gap opening plays an unfavorable condition for the stability of the wall, it may be conjugated with other failure mechanism depending on the permeability of silty sand.

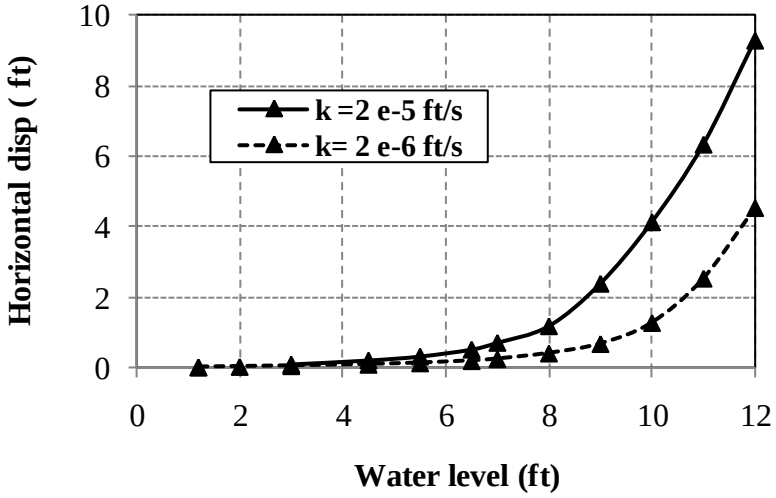

Figure 5.12. Load deflection curve for case (a) for different permeability (ft/s) of silty sand

5.3.6.5 Effect of geometry and relative difference of stiffness of soil layers

To see if the gap is the cause of the failure for all soil conditions, and geometry of the levee or not, the author also investigated the response of 17th Street Canal section applying same loading condition and the same simulation procedures. This section is different in geometry, and the soil layer known as "Lacustrine Clay" at the elevation where the tip of the sheet pile rest, is very soft in nature which is different than that of the London Avenue Canal. No gap condition was taken and the response for the two geometric conditions was compared to see if gap occurs on those sections or not.

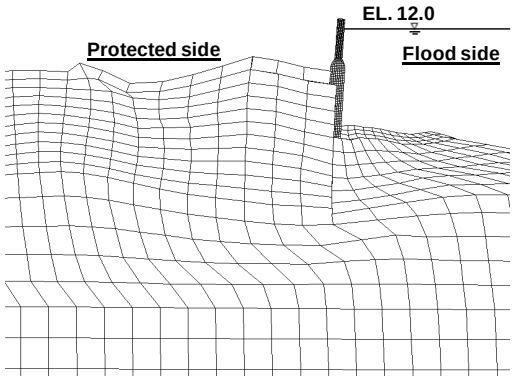

(a) 17th street canal floodwall(10 times exaggerated)

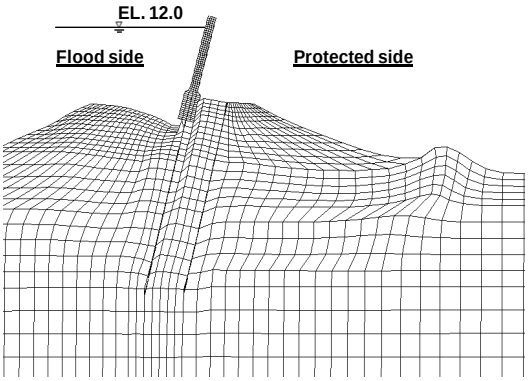

(b)London Avenue Canal (20 times exaggerated)

Figure 5.13. Configuration of the wall at 12 ft WL

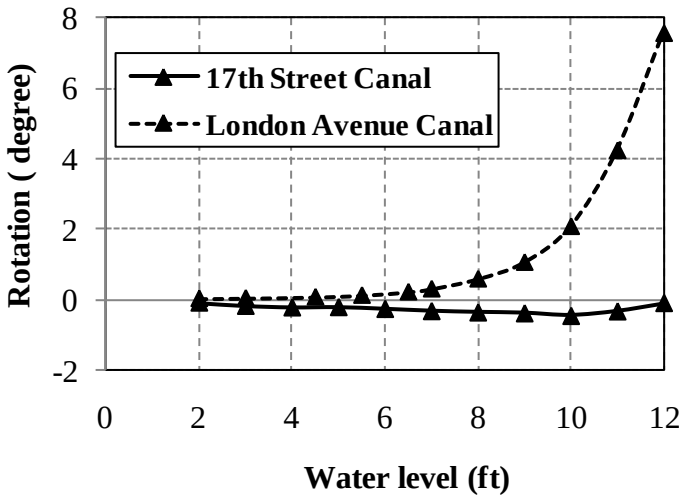

Figure 5.14. Rotation of the wall at different WL

Note: Positive is taken leaning towards protected side;

If the deformation configuration of the floodwall and the levee at the WL of 12 ft in Figure 5.13 is compared, it is seen that the top of the wall for 17th street canal leans towards flood side, while that of the London Avenue canal leans towards protected side.

Figure 5.14 shows the rotation angle of the floodwall for those sections. From the figure, it can be seen that for 17th street canal, the wall is rotated towards the flood side which increases upto 10 ft WL and decreases above that WL. From these results, it might be interpreted that since gap did not occur initially for 17th street canal, the cause of failure might be the shearing of the weak soil layer; gap occurred only after the soil mass slide. Therefore, in this case, the formation of gap might be the result of failure.

The possible retrofitting technique for this failure mode is reinforcing the weak Lacustrine clay and marsh layer with Deep Mixing Method (DMM) which is being practiced there. Author simulated the case incorporating DMM by increasing the stiffness of both marsh layer and Lacustrine clay by 2 and 5 times the original stiffness and also increasing the strength of the Lacustrine clay. By doing this, the author found that the deformation of the Lacustrine clay decreases, but it was also found that the decrease in this deformation eventually change the deflection pattern of the floodwall promoting the initiation of gap. It was found that gap initiates when the elevation of water level was 8 ft and 9 ft for the increase in stiffness by 5 times and 2 times the original one respectively.

In the case of London Avenue Canal, hydraulic load on the wall is large enough to cause the wall to lean on the land side, which obviously initiates formation of gap. This is also clear from Fig.14 where the rotation angle always increases as WL increases. So in this case, the gap formation is the cause of the failure.

5.4 EFFECT OF BENTONITE APRON ON THE PERFORMANCE OF THE FLOODWALL

5.4.1 Background

In the previous section, the author justified that the gap is always unfavorable (even if it is the consequence of failure), and the counter measure to avoid its occurrence is inevitable to improve the performance of the floodwall against severe loading conditions. One of the counter measures is the application of the bentonite apron**.** The experimental work (Kidd 2011) justified that bentonite is effective in self sealing mechanism. But it is still doubtful ,whether it has the adverse effect by exerting high swelling pressure on the wall than the actual water pressure if gap would allowed to occur, or not. In this section, the author tried to verify by numerical study that the bentonite apron is a feasible approach in self healing mechanism in the real floodwall for the real loading conditions without creating an adverse effect by exerting high swelling pressure on the wall.

5.4.2 Modeling Approach

Same model section of last section was used for this part of study except that the cofferdam had been removed to model the realistic scenario, and the loading condition was increased upto potential water level of 12 feet A bentonite apron of 1ft by 1 ft cross section was placed adjacent to the wall 1 ft below the levee crest on the canal side as shown in Figure 5.15.

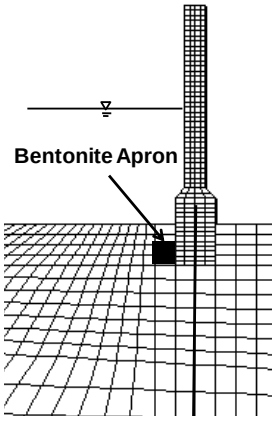

Figure 5.15. Layout of bentonite apron

From the numerical seepage analysis, it was found out that the soil in the proximity of the bentonite apron was essentially dry upto 3 ft (0.9 m) WL. It was only saturated during and after 4.5 ft (1.35 m) WL. So in the numerical analysis, the author assumed that the bentonite apron started to exert the swelling pressure around the soil and the wall at and above the WL of 4.5 ft (1.35 m).

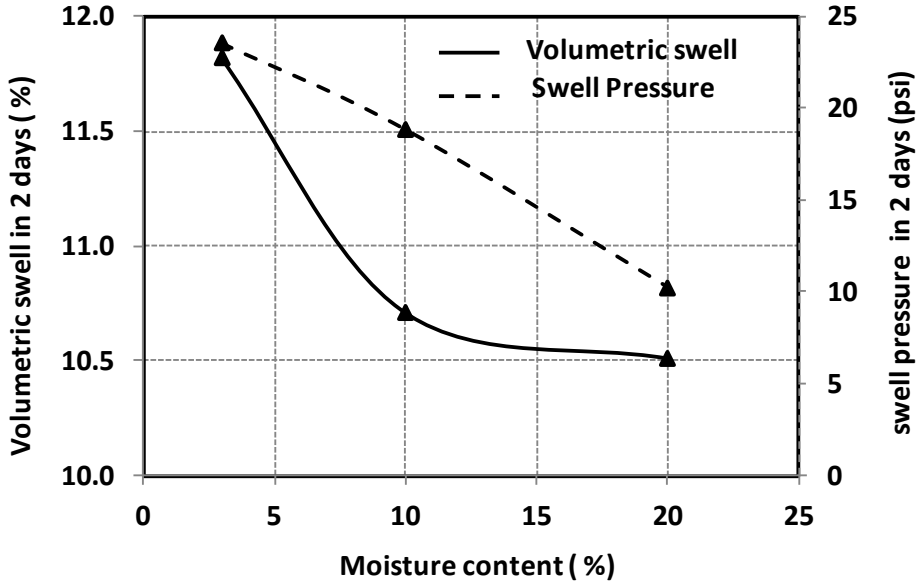

Figure 5.16a. 2 days swelling pressure and volumetric swell vs. moisture content for S70B30

The swelling pressure - deformation relationship was obtained from the laboratory tests. To characterize this relationship, the maximum swelling deformation was found out for 30 and 70 percent bentonite sand mixture (S70B30), since this mixture was proved in the lab to be the optimum mixture for the self sealing mechanism. This swelling deformation is essentially the deformation corresponding to the zero swelling pressure. Again the maximum swelling pressure corresponding to zero swelling deformation was also found out from the laboratory test for the same mixture

For this mixture too, the swelling pressure and the volumetric strain also varies with moisture content of the prepared sample. Two days swelling pressure and volumetric strain for varying moisture content is shown in Figure 5.16a. From Figure 5.16a, it is seen that both swelling pressure and volumetric swell decrease as the moisture content of the sample is increased. This is obvious and trend is similar to the one represented by Soil Water Content Characteristic (SWCC) curve. The moisture content range chosen in the lab test is the usual range observed in the field. For the numerical simulation, the extreme case (lowest volumetric swell and highest swell pressure) was taken, so that if the wall is safe and the plug swells enough to seal the gap for that case, it works for other cases too. Therefore, we used the swelling pressure for the minimum moisture content (3.6%) and the volumetric strain for the maximum moisture content (20%) in our simulation

For this case, the volumetric strain and swelling pressure vs. time relationship obtained from the lab is shown in Figure 5.16b

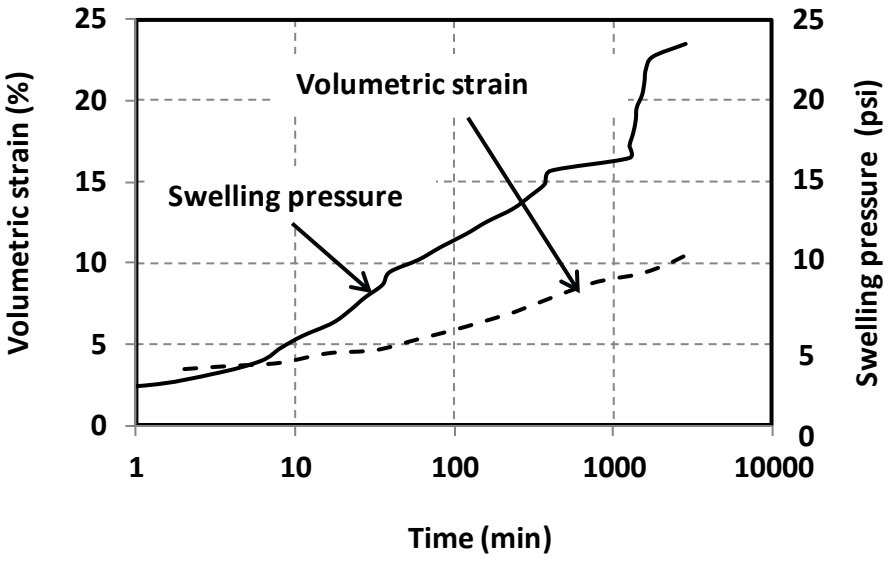

Figure 5.16 b. Volumetric strain and swelling pressure vs. time for S70B30

Since the laboratory test is conducted in the constrained condition (K_0 condition) to measure the swelling pressure and triaxial condition to measure the swelling deformation, unconstrained swelling pressure from the constrained (one-dimensional) swelling pressure can be evaluated by using the following equation.

$$\sigma_s = \frac{\sigma_{s,1}(1+2K_0)}{3} \qquad (5.13a)$$

Using $K_0 = \nu/(1-\nu)$, and simplifying,

$$\sigma_s = \frac{\sigma_{s,1}(1+\nu)}{3(1-\nu)} \qquad (5.\ 13b)$$

where, v = Poisson's ratio; K_0 = coefficient of earth pressure at rest condition; $\sigma s_{,1}$ = one dimensional (constrained) swelling pressure; and σ_s = unconstrained swelling pressure. Although the swelling pressure and deformation does not have linear relationship in reality, it was

idealized to be linear. This simplification is adopted since the material model to reflect time dependent swelling characteristic is unavailable in FLAC^{3D}.Using the above relationships, the linear relationship between deformation and the swelling pressure for the unconstrained case at any time, *t* after the saturation can be established. This can be proposed as

$$(\sigma_s)_t = \left\langle \sigma_{s,0} - \frac{\sigma_{s,0}}{\varepsilon_{s,0}} \varepsilon_s \right\rangle \tag{5.14}$$

where, $(\sigma_s)_t$ = swelling pressure for corresponding swelling strain ε_s at time t; $\varepsilon s_{,0}$ = free swelling deformation; and $\sigma_{s,0}$ = reference swelling pressure at zero strain. In the above equation, minimum swelling pressure can never be below zero as represented by Macauley brackets, < >. But at the same time, the above equation also shows that for the compression case, the swelling pressure would go on increasing with the increase in compressive strain. This relationship can be illustrated as Figure 5. 17.

The relationship between the swelling pressure and the deformation of the bentonite apron can be used in the FLAC^{3D} simulation using the' fish function'. The method includes the monitoring of the deformation of the bentonite apron at each computation step, and using the above relationship, the swelling pressure exerting on the nearby soil and wall elements can be calculated. Since the calculated swelling pressure can be comparatively high that might cause the numerical oscillations, attempt was made to apply it gradually.

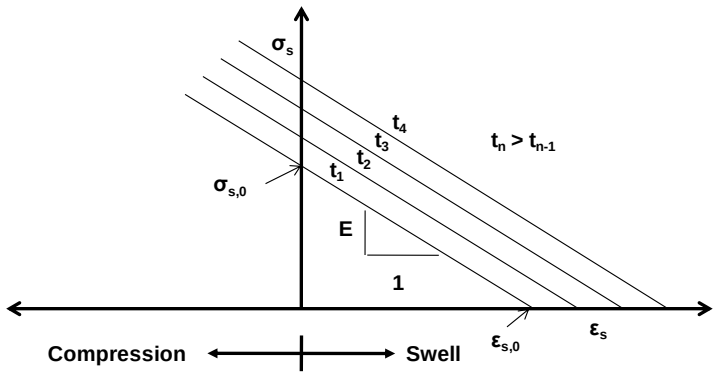

Figure 5.17. Swell deformation characteristics

The experiment showed that that the bentonite apron completely sealed the gap (Kidd 2011). So, in the numerical simulation, after applying the swelling pressure, the water pressure and pore water pressure below the bentonite apron was presumed to be zero but that above the apron would essentially act on the wall.

The author also monitored the swelling pressure for each water increment to see if the residual pressure is enough to cause swelling in the subsequent increment of WL to seal the gap or not.

5.4.3 Result and Discussion

The load deflection curve for two conditions were compared such as 1) no gap condition; and 2) Bentonite apron, and is shown in Figure 5.18. The result shows that the bentonite apron does not have any adverse effect on the performance of the wall as long as the deflection is considered. The figure shows that the deflection of the wall when the bentonite apron was used is almost same as that of no gap condition. The author also compared the result for the different value of permeability of silty sand. From Figure 5.18, it is seen that that for the high permeability of silty sand, the deflection of the wall in either case is higher from 10 feet (3.0 m)

of WL whereas for lower permeability, it is not that high. This result shows that if the silty sand is highly permeable, then the other countermeasure to relief the seepage force should supplement the application bentonite apron. In the other case, bentonite apron is sufficient.

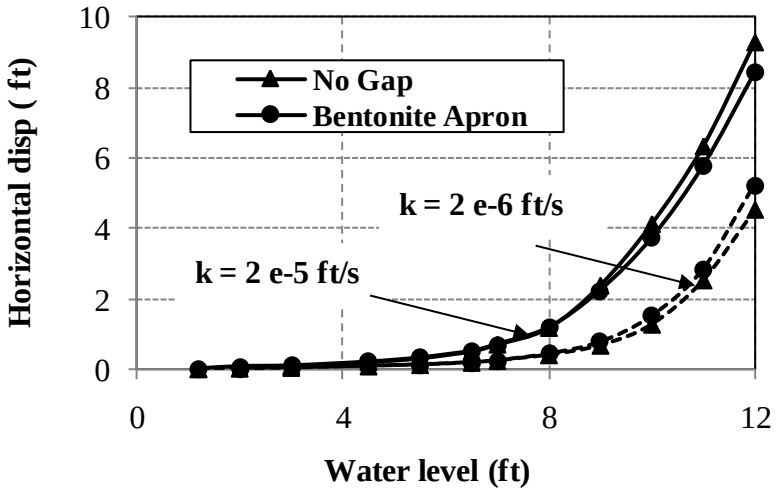

Figure 5.18. Load deflection curve at the top of the wall (***Note:*** 1 ft = 0.3m)

To see if there is a residual swelling pressure for each load increment or not, the swelling pressure was plotted for each water level and is shown in Figure 5.19. From the figure, it is seen that the swelling pressure is not zero before it reaches 12 ft (3.6 m) WL which means that the bentonite apron has enough swelling capability to seal the gap for the next successive increase in water level. This was also proven by the experimental result as shown in Figure 5.20 where the leakage of water through gap was very negligible, which proved the potentiality of bentonite apron to swell and seal the gap.

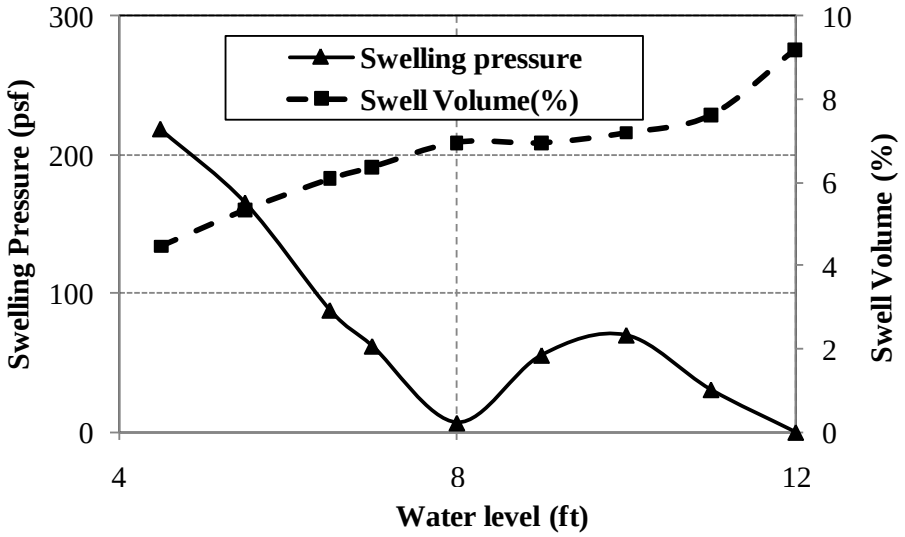

Figure 5.19. The residual swelling pressure for each water level (**Note:** 1 ft = 0.3m; 1 psf = 47.88 Pa)

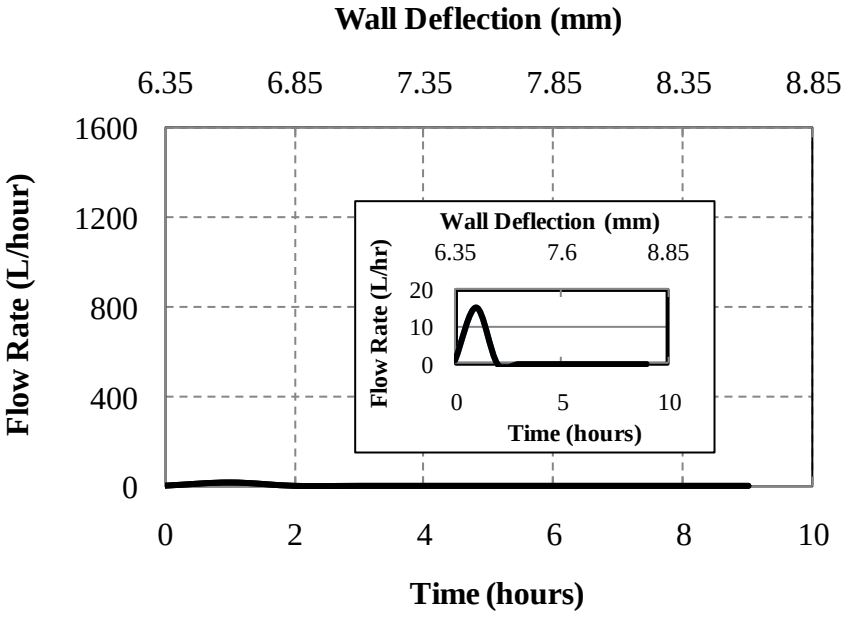

Figure 5.20. Leakage of water through gap vs. time for S70B30 (Kidd 2011)

5.5 SUMMARY AND CONCLUSIONS

The planning, development and implementation of the retrofitting techniques depends on the correct understanding of failure mechanism involved in the failure of I-walls. So diagnosing the cause of the failure is an important aspect of designing the appropriate retrofit techniques. Many researches conducted aftermath of Hurricane Katrina pointed out that one of these failure mechanisms is the gap formation adjacent to the floodwall on the flood side.

In contrary to their assertion, although evidence of gap formation was observed at almost all breaches during Hurricane Katrina, whether those gap formation were the cause or the result of failure might be a controversial issue. So in this study, an attempt was made to categorize and identify three conditions, in which, gap formation is considered to be the main cause; secondary cause; or the consequence of the failure. Related to each of these conditions, different types of countermeasures evolve. For the first condition, bentonite apron alone could be the effective countermeasure against the failure of the floodwall. For the second condition, the bentonite apron should be supplemented by other countermeasures. And for the last condition, where gap opening is not the cause of the failure, but the consequence of the failure, bentonite apron is not the effective countermeasure since restricting the gap opening alone is not that effective.

Once the condition where gap opening is found out to be the primary or secondary cause, the author also tried to check the effectiveness of the bentonite apron so that it would not exert excessive pressure on the wall ,and at the same time it maintains the swelling potential for the successive loading conditions. The detailed findings of the study are outline below.

1) Brandon et al. (2008) derived the formulations to calculate the horizontal pressure acting on the I-wall for gap conditions and no gap conditions, and the depth of gap using total stress approach. This study derived the formulations using effective stress

approach and found that the gap condition is always critical than no gap conditions in transient flow condition, whereas for the steady flow condition, it depends on hydraulic gradient. Since due to the short duration of the loading, and the undrained condition of the soil in New Orleans that maintains transient flow condition, gap condition is always critical.

2) Although gap condition is always critical, whether gap is the cause of the failure or the result of the failure depends on the geometry of the levee and the relative difference in the strength and stiffness of the soil layers. The study showed that the geometry and the soil condition of London Avenue canal signify the gap to be the cause of the failure, while that for 17th street canal; it is the result of failure. If the gap is the consequence of the failure as in 17th street canal, then preventing gap formation will not alone prevent the failure. There should be other countermeasure to safeguard against failure of floodwalls. This can be achieved by improving the foundation soil such as DMM. However, simulation result shows that application of DMM in foundation soil promote the initiation of gap at high water level. So the gap sealing mechanism should accompany DMM method for the effective performance of the floodwall.

3) For the situation when gap is the cause of the failure, there might be two cases .In the first case the gap formation is the primary cause of the failure whereas in the second case, it is the secondary cause of the failure. For the condition where gap is the secondary cause of the failure, bentonite apron alone will not be effective and therefore other counter measure should supplement it. Absence of either countermeasure will result in the failure of the wall. To be more specific, for the site

where the silty sand is highly permeable, countermeasures to relief seepage force as well as bentonite apron should be implemented. This is quite obvious for London Avenue Canal, because most of the silty sand layer in this study is dominated by the sand of high permeability.

4) For the conditions where gap is the primary cause of the failure of the floodwall, and levees, bentonite apron plays a vital role in self healing mechanism. As long as the performance of bentonite apron is concerned, it does not exert an excessive pressure on the wall to cause severe deflection. On top of that, it has the potential to expand upto 11 ft of WL.
5) Apart from evaluating the performance of the bentonite apron, this study also uses some unique approaches to speed up the transient flow analysis and set forth the formulations to relate the swelling pressure with the volumetric deformation within the required time domain.

6. EFFECTIVE STRESS BASED ANISOTROPIC ANALYSIS OF I-WALL SYSTEMS IN NEW ORLEANS

6.1 BACKGROUND

In the human history, the life and property loss associated with hurricanes had brought a lot of attention to engineering community. After Hurricane Katrina, investigation teams primarily Independent Levee Investigation Team (ILIT) and Interagency Performance Evaluation Taskforce (IPET) were formed and many investigations were conducted. One of the purposes of these investigations was to identify the major failure mechanism to devise the proper countermeasures for the next hurricane season. The major work and the findings are well documented in IPET (2007) and ILIT (2006), and in the special issue of ASCE Journal of Geotechnical and Geoenvironmental Engineering (e.g. Sasanakul 2008; Seed et al. 2008[a]; Seed et al. 2008[b]; Seed et al. 2008[c]; Seed et al. 2008[d]; Brandon et al. 2008; Sills et al. 2008; Ubilla et al. 2008; Duncan et al. 2008).

As mentioned earlier, numerical analysis was taken as the key tool for such studies .The numerical studies consisted of limit equilibrium analysis to find the factor of safety and also the finite element/ finite difference method (stress- deformation analysis) to evaluate the soil structure interaction problems. Stress- deformation analysis were mostly done using commercial software like FLAC (Itasca Consulting group 2006) and PLAXIS 2D (Brinkgreve 2007).

One of the vital parts of the successful stress deformation analysis is the constitutive behavior of the soil. This implies that choosing an appropriate soil constitutive model in the numerical analysis is very crucial. Most of the analyses that are documented in IPET (2007) and ILIT (2006) were conducted by considering the soil behavior with Mohr Coulomb (MC) model. These models are simple, but one of the shortcomings is the proper strain hardening cannot be incorporated. Use of this type of simple formulation may not be sufficient to capture the detailed behavior of levees and floodwalls.

To improve the outcome of the numerical analysis, some analyses were conducted using advanced material models, where the soil behavior is described in effective stress so that the coupled effect of both the effective stress and the pore pressure generation, and volume change during shearing, are ensured. For instance, the two dimensional version (Wang and Makdisi,1999) of Bounding Surface Hypoplastic Model (Wang 1990, Wang et al., 1990) was used by the IPET team to model the response of sand in London Avenue canal section. The model was also used for the total stress analysis for 17th street canal sections. Likewise, the ILIT team also used the effective stresses based Modified Cam Clay (MCC) model (Roscoe and Burland 1968) vis-à-vis "soft soil" model in PLAXIS (Brinkgreve 2007) to simulate the response of the foundation soft clay and marsh layers in 17th street canal section and Inner Harbor Navigation Canal (IHNC) south breached section so that the isotropic hardening (volumetric) could be fully incorporated.

Out of the 55 total breaches (Knabb et al.) of New Orleans levees and floodwall section, 17th street canal breach was one of the severe breaches during Hurricane Katrina. Most of the forensic investigation (IPET 2007) pointed out that "Lacustrine Clay" deposit which is of soft consistency (IPET 2007) was the responsible soil layer for such failure. The MC model or the

advanced material model mentioned above may not sufficiently represent the constitutive behavior of such soil because these soils tend to exhibit anisotropy. The so called material anisotropy is one of the fundamental feature of clay deposits which are developed through K_0 consolidation during the successive deposition in historic time period so that the stress condition is not hydrostatic; and the rotation of the principal stresses due to the construction of the levee on top of them. Ling et al. (2002) classified the first category to be the "inherent anisotropy" and the later one the "stress-induced anisotropy". This would yield the fact that the yield surface is no longer symmetrical about the mean effective stress axis. Graham et al. (1983); and Rodriguez (1992) also showed experimentally that the yield surface of the anisotropically consolidated clay tends to align along the K_0 axis .The yield curve of such kind results in the strength and stiffness of the soil significantly different for the vertical and horizontal direction. So the necessity of incorporating anisotropy in the soil constitutive model is necessary to capture realistic features of the soft soils like "Lacustrine Clay"

There are many soil constitutive models which can model the anisotropic behavior of the soil such as Anisotropic Modified Cam Clay (AMCC) model (Dafalias 1987); S-CLAY1 (Wheeler et al., 2003); SANICLAY (Dafalias et al., 2006); and other Bounding surface plasticity models (Dafalias and Herrmann 1982; Anandarajah and Dafalias 1985, 1986; Dafalias and Herrmann 1986; Kaliakin and Dafalias 1990, Ling et al. 2002, Whittle and Kavvadas, 1994). SANICLAY (Dafalias et al., 2006) and S-CLAY1 (Wheeler et al. 2003) are developed as sequel from the AMCC model (Dafalias 1987) based on the classical plasticity theory which differ only in the flow rule (SANICLAY) and the evolution of the anisotropy (S-CLAY1) which are proposed, and effective, to simulate the behavior of soils in dynamic loading conditions, and the conditions where the plastic shear strain is dominant to plastic volumetric strain, respectively.

Bounding Surface Models on the other hand are based on different plasticity theory appropriate to simulate the behavior of over consolidated cohesive soil well. Since soil condition in New Orleans is normally consolidated or slightly over consolidated, the bounding surface model may not be necessary to simulate the behavior of the soil in New Orleans. So, as long as the monotonic condition exists and since the soil concerned is normally consolidated to lightly over consolidated, incorporation of the anisotropy in an elasto- plastic model formulated by Dafalias (1987) is sufficient to realistically represent the soil behavior for the New Orleans cohesive soils.

Therefore, in this study, (AMCC) model developed by Dafalias (1987) is used to characterize the soil in explicit non linear finite difference code, **F**ast **L**angrangian **A**nalysis of **C**ontinua in three dimensions (FLAC^{3D}) (Itasca consulting group 2006) as the main platform. The backbone of this model is primarily developed by focusing the anisotropy of the stress system related with the in situ stress condition, and or stress induced by subsequent shearing. As the built in constitutive models in FLAC^{3D} does not incorporate the anisotropy suitable for the soft soil there is a need of implementing the chosen soil model in it using the user defined model capability.

6.2 THEORETICAL FRAMEWORK OF THE MODEL

Dafalias (1987) introduced AMCC model as a sequel to Modified Cam Clay (MCC) model (Roscoe and Burland, 1968) constructed by adding anisotropy in the work dissipation assumption given by

In the above formulation, triaxial space for stress and strain is assumed so that $p = (\sigma_a + 2\sigma_r)/3$, $q = (\sigma_a - \sigma_r)/2$, $\varepsilon_v = (\varepsilon_a + 2\varepsilon_r)/3$ and $\varepsilon_q = 2(\varepsilon_a - \varepsilon_r)/3$, where, the subscripts *a* and *r* denotes the axial and radial directions of the triaxial space; and σ and ε denotes

usual effective stress and strain quantities. In the above equation, M = critical stress ratio; and α = non dimensional anisotropy quantity accounting for the effect of internal residual stress, and the coupling of the volumetric and the deviator plastic strains $d\varepsilon_v^p$ and $d\varepsilon_q^p$ which can be quantified using the flow rule

$$d\varepsilon_v^p = < L > \frac{\partial f}{\partial p} \; ; \; d\varepsilon_q^p = < L > \frac{\partial f}{\partial q} \tag{6.2}$$

where, L= Loading index and f = 0 is the yield function (associated flow rule) which is yet to be defined. The Loading index is inside the Macauley brackets < > which indicates that < L > = 0 when L <0 (unloading case) and < L > = L when L >0 (loading case).

The elastic counterparts of the volumetric and deviator strain rates can be related with the isotropic hypoelastic relations

$$d\varepsilon_v^e = \frac{dp}{K}; \quad d\varepsilon_q^e = \frac{dq}{3G} \tag{6.3}$$

Where, the elastic bulk and shear modulus K and G are given as:

$$K = \frac{p(v_{in})}{\kappa}; \quad G = \frac{3K(1-2\upsilon)}{2(1+\upsilon)} \tag{6.4}$$

where ,v_{in} = is the initial value of specific volume, v ($v_{in} = 1 + e_{in}$) in which e_{in} =initial values of the void ratio e; and κ and ν = slope of the swelling line in e-lnp space and the Poisson's ratio, respectively. When using v-log p relations, v is taken instead of v_{in}

In the above relations, the additive decomposition of the total strain rate into elastic and plastic parts $d\varepsilon_{ij} = d\varepsilon_{ij}^e + d\varepsilon_{ij}^p$ is assumed.

Again, rearranging the terms in the Eq. (6.1) with Eq. (6.2), Eq. (6.5) is obtained,

$$\frac{d\varepsilon_s^p}{d\varepsilon_v^p} = \frac{2\eta - 2\alpha}{M^2 - \eta^2} = -\frac{dp}{dq} \tag{6.5}$$

Where η can be defined as the stress obliquity and can be written as:

$$\eta = \frac{q}{p} \tag{6.6}$$

If Eq.(6.6) is further expanded with rearranging terms in Eq. (6.5), then the yield function for the AMCCM can be obtained as Eq. (6.7);

$$f(p, q, p_{c,}\alpha) = q^2 - 2\alpha pq + \alpha^2 pp_c + M^2 p(p - p_c) = 0 \tag{6.7}$$

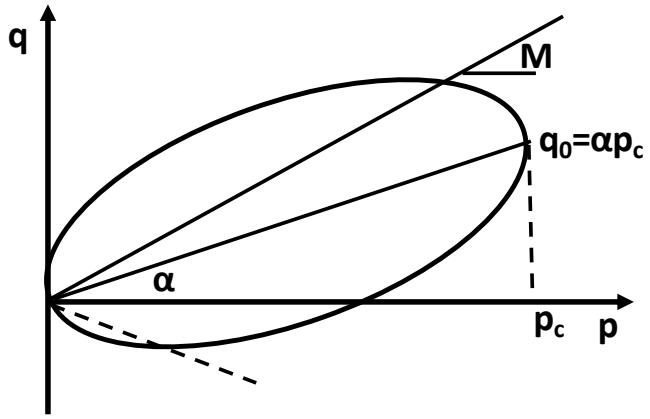

Figure 6.1. Schematic illustration of the anisotropic yield surface in the triaxial p-q surface (Replotted from Dafalias 1987)

Where p_c is the value of p at $q = \alpha p$, and termed as the isotropic hardening variable. The yield surface consists of the distorted and rotated ellipse which is illustrated in Figure 6.1, where α

determines the degree of rotation of the yield surface. While using this model, it should be noted that to have the real value of *p, q* in Eq. (6.7), and the anisotropy should always be less than *M*. And it is also evident from Eq. (5) that $d\varepsilon_v^p$ is zero at critical state irrespective of the value of α. If α is zero, Eq. (6.7) reduces to yield function for MCC model

The same evolution law for the MCC model can be used for the isotropic hardening of the internal variable p_c and can be written in the incremental form as:

$$dp_c = < L > \bar{p}_c = < L > \left(\frac{v_{in}}{\lambda - \kappa} \right) p_c \left(\frac{\partial f}{\partial p} \right) \tag{6.8}$$

Similarly, anisotropic hardening for the internal variable α can be proposed by using the evolution equation which is given for triaxial stress condition in the incremental form (Dafalias 1987) by

$$d\alpha = \langle L \rangle \bar{\alpha} = \langle L \rangle \left\{ \frac{v_{in}}{\lambda - \kappa} \left| \frac{\partial f}{\partial p} \right| \frac{c}{p_c} (q - x\alpha p) \right\} \tag{6.9}$$

The incremental form is for each time step and they are not the true time step as in the rate dependency condition but fake time step to ease for the computational purpose. In other words, after each time step, the variable has to be updated using the following equation.

$$\alpha^{new} = \alpha^{old} + d\alpha \tag{6.10}$$

In the above equation, *x* and *c* are two new model constants in which x controls the level of anisotropy which can develop under a constant *q/p* loading and *c* controls the pace at which such anisotropy develops.

The constant *x* can be estimated using the equation below (Dafalias 1987)

$$x = \frac{2\varepsilon\eta_k[(1-(\kappa/\lambda)]}{\eta_k^2 + 2\varepsilon\eta_k[1-(\kappa/\lambda)] - M_c^2} \tag{6.11}$$

where

$$\eta_k = \eta_{k0} = \frac{3(1-K_0)}{(1+2K_0)} \tag{6.12}$$

$$\varepsilon = {d\varepsilon_v}\big/{d\varepsilon_q} = 3/2 \tag{6.13}$$

In Dafalias et al. (2006), *x* is defined by using the equation

$$x = \frac{2\varepsilon\eta_k[(1-(\kappa/\lambda)]}{B\varepsilon\eta_k^3 + \eta_k^2 + \varepsilon\eta_k[2[1-(\kappa/\lambda)] - BM_c^2] - M_c^2} \tag{6.14}$$

For the K_0 consolidation test

$$B = -\frac{2(1+\nu)\kappa}{9(1-2\nu)\lambda} \tag{6.15}$$

In original paper, B was regarded as zero, since it is generally a small value. For such condition to be valid, the poison's ratio is given by the relation and is the normal value for soils.

$$\nu = \frac{9\lambda - 2\kappa}{2\kappa + 18\lambda} \tag{6.16}$$

There is always a higher limit of α. According to Dafalias (1987), the saturated value α, can be evaluated as:

$$d\alpha = \langle L \rangle \left\{ \frac{v_{in}}{\lambda - \kappa} \left| \frac{\partial f}{\partial p} \right| \frac{c}{p_c} (q - x\alpha p) \right\} = 0 \tag{6.17}$$

$$\Leftrightarrow \alpha = \frac{\eta_k}{x} = \frac{\eta_k^2 + 2\varepsilon(1-(\kappa/\lambda))\eta_k - M^2}{2\varepsilon(1-(\kappa/\lambda))} \tag{6.18}$$

The initial value of α is equal to the inherent anisotropy which arises due to the structured anisotropy and the initial stress condition (inherent anisotropy). If only an initial stress anisotropy is considered, then the initial value of α can be calculated using Eq. (6.19)

$$\alpha^{in} = \frac{\eta_k^2 + 3(1-(\kappa/\lambda))\eta_k - M^2}{3(1-(\kappa/\lambda))} \tag{6.19}$$

η_k is given by the relation in Eq. (6.13). Eq. (6.19) is valid for the case when K_0-consolidation is followed by the shearing. If in case the experiment starts from the slurry state, then α^{in} is always zero.

It is also equally important to understand the plastic modulus and its derivation for this model. Before the plastic modulus is defined, the consistency condition $df = 0$ is applied to Eq.(6.7) and in conjunction with Eq.(6.8) and Eq.(6.9) the loading index L can be calculated as

$$L = -\frac{\left(\frac{\partial f}{\partial p} dp + \frac{\partial f}{\partial q} dq\right)}{\left(\frac{\partial f}{\partial p_c} dp_c + \frac{\partial f}{\partial \alpha} d\alpha\right)} = -\frac{p[(M^2 - \eta^2)dp + 2(\eta - \alpha)dq]}{\left(\frac{\partial f}{\partial p_c} dp_c + \frac{\partial f}{\partial \alpha} d\alpha\right)}. \tag{6.20}$$

The denominator with negative sign of Eq.(6.20) can be termed as the plastic modulus and when it is expanded the following equation is evolved.

$$H = \frac{v_{in}}{\lambda - \kappa} p_c p^2 \left[1 - \left(\frac{\eta}{M} \right)^2 \right] \left[1 - \left(\frac{\eta}{M} \right)^2 \pm \frac{2c}{M^2} \left(\frac{p}{p_c} \right)^2 \left(\eta - \frac{p_c}{p} \alpha \right) (\eta - x\alpha) \right] \quad (6.21)$$

For the generalized multi axial stress space condition, the yield function can be written as:

$$f = \frac{3}{2} \left\{ (s_{ij} - p\alpha_{ij}) \left(s_{ij} - p\alpha_{ij} \right) + (p_c - p) p \alpha_{ij} \alpha_{ij} \right\} + M^2 p (p - p_c) = 0 \quad (6.22)$$

Where the incremental form for the isotropic hardening can evaluated as:

$$dp_c = < L > \bar{p}_c = < L > \left(\frac{v_{in}}{\lambda - \kappa} \right) p_c tr \left(\frac{\partial f}{\partial \sigma_{ij}} \right) \quad (6.23)$$

And the incremental form for the kinematic hardening is evaluated as:

$$d\alpha_{ij} = \langle L \rangle \bar{\alpha} = \langle L \rangle \left\{ \frac{v_{in}}{\lambda - \kappa} \left| tr \frac{\partial f}{\partial \sigma_{mn}} \right| \frac{c}{p_c} (s_{ij} - xp\alpha_{ij}) \right\} \quad (6.24)$$

In the generalized multi-axial space condition, the value of M is not constant, and depends on the stress path as characterized by the Lode angle and lies between the values corresponding to the extension and compression cases.

One of the distinctive features for the Constitutive model is the generation of the excess pore pressure during the undrained shearing which is specifically determined by the pore pressure coefficient. In this section, it is quite relevant to derive the pore pressure coefficient for the model in hand for the triaxial case which is not done in the original paper. In incremental form, the total, effective stress (with apostrophe) and pore pressure is related as

$$\delta u = \delta p - \delta p' \quad (6.25)$$

If the pore pressure parameter is considered to link the pore pressure changes with the changes in the applied total stresses,

$$\delta p' = -a\delta q \tag{6.26}$$

Combining these two equations for saturated soil condition,

$$\delta u = \delta p + a\delta q \tag{6.27}$$

Where a = the pore pressure coefficient.

The total stress path for the undrained triaxial compression test in incremental form is given by

$$\delta q = 3\delta p \tag{6.28}$$

Now within the yield surface, when the soil is behaving elastically in undrained condition, then the change in effective mean pressure is zero i.e.

$$\delta p' = 0 \tag{6.29}$$

Within the yield surface Skempton's(1954) pore pressure coefficient is 1/3, the changes in pore pressure with respect to incremental stresses .This gives the relation for the changes in pore pressure with respect to incremental stresses.

$$\delta u = \delta p = \frac{\delta q}{3} \tag{6.30}$$

When the soil is behaving plastically after hitting the initial yield curve, then the different relationship can be established. Differentiation of the obliquity [Eq. (6.6)] relationship gives,

$$\delta q = \eta \delta p' + p' \delta \eta \tag{6.31}$$

Dividing Eq. (6.31) with δp' Eq. (6.32) is obtained.

$$\frac{\delta q}{\delta p'} = \eta + p' \frac{\delta \eta}{\delta p'} \tag{6.32}$$

And using,

$$\frac{\delta q}{\delta p'} = -\frac{1}{a} \tag{6.33}$$

From Dafalias (1987),

$$\frac{\delta p'}{p'} = -\left(\frac{\lambda - \kappa}{\lambda}\right) \frac{2(\eta - \alpha)}{M^2 + \eta^2 - 2\eta\alpha} \delta \eta \tag{6.34}$$

So, substituting Eq. (6.32) and Eq. (6.33) in Eq. (6.34) and simplifying,

$$a = \frac{2(\lambda - \kappa)(\eta - \alpha)}{\lambda(M^2 + \eta^2 - 2\eta\alpha) - 2(\lambda - \kappa)(\eta - \alpha)\eta} \tag{6.35}$$

At critical state when η = M,

$$a_{cri} = \frac{\lambda - \kappa}{\kappa M} \tag{6.36}$$

6.3 IMPLEMENTATION OF AMCC MODEL IN FLAC^{3D}

In the previous section, the theoretical background of the constitutive model was discussed which acts as the basis for the model implementation. In FLAC^{3D}, solution of

boundary value problems can be separated into two levels. In each element (local level), the constitutive relations are solved using the appropriate algorithm to obtain the stress from the strain increment so that the yield criterion is satisfied. It has the user interface which allows implementing the new constitutive model. Then in the next level (global level), iterations are done to satisfy the boundary conditions until the unbalanced force falls within the convergence criterion. In this level, it adopts the Explicit Dynamic Solution (EDS) scheme which has the capability to overcome numerical instability problem even for the physically unstable problem. The computational procedure for EDS is shown in Figure 6.2

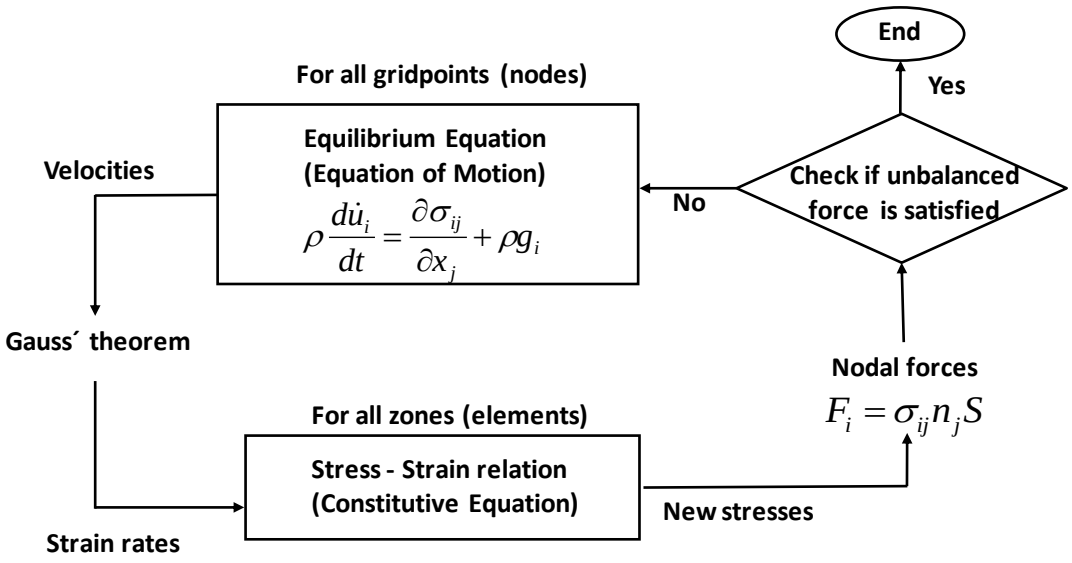

Figure 6.2. Schematic of EDS in FLAC^{3D}

In the local level, while implementing the constitutive model, many integration algorithms (e.g. return mapping algorithm, Newton Raphson method) are available where the return mapping algorithm (sometimes called the plastic correction approach) is more popular. In this technique, the current stress level is evaluated by two steps as shown in Figure .6.3. Initially, elastic stress is predicted from the total strain increment by integrating the elastic constitutive

equation and later the plastic corrector is applied from the plastic part of the total strain increment to bring back the predicted stress so that it falls on the updated yield surface. In doing so, various numerical schemes like explicit, refined explicit or the implicit have been proposed (Simo and Ortiz 1985; Simo and Taylor 1985; Simo and Hughes 1998; Krieg and Kreig 1977; Asensio and Moreni 2003; Criesfield 1991; Borja and Lee 1990; Sloan et al. 2001; Sheng et al. 2000).

Whereas the implicit numerical techniques are more robust and unconditionally stable, it requires extensive computational effort specially for the complex non linear constitutive equations while the explicit technique is computationally economical although it is only conditionally stable (requires small time steps) .The art of choosing the explicit or the implicit depends primarily upon the type of global solver. Since FLAC^{3D} is the explicit solver with small step size, the explicit return mapping scheme is used in this development.

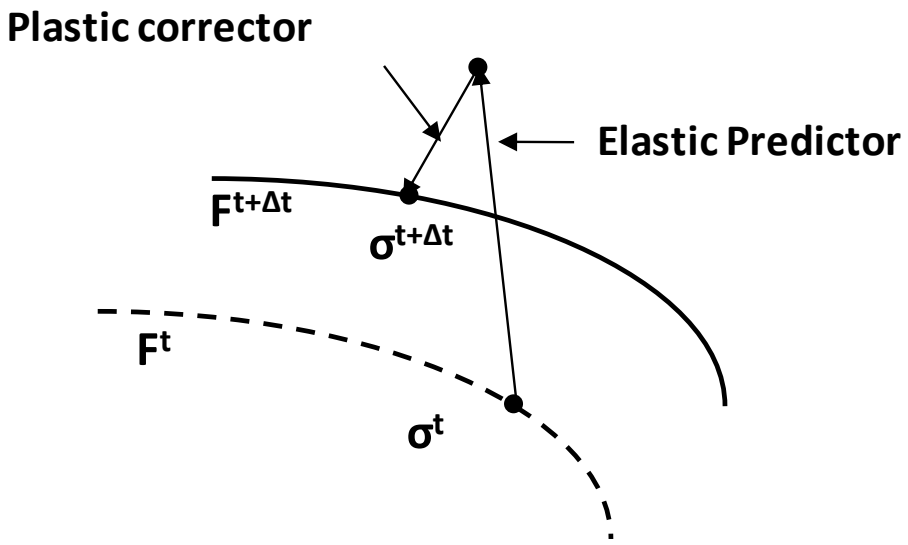

Figure 6.3. Schematic of return mapping algorithm

While calculating the plastic corrector in the explicit return mapping technique, the plastic multiplier (loading index) needs to be evaluated. Whereas in most literatures (e.g. Ortiz and Simo 1986), the loading index is evaluated by satisfying the condition of consistency using the relation $df = 0$ (the stress gradient is orthogonal to the flow gradient), in this development, the loading index was calculated by satisfying $f(\boldsymbol{\sigma} + d\boldsymbol{\sigma}) = 0$ as FLAC^{3D} uses this mechanism to implement built in models, so that the coherence is maintained. As long as the strain increment is kept small (< 0.5 %), $f(\boldsymbol{\sigma} + d\boldsymbol{\sigma}) = 0$ gives accurate results (Rousè 2006). Using this procedure, the calculation of plastic modulus (hardening parameter) can be forfeited

While calculating the plastic corrector in the explicit return mapping technique, the plastic multiplier (loading index) needs to be evaluated. Whereas in most literatures (e.g. Ortiz and Simo 1986), the loading index is evaluated by satisfying the condition of consistency using the relation $df = 0$ (the stress gradient is orthogonal to the flow gradient), in this development, the loading index is calculated by satisfying $f(\sigma + d\sigma) = 0$ as FLAC^{3D} uses this mechanism in built in models to maintain coherence. Using this procedure, the calculation of plastic modulus (hardening parameter) can be forfeited.

The basic constitutive driver using the above mentioned technique can be written as (Itasca 2006). The superscript new and old denotes the stress at current and previous time steps.

$$\boldsymbol{\sigma}^{new} = \boldsymbol{\sigma}^{trial} - < L) \mathbf{D} \ : \left(\frac{\partial f}{\partial \boldsymbol{\sigma}} \right) \tag{6.37}$$

From the condition of $f(\boldsymbol{\sigma} + d\boldsymbol{\sigma}) = 0$,

$$f(\boldsymbol{\sigma}) + f^{*}(d\boldsymbol{\sigma}) = 0 \tag{6.37a}$$

Where,

$$f^*(d\boldsymbol{\sigma}) = f(d\boldsymbol{\sigma}) - f(0) \tag{6.37b}$$

Since $f(\boldsymbol{\sigma}) = 0$, from Eq. (6.34a),

$$f^*(d\boldsymbol{\sigma}) = 0 \tag{6.37c}$$

$$f^*(\boldsymbol{\sigma}^{trial} - L\mathbf{D} : \frac{\partial f}{\partial \boldsymbol{\sigma}}) = 0 \tag{6.37d}$$

$$f^*(\boldsymbol{\sigma}^{trial}) = f(\boldsymbol{\sigma}^{trial}) \tag{6.37e}$$

$$f(\boldsymbol{\sigma}^{trial}) = -L\left[f\left(\mathbf{D} : \frac{\partial f}{\partial \boldsymbol{\sigma}} \right) - f(0) \right] = 0 \tag{6.37f}$$

Arranging the terms in Eq. (6.37f),

$$L = \frac{f(\boldsymbol{\sigma}^{trial})}{f[\mathbf{D} : (\partial f / \partial \boldsymbol{\sigma})] - f(0)} \tag{6.37g}$$

And

$$\boldsymbol{\sigma}^{trial} = \boldsymbol{\sigma}^{old} + \mathbf{D} : d\boldsymbol{\varepsilon} \tag{6.38}$$

In the above equations, D = stiffness matrix

The detailed flow chart for the implementation of the model is shown in Figure 6.4.

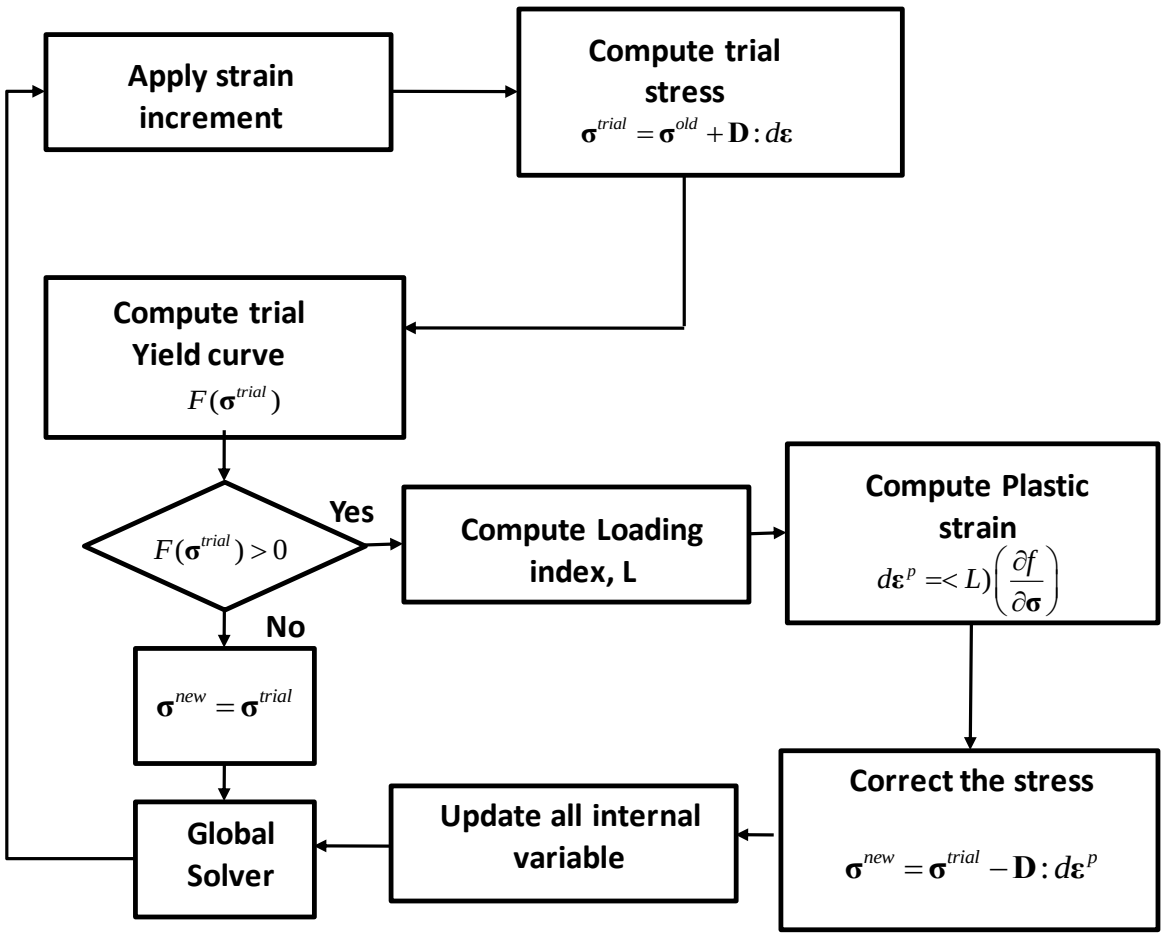

Figure 6. 4. Implementation Algorithm of AMCC model in FLAC^{3D}

***Note*:** D= Stiffness Matrix

In Figure 6.4, the numerical implementation of the constitutive model is done for the elements where the strain rate is given as the input parameter and the stress is given out. Within this process, strain rate is assumed to remain constant. The following steps shows in details how the model is implemented in FLAC^{3D}.

1. In the first step the initial elastic guess σ_{ij}^{trial} is made from the strain rate using the equation,

$$\sigma_{ij}^{trial} = D_{ijkl}\varepsilon_{kl} \tag{6.39}$$

Then from σ_{ij}^{trial}, the trial mean pressure and deviator stress p^{trial} and q^{trial} are calculated using the equation

$$p^{trial} = -\frac{1}{3}\sigma_{ii}^{trial} \text{ and } q^{trial} = \sqrt{3J_2^{trial}} \quad (6.40)$$

Where J^{I}_2 is the second deviator invariant given by

$$J_2^{trial} = 1/2 s_{ij}^{trial} s_{ij}^{trial} \quad (6.41)$$

And s_{ij} is the deviator strain given by

$$s_{ij}^{trial} = \sigma_{ij}^{trial} - 1/3\sigma_{ij}^{trial}\delta_{ij} \quad (6.42)$$

δij is the kronecker delta and is equal to 1 when i=j and 0 when i # j

2. With this stress state, the yield criterion is checked if it meets the criterion using the following equation. The symbols represent the same quantity described in the earlier chapter.

$$f(p^{trial}, q^{trial}, \alpha) = (q^{trial})^2 - 2\alpha p^{trial} q^{trial} + \alpha^2 p^{trial} p_c + M^2 p^{trial}(p^{trial} - p_c) \quad (6.43)$$

3. If the stress state satisfies the yield criterion, then the stress state will be the same as the elastic guess. If on the other hand, yield criterion is violated, then consolidation pressure is updated. In this situation, new mean effective pressure and deviator stress p^{new} and q^{new} are calculated using the following equation:

$$p^{new} = p^{trial} - LKc_a$$

$$q^{trial} = q^{trial} - L3Gc_b \quad (6.44)$$

Where

$$c_a = M^2(2p - p_c) + \alpha^2 p_c - 2\alpha q$$

$$c_b = 2q - 2\alpha p \tag{6.45}$$

And L can be calculated using the following equation

$$aL^2 + bL + c = 0 \tag{6.46}$$

Where

$$a = (MKc_a)^2 + (3Gc_b)^2 - 6\alpha GKc_a c_b$$
$$b = -[Kc_a c_a^{trial} + 3Gc_b c_b^{trial}]$$
$$c = f(q^{trial}, p^{trial})$$

Then the stresses are updated using the following equation

$$\sigma_{ij}^{new} = s_{ij}^{new} + p^{new}\delta_{ij}$$
$$s_{ij}^{new} = s_{ij}^{trial} \cdot \frac{q^{new}}{q^{trial}} \tag{6.47}$$

4. The kinematic hardening term is updated using the following equation

$$\dot{\alpha} = \langle L \rangle \left\{ \frac{v_0}{\lambda - \kappa} |c_a| \frac{c}{p_c} (q - x\alpha p) \right\} \tag{6.48}$$

$$\alpha^{new} = \alpha^{old} + \dot{\alpha} \tag{6.49}$$

5. The hardening term is checked if it reached the saturation point or not by using the following equation

$$\alpha = \frac{\eta_k}{x} = \frac{\eta_k^2 + 2\varepsilon(1-(\kappa/\lambda))\eta_k - M^2}{2\varepsilon(1-(\kappa/\lambda))} \tag{6.50}$$

6. Then the elastic and plastic volumetric strain is calculated.

$$\varepsilon_v^e = -\Delta\varepsilon_{ii} \tag{6.51}$$

$$\varepsilon_v^p = \lambda^v c_a$$

7. After that the zone stress and train are updated using the mixed descretization scheme
8. Specific volume is then calculated

$$v^{new} = v^{old}(1+\Delta\varepsilon_{ii}) \tag{6.52}$$

9. The updated bulk modulus is then calculated as

$$K = \frac{v^{new} p^{zone}}{\kappa} \tag{6.53))}$$

10. Then the updated p_c is calculated

$$p_c^{new} = p_c(1+\Delta\varepsilon_v^p \frac{v}{\lambda-\kappa}) \tag{6.54}$$

The model was numerically implemented in FLAC^{3D} using its User Defined Model (UDM) capability. It was written in C++ following the above procedure, and was compiled as a dynamic link library (DLL) file that can be loaded whenever it is needed. While compiling in C++, the base class "Constitutive model" already exists in the main program, and the derived class was constructed which has altogether 16 member functions. These member functions are associated with registration of the model, indicating state, assigning property, initializing the property or state variables, running the constitutive model, updating the parameters and stresses, and to save or restore the model.

6.4 INPUT PARAMETERS OF THE MODEL AND ITS DETERMINATION

Apart from the parameters of the MCC model, three extra parameters are needed in this model: the initial value of α^{in}, the evolution parameters *x* and *c*. So in total, this model has eight

independent parameters. Following steps shows how the eight independent parameters can be evaluated.

1. The constants λ, κ, and ν_λ have meaning in soil mechanics which can be found easily from the plot of consolidation and swelling curves.
2. The elastic parameters like shear modulus (G) or poisons ratio (ν) can also be determined from the experiment or from some empirical relations. Only one out of two is required as the input parameter.
3. Critical line slope, M can be derived from the friction angle using the relation $M = 6\sin\phi/(3-\sin\phi)$ for compression.
4. Initial anisotropy for the shearing case after one dimensional consolidation, α^{in} can be calculated using the Eq. (19) for the anisotropic consolidation.

For the consolidation test, the initial α is essentially zero, and the saturated α is the one given in Eq. (6.19).

5. x and c are the non classical parameters which are involved only in the constitutive model in hand . For the consolidation test, the variable x is constant as the obliquity is constant and can be obtained from Eq.(6.15)

For the shearing case, x may not necessarily be constant value. Since x is dependent upon the stress and strain of the material, it is not an inherent property and can be calculated from other parameters. Otherwise, it can be calculated using the parametric study. Parameter c is the pace at which the anisotropy is developed and can be estimate using the back numerical calibration.

Apart from these parameters, other internal variables which are important in the model formulations are determined using the following steps.

1. K_0 varies for different soils and can be found from the reference. Using this, the stress states can be calculated from which the mean pressure can be easily calculated.
2. From the mean pressure, for the normally consolidated soil, the pre-consolidation pressure can be found out by $p_{co} = p_c = p$ and $q_c = \alpha_{k0} . p_c$
3. for normally consolidated soil, the initial specific volume can be calculated as

$$\nu_0 = \nu_\lambda - \lambda \ln\left(\frac{p_{co}}{p_1}\right) \tag{6.55}$$

4. The Bulk modulus always varies and can be calculated using equation (4)

6.5 VERIFICATION

Before the coded model could be used for the practical purpose, it is necessary to verify the model against the analytical solution. So the model is verified for the anisotropic consolidation, drained and the undrained shear test for the triaxial condition and the computational results is compared with the analytical solutions. Figure 6.5(a) shows the model and boundary condition used for verification. For the verification, one element model is sufficient to save the computational time.

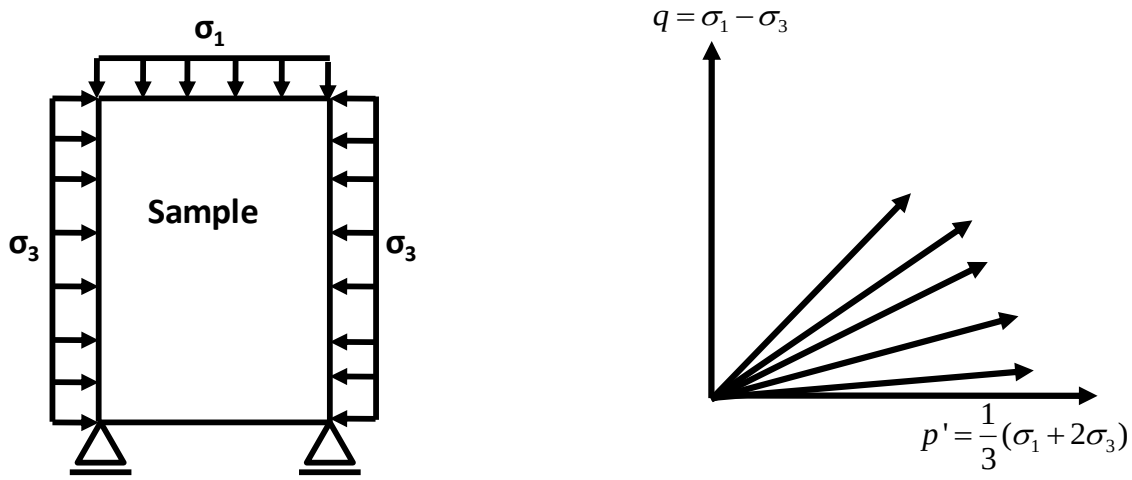

(a) 2-D view of the model (b) Different stress path

Figure 6. 5. Single element model and the stress paths for anisotropic consolidation

6.5.1 Anisotropic Consolidation

The parameters for the verification are adopted from the Dafalias (1987). The parameters are shown in Table 1.The consolidation test was done for the sample which was prestressed at the stress level shown in the table with the value of K_0 as 0.6. The value of constant x and initial α was calculated using Eq.(15) and Eq.(18), respectively following the K_0 consolidation path. Fig. 5(b) shows different stress paths during the numerical simulation of the anisotropic consolidation test which defines the yield points of the characteristic curve.

Table 6.1. Parameters for the Anisotropic Consolidation test

λ	κ	M_c	x	c	α_{in}	P_c (kPa)	e_o
0.27	0.06	0.806	1.38	1.0	0.395	1.41	0.67

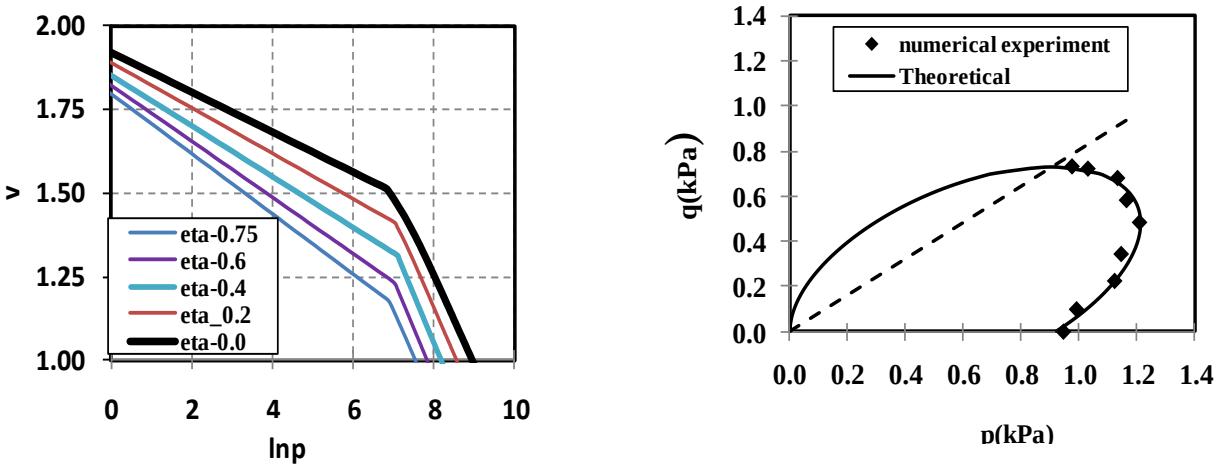

Figure 6. 6. Specific volume vs. ln p' (a) and the theoretical and analytical yield curve (b)

Figure 6.6 shows the result of the numerical experiment for anisotropic consolidation test. Figure 6.6 (a) shows the pronounced demarcation of the elastic and plastic domains denoted by the marked change in the stiffness of the loading for all the stress paths. Those boundary points are plotted on the q-p space as shown in Figure 6.6(b), in which the plotted points matched well with the mathematical model corresponding to the state variables used in the numerical analysis.

6.5.2 Drained Shear Test

The parameters used for the drained analysis were same as those parameters used in anisotropic consolidation except for initial anisotropy. Initial alpha at the beginning of the shearing was calculated to be 0.29 using Eq. (6.18) and K_0 as 0.64 .For shearing; x is variable quantity since stress ratio (ή) doesn't remain the same. So "fish function" can be used to calculate the value of x for the varying stress ratio which is updated for each time step. But in this analysis, the constant value of x was taken. The influence of x on the response is evaluated

using the sensitivity analysis in the next section. The initial stress condition was $q = 198\ kPa$, and $p = 418\ kPa$ (Dafalias 1987).

The analytical solution of the model for drained case at the critical state is given by the following equations

$$p_{cr} = \frac{(3p_0 - q_0)}{3 - M} \tag{6.56}$$

$$q_{cr} = Mp_{cr} \tag{6.57}$$

$$p_c = \frac{2p_{cr}}{1 + \alpha / M} \tag{6.58}$$

$$v_{cr} = v_\lambda - \lambda \ln\left(\frac{2p_{cr}}{p_1^{'}(1 + \alpha / M)}\right) + \kappa \ln\left(\frac{2}{1 + \alpha / M}\right). \tag{6.59}$$

In the above equations, p_{cr} , q_{cr} = mean effective stress and deviator stress at the critical state respectively; v_{cr} = specific volume at critical state; v_λ = specific volume for the reference effective mean pressure p_1. Other symbols are the usual symbols already described in the previous sections.

Figure 6.7(a.) shows the development of different state variables like mean effective pressure (p), deviator stress (q), specific volume (v), isotropic hardening variable (p_c), and anisotropic hardening variable (α) in the triaxial drained test. Figure 6.7(b) shows the initial yield curve at the initial stress condition and the final yield curve at the critical state where the rotation and the enlargement of the yields surface were occurred during the shearing.

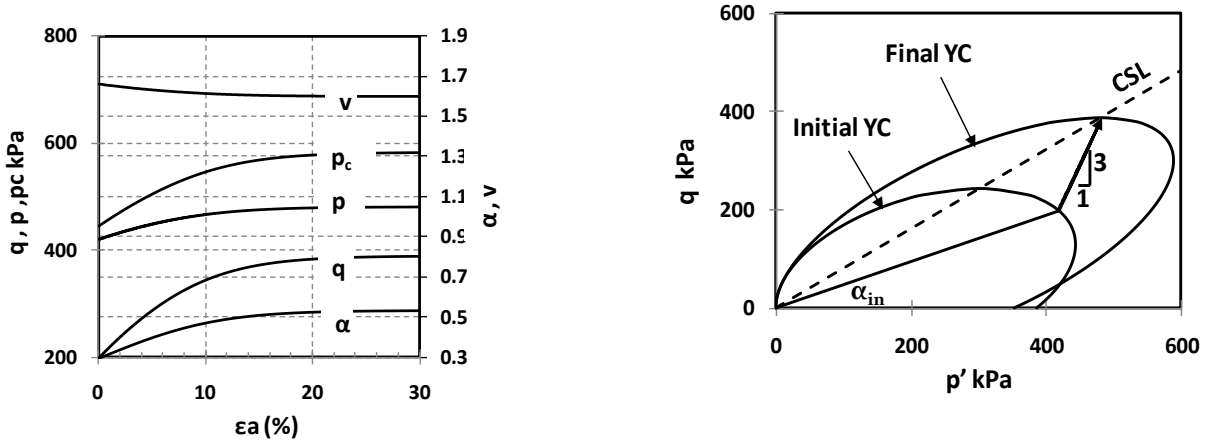

Figure 6.7. (a) Development of different state variables (b) initial and final yield curves

To verify the code, theoretical values of state parameters like q and v at the critical state were compared with that of the numerical ones. The theoretical value of q_{cr} calculated using Eq.(58) is 388 kPa which is equal to the numerical one having 0% error. Similarly, theoretical and numerical value of specific volume at critical state is 1.59 and 1.6, respectively which yields the error of 0.6%. Those errors are very small which shows correct coding of the implemented model.

6.5.3 Undrained Shear Test

The analytical solution of the model for undrained case in the critical state can be described one by one as the following. According to Dafalias (1987),

$$\frac{p}{p_{in}} = \left[\frac{\eta_{in}^2 - 2\alpha_{in}\eta_{in} + M^2}{\eta^2 - 2\alpha\eta + M^2} \right]^{1-\kappa/\lambda} \tag{6.60}$$

From the yield criterion, if the stress state is considered to be on the yield curve and taking all the parameters that lies on the yield curve with the subscript (in) then the following relation can be proposed.

$$\eta_{in}^2 - 2\alpha_{in}\eta_{in} = M^2(R-1) - \alpha_{in}^2 R \tag{6.61}$$

Where R is the over-consolidation ratio given by:

$$R = p_{co}^{'} / p_o^{'} \tag{6.62}$$

Now plugging Eq. (61) in Eq.(60) and simplifying,

$$\frac{p}{p_{in}} = \left[\frac{M^2 R - \alpha^2 R}{\eta^2 - 2\alpha\eta + M^2} \right]^{1-\kappa/\lambda} \tag{6.63}$$

And in the critical state, when η = M,

$$p_{cri} = p_0 \left[\frac{M^2 R - \alpha^2 R}{2M^2 - 2\alpha M} \right]^{1-\kappa/\lambda} \tag{6.64}$$

Similarly,

$$\begin{aligned} q_{cr} &= M p_{cr} \\ v_{cr} &= v_0 \end{aligned} \tag{6.65}$$

$$u_{cr} = \frac{q_{cr} - q_0}{3} + p_0^{'} - p_{cr}^{'} \tag{6.66}$$

Where u_{cr} =pore pressure at the critical state. Specific volume (v) remains constant as long as the undrained shearing is conducted.

In Figure 6.8 development of different state variables are plotted against the axial strain for the normally consolidated soil with R=1 (Figure 6.8a) and for the heavily over consolidated soil R=4.43 (Figure 6. 8b).

Table 6.2 compares the theoretical and numerical values of the state parameters at critical states, and from the table, it can be seen that the errors in the numerical analysis is just nominal.

The complete verification program shows that the implemented model represents the theoretical model accurately so that the application of numerical model practically can be fully justified.

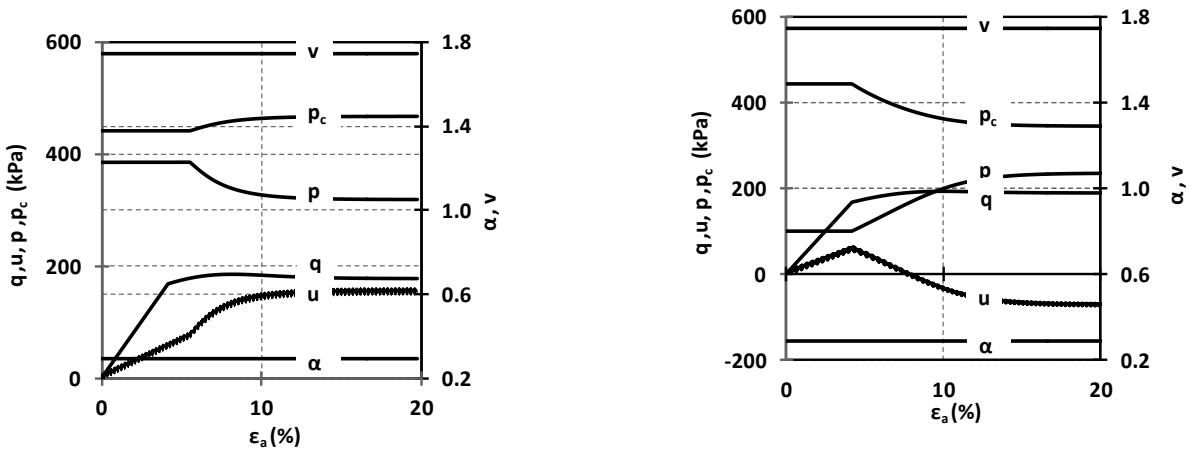

(a) (b)

Figure 6.8. Development of different state variables for R=1 (a) for R=4.43(b)

Table 6.2. Comparison of the numerical and the analytical solution

S.N.	Variable	Theoretical		Numerical		% Error	
		R=1	R=4.4	R=1	R=4.4	R=1	R=4.4
1	q_{cr} (kPa)	276	167	273	178	**-1**	**5.6**
2	u_{cr}	102	-53	106.8	-53	**4**	**0**

6.6 SENSITIVITY ANALYSIS

The sensitivity analysis is done to reflect the sensitiveness of each parameter to the soil response at different loading conditions. This is particularly important while calibrating the parameters. For this analysis, the important parameters like x and c were chosen for which the sensitivity analysis was done.

Table 6.3. Parameters for sensitivity analysis

λ	**κ**	**M_c**	**Pc(kPa)**	**α^{in}**	**G (kPa)**	**K_{max}(kPa)**	**e_o**
0.27	0.06	0.806	443	0.29	1341.2	3736200	0.67

Table 6.3 shows the parameters used for the sensitivity analysis. The sensitivity analysis of parameters x and c was done for both drained and undrained analysis and the result is shown in Figure 6.9. In the drained analysis, the axial strain and the anisotropic hardening at the critical state are compared for different values of x and c. The value of x cannot be less than one at the critical state since it is given by the equation

$$x = \eta / \alpha \tag{6.67}$$

And since $\eta_{cr} = M$ and $\alpha \le M$, x cannot be less than one. And similarly, at the beginning of shearing, $x \ge \eta_{k_0} / \alpha_{k_0}$. So the values of x for the sensitivity analysis can be defined within the domain defined by $1 \ge x \ge \eta_{k_0} / \alpha_{k_0}$ and parameter study was conducted for x = 1.0, 1.3, and 1.63. Figure 6.9a shows that the higher the x becomes, the higher the axial strain $\varepsilon_{a,cri}$ becomes and the lower the α_{cri} becomes, for the drained condition. That is interpreted as the soil becomes stiffer as

x becomes lower. Figure 6.9b shows that the higher the *x* becomes, the lower the deviator stress q_{cri} becomes and the lower the back stress parameter α_{cri} becomes, for the undrained condition. That is also interpreted as the soil becomes stiffer as *x* becomes lower.

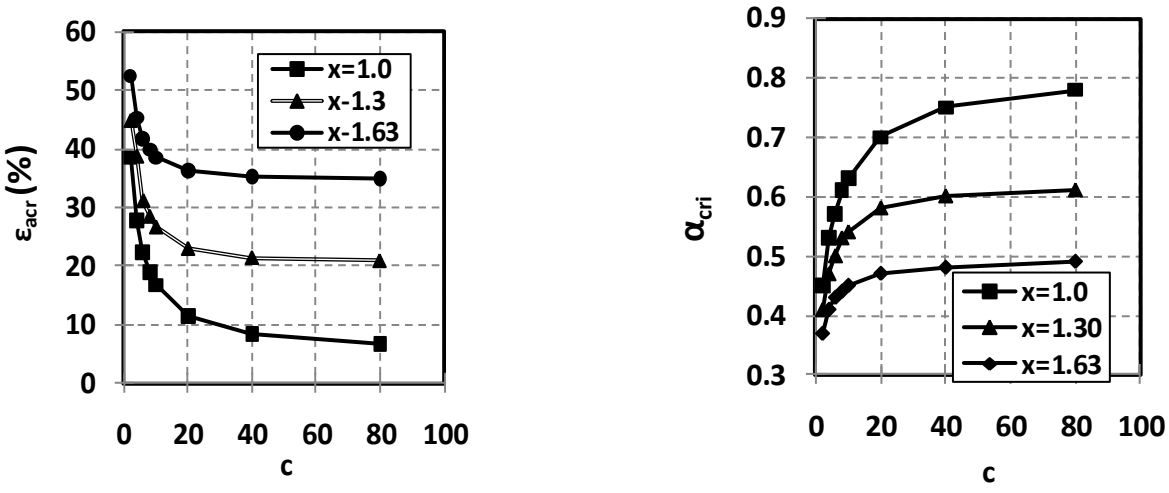

(a) Drained analysis

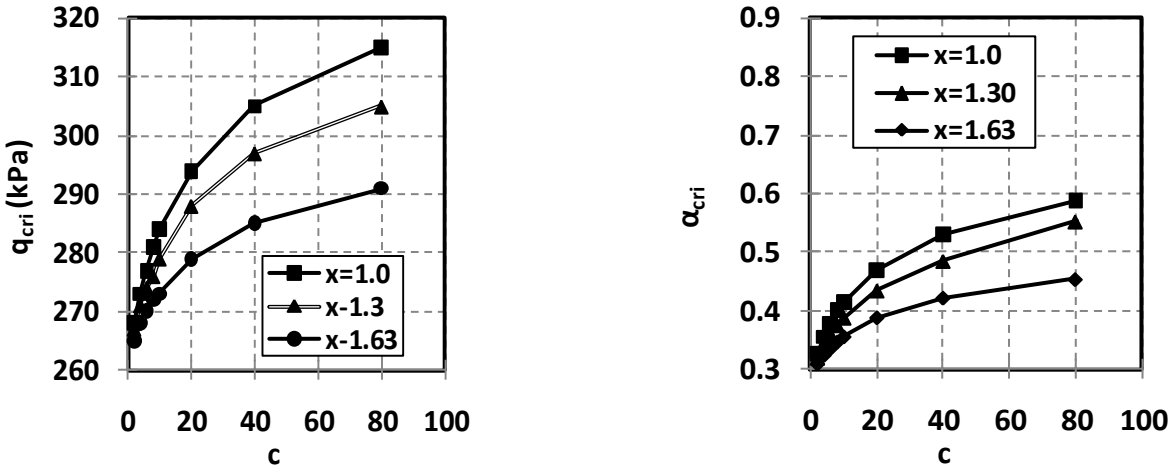

(b) Undrained analysis

Figure 6.9. Sensitivity analysis

Parameter *c* defines the pace at which the anisotropy evolves. In the sensitivity analysis, variables such as deviator stress (q), axial strain (ε_a) and anisotropic hardening (α) at critical states were compared for different values of *c* and *x*, and are illustrated in Figure 7. From Figure 6.9a, it can be seen that for the drained condition, axial strain at critical state decreases as the value of *c* increases. However, the influence of *c* beyond the value of 20 is not significant. From Figures 6.9a and 6.9b, it can be seen that the anisotropic hardening variable at critical state increases as *c* increases, and as *x* decreases. Again, the influence of *c* is not significant beyond 20. Similarly, the deviator stress at critical state for undrained analysis also increases as *c* increases which is significant until 20 (Figure 6.9b), but as *x* decreases. From this sensitivity analysis, it can be seen that taking the typical range of *c* that is less than 20 is reasonable. It can be also seen that taking lower *c* results in conservative results (lower volumetric strain and deviator stress).

In the case of soils in New Orleans, the constant *x* varied with η and starts from 1.54 (Note: This number was 1.63 in Dafalias 1986) for K_0 condition and has the potential to drop to 1.0 at the critical state condition. Since this study was mostly interested to see the behavior at critical state, choosing x = 1 seemed logical. For the constant *c*, the initial run, *c* =1 was adopted for the conservative results. However, due to the fact that *c* has the substantial influence on the behavior of soil, additional two sets of numerical simulation were conducted that is *c* = 10 and 20, and results are discussed in later section of this study.

6.7 VALIDATION OF THE MODEL

The model was validated with the experimental results of the Winnipeg clay (Graham et al. 1983) and lacustrine clay (Messerklinger 2006) which have properties that bound those of the

"Lacustrine Clay" of New Orleans. The validation procedure for each of those clays is described separately as below.

6.7.1 Winnipeg Clay

Graham et al. (1983) conducted the stress controlled test on the 76mm diameter triaxial samples of natural plastic Lake Agassiz clay from Winnipeg, Canada. Index properties of Winnipeg clay is given in the table below (Graham et al. 1983)

Table 6.4. Index properties of Winnipeg clay (Graham et al. 1983)

S./N.	Properties	value
1	Natural water content, w_n (%)	54-63
2	Liquid limit, LL (%)	65-85
4	Plasticity Index, PI (%)	35-60
9	Undrained shear strength, su (kPa)	50-75
10	Sensitivity	3-4
11	Compression Index	0.6-1.1
12	Clay fraction (%)	70-80
13	Normally consolidated, ϕ (deg)	17.5
14	Dominant mineralogy	Smectite
15	Depth (m)	8-12

The samples after trimmed were reconsolidated to their in-situ stresses. The samples were then loaded in different stressed paths in *p'-q* stress space to produce the well defined yield envelops in *p' q* space for four different pre-consolidation pressures. This yield envelops was used in this study to validate the model that will be used. Altogether, 28 tests were conducted experimentally for 4 different pre-consolidation pressures. From the experiment, the following parameters was found as listed in Table 6.5.

Table 6.5. Parameters for the Winnipeg clay (Graham et al. 1983)

M	λ	κ	e_0	K_0
0.668	0.305	0.078	-	0.64

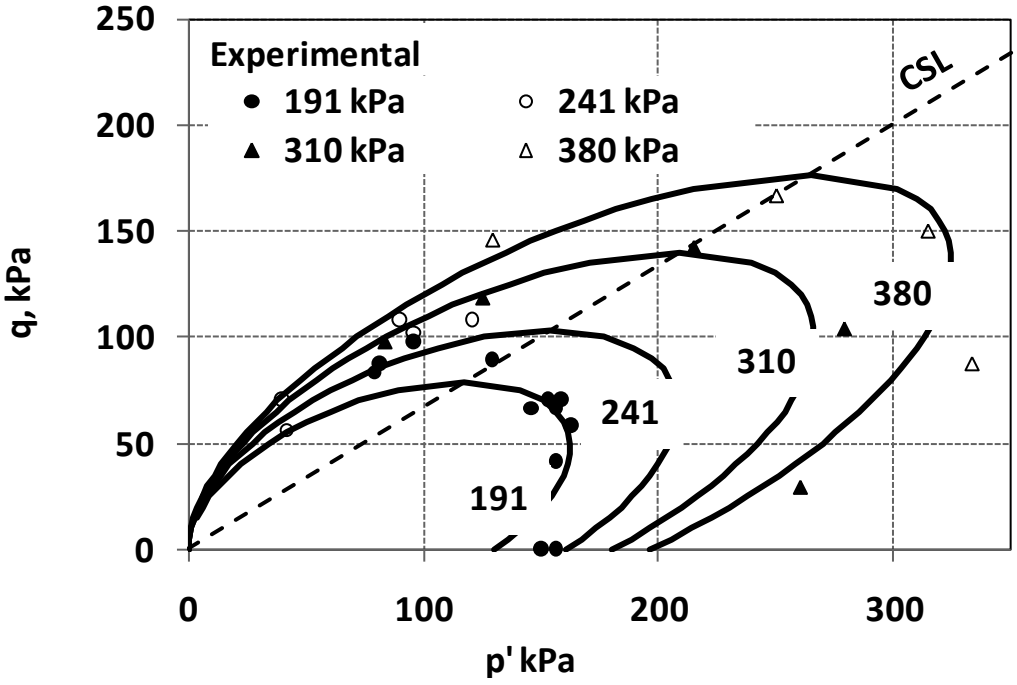

Figure. 6.10. Experimental (Graham et. al. 1983) and analytical results for the Winnipeg clay

The comparison of the theoretical and the experimental results are shown in Figure 6.10. Four yield surfaces that correspond to four yield curves were drawn. In the original paper, Graham et al (1983) also plotted the *q-p'* plots with the stresses normalized with respect to the pre-consolidation pressure so that one yield surface could be defined. In this study, normalization was not done. It is seen that the yield curves derived from the formulation used in this study match well for the experimental data. From the study, it was found that the anisotropy slightly vary for 4 pre- consolidation pressures with the average of 0.36 and standard deviation of 0.167.

6.7.2 Lacustrine Clay

Messerklinger (2006) did 13 drained test to identify the yield envelop for the Swiss Lacustrine clays. Index properties of lacustrine clay are shown in the table below. She plotted the *q-p'* plots from the data points (yield points) obtained by plotting p'-e_v and q-e_s plotting as shown in Figure 6.11 (11 such points are shown in the figure).

Table 6.6. Index properties Lacustrine Clay (Messerklinger 2006)

S./N.	Properties	value
1	Natural water content, w_n (%)	26.5
3	Plastic Limit, PL (%)	14.4
4	Plasticity Index, PI (%)	12.3
5	Specific gravity, G_s	2.74
7	Clay fraction (%)	20
8	Normally consolidated, ϕ (deg)	31

The experimental result for the initial yield curve for the lacustrine clay (Messerklinger 2006) and the best match yield curve for those data points are shown in Figure 6. 11. The best yield curve that suits the data points well has the anisotropy of 0.806. Although the yield curve does not pass perfectly through all experimental data points, it however shows the general pattern on how the yield curve for soft soil aligns in *q-p'* space.

From the above validation results, it is seen that the theoretical model used in this study validates well with the laboratory test data for the anisotropic consolidation test for the soft soils whose index properties bound those of the Lacustrine Clay of the New Orleans. Considering this capability, the model can be used for the numerical simulation of the real problems with minimal error

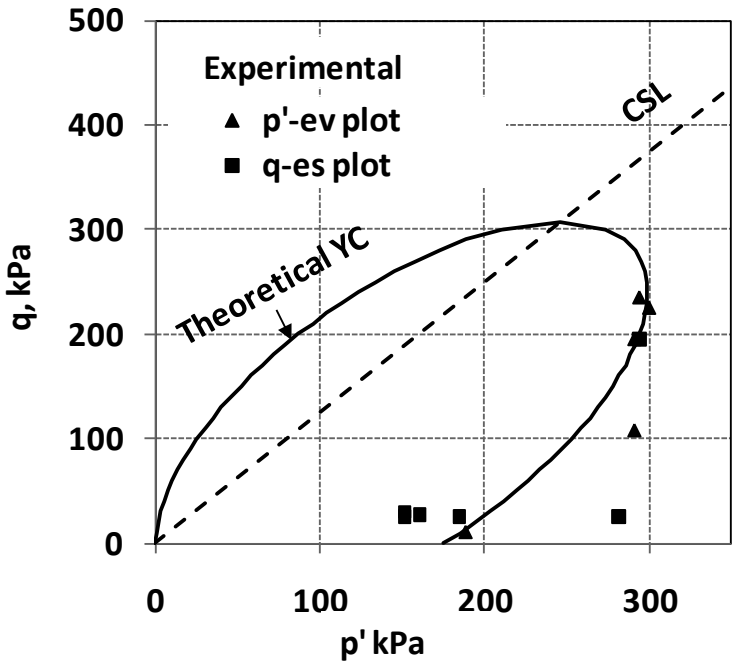

Figure 6.11. Experimental (Messerklinger, 2006) and analytical result for lacustrine clay

6.8 APPLICATION OF THE MODEL

The implemented model is applied in the evaluation of the stress and strain for 17th street canal floodwall section in New Orleans which was breached by hurricane Katrina.

Figure 6.12. Shows the typical soil profile for 17th street canal which comprises Baysound clay, Beach sand, lacustrine clay, marsh layer and the levee fill material as classified by IPET (IPET 2007). Out of these soil layers, marsh layer and the Lacustrine clay layers are of soft consistency. Since the forensic studies and the preliminary studies documented in IPET report (IPET 2007, Volume V.3 pp 36) show that the shear strength of lacustrine clay plays a crucial role on the stability of the levee than other soils as the critical surface intersect mainly through this layer than the other soil layers.

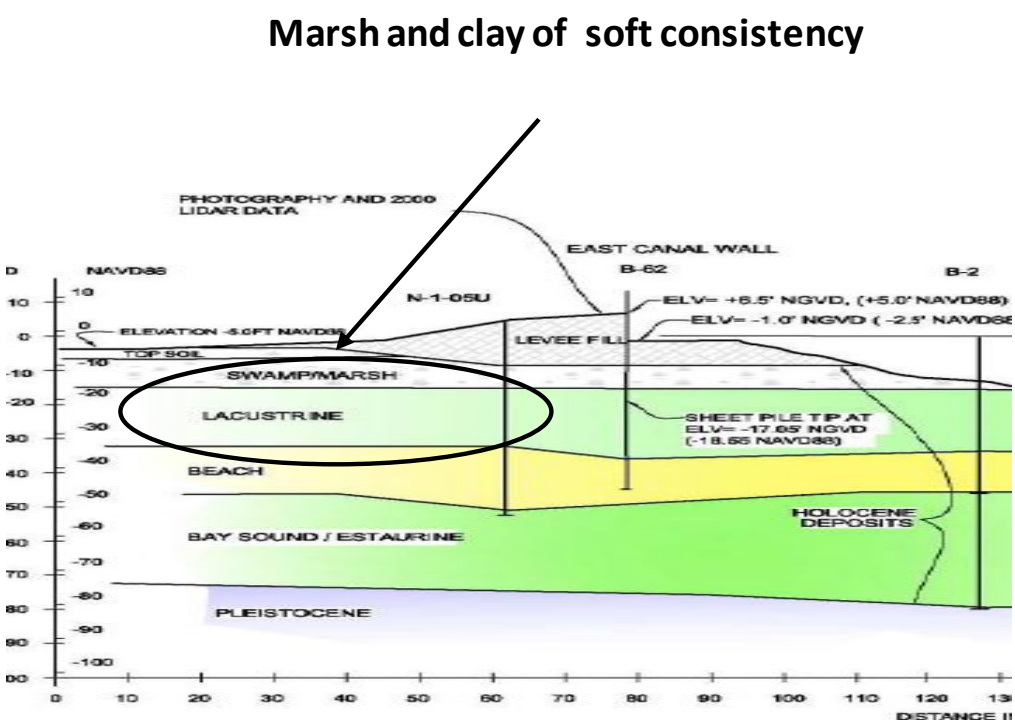

Figure 6.12. Cross section and soil profile for 17th street canal (Adapted from IPET 2007)

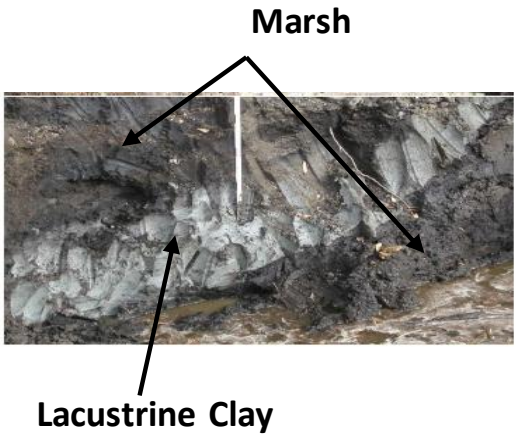

Figure 6.13. Shearing of Lacustrine clay (Adapted from IPET 2007)

Figure 6.13 shows how this layer(gray layer) displaced into the marsh layer (dark layer). Considering this, the model was used to simulate the behavior of Lacustrine clay. The results of the simulation were then compared with the other built in constitutive model.

6.8.1 I-Wall Section and Soil Profile in 17th Street Canal, New Orleans

The FLAC^{3D} numerical model used for the numerical simulation is adapted from Figure 6.12 and is shown in the Figure 6.14. The model consists of I–wall comprising a concrete capping over the sheet pile and the levee section. The sheet pile tip rests at the elevation (EL.) of -19.0 feet and the I-wall capping extends upto EL. 14 feet .The soil stratigraphy consists of five layers. The first layer is the levee fill material of (CH and CL) from crest level of the levee to the EL.-10.0 ft at the centerline of the levee. The second layer (EL. -10.0 ft to EL.-16.0 ft) is highly compressible organic clay known as the marsh layer. Below marsh layer, the third layer (EL. -16.0 to EL.-34.0 ft) is a weak clay (CH) of soft consistency known as the Lacustrine clay (IPET 2007).

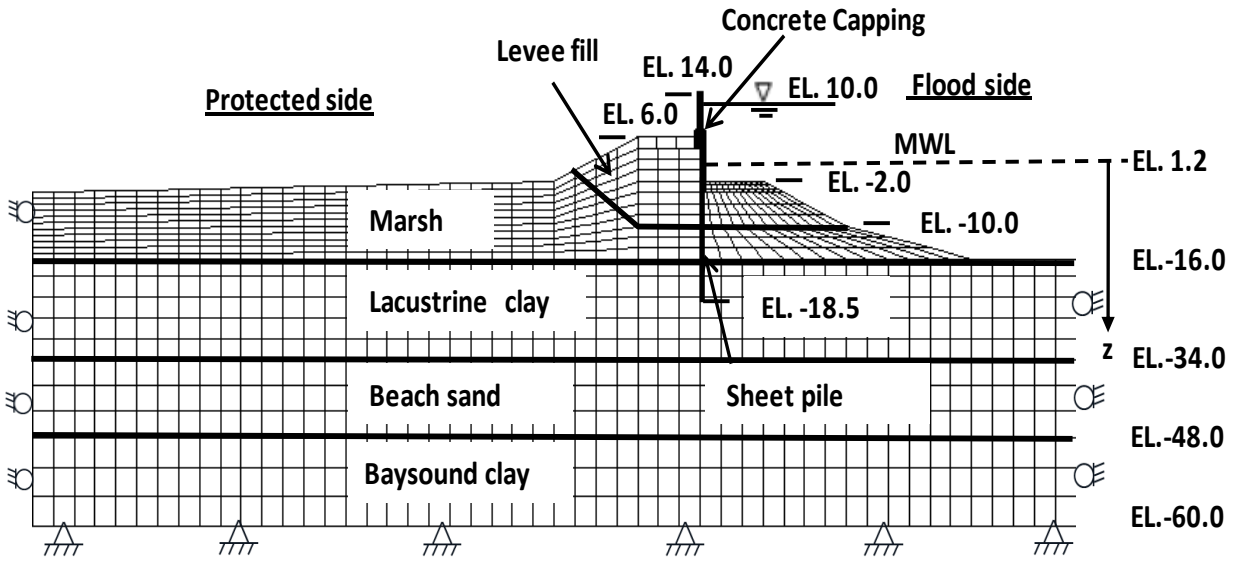

Figure 6.14. The numerical model

The sand layer (EL. -34.0 ft to EL.-48.0 ft) lies underneath lacustrine clay layer which is termed as Beach sand by IPET 2007. Underneath sand layer from El. -48.0 ft to El. -60.0 ft lies the stiff clay known as the Baysound clay.

The soils are modeled with the brick element with elasto-plastic constitutive model. The shear strength and stiffness parameters of the soil layers shown in Figure 6.14 are obtained partly from IPET 2007 and partly from Seed et al. 2008[c] and are shown in the Table 6.7.

The parameters that are used are the effective stress parameters.

Table 6.7a. Soil Parameters at 17th Street Canal

S.N.	Soil layer	Model	Strength/ Stiffness						Permeability
			γ_d(slug/ft^3	E(psf)	ν'	Φ'	K_0	n	k_h(ft/s)
1	Levee fill	Mohr Coulomb	2.61	7.56e4	0.35	32	0.6	0.4	3.20e-8
2	Marsh-toe	Mohr Coulomb	1.71	2.52e4	0.35	36	0.6	0.4	3.20e-6
3	Marsh-center	Mohr Coulomb	1.71	3.35e4	0.35	36	0.6	0.4	3.20e-6
4	Lacustrine Clay	Vary[a]	2.18	Vary[b]	0.35	22	0.61	0.4	3.20e-8
5	Beach Sand	Mohr Coulomb	2.95	1.26e5	0.29	36	0.41	0.4	0.00049
6	Baysound Clay	Mohr Coulomb	3.11	4.19e5	0.35	32	0.6	0.4	3.20e-8

Note: a) there is a variation of the soil model b) the value of E varies with depth.

Table 6.7b. Critical state soil parameters for Lacustrine clay

α^{in}	M	λ	κ	e_0
0.342	0.856	0.17	0.03	0.67

In the numerical simulation, all the soil layers except Lacustrine clay are modeled using the Mohr Coulomb Model whereas Lacustrine clay is model with three different types of model such as Mohr Coulomb Model, Modified Cam Clay Model and the Anisotropic Cam Clay Model to distinguish the responses of those models.

In Seed et al 2008, the marsh layer and the Lacustrine clay layer are modeled using the soft soil in their Plaxis analysis which is actually the MCC model. So the friction angle (ϕ') for those soil layers and the Cam clay model parameters for the Lacustrine Clay are adopted from Seed et al. 2008[c]. Similarly the Poisons ratio for levee fill material is adopted from the same paper and the same value is adopted for other cohesive soil where as for sand, it is obtained indirectly using $\nu = K_0 / (1 + K_0)$ (e.g. Terzaghi 1943) where K_0 is the coefficient of lateral earth pressure at rest which is calculated using Jaky (1943) ($K_0 = 1 - \sin\phi'$). The remaining parameters of those soil layers and the other soil layers are adopted from IPET 2007. Since IPET 2007 does not provide the effective stress soil stiffness parameters, the Young modulus of elasticity (E) is calculated from the Poisons ratio and the total stress shear modulus, since shear modulus for the total stress analysis and the effective stress analysis are equal.

As long as the sheet pile and the concrete capping are concerned, concrete is modeled with brick type elements while sheet pile is modeled with special type of shell element in FLAC^{3D} known as "embedded liner" with the interface slaved in it. The mechanical properties of concrete and steel are readily available in any text books and the properties are the same as described in Adhikari et al.2009.

The boundary conditions used in the numerical simulations is shown in Figure 6.14. The vertical boundaries are provided with roller conditions so that only vertical movement is allowed

whereas the bottom horizontal boundary is provided with the hinged boundary conditions so that the movement in all directions is restricted.

The loading conditions follow the hydrograph illustrated in Figure 6.15. The same simulation procedure is followed as documented in the previous section. Semi coupled fluid mechanical analysis is done since fully coupled analysis takes more computational time.

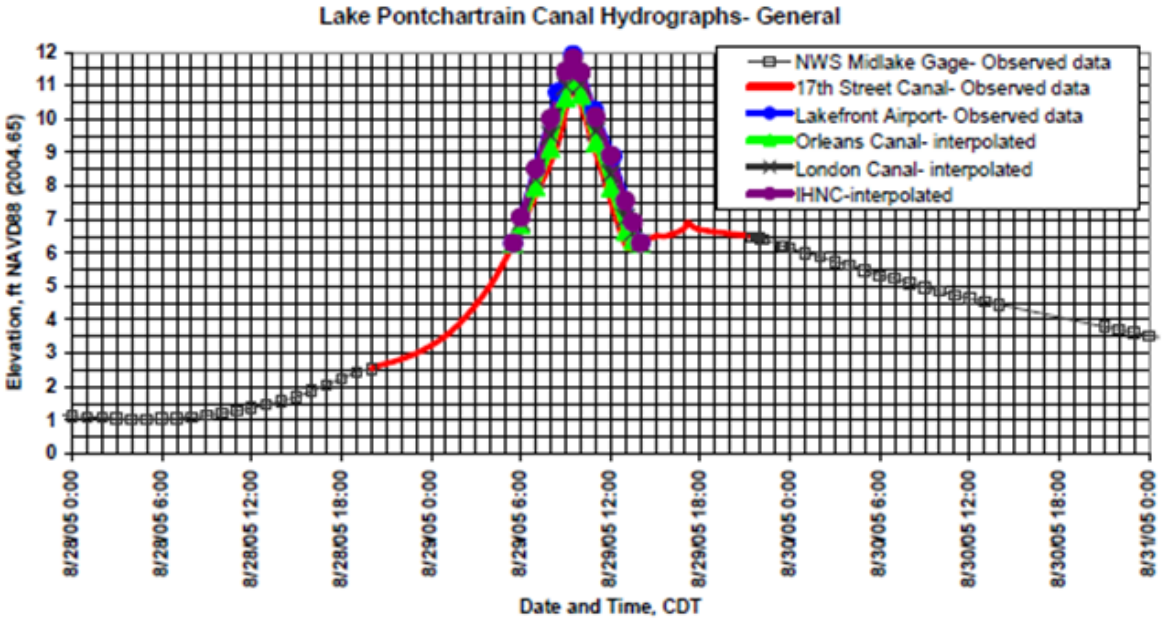

Figure 6.15. Hydrograph at Lake Pontachrain canals (adapted from IPET 2007)

6.8.2 Result and Discussion

In this section the main objective is to compare the results from the AMCC model with MC model and MCC model. So three sets of semi coupled fluid mechanical analysis was conducted to see the effect of constitutive models on the response of the floodwall levee section under different hydraulic loadings. In the following subsections, the responses of the different constitutive models are compared for overall deformation pattern, the yielded zones and the

effect of anisotropy for drained analysis. Though undrained analysis provides the conservative design, drained analysis is adopted which is reasonable enough for the comparison proposes.

6.8.2.1 Comparison of deformation

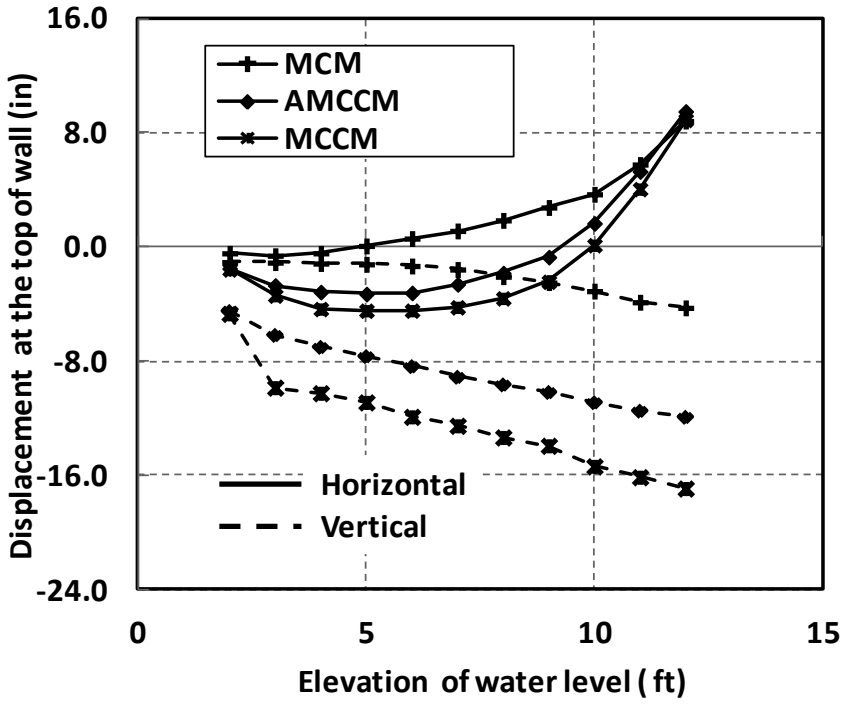

Figure 6.16. Horizontal and vertical deflection of wall top for different water levels

Figure 6.16 shows the comparison of horizontal and vertical displacement at the top of the floodwall for gradually rising water levels for MC, MCC and AMCC models. From the Figure 6.16, it is seen that the wall top deflects and settles more in the order of MCC, AMCC, and MC models from greatest to smallest. This phenomenon is understandable because the AMCC model better traces the hardening behavior of soils than the traditional isotropic MCC model; consequently, the AMCC model is supposed to show a stiffer response than the MCC model.

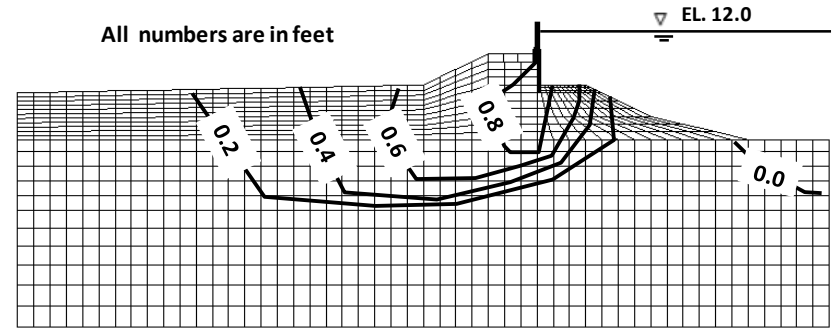

(a)

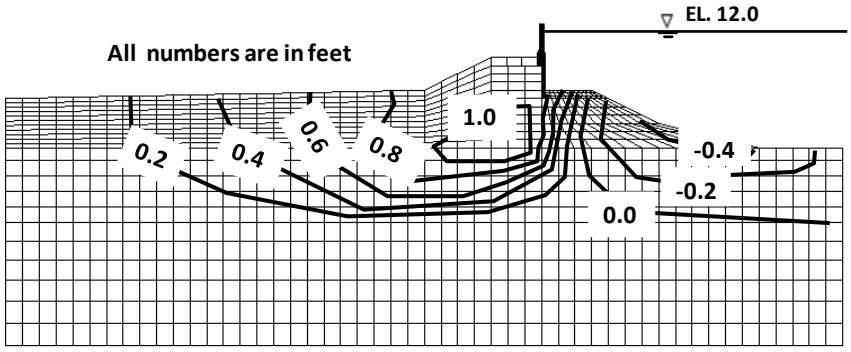

(b)

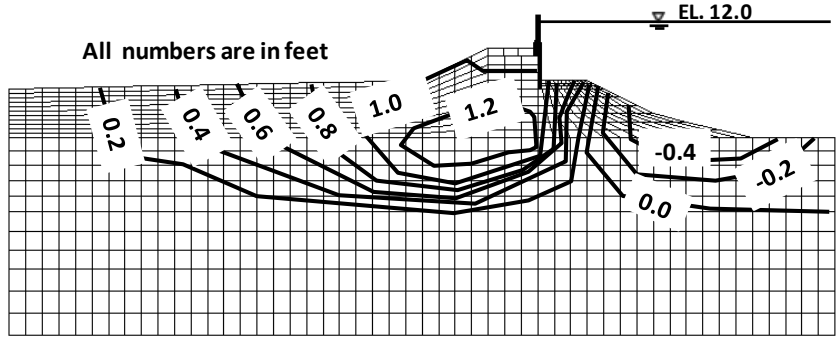

(c)

Figure 6.17. Horizontal deformation of soils for different soil constitutive models at 12.0 ft WL. (a) MC model, (b) AMCC model, (c) MCC model

(MCCM, induced anisotropy is disregarded.)

While MCC and AMCC models incorporate the full consolidation deformation in drained condition, MC model implicitly assumes that the consolidation is already complete (if the consolidation is not coupled by a separate subroutine); therefore MC model showed a stiffer response exhibiting lower deformation than either MCC or AMCC models. Figure 6.17 shows the horizontal soil deformation for different models for a 12 ft (3.6 m) water level (WL). From this figure, it is also seen that the horizontal soil deformations are in the order MCC, AMCC, and MC models from greatest to smallest and underlying mechanism should be similar to the one for Figure 6.16.; MC model showed the stiffest response and it may lead to a non conservative result.

6.8.2.2 Comparison of yielded elements

Figure 6.18 shows the comparison of yielded elements for different constitutive models. From Figure 6.18 it is seen that the number of yielded elements for MC model is much less than AMCC or MCC model. This behavior indicates that the MC model shows a stiffer response than AMCC or MCC models. Yield criteria of the MC model are the same as failure criteria, and it does not recognize yielding before the stress point hits the failure envelope. On the other hand, AMCC and MCC models recognize proper yielding when stress points of soil evolve toward the critical state line. It should be noted, therefore, that the yielded elements in MC model really are the failed elements. But it is unavoidable that MC model may result in a risky interpretation by showing reduced area of the plastic zone. AMCC model showed somewhat lower number of yielded elements than MCC model, and that is reasonable considering AMCC model better traces the strain hardening behavior with slightly stiffer behavior.

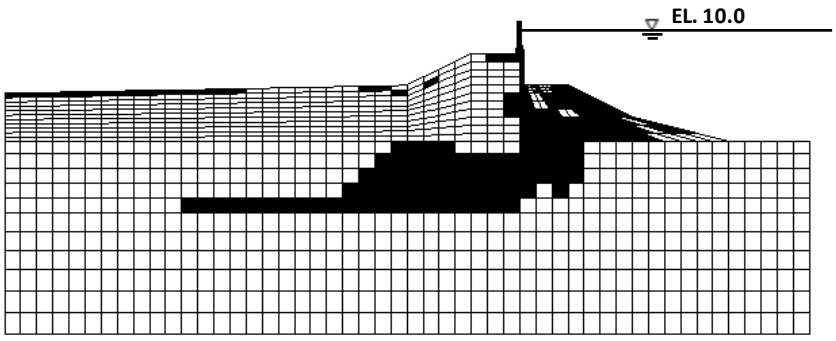

(a)

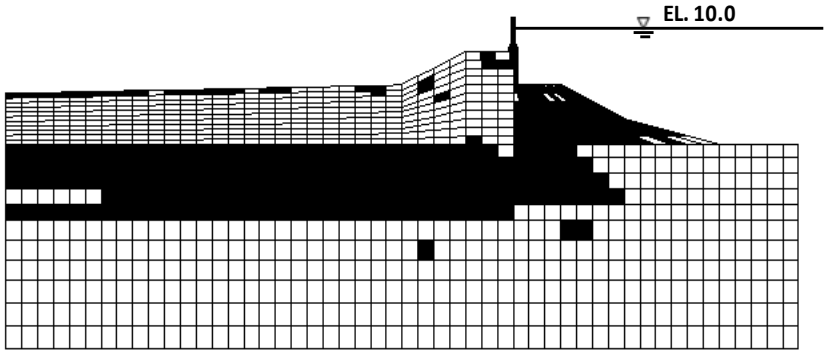

(b)

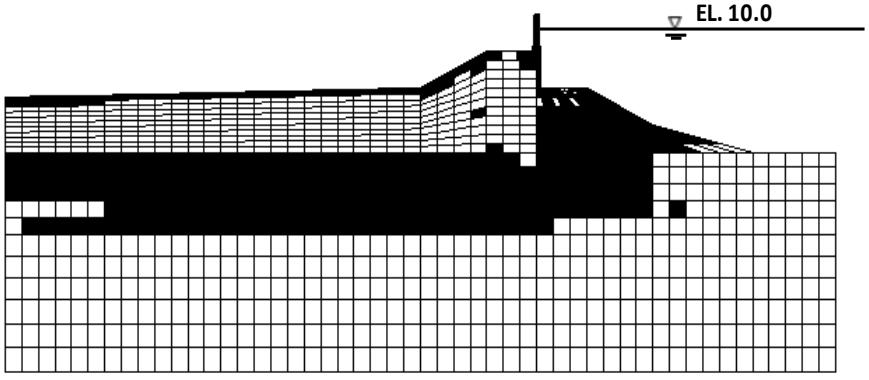

(c)

Figure 6.18. Yielded elements of soils for different soil constitutive models at 10.0 ft WL. (a) MC model, (b) AMCC model, (c) MCC model

6.8.2.3 Effect of anisotropy

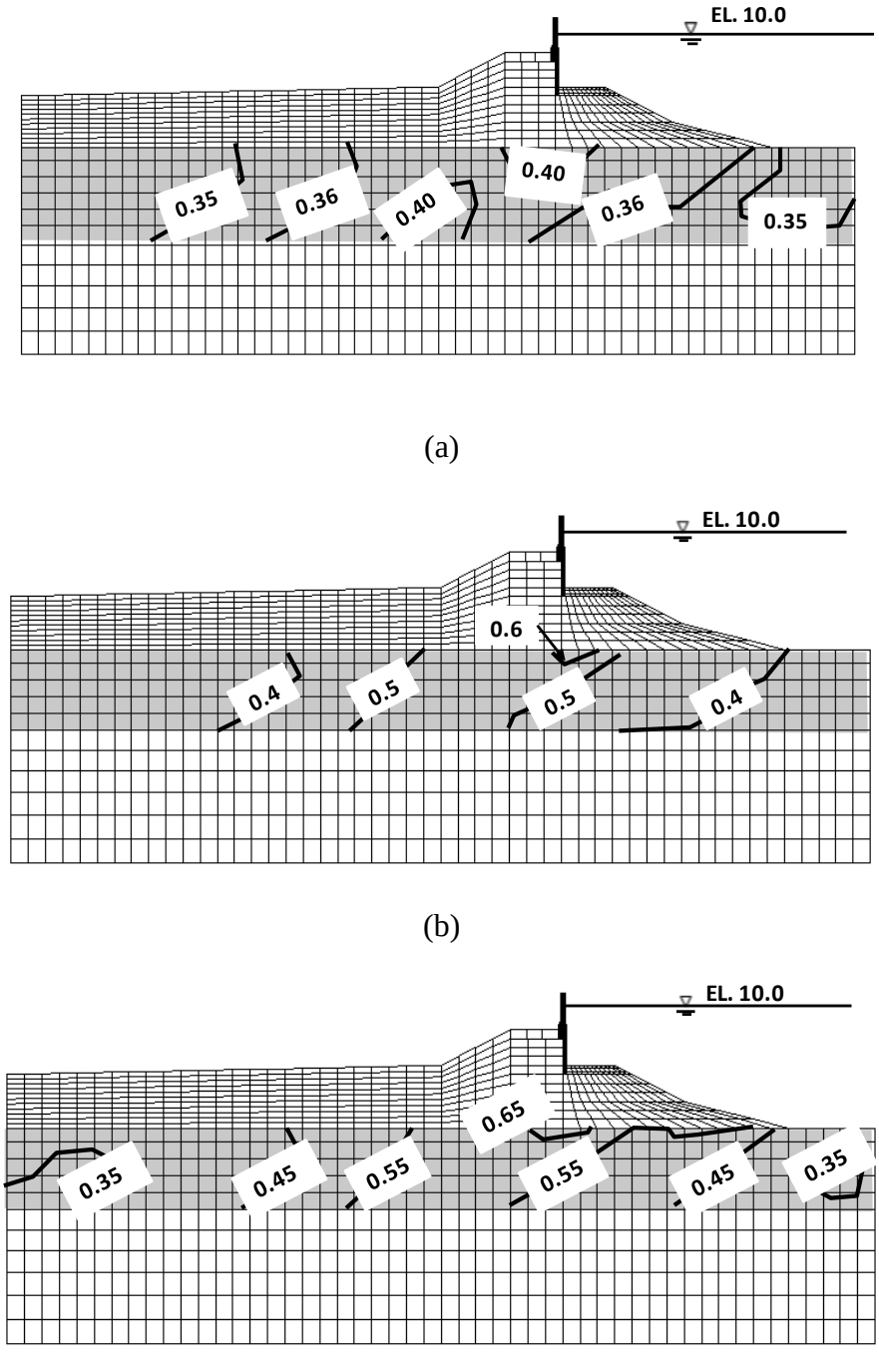

Figure 6.19. Value of Anisotropy for the different value of c at 10.0 ft WL. (a) c = 1, (b) c = 10, (c) c = 20.

From Figures 6.16 and 6.17, it was found that the incorporation of anisotropy results in a more reasonable overall deformation of the soil and the size of yielded zones. The evolution of α depends upon the parameter *c*, and therefore two additional sets of simulation were run to see the effect of *c* on the anisotropy.

Figure 6.19 shows the value of anisotropy (α) at 10 ft WL for different values of *c* (for x = 1). It shows that the value of α increase as *c* increases. But at the same time, the increase of α when *c* is 20 is not that significant as compared to when its value is 10. Since the plastic deformation decreases when anisotropy increases, the deformation decreases when *c* increases. This is reflected in Figure 6.20b. It is seen that the influence of *c* even beyond the value of 10 is less significant. From Figure 6.20b and Figure 6.19, it is also seen that the low *c* results in low back stress, higher deformation as a result of yielding at lower deviator stress. It is noted that Figures 6.16 to 6.18 should be interpreted as the condition where the anisotropy is lightly incorporated; there is a high possibility that the difference between isotropic MC model and AMCC model may be more substantial. However, the difference between the isotropic MC model and AMCC model is clearly addressed even with the lightly incorporated anisotropic model.

Figure 6.19 also shows that α is higher at high strain region as anisotropy is higher in that region. It is then interpreted as that AMCC model should be used to evaluate the behavior of large deformation problem (Note that $\alpha = 0$ for isotropic analysis). However, the overall distribution of α at low deformation region is not very different from the initial value (0.343), which explains why overall behavior of AMCC model was not much different from MCC model except the critical area which may mislead the engineer in evaluating critical zones.

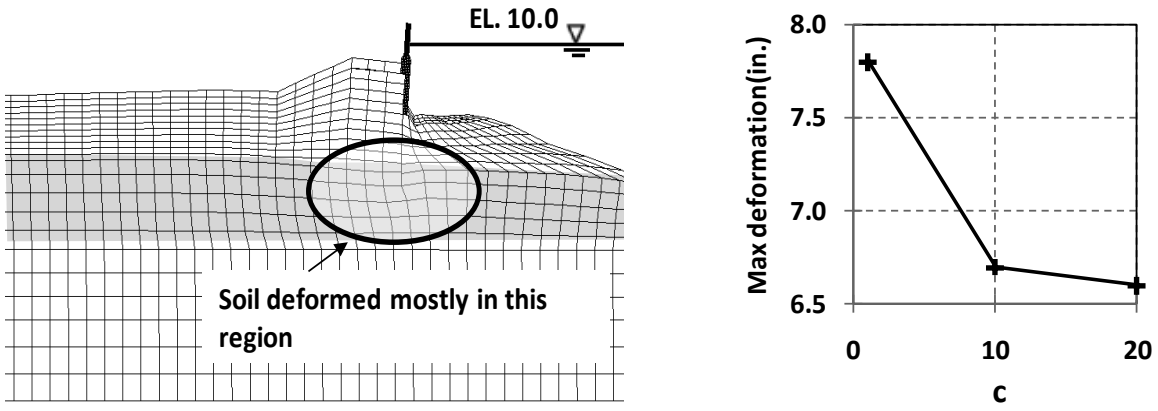

(a) Deformed shape (b) Effect of c on the deformation

Figure 6.20. Effect of anisotropy and the deformed shape

6.9 SUMMARY

This paper outlined how the AMCC model formulated by Dafalias (1987) was implemented in commercial code FLAC^{3D}, its verification, and the sample application of the implemented model. The following shows the detailed summary and conclusions of the study.

1. The AMCC model formulated by Dafalias (1987) was coded in C++ with the return mapping algorithm (plastic correction approach), and was successfully implemented in commercial code FLAC^{3D}
2. The Numerical Model when compared with the mathematical model matched well for anisotropic consolidation, drained and undrained triaxial tests for the triaxial conditions. The verification program shows that the model can capture the K_0 consolidation of the soil effectively and the and the induced anisotropy associated with it

3. AMCC model was validated with the experimental data of the clays exhibiting anisotropic behavior that is similar to the New Orleans soft soil and the experimental data fitted well with the AMCC model.
4. It showed that MC model could lead to unconservative conclusion by showing substantially smaller area of yield zone compared to MCC and AMCC models.
5. MCC model showed least stiff response, but overall prediction was not substantially different from AMCC model; this indicates the overall effect of anisotropy was not substantial in the simulated case.
6. However, the back stress (anisotropy) parameter α started from 0.342 and evolved up to 0.40 (for c = 1) and 0.65 (for c = 20) at the middle of the levee where the highest deformation occurred. This number indicated that the anisotropy becomes more severe at high deformation region.
7. The sensitivity analysis showed that the value of c beyond 20 does not have the significant influence on the responses of the model.
8. The developed model was applied for numerical simulation the 17^{th} street floodwall section of New Orleans, and to this end, results show that the MC model under predicts the deformation while the isotropic MCC model over predicts the deformation of soil as compared to AMCC model. Therefore the design based on the MC model could be non conservative. So to have the optimum design of the levees and the floodwall, the anisotropic soil constitutive model should be used in the numerical simulations.

7. DEVELOPMENT OF DEFLECTION CRITERION TO PREDICT AND MONITOR FAILURE OF THE FLOODWALLS IN NEW ORLEANS

7.1 BACKGROUND

The performance of floodwalls in New Orleans is basically related with the slope stability problems. So it is utmost necessary to understand the physics behind the stability of the levees and embankment and the methods that have been used so far to address the stability problems. There are many classical limit equilibrium methods to deal with slope stability analysis such as Ordinary Method of Slices (Fellenius 1936); Bishop's Modified Method (Bishop 1955); Force equilibrium Methods (e.g. Lowe and Karafiath 1960); Janbu's generalized procedure of slices (Janbu 1968); Morgensten's and Price's Method (1965); and Spencer's Method (1967).

The classical method of slope stability analysis using limit equilibrium method has many limitations; so the finite element approach has evolved. The major algorithm for the finite element analysis of the slope failure is based on the strength reduction technique. According to this technique, the series of trial factor of safety are used to adjust the cohesion, *c'* and friction angle, ϕ' using the following equations

$$c'_{trial} = \frac{c'}{SRF} \tag{7.1}$$

And

$$\phi'_{trial} = \arctan\left(\frac{\tan\phi'}{SRF}\right) \tag{7.2}$$

Where *SRF* is the strength reduction factor and the factor of safety SF is the value of *SRF* that makes the slope to fail. The choice of this series of *SRF* is made by using the "bracketing and bisecting procedure" proposed y Dawson et al. (1999)

This procedure has been applied in many studies (e. g. Zienkiewicz et al., 1975; Donald and Giam, 1988; Ugai, 1989; Matsui and san, 1992; Ugai and Leshchinky, 1995; Dawson et al., 1999; Griffiths and Lane, 1999; Manzari and Nour, 2000 etc.). Lot of comparisons have been made between the limit equilibrium and numerical methods by Han and Leschinsky (2004); Cheng et al.(2007); Cundall (2002); and San et al (1994), and the studies found that the factor of safety are more or less comparable and justified the advantages of the finite element analysis as indicated in paper by Grifiths and Lane (1999).

As a leap in the progress of stability analysis, a reliability analysis was adopted to complement factor of safety calculations around 1990's (e.g. Wolff and Harr, 1987; Li and Lumb 1987; Hassan and Wolff 1999; Duncan 2000; and El-Ramy et al. 2003). These analyses are done to test the reliability of the factor of safety depending upon the reliability of the data that have been used during the analysis.

Limit analysis theorems have also been used to evaluate the slope stability problems using the upper bound and lower bound theorem. This method though not popular, is however

superior to the limit equilibrium method since later violates both kinematic and static admissibility.

7.2 CURRENT ANALYSIS METHODS IN NEW ORLEANS

Though there has been a lot of improvement in the slope stability analysis, in the case of New Orleans levees and floodwall system, USACE has been adopting the conventional methods using the limit equilibrium and deterministic approach for sake of convenience. For example, USACE (2008) uses the Spencer Method (1967) or the Method of Planes (MOP) for the stability analysis of embankment slopes. The updated design guidelines specify that the risk based analysis is in the development mode. The new design guidelines also specify that the stick up height of the I-walls to be less than 4 feet so that the deflection of the wall lies within the satisfactory value, but there is no clear guidelines of the deflection criterion to be adopted in the design.

The slope analysis methods mentioned above are developed on the basis of failure criterion on stress based (static) approach. Stress based approach is easy to compute and is easy in new design or can be used as the predictive tool of the failure, but it has the limitation that it is difficult to be used as the monitoring tool. So the new method to evaluate the performance of floodwall is needed so that it can be used as the efficient monitoring tool. Since the floodwall is the combination of the wall and the embankment, it might be logical to combine the stability of the embankment with the deflection of the wall to develop a new criterion. The advantage of this method is that the stability of the embankment is easy to evaluate numerically and theoretically, and the deflection of the structure is easy to measure practically. This would emerge the deflection based criterion, which is similar to deformation based criterion (serviceability limit

state) but not exactly the same and this method is unique for the floodwalls or retaining walls only.

7.3 PROPOSED METHOD OF ANALYSIS IN NEW ORLEANS

The deflection based criterion mentioned above could be developed by correlating deflection of wall with the respective slope failure of the embankment. One of the simple way of achieving is by finding the deflection of wall for certain load level and finding the factor of safety for the global failure of the levee (embankment) using the limit equilibrium method.

But, in the case of New Orleans floodwall and levee system, monitoring the existing floodwall and taking an immediate action in the emergency period is uttermost important than the new design of the floodwalls. So it is very important to develop the efficient monitoring and predictive tool in a preventive way to manage and combat disasters by taking the necessary action in time in order to safeguard the people and the property from the devastation during the hurricane season. This could be done by giving enough time for the authorities to evacuate the affected community and at the same time start fixing the breached levee. For example, this efficient monitoring and decision making system may be the "Smart levees" (IJkdijk Foundation) practiced in Netherland. "Smart levees" consist of smart network of sensors monitored from the computers afar. The monitoring system should know when and how the water retaining structure starts to fail when the water level increases.

In order to develop above mentioned predictive and monitoring system, there should be some criterion developed, on the basis of which the initiation of failure can be realized and at the same time the enough time is available for the authority to alert the community. These criteria may be developed on the basis of stress developed on the soil; the pore water pressure; or the deflection of the wall top. Among them, as long as the effective monitoring is considered, the

most efficient criterion to assure convenient and reliable measurement could be the deflection of the wall. As already been mentioned that since there is a need of the enough time to send the warning signal, the monitoring system should encompass the system that incorporates the indicators (may be factor of safety, deflection etc) band comprising the initiation of failure to the incipient failure. This could be achieved by using lower bound and upper bound theorems rather than the limit equilibrium method. So this study will introduce the new analysis technique based on the deflection criteria reinforced with upper and lower bound theory.

7.3.1 Lower and upper bound deflection

In the limit analysis (Atkinson 1978), the upper bound load corresponds to external load which is upper bound to the collapse load so that when structure is loaded to this value, it must collapse. This theorem uses the compatibility criterion but ignores the equilibrium condition. Lower bound load, on the other hand is the external load which is lower bound to collapse load so that the structure when loaded to this load, it must not collapse. This theorem utilizes the equilibrium condition with material laws ignoring the compatibility conditions.

The upper bound and lower bound approach are also important to allow variability and uncertainty. The uncertainty is more if difference between them is high and low if the difference between them is low. Utilizing the range of the external loads, upper bound and lower bound analyses are particularly practical in monitoring and predicting the behavior of the floodwalls. In the event of flood, external load is directly related to the height of the canal water and thus the load on the wall increases gradually, allowing the time to span from the lower bound to the upper bound conditions. This bandwidth of time can be utilized by authority to send the warning to the community and be prepared for fixing the floodwall. In Limit equilibrium method, no direct information regarding deformations can be provided. And since it does not provide any band of

the external loads, it might be very difficult to utilize its result while developing predictive or monitoring tools ensuring enough time to take actions.

Since the author is more concerned with the collapse deflections (easy in measuring), the collapse load and the deflections are correlated to find the deflection band comprising the lower bound deflection and upper bound deflection. Similar to the definition of external load, lower bound deflection is the deflection below which failure cannot occur, and the upper bound deflection is the one above which failure must occur. The upper bound and lower bound deflection of the wall top are correlated with the failure (yielding) of the zone in the grid. The deflection of the wall top is the stress-strain problem, where as the failure of the levee embankment is the stress equilibrium problem combined with material yielding. This can also be termed as the local factor of safety

7.3.2 Numerical Prospective

In the process of evaluating the bound deflections, stability problem can be addressed using the numerical approach based on the strength reduction method. Since in Finite element or Finite difference software like FLAC^{3D}, the quantification of global failure is almost impossible using the main program, a new technique can be implemented using an algorithm which is done according to (e.g. Mohr Coulomb criterion)

$$FS = \frac{1}{SMF} = \frac{2c\cos\phi + (\sigma_1 + \sigma_3)\sin\phi}{\sigma_1 - \sigma_3} \qquad (7.3)$$

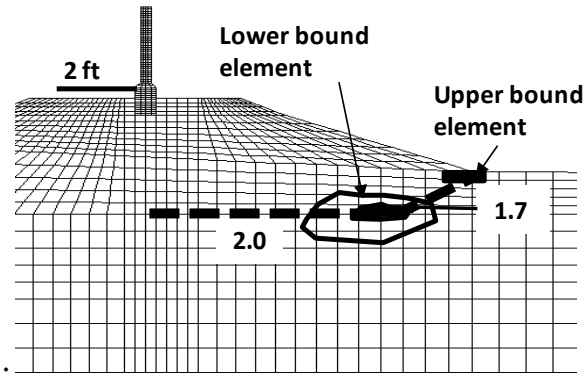

Figure 7.1. Upper bound and Lower bound element (zone)

Using this algorithm, the factor of safety of each element (zone) can be monitored .In terms of the yielding of the zones, lower bound deflection is the one for which the first element (lower bound element) of the levee embankment starts to yield locally. According to Michalowski (1989) the upper bound solutions also satisfy the force equilibrium equations. This can be solved by either considering the energy equilibrium technique (compatibility criteria), or the global force equilibrium equations. At global failure, since the material does not violate the yield criteria, all the failed elements in the failure zone also exhibit FS=1. The boundary between the failed zones and the unyielded zones defines the global failure surface so that the failed zone acts as the rigid plastic zones having the rigid body motion. Therefore, FS=1 for last element to yield before the global failure took place, implicitly means the global FS=1. The upper bound deflection of the wall, thus, implicitly corresponds to global failure of the Levee-wall system. Considering this philosophy, the upper bound deflection is the deflection of the wall in which the last element (upper bound element) of the levee (embankment) yield before the global failure occurs (see Figure 7.2). In order to find lower and upper bound values, propagation of shear band in the embankment is thus monitored which varies according to the nature of the slopes, soil conditions, and the nature of the loading.

7.4 APPLICATION EXAMPLE IN NEW ORLEANS

The above discussed philosophy is applied in one section in the New Orleans floodwalls. To develop the criterion for the full phased monitoring system, other sections (mostly critical sections) should also be evaluated in the similar manner.

7.4.1 Soil Profile and Parameters

The section chosen is the site where the Full scale load test was done. According to HPO (2008), the load test site consists of four layers of foundation soil and the embankment backfill soil layer as shown in Figure 7. 2. The lowermost soil layer is the stiff clay known as Bay sound clay. This layer extends below Elevation (EL.) of -44.4 ft measured in North American Vertical Datum of 1988 (NAVD88) scale. The stiff clay is overlain by Beach Sand that extends from EL. -44.4 ft to EL.-21.4 ft Above the Beach Sand layer, up to EL. -11.4 ft is the silty-sand layer which is overlain by the marsh layer. The marsh layer is divided into two parts namely Marsh-crest and the Marsh-toe as they exhibits different shear strength. The embankment with backfill material extends up to EL. 2.2 ft above the marsh layer. The FLAC^{3D} numerical model was constructed to represent those layers with sheet piles and the concrete floodwall. The sheet pile is embedded inside the reinforced concrete to EL. 2.75 ft from the base of I-wall. The reinforced concrete floodwall extends from EL. 0.2 ft up to EL. 13.2 ft and the tip of the sheet pile is at EL. -21.4 ft Table 7.1 shows the calibrated parameters. The details about the calibration of the soil parameters are discussed in chapter 3. The evaluation of properties of sheet pile, concrete capping and interface and is summarized in Table 7.2.

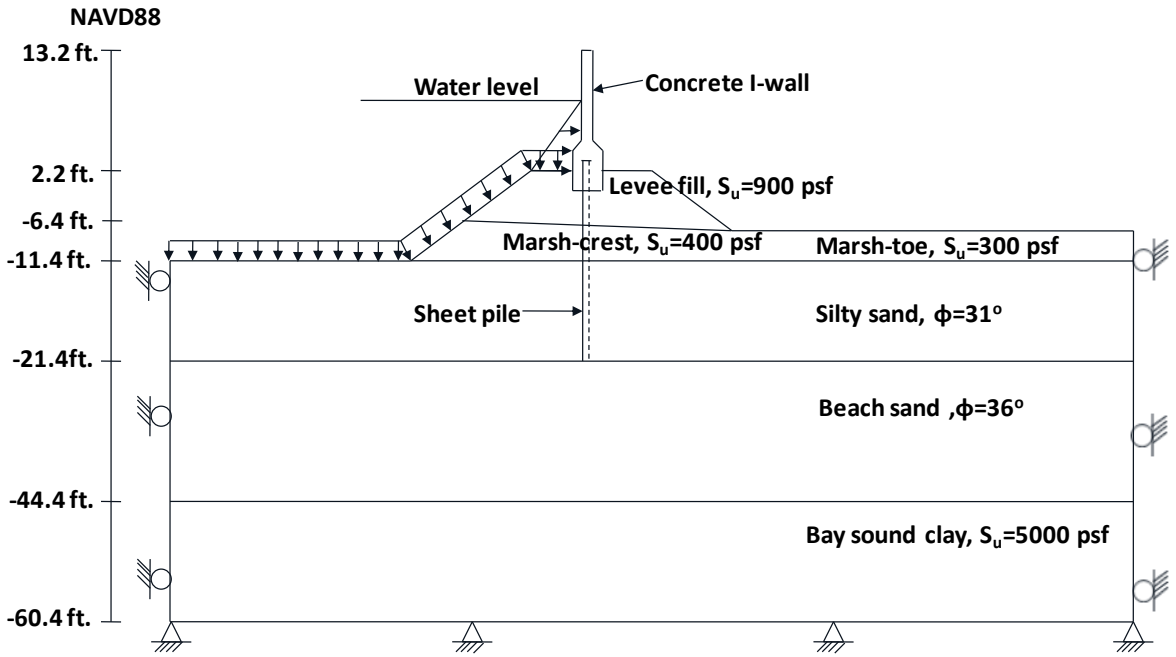

Figure 7.2. Soil Profile and geometry

Table 7.1. Soil parameters used in the analysis

Soil layer	Shear Strength	Saturated density (slug/ft^3)	Elastic modulus (psf)	Poisson's ratio
Levee-fill	s_u=900 psf,ϕ_u=0°	3.39	8.28e4	0.48
Marsh(Toe)	s_u=300 psf,ϕ_u=0°	2.49	8.28e4	0.48
Marsh(Center)	s_u=400 psf, ϕ_u=0°	2.49	1.1e5	0.48
Silty Sand	c=0 ,ϕ=31°	3.66	2.76e5	0.43
Relic Beach Sand	c=0 ,ϕ=36°	3.79	4.83e5	0.41
Bay sound Clay	s_u=5000 psf,ϕ_u=0°	3.89	5.5e6	0.48

Table 7.2. Structural properties

Structures	Element	Structural properties			Interface properties	
Sheet pile	Embedded liner	E	4.2	Gsf	k_n	Varies with depth $k_s \approx k_n \approx 10 \cdot \left[\frac{(K + 4/3G)}{\Delta z_{\min}} \right]$
		ν	0.3			
		thickness	0.33*	in		
		Density	15.14	Slug/ft^3		
Concrete I-wall	Brick element	G	0.216	Gsf	k_s	
		K	0.285	Gsf		
		Density	4.72	Slug/ft^3	c_i	$c = 0.67 s_u$
					δ_i	$\delta = 0.67\phi$

7.4.2 Simulation procedure

Normally there are two types of stress analyses namely effective stress and total stress analyses. These analyses are dependent on the loading conditions. The total stress analysis are done for the design of embankments during construction, rapid drawdown and earthquake since in these loading conditions, the pore water pressure are not allowed to dissipate. For the case of steady state seepage condition and the partial pool conditions, the effective stress analysis may be done given the condition that the soil are totally drained and the piezometrical heights are available.

USACE (2003) in their revised edition of EM 1110-2-1902, however, recommend using the total stress analysis for the slow draining soil using undrained strength and effective stress analysis for the free draining soil using the drained strength. It states that the soil having permeability coefficient higher than 10^{-4} cm/ sec is taken as the free draining soil and that lower than 10^{-7} cm/sec is taken as the undrained soil. In the case of the steady state condition, no matter

what the soils are, the effective stress analysis is done. This agrees well with the Duncan (1996) concept. It assumes that in case of the surcharge pool, it does not persists for a long time to establish the steady seepage condition. In the case of the drawdown , USACE (2003) recommends to use the effective stress analysis for the free drained material whereas for the low permeability material, the three stage computation process developed by Lowe and Karafiath and modified by Wright and Duncan (1987) and Duncan, Wright and Wong (1990) are used.

In the case of the New Orleans levee analysis the type of the analysis that may be used can be in accordance with Duncan (1996) with slight modifications. According to Duncan (1996), the type of analysis might be as for multistage loading condition in which a period of consolidation under one set of load is followed by a change in load under undrained conditions. According to him, the total unit weight for all soil is included where as the drained strength for the free drained soil and undrained strength for the undrained soil are given as the input parameters; and pore pressure from the steady state condition is given for the free drained soil where as it is kept zero for the undrained soil.

In this study, the method proposed by Duncan (1996) is slightly modified since the free draining soil is sandwiched in between the undrained soil layers so that the pore pressure in the sand layer is not much changed during the multistage loading condition. So, the pore pressure in this layer is not incorporated during the analysis, since the total unit weight is taken for the analysis. Otherwise if pore water pressure is given, the hydrostatic force is double counted

Apart from using the total stress approach, it was established in Chapter 3 that the gap formation and the strength reduction of the marsh layer is the major failure mechanism of the floodwall. So this has been incorporated in the analysis too. FLAC^{3D} is used as the numerical tool for the analysis.

7.4.3 Result and Discussion

Figure 7.3 show the contour of the factor of safety calculated using Eq. (7.3). As the water level increases, the shear band also increases. In the figure, the area enclosed by the contour having factor of safety of one denotes the failed zone. From the figure, it is seen that the shear zone first develops in the weak marsh layer, somewhere under the mid slope. The failed zone then propagates on either side of it as the water level increases. The element that fails first is traced out, and the water level and the deflection of the top of wall corresponding to that failure are noted. This gives the lower bound deflection

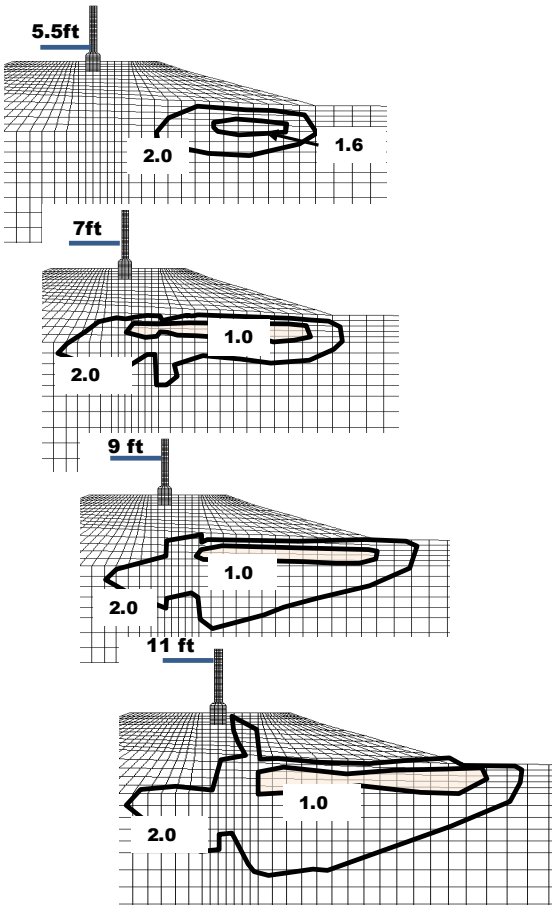

Figure 7.3. Expansion of failure zone with respective water level elevation

Then the water level and the deflection at which the last zone (the zone at the toe of the levee) is noted and termed as the upper bound deflection. It is not necessarily that the upper bound element is always a toe element. Upper element signifies that the global failure is incipient and it is based on the modeler decision.

Figures 7.4 and 7.5 shows deflection vs. factor of safety for lower bound and upper bound elements. The numbers shown inside the graph shows the elevation of the water level. In the figure, the solid lines shows the actual factor of safety of the respective element and the broken line indicates failure condition (FS=1). From these figures, it is seen that the lower bound deflection is 1.5 in. at water level elevation of 6.5 feet and the upper bound deflection is 7 in. at around the water level elevation of 10.5 feet. The result of this study is similar to what the previous studies have found out that the walls in London Avenue Canal failed around 10 feet water level elevation during Katrina.

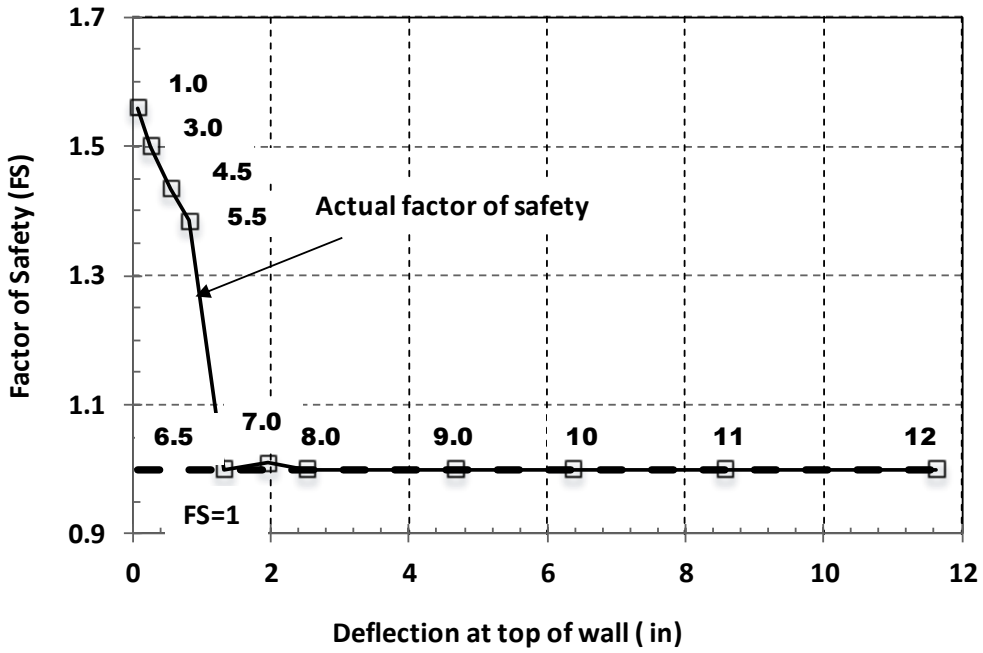

Figure 7.4. Lower bound deflection vs. factor of safety

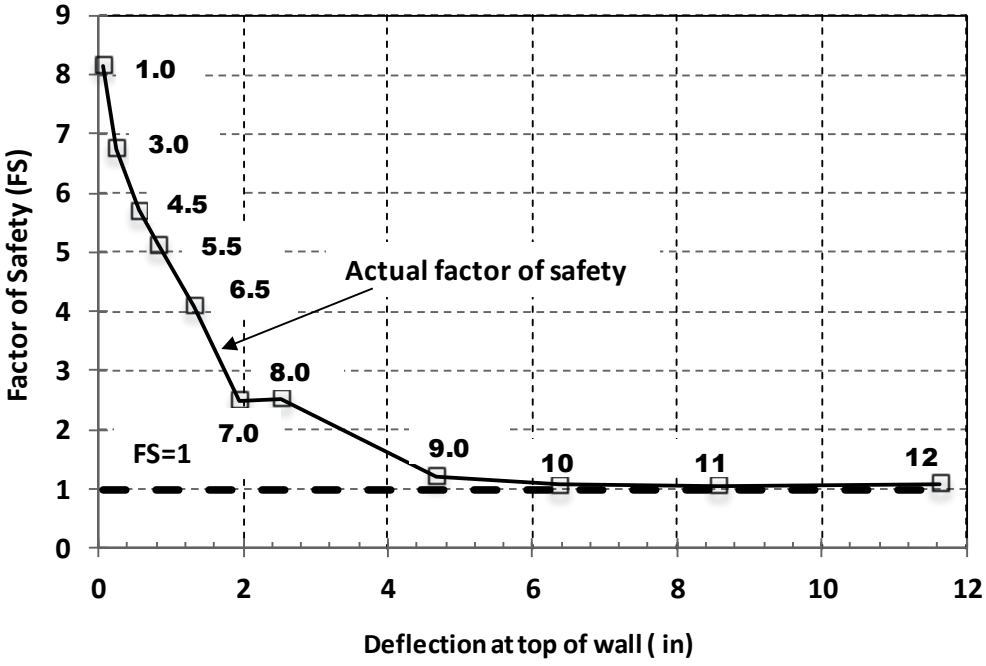

Figure 7. 5. Upper bound deflection vs. factor of safety

If we look at the hydrograph of the canals in New Orleans, the time span elapsed from the Water elevation of 6.5 feet to 10.5 feet is about two hours. This two hour can be utilized by the authority to prepare for the levee fixing and the evacuation program. Figure 7.6 shows the failure zone at 12 feet water level and the it shows the complete global failure, where the failure mechanism is the shear failure at the interface between the silty sand and the Marsh layer.

For the reliable monitoring, it is however suggested that the continuous measurement of the deflection has to be made in between those bounds so that the depletion of the water level could be observed or sometimes to figure out the earlier near failure conditions. In those cases, tracing only two bounds of deflections might not be sufficient.

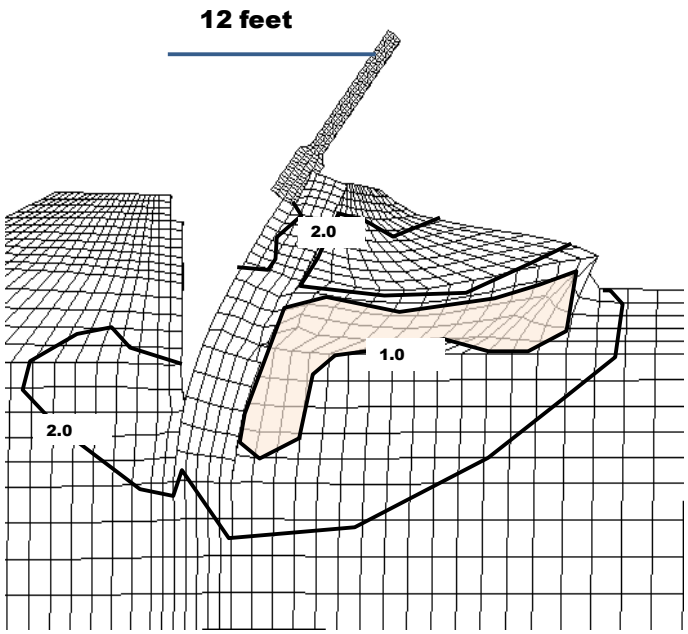

Figure 7. 6. Failure zone and the deformed mesh

7.5 CONCLUSIONS

From this study, following conclusions are drawn out.

- From this study an initial effort was made to establish the deflection criterion based on the lower bound and upper bound methods.
- The established criterion was applied in London Avenue Canal section the New Orleans levees. From the analysis, it was found that the lower bound and upper bound deflection are 1.5" and 7" with a time span of 2 hours in between. For the more reliable monitoring, however, the continuous monitoring of the deflections in between has to be done.
- This method can be utilized for only slope failure related problem, but may not be applicable for the seepage failure mode.
- For the full flexed Monitoring system, a series of analyses are needed to be done in critical sections following the similar method developed in this study.

8. CONCLUSIONS AND RECOMMENDATIONS

8.1 SUMARY AND CONCLUSIONS

Hurricane Katrina revealed many design flaws of the floodwall systems in New Orleans and urged the geotechnical engineers to improve the design criteria and the countermeasures of this protection system for the next hurricane season. The main counter measure programs that the USACE now practicing is heightening the floodwalls (100 year return period) and improving the sub surface soil conditions using the deep soil mixing techniques. In the vicinity of New Orleans, in Mississippi river sides, they are also installing the relief wells and the berms to control the failure due to seepage. But these techniques seem to be quite expensive in terms of economical ground, and therefore, alternative economical but effective techniques needed to be sought out.

The failure of these flood protection system occur mainly because it didn't behave as if it was a system in the global sense, and failed due to localized failure as discussed in chapter 1 and 2 ; gap formation being the main cause. So the effectiveness of the countermeasure, therefore, lie how effectively they prohibit those failure mechanisms. The techniques that the project proposed are the structural cap to integrate I-walls which are composed of different panels and to apply the Bentonite apron to seal the gap formed adjacent to the floodwall on the flood side. The objective of the first countermeasure is to ensure that the floodwalls behave as one system and the second countermeasure is to prohibit the local failure of the walls. The combination of these countermeasures ensures the resilient hurricane protection system.

The evaluation of these new methods can be done by experimentation, centrifugal tests, full scale test and the numerical analysis. This study is focused on the last approach.

The main objective of this study was to numerically evaluate the effectiveness of the economic retrofitting techniques for the floodwalls and to implement the advanced constitutive model in FLAC^{3D} to capture the anisotropic behavior of the soft soils. Apart from it, this study also aimed to make an initial effort to develop the deflection based failure criteria that can be instrumental in developing the monitoring tool.

Before the effectiveness of the cap was evaluated, there was a need to calibrate the stiffness of the subsurface soil and to develop the new modeling approach. For this, the full scale load tests on the London Avenue Canal conducted by USACE (USACE 2008) were chosen to verify the approaches undertaken to simulate the I-wall and to calibrate the model stiffness parameters. In the study two hypotheses like the gap formation and the reduction of soil strength were tested. The detailed conclusion of the study is already mentioned in the respective section. From the study, it was found that the stiffness parameters of the soil need to be increased by 1-12 of the stiffness documented in IPET. Apart from that the study also showed that the gap formation and the reduction of the shear strength of the marsh layer played a crucial part on the behavior of I-wall due to water loads. From the study, it was found out that the shearing of marsh layer trigger the failure of the I-wall which is due to the reduction of strength induced by increase in water content.

Using the calibrated modulus and the verified numerical procedure, the effectiveness of the structural cap was evaluated. (The main objective of the study was only to evaluate the effectiveness of the cap: the detailed design and the evaluation of the designed cap is mentioned in the other papers and not included in this dissertation). In the study, the anisotropic stiffness of

the sheet pile was incorporated and the it was found out that the anisotropy was influential upto 0.1 and below it, it was not that influential when the displacement and the moment distribution was taken into account. Since the cracking of the concrete has also great influence in the response of the floodwalls, it was also incorporated in the analysis. Since the longitudinal and vertical distribution of the reinforcement is not same for the typical floodwall sections, the rigidity in these two directions were assigned differently. Three potential failure mechanisms were investigated in the analysis such as variation of soil strength along the length of the levee/ floodwall; localized erosion; and the localized structural failure of the floodwall. From the study it was found that the structural cap was efficient mechanism to integrate the floodwall system by minimizing the relative displacement of the adjacent panels. However, the cap was not efficient to reduce the overall displacement of the wall for first two cases whereas it was good for the third case .The study also found out that the existing floodwall section New Orleans floodwalls is critical for the first two cases in terms of the moment capacity as they were designed mainly to withstand the hydraulic loads rather than to withstand the moment created due to non uniform erosion or the variation of soil strength along the floodwall length. The study recommends incorporating these effects in the future design of the floodwalls.

The study also conducted the research to evaluate the effectiveness of the bentonite apron as the self sealing mechanism. Before the effectiveness of the bentonite apron was evaluated, the conditions were categorized for which the gap was the sole cause of the failure, the consequence of the failure, or the secondary cause of the failure so that the effective implementation of the bentonite apron could be justified. For the condition where the gap is the result of the failure, the bentonite apron may not be the feasible technique. In the case where the gap is the secondary cause of the failure, the bentonite apron should be accompanied by other retrofitting technique.

Absence of either of this approach would lead the failure of the floodwall. In case where gap is the cause of the failure, bentonite apron is an effective countermeasure to seal the gap. But it was necessary to verify that bentonite apron will not exert an inadmissible swelling pressure and at the same time, it has the potential to swell at any water level so that the effective self sealing could be achieved. It was found out that the bentonite apron does not exert a high pressure on the wall and at the same time swelling potential was maintained.

In the earlier sections, the effectiveness of retrofitting techniques was evaluated with the simple Mohr Coulomb Model. The Mohr Coulomb Model is simple to apply but may not be sufficient to model the behavior of soft soils where the strength anisotropy and the strength dependency on the volumetric behavior prevail. So this study incorporated the implementation of the advanced constitutive model known as "Anisotropic Modified Cam Clay Model" (Dafalias 1986) in the numerical code FLAC^{3D}. The model was coded with C++ programming and saved as the Dynamic Link Library (DLL) file which can be loaded any time. The numerical code was then verified with the analytical model and it was found that it matches very well. At the same time, the mathematical model was also validated with the experimental results of the clayey soil similar to the lacustrine clay of New Orleans. The experimental result matched well with the analytical result. So we were confident that model that we were going to use can be well suited to model lacustrine clay of New Orleans. Sensitivity analysis was also done to see the sensitivity of the parameters in the model so that it would be easy in calibrating the parameters. Then the model was applied to simulate the behavior of the 17th street Canal floodwall section of New Orleans. The results from the anisotropic model were compared with the ones with the Mohr coulomb Model and the Isotropic Modified Cam Clay Model. The analysis showed that the anisotropic model resulted in a similar overall deformation to Mohr-Coulomb isotropic model.

However, the anisotropic model showed more widely spread yielded elements and higher shear strain gradient in the lacustrine clay layer, reconfirming that the lacustrine clay layer played a major role for the failure in 17th St. Canal. This result also signified that isotropic Mohr-Coulomb might be good for evaluating overall behavior in moderate deformation problems, while anisotropic Modified Cam Clay model was good even for large strain problems where more accurate evaluation of yielding is needed.

Other than designing and constructing the new floodwalls or retrofitting the existing floodwalls, it is also important to develop monitoring tools that aid the effective emergency management and evacuation program for the next hurricane season. The criterion developed so far, and the analytical tool used so far may not be efficient to develop the proper and efficient monitoring too. In order to develop such monitoring tool, deflection based failure criterion is necessary. This dissertation demonstrated an initial effort to develop and apply deflection based criterion with the example case. To develop the full phased deflection criterion for the use in monitoring system, however, an extensive work has to be done for at least critical floodwall sections using the similar approach discussed chapter 7, so that in future, initiation of failure can be detected well before the breach of the floodwall to allow enough time for evacuation and levee fixing program

The detailed conclusions from the study are already stated in the respective chapters (please see chapter 3 to 7)

8.2 FUTURE STUDY

This study was mainly focused on the application and implementation of the established theory rather than establishing new knowledge. So the long string of the research and publications following this research cannot be guaranteed. Albeit, to bridge some limitations of

this study and to make it complete, the author recommends some further studies that was not covered during the study. Following are some recommendations.

a. In this study, only the effectiveness of the cap was pre-evaluated. The study was primarily focused to study the three cases in which there is a soil strength variation along the levee length, localized erosion of the levee material, and the localized failure of the wall occurs. The structural cap behaves effectively to prohibit the relative displacement of the adjacent panels of I-wall. The caps are modeled ideally as the rigid element, which is not the case, necessitating the optimum design of the. This optimum design of the cap is under way where the different size and the stiffness of the cap are adopted in the study and will be documented as future theses and journal articles.

b. It was proven that the Bentonite apron was effective in the ideal condition (laboratory condition) since the relationship between the volumetric strain and swell pressure was characterized in the lab. But in the field, the bentonite apron may get saturated well before the hurricane flooding is introduced so that the swelling potential is well consumed before the flooding and this might reduce the effectiveness of the bentonite apron. So a study is necessary on how to implement this in the field and the methodology required saving them from the initial saturation. Apart from that, a study may be required on to address how the bentonite apron could be implemented on the field for the effective performance. This might require a full scale testing.

c. In this study, the AMCC model was implemented in the triaxial framework. The triaxial framework is good as long the critical angle remains same. But in reality

the critical angle may vary according to the lode angle. In this case, the anisotropy parameter is no longer the scalar quantity but is a tensor quantity. So in the future, this study recommends implementing the AMCC model developed in the multiaxial framework to better simulate the behavior of soft soil.

d. This study only demonstrated the initial effort to develop deflection criterion as the effective tool to monitor the performance of the floodwalls during hurricane ladings. To apply it as the complete monitoring system, a detailed integrated multi disciplinary study comprising principally the geotechnical, numerical, instrumentation, networking and decision making process is required.

LIST OF REFERENCES

LIST OF REFERENCES

American Concrete Institute (ACI). (2005). "Building Code Requirements for Structural Concrete (ACI 318-05) and Commentary (ACI318R-05)", Detroit

Anadarajah, A.M., and Dafalias, Y.F. (1985). "Anisotropic hardening bounding surface constitutive model for clays." *Proc.,5th Int. Conf. on Numerical methods in geomechanics,* Balkema, Rotterdam, The Netherlands, 267-275

Anadarajah, A.M., and Dafalias, Y.F. (1986). "Bounding surface plasticity III: application to anisotropic soils." *J. Eng. Mech.,* ASCE, 112(12), 1292-1318.

Anandarajah, A. and Agrawal, D.(1991). "Computer aided calibration of soil plasticity model." *Int. J. for Numeric. and Anal. Meth. in Geomech.* 15(12), 835-856

Baker,R.(2003). "Inter-relations between experimental and computational aspects of slope stability analysis." *International Journal for Numerical and analytical methods in Geomechnaics,* No.27, 379-401.

Betram G.E. (1940)." An experimental investigation of protective filters. " Soil mechanics series No. 7, Graduate school of Engineers, Harvard University, Cambridge, Mass

Bishop,A.W.(1955). "The use of the slip circle in the stability analysis of the slopes." *Ge'otechnique,* 5(1), 7-17.

Bligh, W.G. (1910). “Dams, Barrages and Weirs on Porous foundations.” Engr. News, 64(26), 708-710

Borja, R.I., Hseih, H.S. and Kavazanjian, E. (1990)” Double yield surface model. II: Implementation and verification.” *J. Geotech. and Geoenv. Eng*., ASCE, 116(9), 1402-1421.

Bowles, J. E. (1996) “Foundation Analysis and design”, McGraw-Hill, New York

Brandon, T. L., Wright, S.G. and Duncan, J. M.(2008) “Analysis of the stability of I-walls with Gaps between the I-Wall and the Levee Fill” *J. of Geotech. Geoenviron. Eng*., 134(5), 692-700

Burland, J.B. (1965). The Yielding and dilation of clay.” *Geotechnique*, 15(), 211-214

Budhu, M.(2000) “ Soil Mechanics and Foundations”, John Wiley & Sons, Inc. , New York; pp 213

Casagrande, A. (1937). “Seepage through dams. Contributions to Soil Mechanics 1925-1940. Boston Society of Civil Engineers, 1940 (reprinted from J. New Eng. Water works Assoc., 51, 131-172) 295

Cathie, D.N. and Dungar, R. (1978). “Evaluation of finite element predictions for constructional behavior of a rockfill dam.” *Proceedings Instrumentations Civ. Engrs., Part 2* (65),551-568.

Cavounidis, S. and Vaziri, H. (1982) “ Effect of plasticity on load transfer in zoned dams.” *Proceedings 4rd int. conf. on Numerical Meth. in Geotech. Eng*., A.A. Balkema, Rotterdam, The Netherlands, 663-669.

Chang, C.S. and Duncan, J.M. (1977). “Analysis of consolidation of earth and rockfill dams.” Geotech. Eng. Report No. TE 77-3, U S Army Eng. Waterway Experiment station, Vicksburg, MS.

Cheng, Y.M. , Lansivaara, T. and Wei, W.B. (2007).” Two-dimensional slope stability analysis by limit equilibrium and strength reduction methods.” *Computers and Geotechnique*, 34, 137-150

Cundall, P.A. (2002). “ The replacement of limit equilibrium methods in design with numerical solutions for factor of safety.” Power Point presentation, Itasca Consulting group, Inc.

Dafalias, Y.,and Herrmann, L.R. (1982). “ Bounding surface formulation of soil plasticity.” Soil Mechanics, Transient and Cyclic Loads, G. N. Pande and O.C. Zienkiewicz, eds, Wiley and sons

Dafalias, Y.,and Herrmann, L.R. (1986). “Bounding surface plasticity II: Application to isotropic cohesive soil.” *J. Eng. Mech*.,112(9),1263-1291

Dafalias, Y.F. (1987). “An anisotropic critical state clay plasticity model.” *Constitutive laws for engineering materials: Theory and applications*, C.S. Desai et al. eds., 513-521

Dafalias Y.F., Manzari, M.T. & Papadimitriou, A.G. (2006)” SANICLAY: A simple anisotropic clay plasticity model” *International Journal for Numerical clay and Analytical Methods in Geomechanics*, 30(12): 1231-1257

Dawson, E.M., Roth, W.H. and Drescher, A. (1999) “ Slope stability analysis by strength reduction.” *Geotechnique*, 49(6),835-840

Della Rossa, M.C., Francani, V. , and Gattinoni, P. (2003). " Studio idrogeologico del terrotorio monszese: individuazione e caratterizzazione delle zone a basaa resistenza." *Quaderni di Geologia Applicata* 10 (2), 103-120.

Denish, J.E., Schnabell R.B. (1983). " Numerical Methods for unconstrained Optimization and Non Linear Equations." Prentice-Hall, Engelwood Cliffs, NJ.

Drucker, D.C., Gibson, R.E. and Henkel, D.J. (1957). " Soil mechanics and work hardening theories of plasticity." *Transactions* ASCE, Vol. 122, 101-106

Dunbar,J.B.,Britsch III,L.D. (2008) "Geology of the New Orleans Area and the Canal Levee Failures" J. of Geotech. Geoenviron. Eng., 134(5), 566-582

Duncan, J.M., Buchigani, A.L. and De Wet, M.(1987). "An Engineering manual for slope stability studies, Virginia Tech, Blacksburg, VA

Duncan, J. M., Wright, S. G., and Wong, K. S. 1990. "Slope Stability During Rapid Drawdown,"

Duncan, J.M. (1996). "State of the Art: Limit equilibrium and finite-element analysis of slopes." *J. Geotech. Geoenv. Eng*., ASCE, 122(7), 577-596.

Duncan, J.M. (2000). "Factor of safety and Reliability in Geotechnical Engineering." *J. Geotech. Geoenv. Engr*., ASCE,126 (),307-316.

Duncan, M., Brandon, T. L., Wright, S.G. and Vroman, N.(2008) "Stability of I-walls in New Orleans during Hurricane Katrina" *J. of Geotech. Geoenviron. Eng.*, 134(5), 681-691

Duncan, J.M. and Buchignani, A.L.(1976) "An Engineering Manual for settlement studies", Department of Civil Engineering , University of California, Berkeley, June 1976, 94-94

El-Ramy, H., Morgenstern, N.R. and Cruden, D.M. (2003). "Probabilistic stability analysis of a tailings dyke on pre-sheared clay-shale." *Can. Geotech. J*., 40(..)192-208.

Everard, N.J. (1993) "Reinforced Concrete Design" Serviceability and Deflections McGraw-Hill, New York, 162-178

Fellenius, W. (1936). "Calculation of the stability of earth Dams." *Proceedings of the 2nd Congress on Large Dams*, Washington D.C., Vol. 4. U. S. Government Printing Office.

Fletcher, R. (1980). "Practical method of Optimization-volume 1: Uncnstrained optimization.", Willy, Chichester, UK.

Forcheimer, P.(1886). "Ueber die Ergiebigkeit von Brunnenanlagen und Sickerschlitzen." Zeitschrift, Architekten und Ingenier-Verein, Hannover, 32(7), 539-564.

Gill, P.E., Murray,W., and Wright, M.H. (1981). "Practical Optimization." Academic press, London

Graham, J., Noonan,M.L., and Lew, K.V. (1983). "Yield states and stress-strain relationship in natural plastic clay." *Can. Geotech. J*.,20(3),502-516

Griffiths, D.V. and Lane, P.A. (1999)."Slope stability analysis by finite elements." *Geotechnique*, 49(3),387-403.

H. Bolton Seed Symposium, Vol. 2, University of California at Berkeley, pp 253-272.

Hagerty, D.J.(1991). " Piping-sapping erosion I: basic considerations." *J.of Hydro. Engr*., 117, 991-1008

Hammah, R.E. Curran, J.H. ,Yacoub, T.E. and Corkum, B. (2004).”Stability Analysis of Rock Slopes using the Finite Elements Methods.” *Proceedings of the ISRM Regional Symposium EUROCK 2004 and 53rd Geomechanics* Colloquy, Salzburg, Austria.

Hammah, R.E. Yacoub, T.E. and Corkum, B (2005). “ The shear strength Reduction Method for the Generalized Hoek-Brown Criterion, *Proceedings of the 40th US Symposium on Rock Mechanics*, Alaska Rocks, Anchorage, Alaska.

Han, J. and Leshchinsky, D.(2004). “ Limit Equilibrium and continuum Mechanics based Numerical Methods for analyzing stability of MSE walls.” *Proceedings of 17th ASCE Engr. Mechanics Conf.*, University of Delaware, Newark, DE.

Hassan, A.M. and Wolff, T.E. (1999). “ Search algorithm for minimum reliability index of earth slopes.” *J. Geotech. and Geoenv. Engr.*, 125(4)301-308.

Hart, R.D., and Detournay, C.(2005). “Geotechnical constitutive model in an explicit, dynamic solution scheme, soil constitutive models: evaluation, selection and calibration” *Proc. of Geo frontiers*, Austin , Texas, ASCE geotechnical publication,128,185-203

Hurricane Protection Office (HPO) of the US Army Corps of Engineers and the St. Louis District Corps of Engineers (2008) “The London Avenue Site Specific Load test”

Hurricane Protection Office(HPO)of the US Army Corps of Engineers and the St. Louis District Corps of Engineers (2008b) “ The London Avenue Site Specific Load test” Appendix-D: Analysis of the London Avenue Canal Load test-Section1 Soil Structure Interaction Analysis,1-17

Interagency Performance Evaluation Task Force (IPET) (2007) “Performance evaluation of the New Orleans and southwest Louisiana hurricane protection system” Final Report of the IPET

Itasca Consulting Group, (2006) “FLAC^{3D} Manual”, Minneapolis, Minnesota

Itasca Consulting Group, (2006) “FLAC Manual”, Minneapolis, Minnesota

Jang, W. (2010). “Erosion Study of New Orleans Levee Soils Subjected to Plunging Water”, Ph. D. Dissertation, University of Mississippi

Jaky, J. (1944) “The Coefficient of Earth Pressure at rest”, In Hungarian (A nyugalmi nyomas tenyezoje)” *J. Soc. Hung. Eng. Arch.* (Magyar Mernok es Epitesz_Egylet Kozlonye),355-358

Janbu, N. (1968). “Slope stability computations.” Soil Mech. and Found. Eng. Report, Technical University of Norway, Trondheim, Norway

Kaliakin, V. N., and Dafalias, Y. F. (1990) ‘‘Theoretical aspects of the elastoplastic-viscoplastic bounding surface model for isotropic cohesive soils.’’ *Soils Found*., 30(3), 11–24.

Kidd, J.T. (2011) “ Developing a Retrofitting System to Mitigate Floodwall Failures of New Orleans” Ms Thesis, University of Mississippi

Knabb, Richard D; Rhome, Jamie R.; Brown, Daniel P (December 20, 2005; updated August 10, 2006). "Tropical Cyclone Report: Hurricane Katrina: 23–30 August 2005" (PDF). National Hurricane Center. http://www.nhc.noaa.gov/pdf/TCR-AL122005_Katrina.pdf. Retrieved 2006-05-30.

Kohgo, Y. and Yamashita, T.(1988). " Finite element analysis of fill type dams- stability during construction by using the effective stress concept." *Proceedings conference numer. Meth. in Geomechanics*., ASCE, New York, 1315-1322.

Kolb, C. R and Saucier, R. T. (1982). " Engineering Geology of New Orleans" *Rev. Eng. Geo*. 5,75-93

Kolb, C. R., and Van Lopik, J. R. (1958). "Geology of the Mississippi River deltaic plain, Southern Louisiana." Technical Rep. No. 3-483,U.S. Army Engineer Waterways Experiment Station, Vicksburg, Mississippi

Lancellota R. (1995). "Geotechnical Engineering", A. A. Balkema, Rotterdam, Brookfield

Lane, E.W. (1934), "Security from under-seepage masonary dams on earth foundations." *Trans* ASCE, 60(4): 929-966.

Li, S.K. and Lumb, P.(1987)."Probabilistic design of Slopes." *Can. Geotech. J*., 24(4),520-535.

Lowe, J., and Karafiath, L. (1960). "Stability of Earth Dams upon Drawdown." *Proceedings of the First Pan American Conference on Soil Mechanics and Foundation Engineering*. Mexican Society of Soil Mechanics, Mexico D.F., pp 537-552.

MacGregor, J.G. (1992) "reinforced Concrete Mechanics and Design" Serviceability, Englewood Cliffs: Prentice Hall, 314-348

MacGregor, J.G. (1992) "reinforced Concrete Mechanics and Design" Flexure: T Beams, Beams with compression reinforcement, and special cases, Englewood Cliffs: Prentice Hall, 126-167

Mattson, H., Klisinski, M., Axelsson,K.. (2001). " Optimization routine for identification of model parameters in soil plasticity." *Int. J. for Numeric. and Anal. Meth. in Geomech.* 25(5),435-472.

Mayne, P.W. and Sawson, P.G.(1981), "The critical State pore Pressure parameter from consolidated- Undrained Shear tests", Laboratory shear strength of soil (STP 740), ASTM, Philadelphia, 410-430

Messerklinger, S. (2006). "Non-linearity and small strain plasticity of lacustrine clay" http://www.enpc.fr/cermes/seminaires/w(h)ydoc05/presentations/Messerklinger-w(h)ydoc05.pdf

Mississippi Levee Board ( ). "Mississippi River Levee Enlargement and Berms Project", Project for people.

Morgenstern N.R. and Price, V.E. (1965). "The analysis of the stability of general slip surfaces." *Geotechnique*, 15(1), 79-93.

Mylleville, B.L. J. and Rowe, R.K. (1988) " Steel reinforced embankments on soft clay foundations." *Proceeding int. Geotech. Symposium theory and Practice of Earth Reinforcement*, A.A. Balkema, Rotterdam, The Netherlands, 437-422.

Ng, C.W.W. and Shi Q.(1998) " A Numerical investigation of the stability of unsaturated soil Slopes subjected to transient seepage" *Computers and Geotechnique*, 22(1) 1-28.

Patrick J. Conroy, Kenneth M. Berry (2008) "Load test of London Avenue canal floodwall", *Midwest Levee Conference*, June 2-5, 2008, St. Louis, Mo.

Perry, J. (1993). " A technique for defining non linear shear strength envelops, and their incorporation in a slope stability method of analysis." *Quarterly Journal of engineering Geology*, N0. 27, 231-241

Pockoski, M. and Duncan, J.M.(2000), " Comparison of computer programs for analysis of Reinforced Slopes." Virginia Polytechnic Institute and state University, VA.

Powel M.J.D.(1964). " An efficient method for finding the minimum of a function of several variables without calculating derivatives.*' Computer J.* 7,155-162

Rogers, J.D., Boutwell,G.P.,Schmitz, D.W., Karadeniz D., Watkins,C.M., Athanasopoulos-Zekkos,A.G., Cobos-Roa,D.(2008)"Geologic Conditions Underlying the 2005 17th Street Canal Levee Failure in New Orleans" *J. of Geotech. Geoenviron. Eng.*, 134(5), 583-601

Roscoe, K.H. and Schofield, A.N. and Worth, C.P. (1958). "On the yielding of soils." *Geotechnique*, 8(), 22-53

Roscoe, K.H. and Schofield, A.N.(1963). " Mechanical behavior of idealized wet clay." *Proceedings of 2nd European conf. on Soil Mech.,* Wiesbaden, No.1, 47-54

Roscoe,K.H. and Burland, J.B. (1968). " On the generalized stress-strain behavior of the wet clay." Engineering Plasticity, Cambridge University Press, Cambridge, 535-609.

Rosenbrook, H.H. (1960). " An automated method for finding the greatest or least value of a function .*" Computer J.* 3, 175-184

Rousè, P. (2006). "Implementation of critical state models within FLAC" *4th International FLAC symposium*, Madrid, 2006.

Rowe, R.K. and Mylleville, B.L.J.(1985) " An approximate method for estimating the stability of geotextiles reinforced embankments." *Can. Geotech. J*., 22(3), 392-398.

San, K.C. Leschinsky, D. and Matsui, T. (1994). Geosynthetic reinforced slopes: Limit equilibrium and finite element analysis." *Soils and Foundations*, 3492), 79-85

Sasankul, I., Vandit-Ellis, W., Sharp, M., Abdoun, T., Ubilla, J. , Steedman, S. and Stone, K. (2008) "New Orleans Levee System Performance during Hurricane Katrina: 17th street Canal and Orleans canal North" *J. of Geotech. Geoenviron. Eng*., 134(5), 657-667

Schofield, A.N. and Worth, C.P. (1968). "Models and Soil mechanics." Critical state soil mechanics, McGraw-hill, London, New York, 20-21

Schofield, A.N. and Worth, C.P. (1968). "Models and Soil mechanics." Critical state soil mechanics, McGraw-hill, London, New York, 146-149

Seco, E.; Pinto, P.S. and Marahna das Nevas, E. (1985). " Hydraulic fracturing in zoned earth and rockfill dams." *Proceedings 11th Int. conf. on Soil Mech. and Found. Engr*., A.A. Balkema, Rotterdam, The Netherlands, 2025-2030

Seed R.B., Bea, R.G., Athanasopoulos-Zekkos, A, Boutwell, G.P., Bray, J.D.; Cheung, C., Cobos-Roa, D., Ehresing, L., Harder, L.F., Pestana, J.M., Riemer, M.F., Rogers, J.D., Storesund, R., Vera-Grunauer,X. and Wartman, J.(2008) " New Orleans and Hurricane Katrina.II: The Central Region and the Lower Ninth Ward" *J. of Geotech. Geoenviron. Eng.*, 134(5), 718-739

Seed R.B., Bea, R.G., Athanasopoulos-Zekkos, A, Boutwell, G.P., Bray, J.D.; Cheung, C., Cobos-Roa, D., Ehresing, L., Harder, L.F., Pestana, J.M., Riemer, M.F., Rogers, J.D.,

Storesund, R., Vera-Grunauer,X. and Wartman, J.(2008) " New Orleans and Hurricane Katrina.IV: Orleans East Bank(Metro) Protected Basin" *J. of Geotech. Geoenviron. Eng.*, 134(5), 762-779

Sekiguchi, H. and Shibata, T. (1979). " Undrained behavior of soft clay under embankment loading." *Proceedings 3rd int. conf. on Numerical Meth. in Geotech. Eng*., A.A. Balkema, Rotterdam.

Sills,G.L.,Vroman, N.D. Wahl,R.E. and Scwanz N.T.(2008) "Overview of New Orleans Levee Failures: Lessons Learned and Their Impact on Natioal Levee Design and Assessment" *J. of Geotech. Geoenviron. Eng.*, 134(5), 556-565

Skempton, A.W. (1954) "The Pore-Pressure Coefficients A and B," *Geotechnique*, 4(4), 143 – 147

Smith, I.M. and Hobbs, R. (1974) "Finite element analysis of centrifuged and built-up slopes." *Ge'otechnique*, 24(4), 531-559

Smith, I.M. and Hobbs, R. (1976) "Biot analysis of consolidation beneath embankments." *Geotechnique*, 26(1), 149-171.

Snitbhan, N. and Chen, W.F. (1976). " Finite element analysis of large deformation in slopes" *Proceedings conference of Numer. Meth. in Geomechanics*, Blacksburg, VA, 744-756.

Spencer, E. (1967). "A method of analysis of the stability of embankments assuming parallel interslice forces." *Geotechnique*, 17(1),11-26

Tanaka, T. and Nakano, R (1976). "Finite element analysis of Miyama rockfill dam." *Proceedings conference numer. Meth. in Geomechanics*., ASCE, New York, 650-661.

Tandjira, V., Low, B.K. and The, C.I. (2002) " effects of reinforcement force distribution on stability of embankments" *Geotextiles and Geomembranes*, No. 20, 423-443

Terashi, M.2009. "Keynote lecture "Current Practice and future perspective of QA/QC for Deep-Mixed ground", *Okinawa Deep Mixing Symposium*, 2009

Terzaghi, K. (1922)."Der Grundbruch an Stauwerken und seine Verhutung (The failure of dams by piping and its prevention)" *Die Wasserkraft*, 17, 445-449.

Terzaghi, K. (1939)."Soil Mechanics: a new chapter in engineering science." *J. Instrumentation in Civ. Engr.*, 12,106-141.

Terzaghi, K. (1939)."The theoretical Soil Mechanics." Wiley, New York, 1-510

Terzaghi, K. (1943) "Theoretical Soil Mechanics" Theory of Semi-Infinite Elastic Solids, John Wiley and Sons, Inc; New York, 367-416

Terzaghi, k. and Peck R.B. (1948)." Soil mechanics in engineering practice." Wiley, New York.

Thamm, B.R. (1979). "Numerical analyses of Embankments over soft subsoils." *Proceedings 3rd int. conf. on Numerical Meth. in Geotech. Eng.*, A.A. Balkema, Rotterdam, The Netherlands, 725-731.

Ubilla J.,Abdoun, T, Sasankul I., Sharp, M., Steedman,S. Vanadit_Ellis,W,Zimme, T.(2008) " New Orleans Levee System Performance during Hurricane Katrina: London Avenue and Orleans Canal South" *J. of Geotech. Geoenviron. Eng*., 134(5), 718-739

Ugural, A.C. (1981) "Stresses in Plates and Shells" McGraw-Hill, New York, 1-16

U.S. Army Corps of Engineers (1994) “Engineer Manual1110-2-2504: Design of sheet pile wall” *Geotechnical Investigation*, Washington DC, 3/1-3/11

U.S. Army Corps of Engineers (2001) “Plans for Lake Pontchartrain, Louisiana and vicinity hurricane protection High level Plans Orleans Parish, LA” London Avenue outfall Canal, Parallel Protection, New Orleans, LA

USACE(2003). “Slope stability.” Engineering Manual 1110-2-1902, Department of the Army corps of Engineers, Washington D.C. http://140.194.76.129/publications/eng-manuals/em1110-2-1902/entire.pdf

U.S. Army Corps of Engineers (2006) “Performance evaluation of the New Orleans and Southeastern Louisiana hurricane Protection system” Rep. of the Interagency performance evaluation Task Force, Washington, D.C. (http://IPET.wes.army.mil)

U.S. Army Corps of Engineers and St. Louis District Corps of Engineers (2008) “The London Avenue Site Specific Load Test-Appendix D”, New Orleans, LA (http://www.mvn.usace.army.mil/hps2/hps_reports.asp)

Wang, C., Salmon, C.G.(1998) “Reinforced Concrete Design” Introduction, Materials, and Properties, Addison-Wesley , Menlo Park, California ,1-31

Wang, Z.L. (1990). “Bounding surface hypoplasticity model for granular soils and its Applications”, Ph.D. dissertation. Univ. Calif., Davis,

Wang, Z.L., Dafalias, Y.F., and Shen, C.K. (1990). “Bounding surface hypoplasticity model for Sand*” J. Engr. Mech.*, ASCE, 116(5): 983-1001.

Wang, Z.L. and Makdisi, F.I.,(1999) "Implementing a Bounding Surface Hypoplasticity Model for Sand into the FLAC Program", *Proceedings of the International Symposium on Numerical Modeling in Geomechanics,* MN, p. 483-490. September 1999

Wheeler, S.J.,Naatanen, A., Karstunen, M.,Lojander,M.(2003). "An anisotropic elastoplastic model for soft clays, *Can. Geotech. J*. 40,403-418.

Whittle, A.J., Kavvadas,M.J. (1994). "Formulation of MIT-E3 constitutive model for Overconsolidated clays" *J. of Geotech. Geoenviron. Eng*., 120(1), 173-198

Wolff, T.F. and Harry, M.E. (1987). " slope design for earth dams." In Reliability and Risk Analysis in Civil Engr. 2, *Proceedings of the 5th Int. conf. on Applications of statistics and Probability in Soil and Structural Engr*., Vancouver, BC, Canada, May , 1987, 725-732.

Wright, S. G., and Duncan, J. M. 1987. "An Examination of Slope Stability Computation Procedures for Sudden Drawdown," Miscellaneous Paper GL-87-25, U. S. Army Engineer Waterways Experiment Station , Vicksburg, MS

Wroth, C.P. and Simpson, B. (1972) "An induced failure at trial embankment: Part II finite element computations. " *proceedings of Earth and Earth-Supported Struct*., ASCE, New York, Vol.1,65-79.

Yang, Z., and Elgama,A.(2003). "Application of unconstrained optimization and sensitivity analysis to calibration of soil constitutive model" *Int. J. for Numeric. and Anal. Meth. in Geomech*. 27,1277-1297

Zangl, L.W.(1979). “Behavior of an asphalt concrete core during dam construction and reservoir filling” *Proceedings 3rd int. conf. on Numerical Meth. in Geotech. Eng*., A.A. Balkema, Rotterdam, The Netherlands, 733-746.

http://www.dotd.state.la.us/press/pressrelease.asp?nRelease=764

http://kellerfareast.com/deep_soil_mining.htm

http://www.wdsu.com/r/19508312/detail.html

http://www.sheetpiles.net/

VITA

Sudarshan Adhikari was born in Dhading district of Nepal. He completed his high school study from Budhanilkantha School, Nepal in 1989 and joined Tribhuvan University, Nepal for his further studies. He completed Diploma in Civil Engineering in 1993, and Bachelors in Civil Engineering in 1997. After his graduation, he worked in different consulting firms and government agencies for 6 years. In 2003, he went to the University of Hanover, Germany to pursue his Mater degree in Geotechnique and Infrastructures. For that he received German Academic Exchange Service (DAAD) scholarship. In 2005, he completed his Master degree and he continued his study there as a guest student to study some civil engineering courses. In 2007 he returned back to Nepal and joined the consulting firm as a geotechnical Engineer and worked there for about 8 months. He then came to USA in 2008 to pursue Ph.D. in Geotechnical Engineering in the University of Mississippi. He worked as the Graduate Research Assistant under the supervision of Dr. Chung R. Song. He received "dissertation fellowship" from the Graduate school to support his study. He also worked as instructor and co-instructor to teach different civil engineering graduate and undergraduate courses. He is planning to graduate in December 2012.